ABOUT THE AUTHOR

Professor Christopher R. Calladine, as a boy from Nottingham High School, won an open scholarship in mathematics and physics to Peterhouse, Cambridge. There, he read engineering and achieved Class I in the Mechanical Sciences Tripos, winning the Rex Moir Prize; and in Part II won the Archibald Denny Prize. He did a Masters Degree in Civil Engineering at the MIT Computation Centre, USA in 1958. Before returning to Cambridge as an academic, he worked for a time in the nuclear power industry solving structural problems. In the late 1960's and 1970's he returned to the USA as a visiting Research Associate at Brown University and as Visiting Professor of Applied Mechanics at Stanford University.

In 1986 he became full professor in his main field of structural mechanics at Cambridge University, where he has been a faculty member in the Department of Engineering since 1960. His main interests have been in engineering plasticity; in shell theory (*Theory of Shell Structures*, Cambridge University Press, 1983); and also in the biological problems of structural mechanics (*Understanding DNA 3rd Edition* with Horace Drew, Ben Luigi and Andrew Travers, Elsevier Press, 2004)

He was awarded the Ludwig Mond Prize by the Institute of Mechanical Engineers in 1996 and the James Alfred Ewing Medal by the Institute of Civil Engineers in 1998. He is a Fellow of the Royal Society, a Fellow of the Institute of Civil Engineers and a Fellow of the Royal Academy of Engineering.

PLASTICITY FOR ENGINEERS:
Theory and Applications

C. R. Calladine, **F.R. Eng., F.R.S.**
Professor Emeritus of Structural Mechanics
University of Cambridge
and
Fellow Emeritus of Peterhouse.

Oxford Cambridge Philadelphia New Delhi

Published by Woodhead Publishing Limited,
80 High Street, Sawston, Cambridge CB22 3HJ, UK
www.woodheadpublishing.com

Woodhead Publishing, 1518 Walnut Street, Suite 1100, Philadelphia,
PA 19102-3406, USA

Woodhead Publishing India Private Limited, G-2, Vardaan House, 7/28 Ansari Road,
Daryaganj, New Delhi – 110002, India
www.woodheadpublishingindia.com

First published by Horwood Publishing Limited, 2000; reprinted 2009
Reprinted by Woodhead Publishing Limited, 2011

British Library Cataloguing in Publication Data
A catalogue record for this book is available from the British Library

ISBN 978-1-898563-70-9

Printed by Lightning Source.

TO MARY

PREFACE

MY MAIN concern in writing this book has been to communicate to students of engineering the important and useful ideas of the Theory of Plasticity. Certain features of the theory—which has by now reached its maturity—are particularly appropriate to the crucial activity of engineering design, and I have tried wherever possible to bring out the "lessons" afforded by the theory as well as to present the "facts".

The book is aimed primarily at engineering students who are already familiar with elementary mechanics, "strength of materials" and "theory of structures"—including perhaps a treatment of plastic collapse of beams—and who are mainly interested in becoming design engineers. An appreciation of stress as being rather more than "tension ÷ area" is absolutely essential to any respectable treatment of the theory of plasticity, and I assume that the reader will be thoroughly familiar with the theory and application of the Mohr circle of stress. For the sake of ease of reference, and to explain an unusual sign convention, a brief description of the theory is given as Appendix I. The other Appendices describe important ideas referred to in the text, with which the student may or may not be familiar, and also a note on units, etc. They are intended to be self-contained.

Experience shows that the solving of numerous problems is an important aspect of success in the study of a technical subject. At many points in the text, therefore, I have left proof or verification of simple points to the reader, and I hope that students will work through the corresponding problems whenever they reach them in the text.

The answers to some of the problems are best presented graphically, and I have occasionally suggested that the best place

to draw the curves is on existing figures in the text. This has the merit of making appropriate comparisons particularly easy.

In some instances back-reference is made in the text to the solution of problems in a previous chapter. The student may therefore find it helpful to keep his problem-work in some sort of order.

In addition to the "text problems" I have provided others, some of which are "open-ended". They range widely in scope, length and difficulty, and the ones which are most demanding are marked with the symbol †.

For the sake of completeness I have included material which I do not expect the average student to take too seriously, particularly at first reading. No great harm will be done, I think, by skipping lightly through the *proofs* of the theorems in Chapter IV, provided the statements and examples of their application are given due attention, or by ignoring altogether the rather specialist topic of slip-line fields in Chapter VIII, or by ignoring the parts of Chapter X concerning axisymmetric flow.

Readers who are familiar with other textbooks on Plasticity will notice that I have avoided wherever possible the use of notation more general than necessary for the immediate purposes, and that I show a marked bias towards the Tresca yield condition, which is in fact not normally so realistic as the Mises condition. I have also attempted to keep the mathematical aspects of the treatment as simple as possible so as not to discourage, I hope, those students who are relatively unsophisticated mathematically but who have considerable intellectual and imaginative powers and later become excellent engineers. I have tried, nevertheless, to bring out at every stage the main general features of the theory and I hope that the method of presentation will not prove an embarrassment to students who later graduate from this introductory volume to the more complete and rigorous textbooks.

Readers of this sort may think my nomenclature a little curious also. For example, I do not use the terms "limit theorems" or "limit analysis" in reference to the important upper- and lower-bound theorems and their manifold application. This is because I regard it as rather unimportant for the purposes of this book to

discuss plastic collapse as the limiting state of elastic–plastic behaviour. Instead I give some suggestive examples and point out—repeatedly—the necessity for scrutiny of the idealisations which must be made, whether consciously or unconsciously, in the development of any theory. I also use the terms "theory of plasticity" and "plastic theory" indifferently.

I have not followed the conventional practice of citing detailed references to the literature. It is plain, I trust, that most of the facts and ideas I present are attributable to others, and I leave it to those who become sufficiently interested to consult any of the works cited in the Bibliography to trace the work back to its sources. The book possesses, nevertheless, some novel features, mainly as a consequence of the systematic application of the lower- and upper-bound theorems. For these I accept full responsibility.

There is little emphasis in the book on matters of computation, and in particular there are no listings of computer programs. The reason is that the book is concerned primarily with the development and application of fundamental ideas in plasticity such as the upper- and lower-bound theorems. These ideas afford a freedom to the engineer in thinking about structural design which cannot be conveyed by a set of standard computer routines.

The mechanical properties of specific materials are quoted in SI units (e.g. Fig. 2.23). Conversion factors for stress, etc. to Imperial units are given in Appendix VI.

The present edition has the same text as the earlier edition (*Engineering Plasticity*, Pergamon Press, Oxford) apart from corrections to the text, a few minor changes and an up-dated Bibliography.

Jacques Heyman, Bernard Neal and Andrew Palmer made many valuable suggestions for improvement of the original manuscript. I am indebted to Jim Greenwood and David Durban for some improvements in this edition.

Finally, I thank John Munro the Series Editor and Ellis Horwood the Publisher for their help with the present edition.

Palmer, Dr. J. Heyman and Professor B. G. Neal, who read the manuscript and made many valuable suggestions for its improvement; and to Miss H. Gunns, who typed the manuscript, and Miss P. A. Charter, who traced the illustrations.

CHAPTER I

INTRODUCTION

THIS chapter is intended to provide an engineering background for the theory of plasticity. It consists of a set of short essays which together define the scope of the subject and some of its aims. Part of the chapter is devoted to a brief discourse on the nature of theories in general, and the way in which engineers, by focusing attention on this area (which is, unfortunately, often regarded as a somewhat murky region) can clarify their thinking about the processes of design.

1.1. Metals and Structural Engineering

The widespread use of metals in structural engineering is largely due to their combination of properties of strength, weldability and ductility.

Strength is obviously desirable in making structures which must withstand severe loading conditions.

Weldability is an obvious attraction from the construction point of view, because it is a means to the effective joining together of components into "continuous" structures.

The word *ductility* describes in general the ability of a bar to be "drawn" into a longer, thinner bar, usually with the aid of a die. The word also has a special well-defined quantitative *technical* meaning, but throughout this book we shall use it in its original, general, sense, as a convenient abbreviation for "ability to undergo plastic deformation". The adjective "plastic" simply describes the idea of moulding a shape, as a potter might mould a jug from a lump of clay. This analogy is not at all inappropriate, because

dimensional changes of tenfold can easily be obtained with a ductile metal, by compression or shearing, for example.

Many metals also possess the very useful property of *elasticity* or resilience if they are only deformed a small amount, typically less than 1 per cent. In this book we shall primarily be concerned with deformation in the plastic range, although we shall devote some attention to situations where it is not clear whether elastic or plastic behaviour is more significant.

An important element of the analogy between plastic deformation of metals and the behaviour of potter's clay is that the moulding takes place *quickly* and *permanently*. It is obviously desirable that a jug, once formed, should not "sag" before it is baked, and the potter therefore makes sure that the clay is mixed with the right amount of water so that it can be moulded by sufficient pressure and yet will not deform appreciably under its own weight in the time which elapses before it hardens. The plastic deformation of metals at room temperature has both of these characteristics; for example, a piece of mild-steel rod or strip at room temperature may be bent into an angle practically instantaneously, and it will retain the same shape indefinitely. In technical language we say that this sort of deformation is *time-independent*.

This use of the word "plastic" as an adjective should not be confused with its use as a noun to describe a large class of non-metallic materials, "plastics"—so-called because they are mouldable under certain chemical and environmental conditions. True, there are some obvious similarities of mechanical behaviour between metals and plastics, but there is an important difference in that the deformation of "plastics" is generally *time-dependent*. Thus, a nylon thread will "creep" over a period of time if it sustains a constant pull, and then gradually "recover" over a period of time if it is later unloaded. This is a marked contrast with the plastic behaviour of metals at room temperature and, indeed, at higher temperature. This kind of time-dependent behaviour, although increasingly important in the design of structures made of plastics, is beyond the scope of this book.

Ductility is an important property of metals as far as structural engineering is concerned for two reasons. First, it makes it possible to re-form the cast ingots of metal into a wide variety of shapes. Complex shapes such as crankshafts can be made by *forging*; prismatic members like I-beams and sheets can be made by successive continuous *rolling* operations; rods and wire can be *reduced* to smaller diameter by *drawing* through a die; sections of various shapes can be formed by *extrusion* through a die; and sheet can be *pressed* into complex shapes like car-body panels. The list could be extended considerably. The technology of these processes is outside the scope of this book: we shall, however, study briefly the *mechanics* of some simple metal-forming processes.

Because metals are softer at elevated temperatures (but below the melting-point) many of the processes listed above are performed on *hot* billets. In fact at these temperatures metals *creep* under sustained load, i.e. exhibit some time-dependent behaviour, but they can nevertheless be regarded satisfactorily as plastic in these processes because the imposed deformations are quick in the time-scale of creep.

Secondly, ductility is a useful property of metals in structural engineering from the point of view of structural failure. A structure made of ductile material will deform considerably if overloaded and will usually still sustain a considerable load in its "bent" condition. Such a structure thus gives helpful warning of impending collapse. In contrast, a structure made of a brittle material would fail suddenly and catastrophically by "snapping" of an overloaded component. Another way of looking at this is to note that with ductility goes the capacity for absorbing considerable amounts of energy. Metals are thus suitable materials for the construction of vehicles, such as cars and ships, which may be involved in unexpected collisions.

Moreover, it is not only at failure that ductility plays an important part in structural integrity. In all structures there are geometrical features which produce local "concentration of stress". Such features include holes of all kinds, angular corners,

notches (whether present by design or accident) and abrupt changes in thickness of sections. Broadly the action of a ductile material at a stress concentration is to "yield" a little, and in so doing to make the stress concentration more diffuse and thus less intense. Multiple-riveted joints provide a good example of this sort of behaviour; the load transmitted through the joint is unlikely to be shared equally between the rivets, but the overloaded rivets will tend to yield a little and produce a more uniform load-sharing. This sort of behaviour was well understood by those who pioneered riveting as a means of joining components: after all, the rivets underwent very considerable plastic deformation when they were being put in, so a little more in the course of their useful life would be unlikely to impair their integrity.

Throughout the book we shall assume that we are dealing with materials which are ductile under all relevant circumstances. We should be aware, however, that some metals and alloys display very little plastic deformation before fracture, and also that some metals which are normally ductile may fracture in a brittle manner under adverse circumstances. Brittle fracture in steels—which are normally ductile—has been the subject of a very large research effort, and although many areas of imperfect knowledge remain, sufficient is now understood for the engineer normally to be able to deal confidently with the problems posed by the phenomenon. For an up-to-date account of the subject see the book by Hall, Kihara, Soete and Wells listed in the Bibliography.

1.2. A Microscopic View

An intelligent question at this stage would be: as the capacity of metals for plastic deformation appears to be such an important property from the point of view of the structural engineer, how does it come about? The answer to this question lies outside the field of *mechanics*—which is what this book is about—and within the province of physics, chemistry and metallurgy; it is well covered in, for example, the book by Cottrell listed in the Bibliography. As we shall make use of some of the relevant ideas in the

next chapter, it is worth while to state here, briefly—and at the risk of oversimplification—that the crux of the matter is the nature of the *metallic bond* between atoms. There are three main kinds of chemical bond: ionic, covalent and metallic. All are a result of the interactions between electrons and atoms, but the metallic bond is peculiar in that there are far-ranging electrons which move freely through the entire set of positive ions as a kind of free electron "gas". It is the flow of this electron gas through the metal under an applied electric field which is responsible for the high electrical and thermal conductivity of metals. The freedom of these bonding electrons also makes the cohesive bonds between adjacent atoms *fully transferable* in the sense that if atoms in a crystal shift positions, the cohesive bonds are just as strong in the new configuration as in the old. It is the consequent possibility of large-scale reorganisation of atoms with no loss of cohesion within the simple crystal structures which is responsible for the unique plastic properties of metals on the macroscopic scale.

1.3. The Theory of Plasticity

The task of plastic theory is twofold: first to set up relationships between stress and strain which describe adequately the observed plastic deformation of metals, and second to develop techniques for using these relationships in the study of the mechanics of metal forming processes, and the analysis and design of structures. We shall see that in the accomplishment of both of these tasks there is plenty of scope for the exercise of individual judgement and taste. The theory is a more powerful tool for engineering analysis and design in the hands of a worker who is well aware of the scope, within the theory, for individual initiative.

1.4. The Nature of Physical Theories

It seems worth while at this stage to digress a little and make some remarks about the problems which are encountered in the

construction of *any* theory. The general aim of these remarks is to elucidate the nature of the relationship between objects and experimental observations on the one hand and ideas on the other. These remarks will in fact provide one of the major themes for the book as a whole.

Our problem is, basically, how the human mind can come to grips with the physical world, and manipulate it. Now one of the most interesting achievements of the human mind has been the development of *mathematics*, which is fundamentally an abstract subject dealing in particular with relationships between symbols, including numbers. We might guess therefore that mathematics would be a useful tool in our task of obtaining an understanding of the physical world. But how can mathematics, which is so clear and precise, and in many ways simple, be applied to the physical world which, although apparently *consistent*, is many-sided and extremely complex? The key to the solution of this problem lies in our making *idealisations* of the physical world. Now we are all familiar with the process of making idealisations, but we may indeed be *so* familiar with it that we almost lose sight of the fact that we are making idealisations at all. Therefore, even though we risk stating the obvious, it seems worth while to give a few simple illustrations.

For example, in discussing the position of a ship at sea, we regard the ship as a *point*. The bows and the stern actually occupy different positions in space and so have different latitude and longitude coordinates. However, it would clearly be a waste of everyone's time to think of quoting two positions for two different parts of the ship at sea, simply because the ship is extremely small compared to the size of the ocean. The situation is reversed, however, if we are thinking of bringing the ship into a dock: here the pilot will be very much concerned with the positions of both bow and stern with respect to the dock.

We can extend these considerations about ships almost as far as we please. The hydrodynamics expert whose job it is to decide the shape of the hull of a ship will regard the ship as a *rigid body* which is moving through the water. On the other hand the

structural engineer will certainly regard the ship's plating as *flexible*, and indeed will probably be concerned with the distortion of the ship as a whole in heavy seas, if for no other reason than to make sure that the propeller shaft bearings remain in sufficiently good alignment. The mechanical engineer will be conscious of the *vibrations* of the ship's structure which may be caused by the engines, so he too will consider the ship as being made of flexible material. Yet, again, the interior designer of a large liner will picture the ship primarily as a floating *hotel*; and so on.

The point of this rather obvious analysis is that *any* mental picture of the ship we may have depends on what questions we are asking about the ship. If we ask "where is the ship?" we think of it as a *point* if it is out at sea, and as an object of a particular *shape* and *size* if it is near a dock. To answer other obviously important questions in the design of a ship we consider it successively as a *rigid body*, a *flexible body*, a *hotel*, etc., etc. There is no real contradiction between any of these different idealisations; not even between a point and a body of a particular shape and size or between a rigid and a flexible body—although at first sight these are absolutely contradictory. Quite simply, in each case the idealisation is the best one for the particular question in hand. The process of idealisation of the physical world is one in which we set up conceptual *models* in which only the *main features* from a particular standpoint are reproduced.

Now we are all familiar with *physical* models. An architect's model of a proposed building, for example, gives an indication of the main features of the building without including a lot of detail. We are not misled by the fact that the model, perhaps, is made of balsa-wood and has unglazed windows into thinking that the finished building will also be made of wood and have simple holes for windows; we understand easily that the sole object of a model of this sort is to give an indication of the layout and proportions of the building in a three-dimensional representation. Precisely the same sort of relationship between reality and model holds for *conceptual models*; the only difference is that conceptual models only exist in the human mind.

Science is rich with examples of conceptual models, and indeed the progress of science is largely a result of the invention of appropriate conceptual models to fit particular experimental observations. A good example of a conceptual model is Maxwell's kinetic theory of gases. In this theory Maxwell uses as a model of gas an empty space containing a number of small, fast-moving, perfectly elastic, heavy balls which bounce indefinitely between the walls of the container, obeying Newton's laws of motion. This simple and imaginative model explains satisfactorily a number—but by no means all—of the phenomena of gases and mixtures of gases. In discussing this theory we are not committing ourselves to a belief that atoms or molecules *are* small spherical particles: we are simply saying that *if* we regard them as such, then in certain circumstances the predictions of the model agree well with experimental observations. In other circumstances—for example at very high pressures—this model becomes inadequate, and we have to seek another.

Nearer to our own field, the useful subject of rigid-body mechanics provides many good examples of conceptual models; indeed, the subject owes its existence to the conceptual model of the *rigid* body. Now no real object is actually rigid: sufficiently large forces will always produce deformation or fracture. However, in many situations the forces tending to distort the body are relatively unimportant compared to those tending to accelerate it, and so it is reasonable to set up and use the concept of the perfectly rigid body. We are all familiar with the language of this branch of mechanics at the schoolboy level: "A heavy particle rests on a smooth flat horizontal table. It is attached to a point on the table by a light inextensible string. . . ." An idealised situation is described very clearly. The corresponding situation in the physical world might be described as follows: "A lump of metal lies on a table. It is attached by means of a piece of string to a nail which has been driven into the table. On investigation it turns out that the coefficient of friction between the lump and the table is 0·1, that the mass of the string is only 1/20 of that of the lump of metal, and that when the mass is suspended by the string in the

gravitational field the string extends by about 1 per cent." By removing from our model the extensibility and mass of the string, and all friction, we arrive at a situation which is amenable to relatively simple analysis using Newton's laws, and we hope that the main features of the behaviour of the model will be broadly similar to those of the real system. We can test the predictions of our model by performing an experiment and comparing the predicted and observed behaviour. If this comparison reveals large discrepancies, we must of course reconsider the features of the model. For example, in this particular situation the absence of friction from the model would lead to large differences in behaviour between the model and the physical set-up in long-term motion, but probably not in short-term motion. If instead of discarding these "secondary" effects in setting up our model we had retained them, all the mathematics would have been very much more complex, and all clarity would have disappeared.

Thus, in making idealisations and setting up conceptual models we run, in general, the risk of removing some feature which is in fact rather important. We cannot of course make any *direct* test of our models against the real physical world: the only test we can make of the validity of our models is to see whether or not predictions based on their use agree with experimental observations made on real physical systems.

As we must *necessarily* make idealisations in setting up our simple models we cannot of course ever expect *complete* agreement between "theory" and experiment, and we must be content with broad agreement on the main features of behaviour. The question of whether agreement is satisfactory or not is thus to some extent a question of taste. In engineering we often have to judge between an extremely crude model which leads to very simple calculations and answers which may agree with experiment to within, say, $\pm$ 20 per cent, and a much more sophisticated model which leads to complex and lengthy calculations and produces answers which are to within, perhaps, $\pm$ 5 per cent of experimental observations.

It is a main thesis of this book, as indeed of plasticity theory in

general, that in the structural engineering design situation it is extremely valuable to have a simple theory which enables the designer to make rough but rapid assessments of the main structural characteristics of various possibilities which he is investigating. It is true that some refinement will probably be desirable in the later stages of design, but it is very important not to waste time and effort on elaborate calculations in the early stages of design if simpler and more radical calculations would provide just the relevant information.

1.5. The Conceptual Simplicity and Power of Plastic Theory

It is implicit in the preceding discussion that one of the barriers to the general progress of science and engineering is the difficulty of choosing appropriate conceptual models. This is one of the points at which the intellect and the imagination are worked hardest; but once the key has been found, so to speak, new realms of understanding are opened up.

The theory of plasticity is based, as we shall see, on an exceptionally simple idealisation of material behaviour, and it has enabled engineers to make enormous advances in their understanding of certain kinds of structural action, and in the setting up of rational design procedures. The development of the theory over the past 30 years has marked a pronounced maturing process in the field of structural engineering, which has led to increased confidence and a growing awareness of the value of imagination and intuition in the processes of structural design. One somewhat curious outcome of this maturing process is that we can now, with the aid of plastic theory, appreciate some of the achievements of the Gothic Cathedral builders who in the "dark ages" evidently had enormous reserves of imagination and intuition. These achievements are practically incomprehensible according to the *theory of elasticity* which, ever since the publication of Castigliano's book in 1879, has provided a major conceptual basis for structural engineering. For a development of this

theme see the paper by Heyman listed under "Masonry construction" in the Bibliography.

1.6. Uniqueness, Indeterminacy and Freedom

This brings us to a fundamental and rather subtle point which is not at all well understood by some engineers. Because lack of appreciation of this point apparently acts as a barrier to the acceptance of plastic theory as relevant to structural design, it seems worth while to look into the question in some depth.

In the theory of elasticity there is a unique relationship between stress and strain, which results in the behaviour of elastic structures being expressed in the form of *equations*. As we shall see later, plastic theory on the other hand has an essential *discontinuity* in the stress–strain relationship, and the theory involves, in consequence, discontinuities and inequalities. This might appear at first sight to make the theory difficult, but it turns out that the situation may be exploited to produce some extremely simple results. Part of the price to be paid for this simplicity is that there is often an apparent degree of indeterminacy about solutions to problems in plasticity. In fact the answers to the *main* questions which are asked are unambiguous, but there is often a degree of flexibility in solutions in the sense that the values of some variables may be chosen arbitrarily—within limits—without affecting the answers to the main questions. To those brought up on elasticity theory this *minor indeterminacy* may well be puzzling, because it is unfamiliar: nothing like it appears in elastic theory where, once a problem has been posed, the values of all the variables may be determined uniquely, in principle, at least.†

Are we to conclude, then, that because some quantities are apparently undetermined the theory of plasticity is in some way sub-standard? Not at all! On the contrary, we conclude that those quantities which are not determined uniquely by plastic theory are in some way of *secondary importance*.

Now the apparently complete determinacy of elasticity solutions

† We exclude from consideration here questions of elastic stability.

is due in part to the fact that elastic structures are normally idealised as being *stress-free* initially. Actual structures are very rarely stress-free as built because, quite apart from having to carry their own weight, they sustain "locked-in" stresses due to slight misfit of the components with each other, due to thermal expansion on welding, and because as-rolled sections invariably have high residual stresses due to differential cooling in the manufacturing process. Some specially critical structures may be put through a "stress-relieving" procedure which aims at removing initial stresses by a sort of annealing process, but in general it can be stated that structures as built contain random unknown residual stresses of significant magnitude. In general therefore the "initially stress-free" idealisation of structures in elastic theory cannot be justified, and the determinism of the stress quantities in the theory can properly be regarded only as a consequence of an unjustifiable idealisation.

Plastic theory deals with the initial-stress problem in a quite different way. It concentrates on the state of the structure at *collapse*, and in fact concludes that initial stresses do not affect the collapse strength of the structure. In other words, plastic theory, instead of *ignoring* initial stresses, shows positively that in some important respects their magnitude is *irrelevant*. This conclusion is closely related to the ideas of "minor indeterminacy" mentioned above.

The emphasis in plastic theory on the importance of some quantities and the relative insignificance of others makes the theory particularly valuable for structural design. Anyone who has attempted any engineering design- or project-work will be well aware that in creative work of this sort there are so many variables that to consider them all would be quite impossible. It is necessary in practice to pick out what appear to be the important variables, and assign reasonable values to the others by intuition if by no other means. In other words, there are usually so many facets to a design problem that there is no unique solution. There is, so to speak, a lot of room for free-will in design, and experienced engineers will often express the profound idea

that engineering design is, to a large extent, an *art*. In an important sense plasticity theory harmonises with this overall design situation, in that it places a premium on the use of imagination and intuition. It is not surprising, therefore, that plastic theory lends itself easily to problems of structural design, as we shall see in the remainder of this book.

1.7. Shortcomings

One of the shortcomings of the present chapter is that it anticipates some of the more important results of plastic theory which probably will not be fully appreciated by the student until he has studied subsequent chapters and worked at problems. The chapter may well make much more sense to the student if he reads it again after he has finished other parts of the book. Difficulties of this sort are encountered frequently in teaching a mature subject; the wholeness of the subject can rarely be communicated quickly, even though the major ideas can be stated, if necessary, in a few words. Usually only a fraction of the ideas in a book "take root" at the first reading, and much more is understood on a second coverage of the same ground.

To correct any possible misunderstandings the student may have at this stage, it seems good to state, explicitly, that the theory of plasticity is concerned exclusively with a definite area in the mechanics of deformable bodies, and that it cannot, by definition, answer questions on many important topics outside its scope. The theory provides no guidance on such important aspects of structural design as vibrations, structural stability and the *probability* of the design loads being exceeded during the lifetime of the structure, to name a few. Plastic theory provides a tool for solving problems in a strictly limited, but nevertheless important, field of structural mechanics.

CHAPTER II

SPECIFICATION OF AN IDEAL PLASTIC MATERIAL

WE CONSIDER in this chapter the general problem of how to set up a model of the plastic behaviour of metal—for use in analysis and design of structures and forming processes—which is at the same time both simple and also in broad general agreement with experimental observations. The development of our model will be done in several stages, the last of which involves making as many simplifications as possible without removing what we consider to be the main features.

2.1. Observations on a Tension Test

The simplest mechanical test we can perform on a material is the *tension test*. Figure 2.1(a) shows the result of a simple tension test performed on an annealed wire of commercially pure copper. The wire, originally about 2 mm diameter was held tightly in grips which were arranged so that there was a "test section" about 6 cm long. The grips were pulled in a testing machine which maintained accurate alignment of the specimen and grips, and provided a means for recording simultaneously the pull and the extension of the wire at any time. The specimen was extended steadily. Very similar curves were obtained by testing other specimens at different speeds of extension, over a wide range. We observe that the curve is steep in the region of the origin, and that although it continues to rise, the slope becomes progressively less. We can say that the material *hardens* on deformation, in the sense that it gets stronger the more it is extended. In fact, sooner or later a maximum load is reached, but we will return to this later.

One possibility at this stage—which we shall in fact reject—is to fit an algebraic equation to the curve and to use this in subsequent calculations on the behaviour of structures, etc. We reject this (a) because in general we are interested in solid *blocks* of

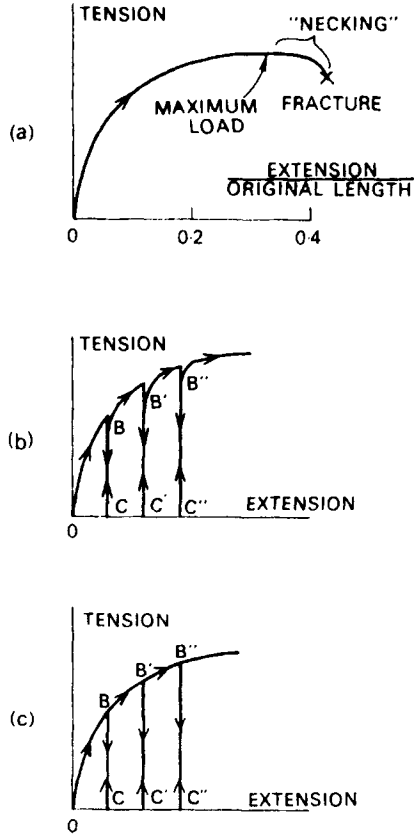

FIG. 2.1. Simple tension tests of annealed copper.

metal rather than wires and (b) because there is much more experimental information available which we shall also want to consider and incorporate in our model.

The result of a second kind of tension test performed in the same machine on a similar specimen is shown in Fig. 2.1(b). It is altogether much more interesting than that of the first test,

because it shows what happens when the specimen is loaded, unloaded and reloaded in succession. While the *loading* parts of the path, i.e. those parts for which the load was rising higher than ever before, are very close to the curve in Fig. 2.1(a), we see that if ever the specimen is *unloaded* the (tension, extension) point in the graph immediately starts off on a different, steeper, almost straight path. Further, on subsequent reloading the load-point follows the unloading path until it almost reaches the initial loading path, when it begins to turn fairly sharply to rejoin the path.

If we are prepared to idealise this kind of "knee" into a "kink", and also neglect a small hysteresis effect, we can schematically redraw Fig. 2.1(b) as shown in Fig. 2.1(c). In this diagram, in view of the directions of the arrows, we can label the steadily rising curve as *irreversible* and the unloading/reloading curves as *reversible*. Further tests show that in fact the loading path is reversible for all load changes within the ranges *BC*, and we can thus describe all the ranges *BC* as *elastic*, using this term to mean *reversible*. Examination of the test records indicates that all of the elastic branches *BC* have practically the same slope, and indeed are parallel to the very first part of the curve of Fig. 2.1(a).

Now suppose that a specimen has been loaded to a point *B*, and then unloaded, and is subsequently subject to a steadily increasing load. As we have already seen, the response of the specimen is at first elastic, but then there is a fairly abrupt (perfectly sharp in the idealised version, Fig. 2.1(c)) change into the irreversible range of behaviour. This irreversible range of behaviour we call the "plastic" range, because we observe on subsequent unloading that in this range some "permanent" deformation has occurred.

As we shall see, it is the fact that there is a *transition* which is almost a *sharp discontinuity* between elastic and plastic behaviour which provides the key to the setting up of simple idealisations of the behaviour of the specimen. The name given to this point of transition is the *yield point*.

We see from Fig. 2.1(b) and (c) that plastic deformation tends to raise the yield-point load; indeed, for this particular annealed

material the *initial* yield point is low and the rate of "hardening" high, and specially careful experimentation is needed to determine the initial yield point.

Further observations that could be made are that the pattern of curves in Fig. 2.1(b) is virtually unchanged if the testing is done at different speeds (but lower than shock-wave speeds) and that the plastic deformation occurs at *constant volume*.

2.2. Behaviour of Metals on the Atomic Scale

It will be appreciated that so far our discussion has been in terms of tension and extension of a bar of material. Later we shall discuss mechanical behaviour in terms of *stress* and *strain*, and use these variables in the subsequent analysis. It is clearly convenient, when dealing with structures and forming processes, to use these *macroscopic* quantities which are obviously appropriate to mechanical testing when it is reasonable to assume that the material is homogeneous. This book is in fact based on the presupposition that discussion of materials in terms of stress and strain is valid.

This is not to deny, however, the importance of metal physics to engineers. As we have already observed in Chapter I, physicists look at metals from the microscopic point of view and often think of metals as collections of atoms. The macroscopic and microscopic views of matter are of course wide apart, but recent advances in metallurgy (see, for example, Cottrell) do in fact enable us to understand in broad terms many of the features of the tension test we have just described in terms of the interaction between atoms. The main lines of the argument can be understood without going into much detail, as follows.

By virtue of the nature of the metallic bond, metal atoms arrange themselves in simple regular arrays in the form of crystals. There are both attractive and repulsive interactions between adjacent atoms; both are highly nonlinear with distance, and the net effect is that for an unstressed metal the atoms have an "equilibrium" spacing. When a metal is loaded in the elastic range the

"bonds" between the atoms are strained, and for sufficiently small relative movements there is practically complete reversibility and a linear relationship between attraction and change of separation from the "equilibrium" position. Thus in the elastic range a block of material will exhibit a linear relationship between changes of load and deformation. The crystals, however, are not absolutely perfect, and there are occasional gaps and misfits in the "lattice". Also in a specimen of metal which has not been specially prepared as a single crystal, there will be many crystals in random orientation, so there will also be mismatch at the crystal boundaries. For sufficiently small applied loads, as we have seen, the material responds, reversibly, by small adjustments of the interatomic distances. For larger loads, however, it becomes "easier" for the material to sustain the load if the misfit atoms move position. In general the movement of one atom will make a neighbour become a misfit, and so it is possible for chains of movement to take place by sequences of "flips" of individual atoms. This process is known as the movement of *dislocations*, and the overall forces required to produce *step-by-step* movements of this kind are much smaller than those required for *wholesale* sliding of planes of atoms over each other. The net result of large numbers of dislocation movements is that observable permanent "plastic" deformation of the specimen takes place. If the load causing plastic deformation is decreased slightly, however, the dislocation chain does not go into reverse, because the forces are relieved on the "next atom in line", and changes are again accommodated elastically. The plastic deformation is thus irreversible. Further, because the broken bonds re-form at practically "equilibrium" separation of atoms, the movement of dislocations, and hence plastic deformation, takes place with no overall change in volume of the specimen. Also, since the atomic bonds are transferred when atoms move around, the elastic properties of the body are unchanged by plastic deformation. On reloading after unloading, the movement of dislocations commences at practically the same load as the previous maximum; hysteresis effects and the rounding of the "knee" (Fig. 2.1(b)) are due to small-scale dislocation

movements at lower stress than the critical level required for large-scale movements. As plastic deformation proceeds the dislocation chains become "piled up" and the stress for plastic flow increases in consequence. However, these effects are removed by annealing: at higher temperatures the mobility of the atoms increases and the atoms can rearrange themselves in a more nearly perfect lattice, without any overall change in dimensions of the body.

The above atomic-scale picture of the deformation of metals thus reveals qualitatively all of the main features of macroscopic behaviour we have described, and we shall return to it as occasion requires for illumination of other points later on.

2.3. Tension and Compression Tests

We have already observed that it would be premature to base a theory of plasticity on the results of tension tests alone, because of all possible ways of deforming a block of material the tension test is clearly only one. An obvious alternative way of deforming a block of metal is to compress it, and because compression is in a sense a simple reversal of tension, we consider it next.

If we compress a straight wire lengthwise it will tend to *buckle* sideways, which is an undesirable complication. We must therefore test stubby specimens, and the most convenient procedure is to squash them lengthwise between smooth, lubricated, parallel plates. Again plastic deformation takes place at constant volume, and axial shortening is accompanied by thickening. In fact even well-lubricated end plates tend to prevent to some extent the lateral "spreading" at the ends of the specimen, and "barrelling" is observed as the test proceeds, as indicated in Fig. 2.2. In our analysis we shall neglect this barrelling and assume that the specimen remains cylindrical at all times.

Figure 2.3 shows the result of a compression test on an annealed copper specimen, with compressive load regarded as a negative quantity. In spite of the difference in *shape* between the curves in Figs. 2.1(b) and 2.3 we can detect encouraging similarities

FIG. 2.2. Stages of deformation in a compression test, showing "barrelling".

between the two graphs: there are both elastic and plastic paths, and relatively sharp transitions between them, in both cases.

As both plastic tension and compression take place at constant volume we might suspect a common mechanism of deformation for the two processes, and hence possibly quantitative correlation between the two tests, in addition to the qualitative correlation we have already noted.

Clearly to make a comparison between specimens of different diameter and length we must normalise our load and deformation quantities with respect to cross-section area and length, respectively: in other words we must work in terms of "stress" and "strain". Now stress and strain can only be described adequately as truly three-dimensional quantities, as we shall see later. However, in the present tests the specimens remain cylindrical (until "necking" occurs in the tension test, as we shall see; and disregarding barrelling in the compression test), so it is reasonable to

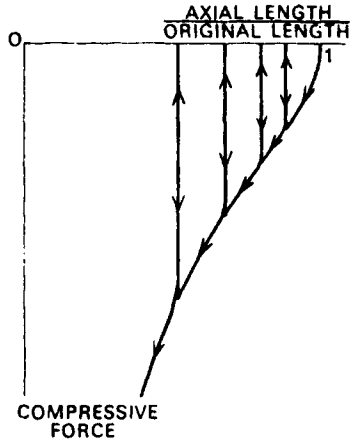

FIG. 2.3. Simple compression test of annealed copper.

use axial load divided by cross-section area as a measure of stress and change in length per unit length as a measure of strain in these particular tests. Let the cylindrical specimen initially have length l_0 and cross-section area A_0, and be subject to a tensile pull P along the geometrical axis of the specimen. At a subsequent time let the length and cross-section area be l and A respectively (see Fig. 2.4).

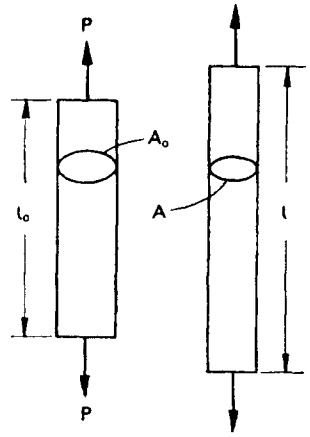

FIG. 2.4. Definition of symbols used to describe tension and compression tests.

The "nominal" or "engineering" definitions of stress, s, and strain, e, are:

$$\left.\begin{aligned} s &= P/A_0 \\ e &= (l - l_0)/l_0. \end{aligned}\right\} \tag{2.1}$$

Note that both s and e are negative in a compression test. Now it is clear that the *shape* of the (s, e) curve will be the same as that of the $(P, l-l_0)$ curve, and so these definitions do not achieve the desired quantitative correlation between Figs. 2.1 and 2.3. It is also clear that in both of these tests, and particularly in the compression test, there are very considerable changes of cross-section area as the deformation proceeds.

To take account of the geometry changes we therefore define a "natural" or "true" stress, σ, as follows:

$$\sigma = P/A \tag{2.2}$$

where A is the *current* cross-section area. A "natural" strain ϵ is not quite so simple to define, because strain is *accumulated* as the length changes: we can however satisfactorily define an *increment* of strain, $\delta\epsilon$, which occurs as the length increases from l to $l + \delta l$:

$$\delta\epsilon = \delta l/l \tag{2.3}$$

Considering infinitesimal changes and integrating between the initial and final lengths l_0 and l_1 (say), respectively, we have

$$\epsilon = \ln(l_1/l_0) \tag{2.4}$$

Here ln stands for "logarithm to the natural base e". Thus again in compression ϵ is negative, because $l_1/l_0 < 1$.

As we have not actually measured changes in cross-section throughout the test, we cannot directly compute the true stress from the observations recorded in Figs. 2.1 and 2.3. However, as we have mentioned already, careful measurements show that in plastic deformation there is practically no change in volume, and we may therefore use this fact to give a relationship between current length and cross-section area. For prismatic specimens of constant volume

$$lA = l_0A_0 \tag{2.5}$$

so

$$\sigma = \frac{P}{A_0} \cdot \frac{A_0}{A} = \frac{P}{A_0} \cdot \frac{l}{l_0} = s\frac{l}{l_0} \tag{2.6}$$

Figure 2.5 shows a re-plot, in terms of true stress and true strain, of the data of Figs. 2.1 and 2.3. Absolute values of σ and ϵ have been plotted so that the tension and compression curves are directly comparable. The two curves are close to each other, and

they indicate that plastic behaviour is remarkably similar in tension and compression, provided due allowance is made for changes of geometry.

The elastic unloading paths have not been shown in Fig. 2.5. It should be remembered, nevertheless, that the curves may be regarded *either* as a plot of true stress against true strain for monotonically increasing loading *or* as a plot of yield stress against strain. The second alternative is of more significance, conceptually, but we should remember—and this becomes of crucial

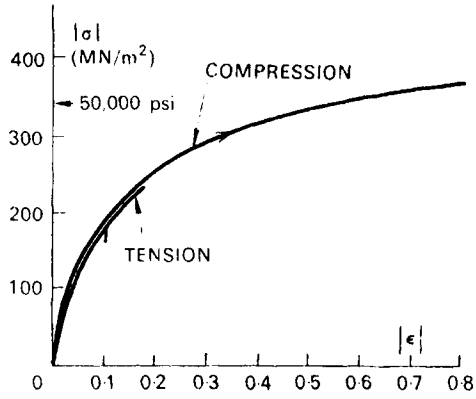

FIG. 2.5. True-stress–true-strain curves for annealed copper.

importance for complex straining paths—that we are really dealing with *accumulation of increments of strain*, rather than with strain as such.

2.4. Instability in the Tension Test

Before going on to discuss truly three-dimensional states of stress, it is worth while to consider, as an introduction to the question of instability and the critical effects of changes in geometry, the phenomenon of *necking* in tension test specimens, and other related topics.

When a bar of ductile material is loaded in a tensile testing machine, it remains prismatic (except possibly for small zones near

the grips or end attachments) well into the plastic range. As the load reaches a maximum, however, the deformation begins to be non-uniform and a *neck* forms (see Fig. 2.6). The neck is associated with decreasing load (see Fig. 2.1 (a)), and the falling part of the tension–extension curve can only be observed if the testing machine is "stiff", i.e. if the testing machine imposes primarily an *elongation* on the specimen rather than a load. Otherwise—if the testing machine applies a steady load—the specimen will not be in equilibrium after the neck has begun to form and the specimen will quickly break.

Suppose that we know the true stress/true strain relationship of the material at strains beyond the inception of necking: Fig. 2.5

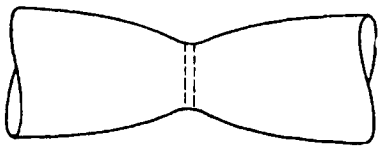

FIG. 2.6. Typical profile of a neck in a tension test specimen.

suggests that we could obtain this information from a *compression* test. Further, let us re-plot this information as σ against l/l_0 (Fig. 2.7): the reason for this choice of elongation variable will be clear later. Let us try to work back from this information to predict the form of the load/extension curve (Fig. 2.1(a)). We need, clearly, to express the nominal stress s in terms of σ. From (2.6)

$$s = \frac{\sigma}{l/l_0} \tag{2.7}$$

Thus, the value of s corresponding to any point B in Fig. 2.7 is given by the slope of the line OB or, equivalently, the intercept on the line $l/l_0 = 1$. Therefore as the load on the specimen increases the point B travels along the curve, until it reaches the point, T, where OB *touches* the curve, when the load cannot be increased

any more. Any subsequent elongation of the bar must take place with *falling* load, and for a value of s below the maximum value there are now two possible paths (both lying on a line of slope s from the origin); one (TC) involving more plastic deformation and the other (TD) involving elastic unloading. In fact the material in the neck follows the path TC, while the remainder of the bar unloads elastically. The important point is that the inception of necking corresponds to a *choice* of loading paths. The neck presumably forms in practice where the wire is locally slightly thin or where the material is slightly weak; once a neck has formed,

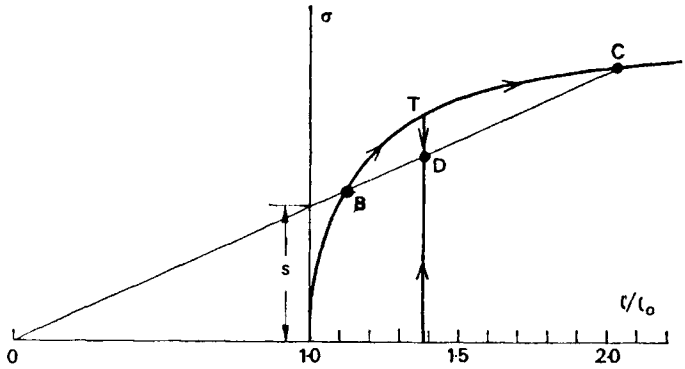

FIG. 2.7. Graphical construction for nominal stress.

however, there is no tendency for other necks to form because the remaining material reverts to elastic behaviour.

Of course a full analysis of the *growth* of a neck would involve consideration of three-dimensional stress in the "hourglass-shaped" region, which is beyond the scope of this book. In the coin-shaped region at the narrowest part of the neck (see Fig. 2.6) the above analysis should be fairly satisfactory, however; but up to and including the inception of necking (i.e. so long as the bar remains prismatic) the above analysis is perfectly satisfactory.

The "tangent" construction for the maximum value of s (called technically "ultimate tensile stress" or U.T.S.) is known as Considère's construction.

2.5. Materials with Upper and Lower Yield Points

The preceding discussion has used as an example the plastic behaviour of annealed copper which, as we have seen, is a material with a low initial yield point and a steadily rising stress–strain curve in simple tension or compression. To have a usefully high yield-point for structural purposes, copper must have undergone a process of deformation, such as rolling or drawing, to harden the material. In contrast, other metals in the annealed or heat-treated condition have usefully high initial yield points. Examples are aluminium alloys and steels (see below). Apart from this feature, however, all of the preceding description (elastic range, yield point, plastic range, etc.) applies equally well.

Among materials with high initial yield stress are those which exhibit the somewhat curious phenomenon of upper and lower yield points. As the very useful material mild-steel is in this class it is appropriate to discuss the matter a little further.

The true-stress–elongation curve for a typical annealed mild-steel is as shown in Fig. 2.8. l/l_0 is plotted because we shall use the generalised Considère construction, but the scale has been broken because the region of interest involves extensions of the order of 1 per cent. Suppose we hang weights on a vertical wire of annealed mild-steel which is exactly straight, so that there is no variation of stress across a section. The material is elastic until point B is reached. As the curve falls but subsequently rises there will be another point of stable equilibrium at C: BC produced passes through the origin, but since the slope is so small BC is practically parallel to the l/l_0 axis. Dynamic effects, which might be expected in the jump B–C, will be absorbed in the slightly viscous (i.e. slightly time-dependent) nature of plastic flow. In this experiment we would therefore observe a jump from the elastic range to a homogeneous plastic elongation of the order of 1 per cent. Now suppose that we perform a second experiment on the same sort of wire in which, by means of a screw, we apply a steadily increasing *elongation* to the wire, and have a device for measuring the load. In the elastic range up to point B

the behaviour is the same as before, but thereafter it is different, as the load is observed to *drop* to a lower yield-point corresponding to line *DF* in Fig. 2.8. At this load the material can be in equilibrium *either* in the elastic range *or* in the plastic range with a definite plastic strain corresponding to point *F*. In an experiment on a *polished* specimen the sudden drop in load is accompanied by the appearance on the surface of narrow bands where the polish is disrupted, called Lüders' bands after their first observer. These bands lie on planes which cross the specimen at 45° to the axis, and in terms of Fig. 2.8 they correspond to material at point

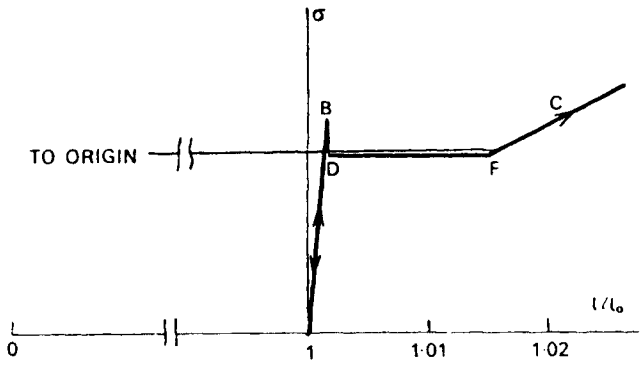

FIG. 2.8. Tension test on annealed mild-steel.

F. As the elongation increases these bands multiply and spread until when the elongation of the specimen *as a whole* has reached point *F*, the polished surface has entirely disappeared. Subsequent elongation causes the load to rise, and the deformation is homogeneous as the load point travels up the curve *FC*. . . . Now as the Lüders' bands are at 45° to the axis it is clear that the deformation is truly three-dimensional and that consequently Fig. 2.8, which refers essentially to a one-dimensional situation, is inadequate for a deep analysis. In several respects, however, Fig. 2.8 is useful: in particular it explains how an *overall* elongation of the specimen of (say) 0·8 per cent is made up of about half of the material at 1·6 per cent plastic strain, with the remainder

still elastic. For mild steel the deformation is thus highly non-uniform on a microscopic scale. This non-uniformity is easily observed when a mild-steel structure is tested if a brittle coating has been applied to the surface. Whitewash or plumber's resin are suitable for application as brittle coatings, but the mill-scale found on as-received hot-rolled sections gives a somewhat similar effect.

2.6. The Bauschinger Effect

We have already seen (Fig. 2.5) that for two specimens of the same material tested under steadily increasing tension and compression respectively the yield stress for continuing plastic deformation is the same function of the accumulated plastic strain, when due allowance is made for changes in geometry, and sign. We might imagine, therefore, that if a specimen were, say, loaded in tension into the plastic range and then unloaded, the yield stress on subsequent loading in tension or compression would be the same, as indicated in Fig. 2.9(a). Unfortunately, physical reality is not quite so simple, and experimental results in general are more as shown in Fig. 2.9(b). Perhaps the most straightforward interpretation of the results is that the hysteresis loops in Fig. 2.1(b) which are "narrow" for unloading to zero and reloading become "wide" when the unloading is continued to a negative load about equal to the previous positive load. After the hysteresis loop has been traversed, the original curve is regained, but as the lower end of the loop is much more rounded than the knees of Fig. 2.1(b) we cannot claim that the behaviour beyond point F (Fig. 2.9(b)) is similar in the tension and compression directions. This is known as the Bauschinger effect, and is often thought of as a reduction of the yield stress on loading in the direction opposite from the previous direction.

In fact the Bauschinger effect is observed in polycrystalline specimens of metal but not in single crystals, and it may be explained qualitatively in terms of an aggregate of randomly oriented "non-Bauschinger" crystals; the interaction between the

crystals "blurs" the sharpness of the yield point on reversed loading (see Problem 2.1).

In all future work we shall for the sake of simplicity ignore the Bauschinger effect: that is, we shall assume that if a specimen has a certain yield stress after a given history of loading, the magnitude of the yield stress is the same if the sign of the stress is reversed. This is a reasonable assumption if reversals of stress do not take place in the history of loading of a particular structure or metal-working process—which is the case for the vast majority of situations considered in this book. If stress reversals do take

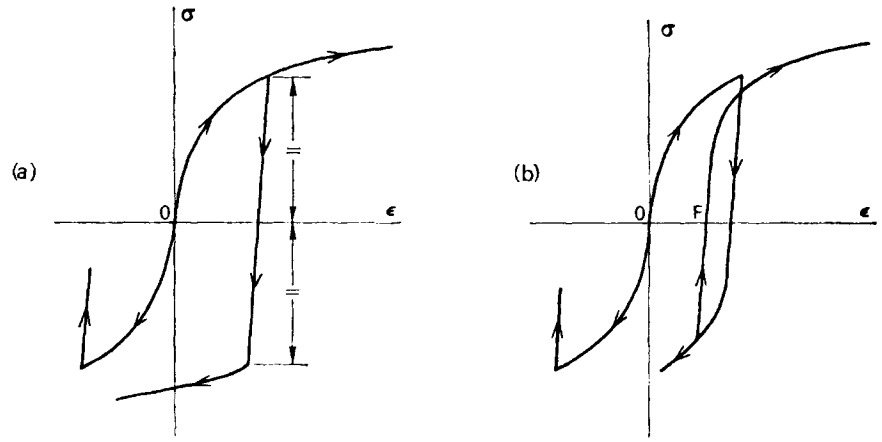

FIG. 2.9. The Bauschinger effect.

place it will be necessary to re-examine this assumption; an example of this will be mentioned in the next chapter. So far we have been considering the Bauschinger effect in terms of simple uniaxial states of stress. Later on we shall interpret our statements about the Bauschinger effect in terms of more general three-dimensional states of stress.

2.7. The Yield Locus

We have already seen that in pure tension and compression tests of ductile metals we find that at any stage in a history of

loading the material has an elastic range of stress, and that if we are prepared to make the idealisations indicated in Figs. 2.1(b) and (c) the extent of the elastic range is defined precisely, in a way which is suitable for formulation in mathematical symbols as follows:

$$\text{For } 0 < \sigma < \sigma_y \text{ the material is elastic.}$$

In this statement σ_y is the *current* yield stress, which may be either an *initial* yield stress for a previously unstressed specimen or a *subsequent* yield stress for a specimen which has already undergone some plastic deformation.

By neglecting the Bauschinger effect we extend the elastic range thus:

$$\text{For } -\sigma_y < \sigma < \sigma_y \text{ the material is elastic.} \qquad (2.8)$$

Note that we can define an elastic range in terms of *limits* on stress, and without any reference to the reversible relationship between changes of stress and strain which is valid within that elastic range.

In general, to develop a satisfactory theory of plasticity we shall need to be able to deal with more complicated, three-dimensional, states of stress. It will therefore be advantageous if we can generalise our ideas of "elastic range" and "yield point" to more complex stress systems.

To proceed in relatively small steps, let us consider next a bi-axial, i.e. two-dimensional, state of stress. Suppose we devise a testing machine which is capable of applying tension and compression independently in two perpendicular directions parallel to the plane of a thin sheet of material, as indicated in Fig. 2.10(a). Also suppose that by plastic straining in the 1-direction we have established an elastic range (no Bauschinger effect) in the 1-direction, bounded by two yield points, as shown on the σ_1 axis of the stress-space of Fig. 2.10(b). Now let us hold σ_1 constant in our testing machine at some value within the elastic range and steadily increase σ_2 until inelastic behaviour is observed. In general experiments of this kind (usually performed on thin-

walled tubular specimens in combined tension and torsion) show that there is a fairly sharp transition from elastic to plastic action: consequently, as an idealisation, we may specify a further yield *point* in σ_1, σ_2 space. Extending the argument, we develop the idea of a *yield locus* in stress space, dividing elastic behaviour from plastic for a material previously strained plastically.

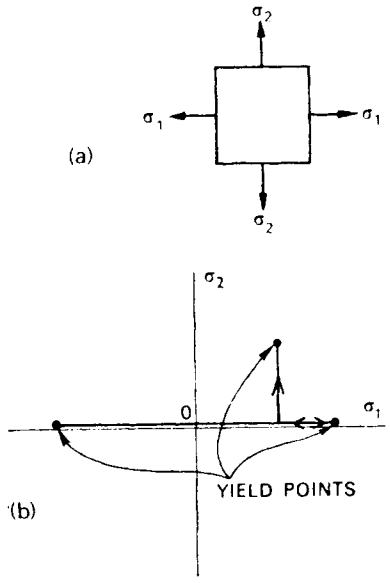

FIG. 2.10. Bi-axial test and corresponding stress-space.

Since the yield locus is the boundary of the elastic domain it is *path-independent* in the sense that a point on it may be approached by many different loading paths within the elastic region, as illustrated schematically in Fig. 2.11.

Experimental work on many metals has amply justified the concept of the yield locus. In so far as it is necessary in an experiment to decide, somewhat arbitrarily, precisely what level of plastic straining marks the end of the elastic range, yield surfaces obtained for the same material by different experimenters may

differ by small amounts. However, such differences do not detract from the validity of the concept of the yield locus.

The yield locus in stress-space may be an *initial* yield locus for a previously unloaded specimen or a *subsequent* yield locus for a specimen with a previous history of plastic straining. We have already seen that in simple tension or compression of a strain-hardening material the yield stress is altered by any plastic deformation, and so in general we expect the yield locus to be *altered* if any plastic deformation takes place. In particular if the

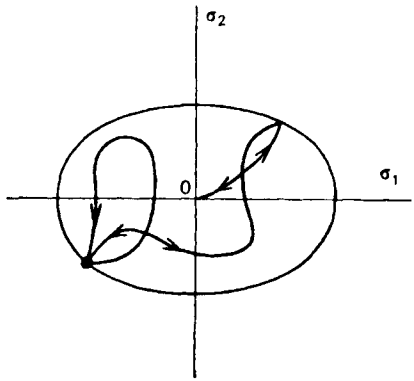

FIG. 2.11. Yield locus in two-dimensional stress-space, schematic.

stress-point goes *outside* a current yield locus it will lie *on* a new yield locus, so that locally at least the yield locus will be carried along with the stress point. In this book we shall be concerned not so much with the way the yield locus changes its shape or size as the load point "pierces" it, but with the general form of the locus for an elementary block of material at a given stage in its history of plastic deformation.

2.8. Yield Surface for Three-dimensional Stress

In general the state of stress at a point in a body is specified by the values of the six independent stress components σ_x, σ_y, σ_z, τ_{yz}, τ_{zx}, τ_{xy} referred to an arbitrary set of orthogonal x, y, z axes

(see Fig. 2.12). It might appear therefore that we would need a six-dimensional stress space in which to represent a general yield locus. However, it is *always* possible to choose directions of orthogonal axes 1, 2, 3 for which the shear stresses τ_{23}, τ_{31}, τ_{12} all vanish, as indicated in Fig. 2.12. These are called *principal axes* and the corresponding stresses—σ_1, σ_2, σ_3—the *principal stresses* (see Appendix I). It is therefore convenient to choose the principal axes as the reference axes, and this incurs no loss of generality

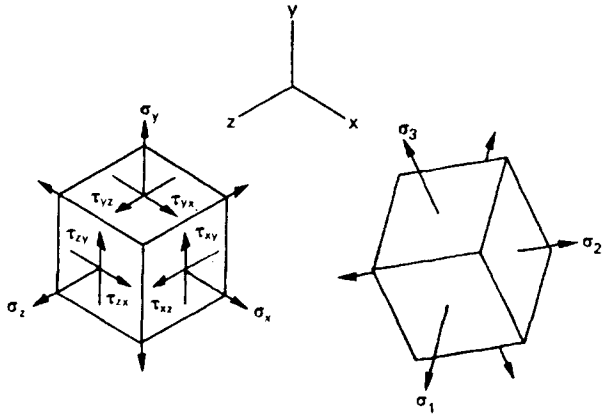

FIG. 2.12. Three-dimensional state of stress.

if the material is isotropic, i.e. has the same properties in all directions.

As all of our visual experience is in three-dimensional space it will obviously be desirable in working out the geometry of yield surfaces to work in terms of a *three-dimensional principal stress space*. However, can we justify the necessary idealisation of our material as isotropic? At first sight this might appear unlikely, because the arrangement of atoms in a crystal lattice, being orderly and having well-defined directions is clearly *geometrically* anisotropic, and thus probably mechanically isotropic also. However, metallographic examination indicates that unless special precautions are taken in preparation, a block of undeformed metal contains in general many grains or crystals with the respective

lattice directions higgledy-piggledy. We would thus expect that the anisotropy of individual grains would be lost and that the material in bulk would be isotropic. However, we might expect that even if a material is *initially* isotropic, subsequent plastic deformation may add a measure of order to the random orientation of grains and hence produce a geometrical anisotropy in the bulk material. Experiments show that the degree of mechanical anisotropy developed during moderately large plastic deformation is not great. It is, therefore, reasonable to build mechanical isotropy into our idealised simple plastic material.

We should note, however, that the degree of mechanical isotropy found, for example, in metal plates which have been reduced substantially in thickness by cold rolling in one direction may in some circumstances demand the introduction of a degree of anisotropy in the theory. We shall not explore this aspect of the theory.

Returning then to the three-dimensional principal stress space, we ask the question: what is the nature of the yield surface for our idealised material?

We use several different pieces of information in answering this question.

First we introduce the experimental observation that the addition of an equal-all-around (hydrostatic) pressure to a specimen of polycrystalline metal does not affect its yield behaviour, at least for pressures of the same order as the tensile yield stress; this has been demonstrated by many direct and indirect experiments. By this statement we mean that if the point $(\sigma_1, \sigma_2, \sigma_3) = (a, b, c)$ lies on the yield surface, then so also does the point $(a+h, b+h, c+h)$ for all h, at least within fairly wide limits.

This observation is not surprising if we think about the atomic-level picture. Response of a metal to hydrostatic pressure by itself is purely elastic, because there is no tendency for dislocations to move if there is no question of change of *shape* of the specimen. This insensitivity of the yield behaviour to hydrostatic pressure is thus broadly associated with the plastic incompressibility of the material.

We ought to note that metals may become brittle under hydrostatic tension, because under these conditions the mode of deformation might change from shear to cleavage; and that some normally brittle materials, like rocks, may flow plastically under shear stress in the presence of high hydrostatic compression. For the present purposes, as noted in section 1.1, we shall assume that the material is ductile under all relevant stress conditions.

It is also worth noting, in passing, that a material like saturated clay, which is *irreversibly* compressible, exhibits plastic yield behaviour under shear stresses which are a function of the hydrostatic pressure. The explanation for this difference between the plastic behaviour of metals and clays undoubtedly lies in their different microstructure—clays are composed of flake-shaped particles of the order of 10^{-6} m long, and the cohesive action is electro-chemical in the presence of water.

Returning to our idealised metal, it follows that any *point* (a, b, c) on the yield surface generates a *line* passing through the point and parallel to the line $\sigma_1 = \sigma_2 = \sigma_3$, which is in the first octant of principal stress space and equally inclined to all three principal stress axes. Hence the yield surface is a *prism* which may be thought of as being generated by sliding a curve along the "space diagonal" $\sigma_1 = \sigma_2 = \sigma_3$.

This being so, all the additional information necessary for us to specify the yield surface completely is the shape and size of the cross-section of the prism. Now by elementary solid geometry, all planes perpendicular to the line $\sigma_1 = \sigma_2 = \sigma_3$ have the equation $\sigma_1 + \sigma_2 + \sigma_3 =$ constant. As it is immaterial which cross-section of the prism we consider, we can set the constant to any arbitrary value. The most convenient value is zero, which corresponds to the plane perpendicular to the axis of the prism and passing through the origin of principal stress space. We call this special plane the π-plane, and the intersection of the yield prism with it the C-curve.

It is a matter of elementary algebra to "reduce" any point on the yield surface to the corresponding point on the C-curve. Let (a, b, c) lie on the yield surface. The corresponding point on the C-

curve has coordinates $(a+h, b+h, c+h)$ and in addition, since it lies on the π-plane, the sum of the three principal stresses is zero; so

$$h = \tfrac{1}{3}(a+b+c)$$

We can thus write, for any point on the yield surface, the identity

$$(\sigma_1, \sigma_2, \sigma_3) \equiv (\sigma_1', \sigma_2', \sigma_3') + (\sigma_o, \sigma_o, \sigma_o) \tag{2.9}$$

where $\sigma_o = (\sigma_1 + \sigma_2 + \sigma_3)/3$

and $\sigma_1' = \sigma_1 - \sigma_o$

$\sigma_2' = \sigma_2 - \sigma_o$

$\sigma_3' = \sigma_3 - \sigma_o$

Note that $$\sigma_1' + \sigma_2' + \sigma_3' \equiv 0 \tag{2.10}$$

The stress $(\sigma_1', \sigma_2', \sigma_3')$ is known as the *deviatoric stress* or *stress deviation*, and $(\sigma_o, \sigma_o, \sigma_o)$ is known as the *hydrostatic* stress. In geometrical terms we have broken down the stress vector in three-dimensional stress space into two components, one (the deviatoric stress) lying in the π-plane the other (hydrostatic stress) being perpendicular to the π-plane.

EXAMPLE: If $(\sigma_1, \sigma_2, \sigma_3) = (6, -2, 1)$, in arbitrary units, find $(\sigma_1', \sigma_2', \sigma_3')$ and σ_o.

Answer: $\sigma_o = (6-2+1)/3 = 5/3$

so $\left.\begin{aligned} \sigma_1' &= 4\tfrac{1}{3} \\ \sigma_2' &= -3\tfrac{2}{3} \\ \sigma_3' &= -\tfrac{2}{3} \end{aligned}\right\}$ check: sum $= 0$

As we have now focused our interest in the nature of the three-dimensional yield surface onto the C-curve in the π-plane, it is now advantageous to draw a proper plane diagram, shown in Fig. 2.13. The drawing shows a view (without perspective) along the space diagonal of the three axes σ_1, σ_2, σ_3 (positive and negative senses) together with what appears as a triangular mesh inscribed on the π-plane but which may equally well be thought of as a view of a cubic lattice in the first octant of the stress space.

The reader should verify that the diagonal view of a unit cube (i.e. a cube whose side represents unit stress) is as shown inset.

In Fig. 2.13 the stress-point (6, 0, 0) is represented by point A_1. The same point also represents the corresponding deviatoric stress (4, −2, −2)—which is as it should be by virtue of the properties of the π-plane. The reader should make sure that he can plot points on a diagram of this sort: see the first part of Problem 2.12.

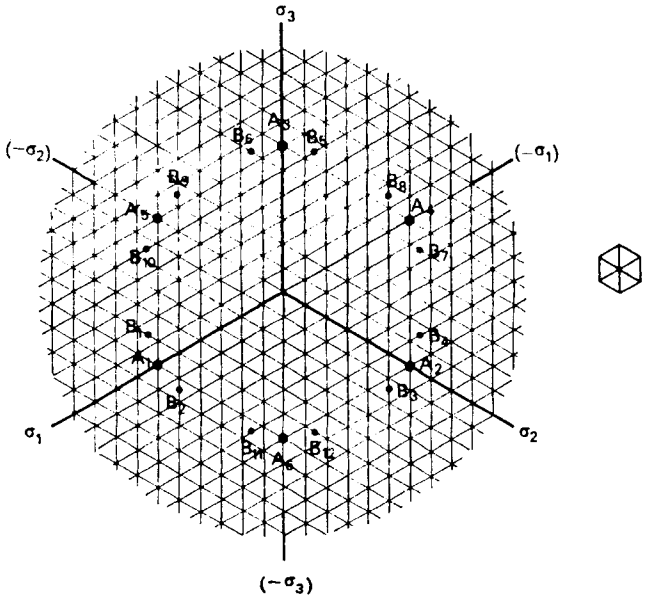

FIG. 2.13. Plan view of the π-plane.

2.9. Symmetry of the *C*-curve

We are now in a position to investigate the nature of the *C*-curve and particularly some aspects of its symmetry. First, suppose that point A_1 (6, 0, 0) lies on the yield surface. Then, if the material is *isotropic*, there is no reason why we should not relabel the axes in all possible ways; we thus conclude that points (0, 6, 0) and (0, 0, 6) also lie on the yield surface, as shown; A_2, A_3. Further, if the material has no Bauschinger effect, the point (−6, 0, 0) lies on the surface, and so, similarly, do points (0, −6, 0) and (0, 0, −6);

A_4—A_6. Thus, by appealing to isotropy and no Bauschinger effect, one point on the surface has become six. Restrictions of this sort are clearly likely to lead to some sort of symmetry in general. In fact the point considered was special in the sense that $\sigma_2 = \sigma_3$. If $\sigma_1 \neq \sigma_2 \neq \sigma_3$ a single point, by virtue of isotropy and no Bauschinger effect, is multiplied into *twelve* points. For example, if point B_1 $(7, \frac{1}{2}, 2)$ is on the yield locus, so are B_2 $(7, 2, \frac{1}{2})$, B_3 $(2, 7, \frac{1}{2})$, B_4 $(\frac{1}{2}, 7, 2)$, B_5 $(\frac{1}{2}, 2, 7)$ and B_6 $(2, \frac{1}{2}, 7)$. The other six points are found by multiplying throughout by (-1). Now considering B_1 and B_2, we see that these are mirror images of each other about the projection of the σ_1 axis onto the π-plane. Also B_2 and B_{11} are mirror images about a line bisecting the projections of the σ_1 and $-\sigma_3$ axes on the π-plane. The problem of specifying the C-curve thus becomes (subject of course to the idealisations of isotropy and no Bauschinger effect) the problem of specifying the C-curve in one 30-degree sector of the π-plane. The curve within this sector can then be used as a "template" for all the other sectors, as indicated in Fig. 2.14.

In the π-plane three of the six axes of symmetry for the C-curve consist of the projections of the uni-axial tension/compression axes. To what do the other three correspond? The answer is (see Problem 2.2) that they are states of pure shear (for which, in general, the principal stresses are of the form $(b, -b, 0)$) or, in general, projections of states of pure shear plus arbitrary hydrostatic pressure. It may be shown (see Problem 2.3) that the angular range of one sector may be covered by combined tension/torsion tests on thin-walled tubes. This is the basis for the classical experiments of Taylor and Quinney (see later) on tubes of aluminium, copper and mild-steel.

2.10. The Tresca Yield Condition

Historically the first yield condition for general states of stress was that of Tresca (1864), who suggested that yield would occur when the greatest shearing stress on *any* plane reached a limiting value k, say. Stating this in terms of principal stresses (using

Mohr's circle of stress, Appendix I) the greatest absolute value of the differences between the principal stresses taken in pairs must equal $2k$ at yield. To plot this yield condition on the π-plane, suppose for example that $\sigma_1 > \sigma_2 > \sigma_3$. Then (see Problem 2.4) the projection of the stress point on the π-plane lies between the projections of the positive σ_1 axis and the negative σ_3 axis. The relevant condition $\sigma_1 - \sigma_3 = 2k$ is a straight line perpendicular

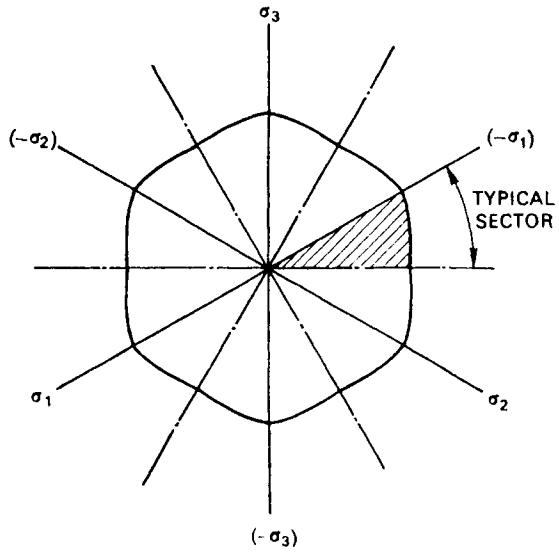

FIG. 2.14. *C*-curve in the π-plane, and axes of symmetry.

to the bisector of the boundaries of the region, as is easily demonstrated. Each of the five other possible orders of principal stress magnitude gives a similar line in the appropriate sector of the π-plane, and the final result is thus as shown in Fig. 2.15. The yield surface is simply a regular hexagonal prism in principal stress space, and in particular it clearly satisfies all the conditions of symmetry previously derived.

The size of the yield surface, i.e. of its cross-section, depends on the yield strength of the material. The surface may be either an initial yield surface or a subsequent yield surface; in the latter case

the value of k is a function of the previous loading history. In either case the geometrical considerations are the same.

2.11. Plastic Deformation

Now the yield locus is the boundary of the elastic zone in stress space. What happens when a stress-point reaches this boundary and plastic deformation takes place? What is the nature of the plastic flow?

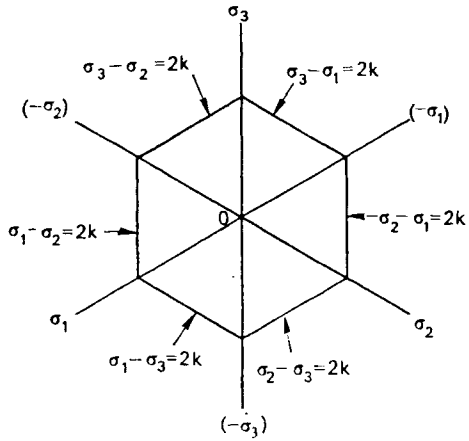

FIG. 2.15. Tresca yield surface: plan view of the π-plane.

It is immediately clear that there will be a *change* in the plastic strain, and that obviously we cannot say anything about the *total* plastic strain because this comprises all the plastic strain which has taken place in the previous loading-history of the specimen. We must always therefore think in terms of the *strain increments* which occur during plastic flow. For a strain-hardening material (Fig. 2.1(b)) the *magnitude* of the plastic strain increment at yield will depend on the magnitude of the stress increment and the slope of the strain-hardening curve. We will return to this topic later.

However, it turns out that for a material which remains isotropic as it hardens (which is our implicit assumption) the

direction of the plastic strain increment vector in a three-dimensional strain increment space is *independent* of the degree of strain hardening, and depends only on the *shape* of the yield surface.

In discussing strain increments we need to know the directions of the axes of principal strain increments. For isotropic material we expect these to coincide with the axes of principal stress. In other words, a rectangular parallelepiped of isotropic material, loaded on its faces by principal stresses, would be expected during any plastic deformation to deform in such a way that its faces remained mutually perpendicular. For example, it would be surprising, for the loading shown in Fig. 2.16, for there to be any shear deformation like that shown if the material were *isotropic*.

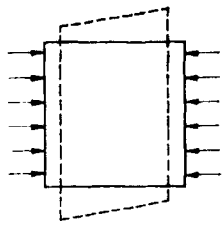

FIG. 2.16. Principal stress and strain-increment axes coincide.

Next, suppose that during the plastic deformation according to Tresca's condition the principal stresses happen to be in the order $\sigma_1 > \sigma_2 > \sigma_3$. The planes on which the shear stress reaches the critical value k are at 45° to the faces of the block as shown in Fig. 2.17(a) and in particular the directions of the maximum shearing stresses are perpendicular to axis 2. It seems reasonable to assume therefore that the deformation increment consists of sliding on the inclined planes shown, and on parallel planes, thus involving in particular *no change of dimension* in the 2-direction. From the plane diagram of Fig. 2.17(b) we can see that, for small plastic strain increments, the decrease in length of the block in the 3-direction equals the increase in length in the

1-direction. If $\delta\epsilon_1$, $\delta\epsilon_2$, $\delta\epsilon_3$ are the three (principal) plastic strain increments, we have therefore

$$\delta\epsilon_2 = 0$$
$$\delta\epsilon_1 \geqslant 0$$
$$\delta\epsilon_3 = -\delta\epsilon_1$$

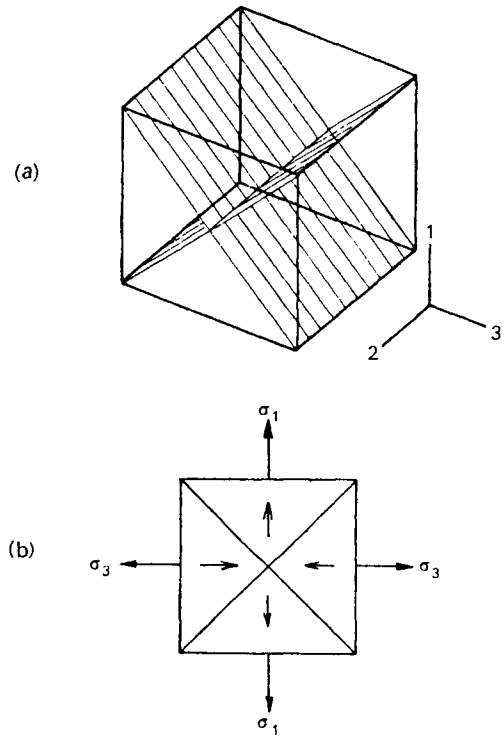

FIG. 2.17. Mode of deformation for shearing of "Tresca" material.

The ambiguous sign indicates that at the yield-point stress there may or may not be any plastic strain increment. This deformation clearly satisfies the constant-volume requirement

$$\delta\epsilon_1 + \delta\epsilon_2 + \delta\epsilon_3 = 0 \tag{2.11}$$

Another way of writing the result is

$$(\delta\epsilon_1, \delta\epsilon_2, \delta\epsilon_3) = \lambda\,(1, 0, -1), \qquad \lambda \geqslant 0 \tag{2.12}$$

Similar results apply at yield for the five other possible algebraic orders of principal stress. This sort of relation is known as a "flow rule".

In the special case where (say)

$$\sigma_1 > \sigma_2 = \sigma_3$$

the situation is more involved, because the shearing stress is equal to the critical value k not only on the planes shown in Fig. 2.17(a) but also on 45° planes parallel to the 3-axis. We can only suppose that slip can occur in *either* of the two possible modes, and we have, *a priori*, no means of knowing what relative amounts of plastic strain take place on the two possible slip systems. All we can say in these circumstances is

$$(\delta\epsilon_1, \delta\epsilon_2, \delta\epsilon_3) = \lambda\,(1, 0, -1) + \mu\,(1, -1, 0), \quad \lambda \geqslant 0, \mu \geqslant 0. \tag{2.13}$$

It is instructive to plot plastic strain increments in a space whose axes are parallel to the principal stress axes. Figure 2.18 shows the combined principal stress/principal strain increment space, viewed along the leading diagonal, as before. In order to associate each strain increment vector with the corresponding stress vector, we plot it with the corresponding stress point as a "floating" origin.

For example, anywhere in the region $\sigma_1 > \sigma_2 > \sigma_3$ the plastic strain increment directions are parallel (see (2.12)) and they are in fact perpendicular to the (Tresca) C-curve locally. Similar relationships apply to the other sides of the hexagon. At the apices of the hexagon we have the ambiguous case (2.13), but the strain increment vector lies between the normals to adjacent sides.

This normality of the strain increment vector to the edge of the hexagon in the π-plane is indeed an aspect of the normality of the strain increment vector to the corresponding *face* of the three-dimensional hexagonal yield prism; this is easily seen by observing that the constant-volume condition (2.11) ensures that the strain increment vector is always parallel to the π-plane which in

turn is perpendicular to the faces of the yield surface. The ambiguous direction of the strain increment vector at the edges of the prism does not violate this "normality" rule: the "normal" to a sharp edge is indeterminate to precisely the degree indicated by (2.13).

2.12. The "Normality" Rule

The "normality" of the associated plastic strain increment vector to the yield surface for the Tresca plastic material is indeed

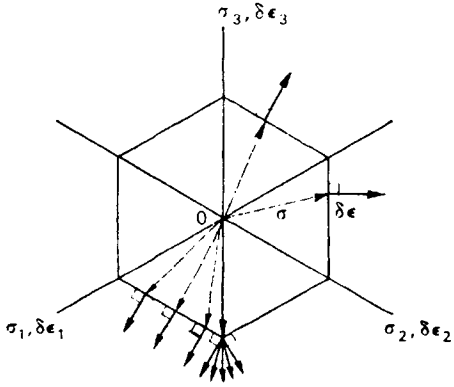

FIG. 2.18. Normality of the strain-increment vector to the Tresca yield surface.

not accidental. "Normality" is a general rule which applies not only to plastic *material* but also, as we shall see, in the appropriate load-space, to *structures* made of plastic material.

Its generality may be appreciated to some extent by means of the idea of *maximum plastic work*. Suppose that we have a structure made of elastic–plastic material (with a well-defined yield point) which is subject to two (for simplicity) independent loads X and Y acting in specific directions as shown in Fig. 2.19(a). In an X–Y load space there will be a "collapse" locus (which corresponds, as we shall see later, to the yield locus for a material)

which in general will enclose a simply-connected region (Fig. 2.19(b)). Suppose that an external agency now *imposes* an incremental *deflection* at the point of application of X and Y, with components δx, δy in the same two directions. We ask the question: what values of X and Y are induced by this agency? The work done in this process is $X\delta x + Y\delta y$, which is the scalar product of vectors (X, Y) and $(\delta x, \delta y)$ in parallel cartesian spaces,

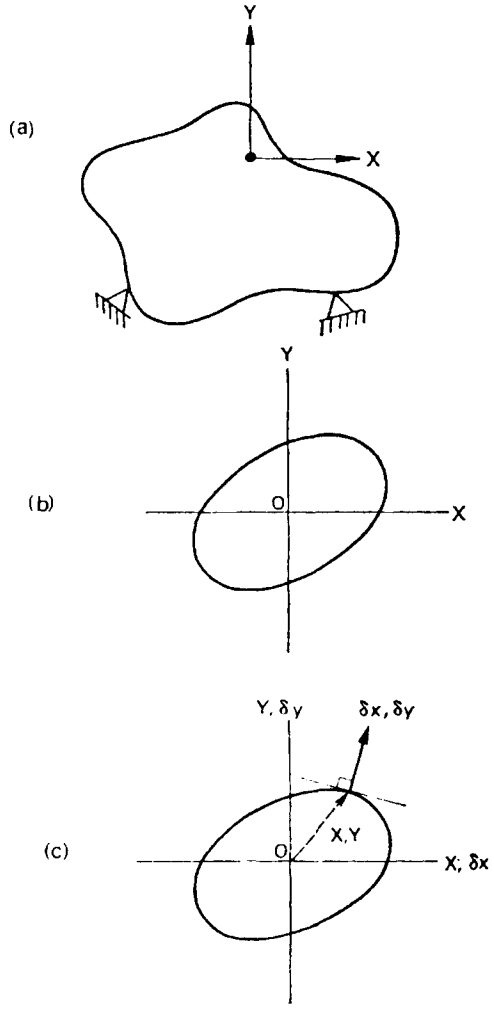

FIG. 2.19. Principle of maximum plastic work.

so we can conveniently use a geometrical interpretation if we superimpose on (X, Y) space a $(\delta x, \delta y)$ space with parallel axes. Given δx, δy, we see (Fig. 2.19(c)) that since the scalar product is found by multiplying the length of the $(\delta x, \delta y)$ vector by the projection of the (X, Y) vector onto it, the work done by the agency is *maximum* if the collapse load corresponds to the point at which the deflection increment vector $(\delta x, \delta y)$ is *normal* to the collapse load locus. As shown in Fig. 2.19, the collapse locus is smooth; the same argument applies equally for collapse loci with corners and flat faces. In the latter case the load is not uniquely determined for an imposed deflection increment normal to a flat, but the work dissipated is determined uniquely: we shall find that this will have repercussions later on.

Thus we conclude that the somewhat intuitive principle of "maximum plastic work" does indeed account for the normality rule. Admittedly the above discussion is sketchy (there has been no reference to elastic deformation, for example) but it does bring out the important point that the displacement increments associated with a collapse locus are related to the loads by means of a *work* relation; the incremental displacement variables are chosen simply so that the scalar product of the load and the displacement increment gives the incremental work done. This provides the link between the forces and incremental displacements in the present discussion and the stresses and incremental strains in the discussion of the Tresca yield condition and the corresponding flow rule; it also enables the same ideas to be generalised to other kinds of load which act on structures, such as couples and uniformly distributed loads or pressures (see Appendix III).

Finally we point out again that the normality rule only tells us the *direction* of the incremental strain vector (i.e. the relative proportions of the various components) or incremental deflection vector in the general case; the *magnitude* of the incremental deformation depends on the amount of strain hardening and other factors.

2.13. The Mises Yield Condition and Associated Flow Rule

Although the Tresca yield condition and associated flow rule will be used almost exclusively in this book (because, as will be seen, they often greatly simplify analysis and design), brief mention must be made of the important yield condition and flow rule due to von Mises.

The Tresca yield condition is open to the following criticism on the microscopic scale. The crystals in a polycrystalline specimen of metal are randomly orientated, and so also, in particular, are their "slip planes". Therefore it is a little naïve to suppose that the simple Tresca maximum shear condition and the associated slip mechanism (see Fig. 2.17) will describe adequately the actual deformation of polycrystalline materials, particularly in the regions of stress space where, according to Tresca, small changes in stress will result in large changes of slip direction. This amounts to saying that the *angularity* of the yield locus of Fig. 2.18 is somewhat unrealistic physically. R. von Mises in 1912 proposed an alternative to Tresca's yield condition which simply replaced the hexagonal C-curve of Tresca by a circle (Fig. 2.20). The equation of this circle in the π-plane is simple, and may be derived easily by noting that the circle, of radius R, say, is defined as the intersection of a sphere of the same radius and the π-plane. The equation of the sphere is

$$\sigma_1^2 + \sigma_2^2 + \sigma_3^2 = R^2 \tag{2.14}$$

and of the π-plane

$$\sigma_1 + \sigma_2 + \sigma_3 = 0 \tag{2.15}$$

Equation (2.15) is identically satisfied by the deviatoric components of stress, σ_1', σ_2', σ_3', so the required equation of the circle is

$$\sigma_1'^2 + \sigma_2'^2 + \sigma_3'^2 = R^2 \tag{2.16}$$

As this equation is in terms of the deviatoric stress components it must also be the equation of the circular cylinder which represents the yield condition in three-dimensional principal stress space.

To fix the size of the circle, let us (arbitrarily) decide to make it coincide with the Tresca hexagon in the π-plane at the apices—i.e. to make it coincide for states of pure tension and compression. Let the yield stress of the material in pure tension be Y. As each of the principal stress axes is inclined at $\cos^{-1}\sqrt{2/3}$ to the π-

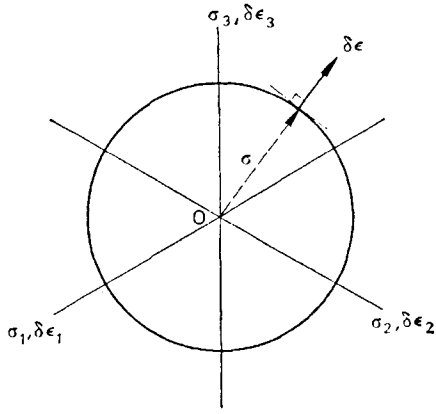

FIG. 2.20. Mises yield surface (plan view of π-plane) and associated strain-increment vector.

plane (Problem 2.5), $R = Y\sqrt{2/3}$ and the equation of the Mises yield condition is thus

$$\sigma_1'^2 + \sigma_2'^2 + \sigma_3'^2 = 2Y^2/3 \tag{2.17}$$

Obviously this equation can be rearranged in several ways (see Problem 2.6), and perhaps the most convenient in practice is:

$$(\sigma_1 - \sigma_2)^2 + (\sigma_2 - \sigma_3)^2 + (\sigma_3 - \sigma_1)^2 = 2Y^2 \tag{2.18}$$

Comparison of this with the Tresca condition (written in terms of the tensile yield stress $Y = 2k$)

$$\text{max. of } |\sigma_1 - \sigma_2|, |\sigma_2 - \sigma_3|, |\sigma_3 - \sigma_1| = Y \tag{2.19}$$

reveals that in effect the Mises condition is related to the R.M.S. value of the principal stress differences, while the Tresca condition concerns only the largest absolute value.

The flow rule associated with the Mises yield condition is also easily derived. The normal to the yield surface, viewed along the space diagonal is *radial* (Fig. 2.20) and it is furthermore parallel to the π-plane. Its direction is thus parallel to the direction of the projection of the appropriate stress vector onto the π-plane, which is of course precisely the deviatoric stress vector. Thus

$$(\delta\epsilon_1, \delta\epsilon_2, \delta\epsilon_3) = \lambda(\sigma_1', \sigma_2', \sigma_3'), \qquad \lambda \geqslant 0 \qquad (2.20)$$

We can readily check that the constant-volume condition is retained, as it should be. Thus in contrast to the Tresca associated flow rule (2.12), there is a one–one correspondence between the directions of the strain increment vector and the *deviatoric* stress vector; in particular there is no ambiguity of direction of the plastic strain increment vector.

2.14. Tresca or Mises Yield Condition?

In the following section we discuss some experiments performed by Taylor and Quinney which were specially designed to investigate what kind of yield surfaces were found in experiments on real materials, and to see, in particular, whether the results supported either the Mises or the Tresca hypothesis, or neither. Before we do this, however, it is instructive to make a direct comparison between the two yield surfaces, shown in Figs. 2.18 and 2.20 respectively. Suppose we specify that the yield stress in tension has a definite value, Y, say. This fixes the intersection of both yield surfaces with the principal stress axes and gives the geometrical result that the Tresca hexagon is inscribed in the Mises circle. In spite of the many obvious differences between the two curves we can see that in some ways they are not dissimilar. For example, the enclosed areas of the curves would be equal if the hexagon were enlarged by only 10 per cent in linear dimensions.

If, as we suppose, the curves intersect at the principal stress

axes we can see that the greatest radial separation between the curves—which occurs in the π-plane directions corresponding to pure shear—is about 15 per cent of the radius of the circle. We can easily work out this separation by using pure geometry, or, equivalently, by comparing the ratio between the magnitudes of the yield stress in pure tension and pure shear indicated by the two hypotheses. In a state of pure shear k, the principal stresses have magnitude $(k, -k, 0)$. Substituting these in the Mises equation (2.18) (noting that the principal stress system $(Y, 0, 0)$ satisfies this equation) we find $k = Y/\sqrt{3}$. According to Tresca, of course, $k = Y/2$, so the greatest numerical discrepancy between the two hypotheses is that between 2 and $\sqrt{3}$, which is about 15 per cent.

If instead of having the surfaces coinciding at stress systems corresponding to pure tension we enlarged the dimensions of the hexagon by $7\frac{1}{2}$ per cent, we could of course make the largest radial discrepancy no more than $\pm 7\frac{1}{2}$ per cent.

2.15. The Experiments of Taylor and Quinney

Taylor and Quinney set out to answer the questions: Is the actual yield condition closer to Tresca's or to Mises's? What are the directions of plastic flow? They performed experiments on three ductile materials in the polycrystalline state: aluminium, copper and mild-steel. Tubes of the three materials, about 12 in. (30 cm) long, $\frac{1}{4}$ in. (6 mm) outside diameter and 0·035 in. (0·89 mm) thickness were loaded in a machine which could apply, independently, tension and torsion. This enables (see Problem 2.3) a complete coverage to be made of one representative sector of stress space. Special checks were made to see that the material was isotropic.

Schematically, the procedure was as follows. A specimen was loaded in tension by pull P up to (say) P_0, and then unloaded (see Fig. 2.21(a)). On reloading in tension a pull P_0 would be required to cause yield. In each case when yield occurred there was a knee rather than a kink in the curve, and the yield load was

estimated by back-projection as shown in Fig. 2.21(b). The combined tension–torsion tests were performed, after the application of tension P_0, by unloading to a smaller tension P_1 which was then held constant while a torque T was steadily increased. When plastic deformation was again observed, the yield value, T_1, was found by the back-projection technique. Tests were performed

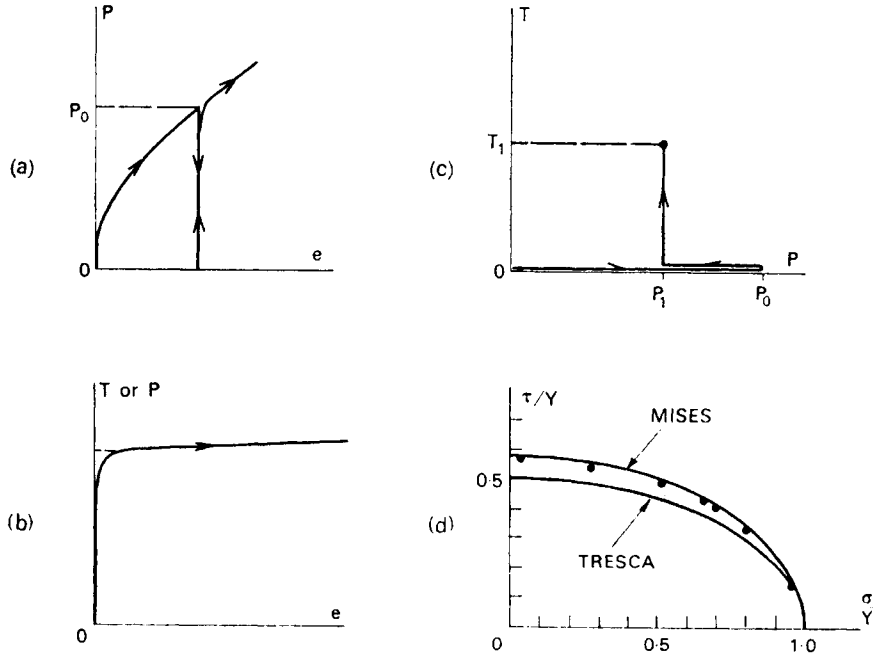

FIG. 2.21. Experiments of Taylor and Quinney on combined tension and torsion of a tube of ductile material.

with different ratios P_1/P_0, and in each case the results were plotted as points P_1, T_1, normalised relative to P_0.

To correlate these results with the Tresca and Mises yield conditions it is not necessary to work in principal stress space: a simple transformation shows (see Problem 2.7) that in P, T space the two yield conditions both produce ellipses, as shown in Fig. 2.21(d). In general, Taylor and Quinney found better agreement with the Mises than with the Tresca yield condition.

Measurements of the incremental plastic extension and twist showed, in general, good agreement between the directions of the deviatoric stress vector and the incremental plastic strain vector, which again—via the normality condition—supports the Mises hypothesis.

2.16. Correlation between Tension and Shear Tests

So far in our discussion of plastic deformation we have considered the nature of the yield surface in stress space, and the *direction* of the incremental plastic strain vector when the load point pierces the yield surface. We now turn briefly to the remaining question of the *magnitude* of the strain increments which occur in the course of a loading programme.

Now in relation to the simple tension test this question seems almost trivial: the magnitude of the plastic strain increment is determined by the magnitude of the stress increment at yield and the slope of the strain-hardening curve. Although this answer is satisfactory for the special case of simple tension, we must bear in mind that we are really seeking an idea which will enable us to predict the plastic strain history for any arbitrary loading path in stress space, which in particular may possibly move around in a three-dimensional zig-zag path, repeatedly crossing the elastic region.

The key to the situation is the question of what factors control the *size* of the yield surface. Having incorporated isotropy and no Bauschinger effect into our model material we found that the yield surface was highly symmetrical, and that if we specified the shape (say Tresca or Mises) it was then *completely* defined by a single parameter. In general therefore we ask the question: what controls the *size* of the current yield surface?

In Fig. 2.1 it seems clear that the magnitude of the yield stress is controlled by the amount of plastic strain which has accumulated. For more general loading we could make the hypothesis that accumulated incremental plastic strain controlled the growth of the yield surface, but we would immediately have to face the

problem of devising a *scalar* measure of incremental strain if we were to add in an appropriate way increments of plastic strain. A way out of this particular difficulty is to postulate instead that the material is *work*-hardening; i.e. that the current yield stress depends on the amount of plastic work which has been done (per unit volume of material) in the entire previous history of plastic loading.

This idea does in fact enable us to predict on the basis of a single test (say a tensile test) the plastic strain changes in any arbitrary loading path.

To illustrate this idea we consider the simple problem of predicting the complete plastic shear stress–shear strain relation which we would expect to find in a pure torsion test on a thin-walled circular tube on the basis of observations on a tension test. Here we define shear strain γ at a point with respect to a set of axes as the change of inclination relative to each other of a pair of lines scribed at right-angles in the material. (Strictly, we should define an *increment* of shear strain.)

For the sake of simplicity we take schematic tension test data as shown in Fig. 2.22(a). The units of stress are arbitrary, and the strain is sufficently small for us to be able to use nominal or true strain (and hence nominal or true stress) indiscriminately. Elastic strains, however, are much smaller, and are negligible.

Suppose first that we adopt Tresca's yield condition. In pure shear of the same material we expect an initial yield stress of 5 units. How can we compute the rest of the predicted τ–γ curve? Let us suppose, tentatively, that the curve is straight. Now because the yield surface expands uniformly, i.e. preserves its shape, we can say that points B and B' (for which $\tau = 15/2$) on the two curves *correspond*, because they both lie on the same yield surface. On our work-hardening hypothesis the plastic work per unit volume done in the tensile test up to B must be the same as the plastic work done in the shear test up to B'. The integral in each case is simply the area beneath the curve, so if γ_B is the value of γ corresponding to B' we have

$$0{\cdot}01\ (10 + 15)/2 = \gamma_B\ (5 + 7{\cdot}5)/2 \qquad (2.21)$$

so $$\gamma_B = 2 \times 0{\cdot}01 = 0{\cdot}02 \qquad (2.22)$$

It is easy to see that a calculation like (2.21) for all corresponding points on the two curves gives the general relation

$$\gamma = 2\epsilon$$

for corresponding strains, and indeed that the argument holds not only for our straight line but also for any general curve. Perhaps the neatest way of expressing the correspondence between the two curves is to say that a graph of 2τ against $\gamma/2$ for

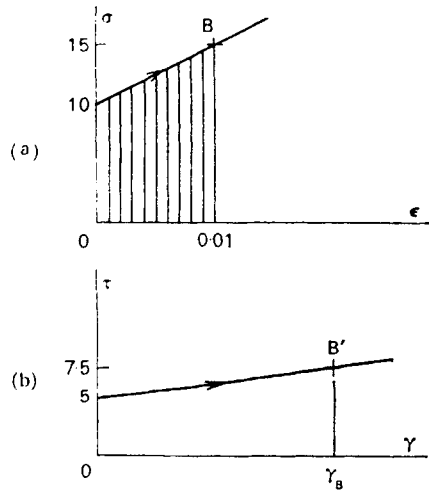

FIG. 2.22. Relationship between tension and torsion tests for a work-hardening Tresca material.

the shear test would—on this hypothesis—coincide with a graph of σ against ϵ for the tension test. Repeating the calculation for a Mises material we find that in this case a curve of $\sqrt{3}\,\tau$ against $\gamma/\sqrt{3}$ should coincide with a graph of σ against ϵ.

These particular correlations can easily be checked experimentally. In general the best fit between the two curves is obtained by plotting quantities intermediate between the two suggestions. Although the above example is extremely simple it does illustrate that it is possible to establish, via the yield condition and a work

equation, the idea of a scalar "effective strain increment". We would expect, in general, the form of this to depend on the form of the yield surface (see Problem 2.8).

2.17. Perfectly Plastic Material

For most of the remainder of this book we shall make use of the simplest possible idealisation of hardening, viz. *zero* strain hardening. A non-hardening ideal plastic material is usually described as *perfectly plastic.*

Nominal stress–strain curves for a few typical structural materials are shown in Fig. 2.23, and at first glance it might seem quite preposterous to suggest that a non-hardening model might be an adequate representation of these materials in analysis or design. A first glance may be very misleading, however.

An important point brought out by Fig. 2.23(a) and (b) is that the *shape* of the plastic stress–strain curve for a particular material may appear quite different over different ranges of strain. Perhaps the most striking instance of this is mild-steel: over a range of plastic strain of, say, 0–1 per cent it exhibits practically no hardening, but over a range of 0–20 per cent the hardening is appreciable. Similar remarks apply to the rolled aluminium–magnesium alloy, and—to a lesser extent—to other materials.

It follows that in choosing a conceptual model for a real material we must be aware of the *range of strain* in which we are interested. In general, in the design of structures we shall be concerned with behaviour over a strain range of the order of 1 per cent in tension, while in the analysis of forming processes we shall obviously be concerned with much larger ranges of strain. It may seem surprising that conspicuous deformation of structures is possible at such small strains, but it is not difficult to see that if a structure consists of slender members like beams or plates appreciable transverse deflections may occur at the expense of relatively small strain (see Problem 2.9).

There is a very large volume of experimental work on structures which supports the use of an ideal perfectly plastic material in the

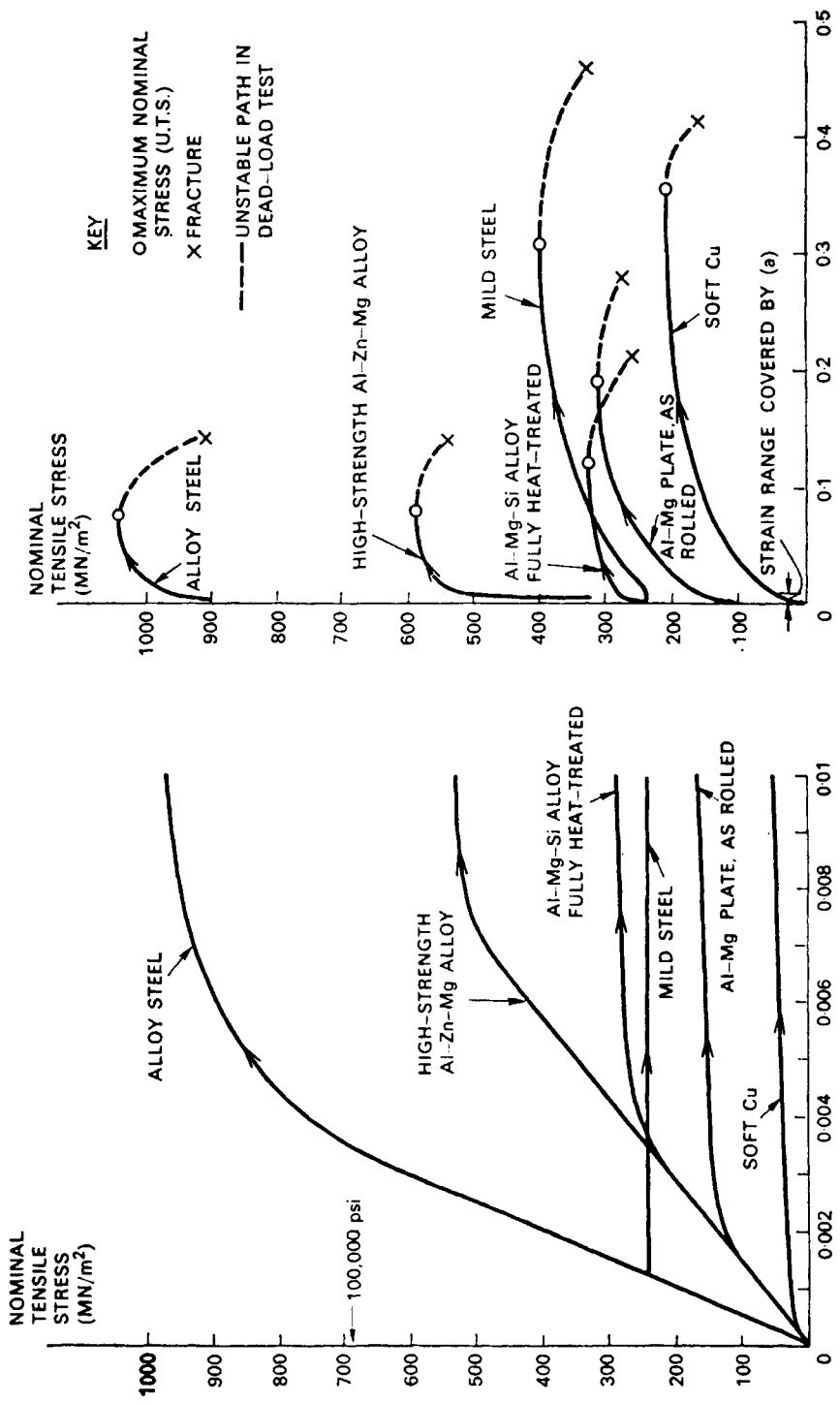

FIG. 2.23. Tension tests on different materials.

development of the theory of plasticity: see the book by Baker, Horne and Heyman listed in the Bibliography. In fact one of the important requirements for the applicability of the simple plastic theory we shall be developing in this book is that the elastic strain range of the material should be sufficiently small for deformation of the structure within the elastic range to be inconspicuous, and sufficiently small *in comparison with the plastic range* for such deformations to be eventually overshadowed by the deformations of the structure due to plastic straining. For some materials, therefore, we should require data over a larger range of strain than that given in Fig. 2.23(a). We shall return to these points in several subsequent chapters.

Having established, then, a *prima facie* case for adoption of perfectly plastic material to represent at least several real metals and alloys in the analysis and design of structures, we turn to the question of suitable idealisations for materials undergoing large plastic strain in forming processes, for which a non-hardening model is not obvious, to say the least, from the curves of Fig. 2.23(b).

Here we must take account of the consequences, as far as calculations are concerned, of the adoption of various possible idealisations of material. It turns out, not altogether surprisingly, that a non-hardening material leads to *simple* analysis of structures and forming processes—at least, simple in comparison with the analysis which would be necessary to deal with more complicated and "realistic" idealisations of the material. One consequence of the choice of a non-hardening material is that powerful *theorems* are available, which in many cases—as we shall see—lead to particularly simple analyses. If, then, there are enormous special conceptual and computational advantages to be gained from the use of a perfectly plastic ideal material, it is worth while to investigate whether even a fairly strongly hardening material may be represented sufficiently well for some purposes by a non-hardening ideal material with a yield stress chosen to be "representative" in some sense over the appropriate range of strain. In fact, practically all theoretical studies that have been made of forming processes

have embodied a perfectly plastic ideal material, and, in general, agreement with experiment has been remarkably good when the value of the "yield stress" has been assigned intelligently. We shall return to this topic in Chapter X.

Finally, to supplement Fig. 2.23 we give some additional approximate data on the strength of metals and alloys in Table 2.1.

Table 2.1

The following are typical, approximate values of ultimate tensile strength and specific gravity of a few metals and alloys. There are very many different iron-, aluminium- and nickel-based alloys, and detailed information on their composition and mechanical properties should be sought in manufacturers' handbooks, etc.

Symbols and units are as listed in Appendix VI.

Material	Specific gravity†	Ultimate tensile strength	
		MN/m^2	psi
Carbon steel, hot rolled:	7·8		
0·2%C (mild-steel)		420	60,000
0·5%C		660	95,000
0·8%C		830	120,000
Alloy steel	7·9	1120	160,000
Structural aluminium:	2·8		
Al-Mg alloy plate, as rolled		315	45,000
Al-Mg-Si alloy, fully heat-treated		315	45,000
High-strength Al-Zn-Mg alloy		600	85,000
Nickel-based alloy (Nimonic)	7·9	1260	180,000
Commercially pure:			
Aluminium	2·7	112	16,000
Copper	8·9	225	32,000
Iron	7·9	295	42,000
Nickel	8·9	485	69,000

† Density of water = 1000 kg/m^3 or 62·4 lb/ft^3.

Problems

2.1. A device consists of two grips, which are constrained to move without rotation, holding three parallel bars, as indicated in Fig. 2.24(a). The bars have equal cross-sectional area and are made of elastic, perfectly plastic, no-Bauschinger-effect material: the elastic moduli are the same but the three yield stresses are different, as indicated in Fig. 2.24(b).

Assuming that buckling is prevented, examine qualitatively the force–displacement relationship for the device when it is subject to an arbitrary force–time programme.

Is there a relationship between the behaviour of this device and the mechanical behaviour of a real, polycrystalline, material? (cf. Fig. 2.9). If so, try and think of a physical explanation for the connection.

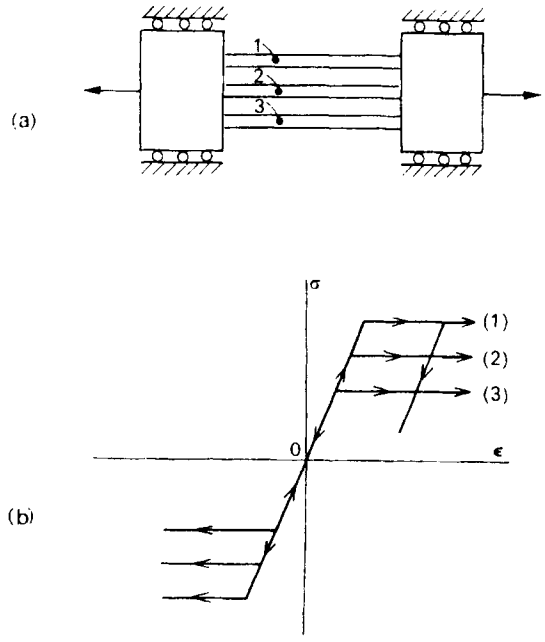

FIG. 2.24. Model of Bauschinger effect: the bars have different yield stresses.

2.2. Verify that the lines in the π-plane which bisect the projections of the axes of principal stress correspond to states of pure shear.

(*Hint. Either* work out the principal deviatoric stresses corresponding to a state of pure shear and plot them on the π-plane, *or* take any two vectors in the π-plane corresponding to known states of principal stress, add them in suitable proportions to give the required resultant direction, and examine the corresponding state of principal stress.)

2.3. Verify that points in the π-plane corresponding to states of stress which can be achieved in a thin tube subject to combined tension and (one-way) torsion lie in a 30° sector.

(*Hint.* Examine the relationships between the three principal stresses in such a test, and plot typical points in the manner indicated in Fig. 2.25. It may help to do Problem 2.4 first.)

2.4. Mark on the π-plane (Fig. 2.25) *regions* corresponding to $\sigma_1 > \sigma_2 > \sigma_3$, $\sigma_2 > \sigma_3 > \sigma_1$, etc.; *lines* corresponding to $\sigma_1 = \sigma_2$, $\sigma_2 = \sigma_3$, etc.; and the *point* corresponding to $\sigma_1 = \sigma_2 = \sigma_3$.

(*Hint.* Work directly with the diagonal view of a cubic lattice, Fig. 2.25, and start by considering simple numerical examples.)

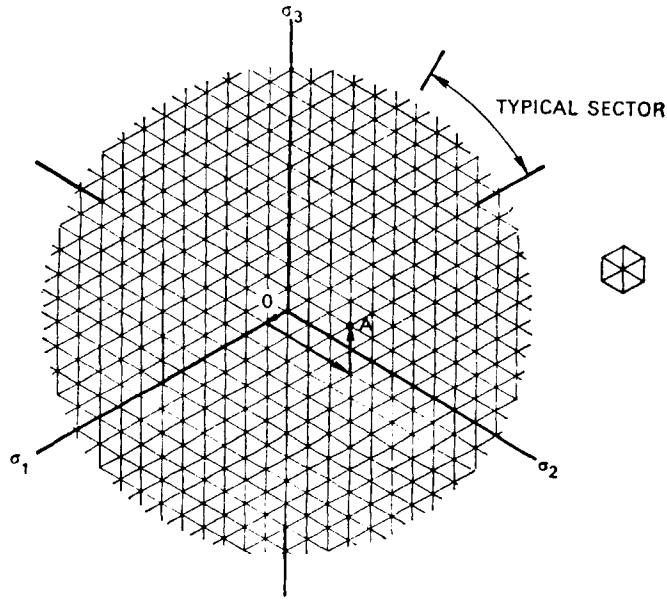

FIG. 2.25. Plan view of the π-plane.

2.5. Work out the cosine of the inclination of the σ_1 axis to the π-plane.

(*Hint. Either* use vector algebra *or* consider the solid geometry of an appropriate tetrahedron.)

2.6. Demonstrate by algebraic manipulation the equivalence of the following formulae for the Mises yield condition in terms of the principal stresses:

$$\begin{aligned} &-(\sigma_1'\,\sigma_2' + \sigma_2'\,\sigma_3' + \sigma_3'\,\sigma_1') \\ &\quad = \tfrac{1}{2}\{\sigma_1'^2 + \sigma_2'^2 + \sigma_3'^2\} \\ &\quad = \tfrac{1}{6}\{(\sigma_1 - \sigma_2)^2 + (\sigma_2 - \sigma_3)^2 + (\sigma_3 - \sigma_1)^2\} \\ &\quad = k^2 = Y^2/3 \end{aligned}$$

(*Hint.* A useful identity is obtained by squaring identity (2.10).)

2.7. In a combined tension/torsion test on a thin-walled tube of circular cross-section (see Problem 2.3) let σ be the tensile stress and τ the shearing stress on planes perpendicular to the axis. Using a Mohr circle construction to find the magnitudes of the principal stresses in terms of σ and τ, find a relationship between σ, τ and Y (the yield stress in pure tension) for yielding of the tube according to (a) the Tresca criterion and (b) the Mises criterion.

2.8.† The scalar "effective stress" $\bar{\sigma}$ of a given state of stress is defined as being numerically equal to the pure tensile stress which is on the same instantaneous yield surface as the given state of stress. Show that for the Mises yield condition

$$\bar{\sigma} = \frac{1}{\sqrt{2}}\left\{(\sigma_1-\sigma_2)^2+(\sigma_2-\sigma_3)^2+(\sigma_3-\sigma_1)^2\right\}^{\frac{1}{2}} = \sqrt{\frac{3}{2}}\left\{\sigma_1'^2 + \sigma_2'^2 + \sigma_3'^2\right\}^{\frac{1}{2}}.$$

The scalar "effective incremental strain" $\delta\bar{\epsilon}$ of a given strain increment is defined in such a way that the product $\bar{\sigma}\,\delta\bar{\epsilon}$ is exactly equal to the total work done by the components of stress on the components of the strain increment. Using the corresponding flow rule (2.20), verify that

$$\delta\bar{\epsilon} = \sqrt{\frac{2}{3}}\left\{\delta\epsilon_1^2 + \delta\epsilon_2^2 + \delta\epsilon_3^2\right\}^{\frac{1}{2}}$$

satisfies the above definition.

2.9. An initially straight slender beam of length l and depth d is bent, in the plane containing its length and depth, into a circular arc such that the deflection of the mid-point relative to the ends is equal to $d/4$.

Assuming that there is no longitudinal strain at the mid-depth of the beam, obtain an expression for the greatest direct strain in the beam in terms of l and d.

(*Hint.* Assume that a shallow circular arc approximates a segment of a parabola, or use the theorem on intersecting chords of a circle.)

2.10. From Fig. 2.7 show that the relationship between true stress σ and nominal strain e at the inception of necking in a simple tension test is

$$\frac{d\sigma}{\sigma} = \frac{de}{1+e}.$$

By making use of the relationship between nominal and true strain (ϵ) find the corresponding relationship between σ and ϵ, and make a geometrical interpretation of it.

Under monotonically increasing tension the true stress/true strain relationship for a certain material is

$$\sigma = B\epsilon^c$$

where B and c are constants.

---

† See the Preface for an explanation of this notation.

Show that necking begins when $\epsilon = c$ and that after a neck has formed the cross-section area A of the un-necked portion of the specimen is given by

$$\ln(A_0/A) = c$$

where A_0 was the original cross-section area.

2.11. Consider a specimen of linear-elastic work-hardening plastic material which may be subject to a general tension/compression loading history.

Show that by subjecting two specimens to different histories of loading it is possible to have two specimens under the same stress at a given time but at different strains, and also two specimens at the same strain but different stresses.

Hence show that for a material of this kind (in contrast to an elastic (reversible) material) the mechanical state of the material in a tensile test cannot be specified by a single variable.

2.12. Figure 2.25 shows a view of the π-plane along the space diagonal $\sigma_1=\sigma_2=\sigma_3$. The mesh is the view of a cubic net in σ_1, σ_2, σ_3 space with mesh size of unit stress.

Plot the projections of the following points onto the π-plane (as demonstrated for A):

	σ_1	σ_2	σ_3
A	1	4	2
B	4	6	2
C	3	−1	3
D	3	−3	0
E	0	−2	−2
F	−3	1	3

Assuming that the material is isotropic and has no Bauschinger effect, transfer all points by reflection about axes of symmetry to the sector of the π-plane indicated. Thus show that some of the load states have proportional deviatoric stresses. Verify this by working out the deviatoric stresses directly, and comparing their ratios.

2.13. A thin-walled cylindrical shell (with closed ends) and a thin-walled spherical shell are subject to interior gauge pressure. Plot on the π-plane points corresponding to the states of stress in the two shell walls.

2.14.† In a certain experiment it is found that yielding of a material occurs under the following states of principal stress:

$$(\sigma_1, \sigma_2, \sigma_3) = (20, 0, 0)$$
and $$(\sigma_1, \sigma_2, \sigma_3) = (21, 7, 0)$$

Assuming that the material is isotropic, that hydrostatic stress does not affect yielding and that there is no Bauschinger effect, plot as many points as you can derive from these observations in σ_1, σ_2 space for $\sigma_3 = 0$ (i.e. plane stress).

What is the relationship of the curve joining these points to the three-dimensional yield surface and the C-curve in the π-plane?

2.15. A perfectly plastic material yields in three-dimensional states of stress according to the Tresca yield condition, and plastic deformation obeys the normality rule.

Plot the yield condition for the material in σ_1, σ_2 space:

(a) for a state of plane stress—i.e. $\sigma_3 = 0$,

(b) for a state of plane plastic strain—i.e. $\delta\epsilon_3 = 0$.

Relate the two yield conditions to the three-dimensional yield surface.

Repeat for a Mises material.

CHAPTER III

FEATURES OF THE BEHAVIOUR OF STRUCTURES MADE OF IDEALISED ELASTIC-PLASTIC MATERIAL

IN CHAPTER II we concentrated on the plastic deformation which occurs when a specimen of metal is stressed, and we set up the simple model of perfectly plastic material, which describes some of the main features of plastic deformation.

In the present chapter we shall consciously endow the material with *elastic* behaviour when the stress-point is within the yield surface, and we shall investigate in some detail the behaviour of a simple structure made of this elastic-plastic material. The object of this exercise is to try to obtain a "feel" for elastic-plastic behaviour in structures, and to seek concepts which will be useful in subsequent discussion of other structures of various kinds.

The example selected for analysis in the present chapter is the thick-walled tube, with closed ends, under internal gauge pressure. The choice of this example is somewhat arbitrary: an obviously desirable ingredient is three-dimensional states of stress, while the evident geometrical symmetry ensures relatively simple equations. We shall analyse the response of the tube to internal pressure which varies arbitrarily with time.

The tube has inner radius a and outer radius b. For part of the discussion we shall for definiteness study a tube with the specific proportions $b = 2a$, but we shall not introduce this restriction until after we have set up all the relevant equations.

For this problem it is obviously best to work in cylindrical coordinates; r is radial distance measured perpendicularly from the axis of the tube, θ is an angular circumferential coordinate

measured from an arbitrary datum and z is axial distance from an arbitrary datum plane perpendicular to the axis. We shall assume that the tube is sufficiently long for "end effects" not to be felt in the zone which we study. End effects may of course be important practically, but the zone remote from the ends provides a sufficiently complex situation for our present purposes.

3.1. Ideal Elastic-plastic Material

The (ideal) material of the tube is elastic-perfectly plastic: in uniaxial tension it has stress–strain relations shown schematically

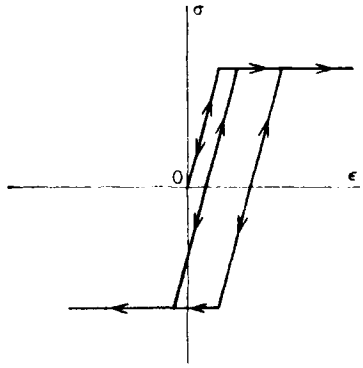

FIG. 3.1. Elastic-perfectly plastic material: a tension test.

in Fig. 3.1. The material is uniform and isotropic. The yield condition is that of Tresca, and the flow rule is associated with it by means of the normality condition. In the elastic range behaviour is described in terms of two elastic constants, Young's modulus E and Poisson's ratio ν. Because by symmetry r, θ and z are the principal stress directions we may write the elasticity relations:

$$\left.\begin{aligned} E\epsilon_r &= +\sigma_r - \nu\sigma_\theta - \nu\sigma_z \quad \text{(a)} \\ E\epsilon_\theta &= -\nu\sigma_r + \sigma_\theta - \nu\sigma_z \quad \text{(b)} \\ E\epsilon_z &= -\nu\sigma_r - \nu\sigma_\theta + \sigma_z \quad \text{(c)} \end{aligned}\right\} \quad (3.1)$$

In these equations, which govern *all* elastic response of the material (see Fig. 3.1), ϵ and σ must be regarded as *changes* of strain and stress respectively within the elastic range.

To make the algebra less cumbersome we shall take $\nu = 0{\cdot}5$, thereby making the material incompressible in the elastic as well as in the plastic range. Real metals have $\nu = 0{\cdot}3$ approximately; however, the effect on the stress and strain distributions of this change is small, and our conclusions will not be affected by this simplification.

3.2. Equations of the Problem

We begin by summarising those equations of the problem which do not depend on the material properties.

The only non-trivial *equilibrium* equation is the radial one (Problem 3.1)

$$\frac{d\sigma_r}{dr} = \frac{\sigma_\theta - \sigma_r}{r} \tag{3.2}$$

The *compatibility* equations express the geometrical relationships between strain and displacement. If u is a (small) radial displacement of a point originally at radius r,

$$\epsilon_r = du/dr \tag{3.3}$$

and, assuming symmetrical deformation,

$$\epsilon_\theta = u/r \tag{3.4}$$

In the axial direction we can at present only state the "long tube" condition for extension of the tube without bending:

$$\epsilon_z = \text{constant} = C \tag{3.5}$$

These relations are purely geometric, and thus hold irrespective of whether the strain is elastic or plastic.

The *boundary conditions* are especially simple:

$$\sigma_r = 0 \text{ at } r = b \tag{3.6}$$

$$\sigma_r = -p \text{ at } r = a \tag{3.7}$$

where p is the interior gauge pressure; tensile stress is regarded as positive. Lastly, in the axial direction overall equilibrium requires

$$p\pi a^2 = \int_a^b 2\pi\sigma_z\, r\, dr \tag{3.8}$$

In writing the last three equations as though the dimensions of the structure, as deformed, were the same as for the original, undeformed structure, we are restricting ourselves to a study of *small deformations* of the structure. This is justified in the present case, because in fact all of the main features of behaviour in which we are interested appear before there is any gross deflection of the structure. This in turn is due to the fact that most metals have such high elastic stiffness that the plastic range is entered at strains usually rather less than 0·005: see Fig. 2.23(a) for some examples. If this were not so, and metals deformed to, say, 10 per cent strain in the elastic range we would have to be very careful about the effects of geometry changes on our equations. We will make some remarks later on in this chapter about geometry-change effects when the tube is in a position to undergo large *plastic* deflections, and we will return to a more general study of these effects in Chapter XI.

To begin the analysis let us suppose that initially when $p = 0$ the tube is stress-free; that is, it has been relieved of any stresses induced in manufacture by a suitable annealing process. This may or may not be a realistic assumption in any particular case.

Because the elastic range is finite, the initial response to a change in pressure is elastic throughout the tube, so we must first make an elastic analysis, which will be valid for sufficiently small interior pressures.

Elastic analysis of this problem is straightforward. One of the many possible procedures for solving equations (3.1) to (3.8) simultaneously is as follows. First use (3.5) to eliminate σ_z from (3.1). Then eliminate u from (3.3) (and 3.4), to give a *compatibility* relation

$$\epsilon_r = \frac{d}{dr}(r\epsilon_\theta) \tag{3.9}$$

Into this substitute for ϵ_r and ϵ_θ in terms of σ_θ, σ_r and C (3.5), using the relations just derived. This gives a first-order linear differential equation in σ_θ, σ_r $\frac{d\sigma_r}{dr}$ and $\frac{d\sigma_\theta}{dr}$, but not in fact involving C. Eliminate σ_θ and $\frac{d\sigma_\theta}{dr}$ using this equation and (3.2) to give a second-order differential equation in σ_r. Solve this subject to (3.6) and (3.7) to give:

$$\sigma_r = p\left(-\frac{b^2}{r^2} + 1\right)\Big/\left(\frac{b^2}{a^2} - 1\right) \tag{3.10}$$

Substitution in (3.2) gives

$$\sigma_\theta = p\left(\frac{b^2}{r^2} + 1\right)\Big/\left(\frac{b^2}{a^2} - 1\right) \tag{3.11}$$

To find the constant C we use these results in (3.1(c)) and substitute in (3.8): this shows that in particular $C = 0$ when $\nu = \frac{1}{2}$; and that for all values of ν

$$\sigma_z = (\sigma_\theta + \sigma_r)/2 \tag{3.12}$$

Results (3.10), (3.11) and (3.12) are in fact independent of the value of ν in general. The result $\epsilon_z = C = 0$ is, however, special for $\nu = 0{\cdot}5$.

This elastic stress distribution only applies of course if p is sufficiently small for the stress point $(\sigma_r, \sigma_\theta, \sigma_z)$ at all radii within the wall of the tube to lie within the yield locus.

Let us find the value of p for which the yield condition is *just* reached at some radius. To do this we plot stress points for different radii on the π-plane of $(\sigma_r, \sigma_\theta, \sigma_z)$ space (Fig. 3.2). In this case it turns out to be simplest to think of plotting $(\sigma_r', \sigma_\theta', \sigma_z')$ directly, because by (3.12)

$$\sigma_0 = \frac{\sigma_r + \sigma_\theta + \sigma_z}{3} = \sigma_z \tag{3.13}$$

i.e. the hydrostatic stress at all radii is equal to σ_z, which is in fact independent of r (see (3.10) to (3.12)). It follows that

$$\sigma_z' = 0$$

and
$$\sigma_\theta' = -\sigma_r' = \frac{\sigma_\theta - \sigma_r}{2} = p\left(\frac{b^2}{r^2}\right)\Big/\left(\frac{b^2}{a^2} - 1\right) \qquad (3.14)$$

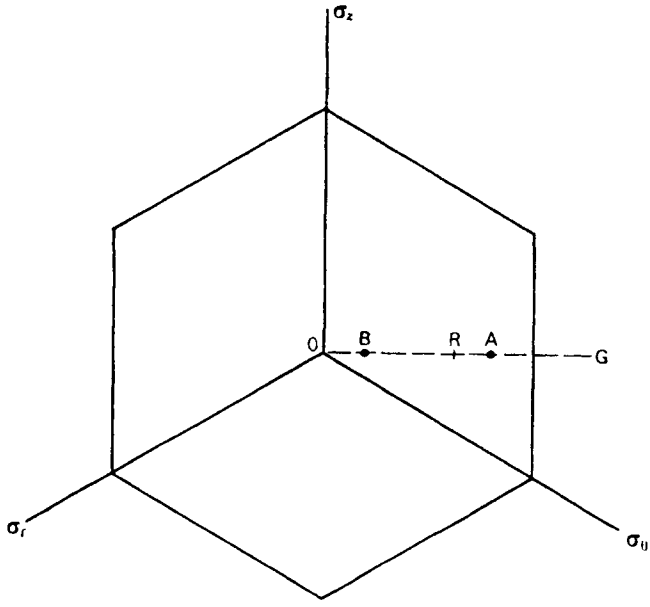

FIG. 3.2. Stress trajectory for a thick tube in the elastic range.

Consequently all stress points referred to the π-plane lie on OG, Fig. 3.2. In other words the state of stress at any point is one of pure shear superimposed on a hydrostatic tension.

Let a typical point, R, on OG represent the state of stress at a general radius r. For a given pressure OR is inversely proportional to r^2, by (3.14). So, if A and B represent the state of stress at the inner and outer surfaces respectively, $OA/OB = (b/a)^2$ irrespective of the pressure, within the elastic range. It is clear from this that if

the pressure is increased steadily the yield-point stress is first reached at the *inner* surface, $r = a$.

To find the corresponding pressure we note that $\sigma_\theta > \sigma_z > \sigma_r$ so that in the relevant region of stress space the yield condition is

$$\sigma_\theta - \sigma_r = Y \tag{3.15}$$

where Y is the yield stress in pure tension. Thus, using (3.14) with $r = a$ we find that the pressure at which the yield point is first reached is given by

$$p = \frac{Y}{2}\left(1 - \frac{a^2}{b^2}\right) \tag{3.16}$$

Notice that the pressure for first yield at $r = a$ is a function of the ratio b/a and not of the absolute size of the tube.

If the pressure is increased above this value, it seems fairly clear that the stress trajectory BA in $(\sigma_r, \sigma_\theta, \sigma_z)$ space (Fig. 3.2), which in the elastic range enlarges proportionally with p, can do so no longer, and therefore presumably distorts in some way to follow the yield surface. This suggests that for increasing pressure an enlarging plastic zone spreads outwards from the inner surface.

To analyse this partly elastic, partly plastic state of affairs, suppose that at some stage in the expansion of the tube the elastic–plastic boundary is at radius c, where $a \leqslant c \leqslant b$, as shown in Fig. 3.3. At $r = c$ let $\sigma_r = -q$; i.e., call the radial *pressure* q at this radius. The outer elastic zone cannot differentiate, so to speak, between pressure q exerted by the plastic zone or q provided by a fluid. It follows therefore that because the outer surface is not loaded the equations we have derived already apply in the elastic region, provided the symbol a is replaced throughout by c. In particular, because the stress must be at the yield point at $r = c$, (3.16) gives

$$q = \frac{Y}{2}\left(1 - \frac{c^2}{b^2}\right) \tag{3.17}$$

Turning now to the plastic zone, we find that the key to the situation is the *yield condition*. Figure 3.2 gives a strong hint that

the relevant region of stress space for the whole plastic zone is $\sigma_\theta > \sigma_z > \sigma_r$, in which the Tresca yield condition is

$$\sigma_\theta - \sigma_r = Y \tag{3.18}$$

Substituting this into the equilibrium equation (3.2) we can integrate directly to give

$$\sigma_r = Y \ln r + \text{constant} \tag{3.19}$$

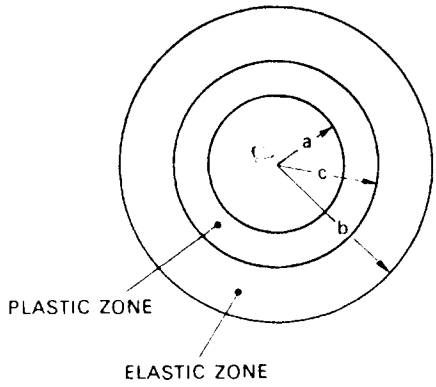

FIG. 3.3. Plastic zone contained within an elastic zone.

The constant is determined by the boundary condition $\sigma = -q$ at $r = c$; using this we find

$$\sigma_r = -q + Y \ln \frac{r}{c} \tag{3.20}$$

We can now use the boundary condition $\sigma_r = -p$ at $r = a$ to give

$$p = q + Y \ln \left(\frac{c}{a}\right)$$

$$= \frac{Y}{2}\left(1 - \frac{c^2}{b^2}\right) + Y \ln \frac{c}{a} \tag{3.21}$$

Hence for any value of c between a and b the corresponding pressure may be calculated. Also for any value of c, σ_θ and σ_r are

determined throughout the tube. Figure 3.4 shows the results for a tube with $b/a = 2$ for various values of c/a.

It is interesting to note that whereas in the elastic analysis sketched above a second-order differential equation was obtained, and the two corresponding constants of integration were

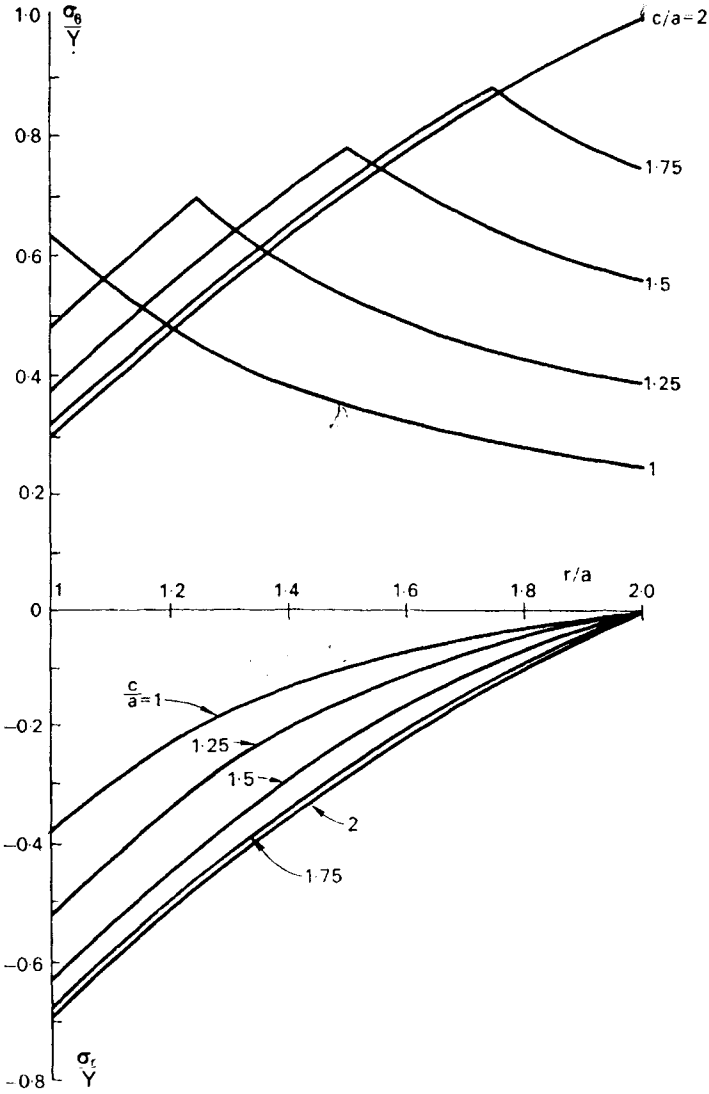

FIG. 3.4. Successive distributions of circumferential and radial stress in the elastic-plastic expansion of a tube: $b/a = 2$.

obtained by using both boundary conditions (3.6) and 3.7), in the plastic zone the stresses are *statically determinate*, and, given the pressure at one boundary, the pressure at the other boundary is determined. Thus the equations in the plastic zone, besides being simpler than those in the elastic zone, are of a different *kind*. The fact that the equilibrium equation and the yield condition can be solved directly without reference to deformation—i.e. that the situation is statically determinate—is a consequence of the *uncoupling* of stress and strain which follows from the special non-hardening form of our idealised plastic material. We shall come across many examples of this situation throughout this book, and we shall exploit the "uncoupling" effect by using certain theorems which we shall prove in the next chapter.

Returning to our solution, we find that this is not yet quite complete because we have yet not checked our assumption that σ_z is the intermediate principal stress throughout the plastic zone.

3.3. Ambiguity of σ_z

We have managed to obtain expressions for σ_r and σ_θ without needing to investigate the other stress variable σ_z. What do we know about σ_z? In terms of stress the only restrictions on σ_z are that, in addition to being the intermediate principal stress in the plastic zone, the boundary condition on equilibrium in the axial direction (3.8)—where the integration is over both the elastic and plastic regions—must be satisfied.

Now it is not difficult to show that the special relationship

$$\sigma_z = (\sigma_\theta + \sigma_r)/2 \qquad (3.12, \text{bis})$$

—which was found by elastic analysis—in fact *always* satisfies the equilibrium relation (3.8): see Problem 3.2. This is therefore a formula for σ_z within the plastic zone which satisfies the requirements stated above. It is clear, however, that the requirement that σ_z is merely the *intermediate* principal stress is not stringent, and

it is not surprising therefore that there are many alternatives to (3.12) which satisfy the above conditions equally well, as we may show easily (Problem 3.3).

Although we have not yet examined the geometry of deformation in partly plastic behaviour of the tube, it is not difficult to see that the *non-uniqueness* of the σ_z component in the plastic zone is attributable to the fact that there is a "flat" on the Tresca yield surface. It is therefore appropriate to ask whether this indicates that there is something "wrong" with the Tresca yield surface. The answer to this must depend on whether the indeterminacy makes any significant difference to the answers we obtain to the major questions we are posing.

From the analysis we have done so far we can see that the indeterminacy in no way affects the relationship between pressure and the radius c of the outer boundary of the plastic zone. Neither, as we shall see, does it affect the relationship between pressure and increase in diameter of the tube. This being so, it appears that the indeterminacy in σ_z, although curious, is of minor practical importance.

It is perhaps worth while to point out that a general aspect of the question of non-uniqueness of stress components arising from the form of the Tresca yield condition is that the indeterminate component of stress does no *work* on the corresponding component of plastic strain increment.

3.4. Elastic-plastic Deformation

We are now in a position to examine the strains and deformations which occur in the elastic-plastic expansion of the tube. The key to the situation is that the radial expansion of the plastic zone is controlled by the elastic deformation of the elastic zone which entirely surrounds it. Our previous analysis indicates that the stress-points in the plastic zone lie on a face of the Tresca yield surface for which the corresponding axial plastic strain increment is zero; consequently it is clear that our idea of regarding the elastic zone as sustaining a pressure q—exactly as if the outer

portion of the tube were filled with fluid—produces no incompatibility of strain and is therefore satisfactory.

It follows that the pattern of strain within the tube in the elastic-plastic condition is a very simple one: there is no axial elongation and, since the material is incompressible in both the elastic and plastic ranges, the deformation may readily be expressed in terms of a single parameter.

A convenient index of the deformation is the circumferential strain, $\epsilon_{\theta b}$, at the outer surface $r = b$; the radial enlargement of the tube is simply (see (3.4)) $b\epsilon_{\theta b}$.

At $r = b$, using (3.10) to (3.12) with c substituted for a and q for p, and substituting for q from (3.17) we have

$$\left.\begin{aligned} \sigma_\theta &= Y c^2/b^2 \\ \sigma_r &= 0 \\ \sigma_z &= \sigma_\theta/2 \end{aligned}\right\} \tag{3.23}$$

Therefore, by the elastic relations (3.1), putting $\nu = 0{\cdot}5$,

$$\epsilon_{\theta b} = \frac{3}{4} \cdot \frac{Y}{E} \left(\frac{c}{b}\right)^2 \tag{3.24}$$

Using this in (3.21) and rearranging we find

$$\frac{2p}{Y} = 1 - \frac{4}{3}\frac{E}{Y}\epsilon_{\theta b} + \ln\left(\frac{4}{3}\frac{E}{Y}\epsilon_{\theta b}\right) + 2\ln\frac{b}{a} \tag{3.25}$$

This relationship between pressure and circumferential strain at the outer surface applies provided $a \leqslant c \leqslant b$, from which, using (3.24)

$$\frac{a^2}{b^2} \leqslant \frac{4}{3}\frac{E}{Y}\epsilon_{\theta b} \leqslant 1 \tag{3.26}$$

When the behaviour is entirely elastic the corresponding equation is, from (3.1), (3.11) and (3.12),

$$\frac{2p}{Y} = \left(\frac{b^2}{a^2} - 1\right)\left(\frac{4}{3}\frac{E}{Y}\epsilon_{\theta b}\right) \tag{3.27}$$

When the elastic-plastic boundary reaches the outer surface, $c = b$ and (3.25) becomes, simply,

$$\frac{2p}{Y} = 2 \ln \frac{b}{a} \tag{3.28}$$

All of these results can be plotted, universally for different values of b/a, on a single diagram, Fig. 3.5. Equation (3.25) is

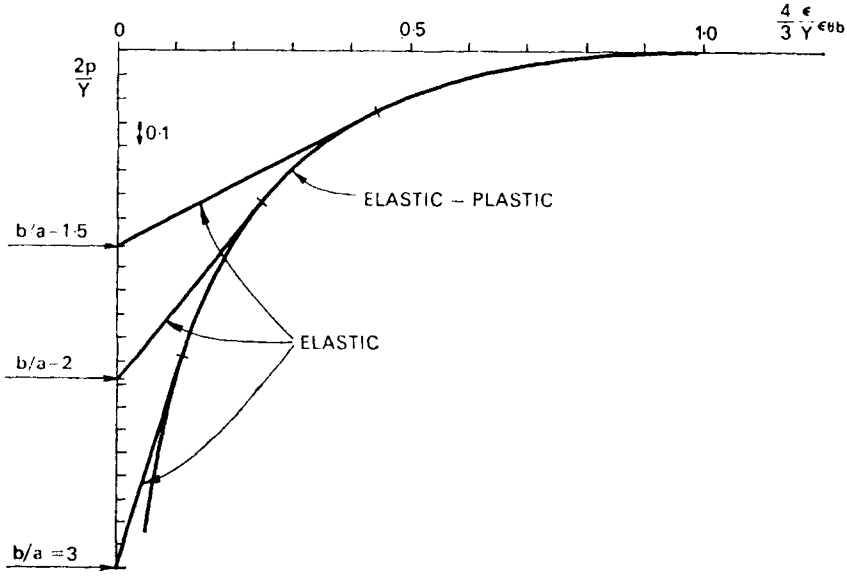

FIG. 3.5. Universal elastic-plastic pressure–expansion curves.

represented by a single curve with, effectively, a different origin for different values of b/a. In fact the line (3.27) is tangential to curve (3.28) at the point corresponding to first yielding (Problem 3.4).

The "full plastic" pressure $p = Y \ln (b/a)$ which is achieved when $c = b$ is maintained if the tube expands further: in the absence of a surrounding elastic ring it is possible for indefinitely large strains to take place, according to the theory so far

developed. In fact the theory is of limited value for predicting behaviour after the disappearance of the elastic zone:

(a) Because if the radial movement of the outer surface is substantial, the faster expansion of the inner surface results in a smaller "current" b/a ratio (Problem 3.5) and, consequently, a falling pressure–expansion curve. A small amount of strain-hardening would, however, counteract this tendency to *instability.*

(b) Because of the possibility of non-symmetrical deformation —corresponding broadly to necking in the tensile test—causing a non-symmetrical bulging and thinning of the tube on one side, especially if the bore of the tube were initially slightly non-central.

However, in spite of these limitations, it is plain from Fig. 3.5 that the *full plastic pressure,* $p = Y \ln (b/a)$ is of great significance as it is the value at which the pressure "flattens" and deflections become (say) an order of magnitude larger than the greatest possible deflections in the elastic range.

It is in a sense misleading to have derived the full plastic pressure as a special case of an elastic-plastic analysis. It can obviously be obtained by direct integration of the equilibrium equation (3.2) together with the yield condition (3.18), from a to b.

We can summarise the analysis so far by saying that for an initially stress-free tube with closed ends, made of elastic-perfectly plastic material and subject to a steadily increasing interior pressure, there are three phases of behaviour:

(i) An *elastic* phase, in which all the material is in the elastic range.

(ii) An *elastic–plastic* phase in which an inner plastic zone is *contained* within an elastic zone. The plastic zone spreads as the pressure increases, but the deflections—which are controlled by the elastic zone—are of the same order as those in the elastic phase.

(iii) A full-plastic phase in which, the outer elastic zone having vanished, the tube is free to expand by plastic

deformation, and achieve much larger deflections than in the elastic range. Apart from second-order effects, plastic expansion takes place at constant pressure called the *plastic collapse* pressure. At this pressure, we predict, the tube will bulge considerably, and may *burst*.

3.5. Behaviour under Rising and Falling Pressure

Suppose now that the pressure, having been raised into the elastic-plastic range is steadily reduced until the gauge pressure is again zero. What happens to the stresses in the tube?

For definiteness we consider a particular case, $b = 2a$, with the pressure (applied to the stress-free tube) having risen to the value corresponding to $c = 1{\cdot}5a$: by (3.21), $p = Y(7/32 + \ln(1{\cdot}5)) = 0{\cdot}624Y$. The distributions of the principal stress under these conditions are shown in Fig. 3.6 (full curves). When the pressure begins to fall, it seems likely that the material which was at the yield stress will have its stress "level" reduced, and will thus immediately re-enter the elastic range. Because we now have some permanent plastic deformation in the contained plastic zone (albeit small plastic strains), we must regard the elastic relations (3.1) as referring to *changes* of stress and strain. As all the material is now (we suppose, and can verify later) behaving elastically, we can use results (3.10) to (3.12) to work out the *changes* in σ_r, σ_θ and σ_z for negative pressure increments. For a complete removal of pressure, for example, we must subtract from the elastic–plastic stress distribution in Fig. 3.6 a stress distribution which would have occurred at the same pressure if the material had remained elastic. This is shown in Fig. 3.6 (broken curves). For clarity σ_z is not plotted: in each state σ_z may be taken as the mean of σ_θ and σ_r, although it is, as we have seen, indeterminate to some extent. We must of course now check that the material is nowhere stressed to yield. This is easily done in the present case because—σ_z being the intermediate principal stress—we simply have to verify that $|\sigma_\theta - \sigma_r| < Y$ everywhere; in Fig. 3.6 this is clearly so.

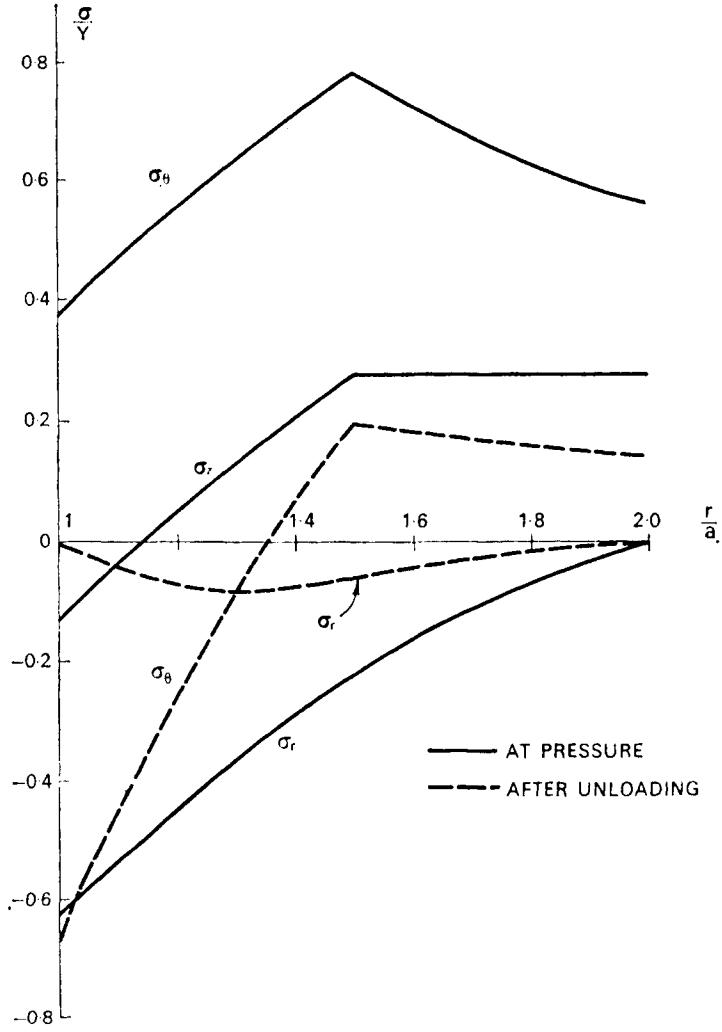

FIG. 3.6. Distribution of circumferential, radial and axial stress at a particular stage in the elastic-plastic expansion of a tube, and after release of pressure.

It is instructive to plot out the stress trajectories in the π-plane, shown in Fig. 3.7. Since $\sigma_z = (\sigma_\theta + \sigma_r)/2$ everywhere (including the *assumption* that this is the case in the plastic zone on first loading) all points lie on a line through the origin perpendicular to the projection of the σ_z axis. Points A, B and C

correspond to the radii a, b and c respectively when $p = 0{\cdot}624\,Y$, and A', B' and C' to the same radii when the pressure has been released. It is clear that the yield condition is not violated in the unloaded state. (This is also true if the above assumption about σ_z in the plastic zone is not made: see Problem 3.6.) Having loaded the tube into the partially plastic range and then unloaded, we are thus left with a *residual stress distribution.*

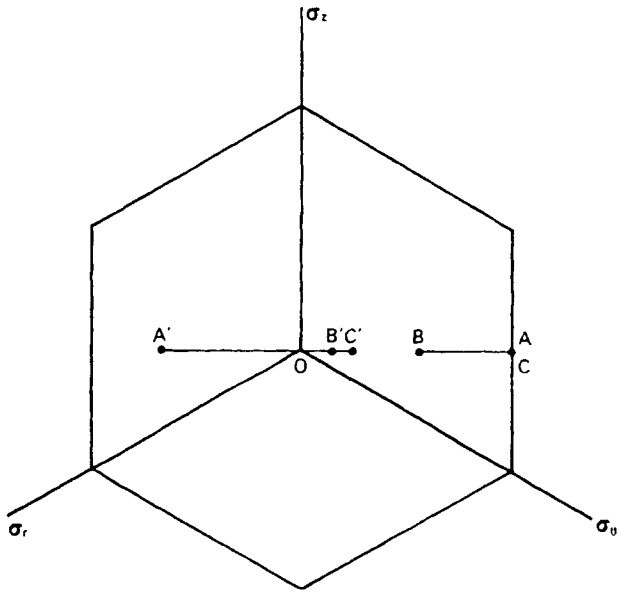

FIG. 3.7. Stress trajectories for partly plastic tube at pressure, and after release of pressure (cf. Fig. 3.6.)

If we now increase the pressure again, the stress points in Fig. 3.7 will retrace their paths between A', B', C' and A, B, C; yielding will recommence at $p = 0{\cdot}624\,Y$ and at higher pressures the behaviour will be exactly as if the pressure had been increased beyond this point in the first loading. The pressure-radial displacement behaviour under this programme of loading is shown in Fig. 3.8; it is closely analogous to the load-extension

behaviour in tensile test of a hardening material shown in Fig. 2.1(c). Any hysteresis effects in a real material, removed by idealisation in Fig. 3.1, would produce broadly similar hysteresis effects in Fig. 3.8.

3.6. The Effect of Residual Stresses

If the tube has been loaded to $p = 0{\cdot}624Y$, unloaded (path *ORS* in Fig. 3.8) and disconnected from the pressure supply, it will be practically impossible to distinguish it by simple inspection

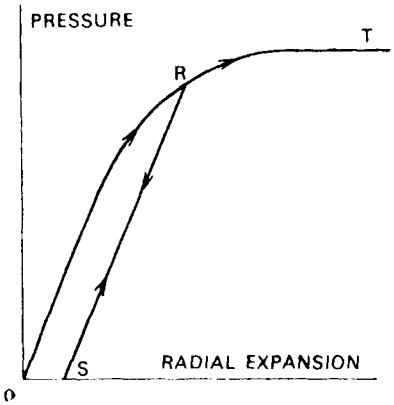

FIG. 3.8. Pressure–expansion curve showing unloading behaviour.

from another similar tube in the annealed, stress-free condition. On pressurisation, however, the pressure-radial displacement curves for the two tubes will be different, as shown in Fig. 3.9. For the pre-pressurised tube the curve will be the same shape as curve *SRT*, Fig. 3.8; the residual stress distribution produced by pre-pressurising postpones the onset of first yielding. In spite of these differences in the elastic and partially-plastic ranges, however, we see that the plastic collapse pressure is the same in both cases, i.e. it is independent of the residual stresses produced by pre-pressurisation. That this is true for *any* initial or residual stress distribution (in equilibrium for zero gauge pressure) can

be seen from a different point of view: the plastic collapse pressure is determined from the equilibrium equation and the yield condition only, therefore any residual stress pattern is "overridden" as plasticity sets in.

Now in real engineering structures residual stresses are practically always present in the zero-load condition, unless special annealing procedures have been carried out to remove them.

Some causes of residual stresses are listed below.

(i) Cold forming operations of components, involving plastic flow: somewhat analogous to the case analysed above.

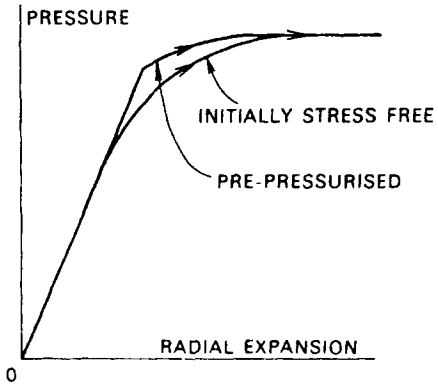

FIG. 3.9. Pressure–expansion curves showing effect of initial stresses.

(ii) Hot forming operations, e.g. forging and rolling. Here the plastic deformation takes place above the annealing temperature, but normally cooling is too rapid for much "stress relief" to take place. Furthermore on cooling the thicker parts cool more slowly, set up compressive stresses —by virtue of the phenomenon of thermal expansion— which tend to anneal out to some extent and result ultimately in tensile stresses in the thicker regions.

(iii) Assembly operations, where components are slightly misaligned before bolting or welding. In the case of welding

there are also thermal effects analogous to those in (ii). Similar effects occur in steel-frame building structures and pressure-vessels if, as often happens, differential settlement of foundations occurs.

(iv) Temperature differences in service. For example, a thick pipe may contain a fluid hotter or colder than the surroundings; this will produce thermal gradients which in turn produce "thermal stresses" necessary to counteract incompatibility of thermal expansion.

It is not uncommon for residual stresses to be as high as half the yield stress of the material. Nevertheless, by virtue of the possibility of plastic action overriding residual stresses and the fact that at collapse the structure is *statically determinate*, residual stresses, while affecting the partially plastic behaviour of a structure, *cannot* affect the plastic collapse load, i.e. the *strength* of the structure.

Throughout our analysis we have assumed, of course, that the material is always capable of providing the necessary plastic strain without prior fracture.

Returning to Fig. 3.9, which we may in fact regard as the load-deflection graph for a general structure, we can see that while a "favourable" residual stress distribution (in this case caused by prior pressurisation of the thick tube) raises the load to cause first yield, an "unfavourable" residual stress distribution (in this case produced perhaps by prior external pressurisation, and in general by any of (i)–(iv) above) will lower the load to cause first yield. Nevertheless, however unfavourable the residual stress distribution may be in lowering the *onset* of yielding in a structure, the *collapse load* is quite unaffected.

This remarkable feature of elastic-plastic behaviour of structures makes calculation of plastic collapse loads an even more significant activity for designers than might have been suspected from our earlier discussion of collapse of initially stress-free structures.

If we had known that the elastic analysis would turn out to be

largely irrelevant as far as the *strength* of the structure is concerned, we might well not have taken the trouble to do it. In the remainder of this book we shall, while bearing in mind the general nature of elastic-plastic behaviour, concentrate primarily on *plastic collapse* calculations.

3.7. "Shakedown"

Another important aspect of the phenomenon of re-adjustment of stress distributions in structures by limited plastic flow of the ductile material is seen in structures which carry repeatedly-applied and alternating loads. A possible mode of failure under these circumstances is low-cycle *fatigue* of part of the structure through cyclic plastic deformation. What tends to happen in many structures is that in the course of the first few applications of loads the structure "does its best", by means of limited plastic flow, to set up residual stress distributions which will minimise the plastic fatigue strains in subsequent cycles.

To provide a simple illustration of this, consider a repeatedly applied pressure $p = 0{\cdot}624\,Y$ to our tube ($b/a = 2$). Supposing that the tube was initially stress free, first yield would be reached at $p = 0{\cdot}375\,Y$ (see (3.16)): it might thus be thought—at least, by any one unfamiliar with plastic analysis—that this would be the limit of pressure for avoidance of repeated plasticity in repeated pressure loading. However, the analysis we have already done shows that a single application of $p = 0{\cdot}624\,Y$ induces a residual stress pattern which enables the structure to respond to repeated pressure application up to this level by purely *elastic* action. We say that the structure will *shake down* to elastic behaviour for repeated pressurisation between $p = 0$ and $p = 0{\cdot}624\,Y$; we draw the analogy with the behaviour of a feather-filled cushion which "shakes down" when repeatedly sat upon.

Figure 3.7 suggests that our particular tube will shake down for even higher pressures: in fact it may easily be shown that shakedown will occur for all pressures up to the plastic collapse pressure. This result however is in a sense a special one for

sufficiently small values of b/a. For values of this ratio greater than about 2·2 shakedown is possible only for pressures *lower* than the plastic collapse pressure (Problem 3.7).

These conclusions about shakedown depend critically on the assumption that there is no hysteresis in Fig. 3.1 and that there is no Bauschinger effect. Neither of these is necessarily justifiable, especially if there are several reversals of stress into the plastic range, as there may well be in practical structures in the early stages of loading. (In contrast, simple plastic collapse is practically insensitive to such hysteresis effects.)

In general, accepting these limitations, we can show that the shakedown pressure would not have been different if the tube had contained residual stresses initially. Initial residual stresses might have altered the pressure at which yield was reached on the *first* application of pressure, but it would not, in fact, have affected subsequent cycles of loading.

It must be admitted that the preceding example of shakedown has been extremely simple: a simple structure subject to only one kind of loading whose sign never changed. Clearly a full discussion of shakedown should involve multiple independent loading systems with the possibility of variation of sign. This is, however, beyond the scope of the present book.

A practical application of shakedown in thick tubes is the "autofrettage" process which has been used for many years in the manufacture of gun barrels. It is clearly desirable that the inner bore of the barrel should retain its dimensional accuracy on repeated pressurisation due to firing. By subjecting the barrel to an *overpressure* before the final surface machining is done, a residual stress system is set up in the barrel which ensures that the bore never goes into the plastic range subsequently, under normal conditions.

3.8. A "Work" Calculation

Before leaving our thick-tube example, we shall demonstrate how it is possible to evaluate the plastic collapse load quite simply

by means of a *work* calculation based on an assumed mechanism of collapse.

In this calculation we shall not be concerned with partly-elastic behaviour, but only with the "full-plastic" or "collapse" state.

We shall perform the calculation intuitively in the following way:

(i) Guess a mechanism of plastic collapse, i.e. investigate the geometry of a plausible mode of incremental deformation.
(ii) For an incremental deformation of this mechanism, integrate the work "consumed" in plastic deformation over the whole body.
(iii) Equate this to the work supplied by the pressure in enlarging the central cavity, and hence find the value of p at collapse.

The first step is to investigate the geometry of incremental deformation of a segment of tube remote from the ends. For the sake of convenience we shall use the symbol $\dot{\epsilon}$ to represent an increment of plastic strain, in place of our previous notation $\delta\epsilon$. This notation suggests a strain-rate, which is indeed appropriate if the time scale is suitably chosen. It is important to think in terms of *increments* of strain rather than *total* strain, because the flow rule (Chapter II) is only meaningful in terms of increments.

We shall suppose that the deformation is symmetrical about the axis. Let the incremental radial displacement at radius r be $\dot{u}$. Then by simple geometry (or by differentiating (3.3) and (3.4) with respect to "time"):

$$\left.\begin{aligned} \dot{\epsilon}_r &= d\dot{u}/dr \\ \dot{\epsilon}_\theta &= \dot{u}/r \end{aligned}\right\} \tag{3.29}$$

In the length of tube we are considering, the behaviour of all cross-sections is the same, so

$$\dot{\epsilon}_z = \text{constant} \tag{3.30}$$

As plastic deformation takes place at constant volume we can write

$$\dot{\epsilon}_r + \dot{\epsilon}_\theta + \dot{\epsilon}_z = 0 \tag{3.31}$$

Substituting for the incremental strains in this we have

$$\frac{d\dot{u}}{dr} + \frac{\dot{u}}{r} = (-) \text{ constant} \tag{3.32}$$

For the present let us assume that the axial elongation is *zero*, and thus set the value of the constant at zero. Integration of the equation gives

$$\dot{u} = C/r \tag{3.33}$$

where C is a constant. It is most convenient to express the constant in terms of the incremental radial deflection, $\dot{u}_a$, at the inner surface, since we shall need this quantity in part (iii) of the calculation. Thus

$$\dot{u} = a\,\dot{u}_a/r \tag{3.34}$$

so

$$\left.\begin{aligned} \dot{\epsilon}_r &= -\,a\,\dot{u}_a/r^2 \\ \dot{\epsilon}_\theta &= \quad a\,\dot{u}_a/r^2 \end{aligned}\right\} \tag{3.35}$$

All of the material in the tube is thus undergoing deformation with one principal strain increment zero and the other two equal and opposite: i.e., a pure shear deformation with respect to planes parallel to the axis and inclined at 45° to a radius. If, as we suppose, $\dot{u}_a$ is positive, we may write, conveniently,

$$(\dot{\epsilon}_\theta, \dot{\epsilon}_z, \dot{\epsilon}_r) = (1, 0, -1)\,\lambda\,(r) \tag{3.36}$$

where $\lambda\,(r)$ is a positive function of r. To calculate the internal work dissipated, say $\dot{D}$ per unit volume, during an increment of deformation, we shall need to know the principal stresses, because $\dot{D}$ is found by summing the increments of work dissipated by the principal stresses:

$$\dot{D} = \sigma_\theta\,\dot{\epsilon}_\theta + \sigma_r\,\dot{\epsilon}_r + \sigma_z\,\dot{\epsilon}_z \tag{3.37}$$

We find the principal stresses by using the normality rule, as in Chapter II. For a Tresca material (3.36) implies that the principal stress magnitudes are in the order

$$\sigma_\theta > \sigma_z > \sigma_r \tag{3.38}$$

This defines a region of principal stress space in which the yield condition is

$$\sigma_\theta - \sigma_r = Y \tag{3.39}$$

Putting $\dot{\epsilon}_r = -\dot{\epsilon}_\theta$ and $\dot{\epsilon}_z = 0$ in (3.37) we have

$$\dot{D} = (\sigma_\theta - \sigma_r)\,\dot{\epsilon}_\theta = Y\dot{\epsilon}_\theta \tag{3.40}$$

using the yield condition (3.39).

Note that the value of σ_z was not determined by the yield condition, but that this did not affect the work calculation.

We can now integrate the internal dissipation of work over, say, unit length of tube, using (3.35) and (3.40):

$$\int_a^b 2\pi r\dot{D}dr = 2\pi Y\int_a^b r\dot{\epsilon}_\theta dr = 2\pi Ya\,\dot{u}_a\int_a^b \frac{dr}{r} = 2\pi Ya\dot{u}_a \ln(b/a) \tag{3.41}$$

We now equate this to the work supplied by the collapse pressure p sweeping through the volume by which unit length of the interior of the tube expands in the deformation, i.e. $2\pi a\dot{u}_a$. We have

$$2\pi a\dot{u}_a p = 2\pi Ya\dot{u}_a \ln(b/a) \tag{3.42}$$

so, finally,

$$p = Y\ln(b/a) \tag{3.43}$$

This is exactly the same result as before (3.28). We have thus obtained a value for the plastic collapse pressure for the tube by two quite different ways:

(i) By using the equilibrium equation in conjunction with the yield condition.

(ii) By considering the geometry of deformation and doing a "work" calculation with the help of the normality rule and the yield condition.

Note that in (i) no reference was made to the *geometry* of deformation and in (ii) no reference was made to the *equilibrium* equation, or indeed to the distribution of stress in the tube.

That two separate approaches are possible is due to the "uncoupling" of the equations which is a consequence of our use of the "perfectly plastic" (non-hardening) ideal material.

Now we must confess that in doing the "work" calculation we "cheated" by making an assumption that the incremental strain in the axial direction was zero. In fact, if we make any other assumption about $\dot{\epsilon}_z$ we obtain a higher value of p (see Problem 3.8). This is an illustration of a general result discussed in the next chapter, which states, in effect, that if we consider a *variety* of possible modes of deformation in doing our work calculation the resulting predicted "collapse load" will in general vary but will always be *greater than* or equal to the actual value. This result is a very useful one, and one which has wide practical implications, as we shall see.

3.9. Summary

The aim of this chapter has been to explore the salient features of elastic–plastic deformation of structures by means of a simple example. Some useful concepts we have encountered are: elastic; partly plastic; contained plastic zone; fully plastic; plastic collapse; collapse load (pressure); residual stress; shakedown; plastic work calculation.

Problems

3.1. By considering the equilibrium of forces on a suitable small element, obtain equation (3.2).

(*Hint.* For an axisymmetric stress field a thin semicircular *hoop* is an appropriate element.)

3.2. Consider a long, thin cylindrical shell with closed ends subject to slightly different internal and external pressures, and show that for equilibrium to be satisfied

$$\sigma_z = (\sigma_\theta + \sigma_r)/2$$

in the parts of the shell remote from the ends. Hence show, by imagining a closed thick-walled cylindrical tube to be "slit" into a number of closed thin-walled shells, that the same relation satisfies the requirements of longitudinal equilibrium for a closed thick-walled tube.

(*Hint.* Either take pressures p and $p + \delta p$ or take an interior pressure δp and superimpose a hydrostatic stress p onto the whole shell.)

3.3. Show that σ_z = constant satisfies the equilibrium equation (3.8) without violating the yield condition (3.15) when σ_r satisfies (3.19) and the ratio of outer and inner radii of the plastic zone is less than about 2·2. Use this solution and (3.12) to generate a family of admissible distributions of σ_z at collapse of the tube.

3.4. Verify that for any given value of b/a, curves (3.25) and (3.27) in a plot of $2p/Y$ against $\epsilon_{\theta b}$ intersect at a value of $\epsilon_{\theta b}$ corresponding to one of the equalities in (3.26); and that the curves intersect tangentially. See Fig. 3.5.

3.5. Show that if a thick tube deforms axisymmetrically, preserving both its length and constancy of volume of the material, the ratio of outer to inner radius decreases as the outer radius increases.

3.6.† Suppose that in the partly-plastic distribution of stress indicated in Fig. 3.6. (full curves) σ_z had *not* been set equal to the average of σ_θ and σ_r in the plastic zone—but had, of course, still been made to satisfy (3.8). Investigate the changes this would make to Fig. 3.7.

3.7. Derive the geometrical condition (Tresca; no Bauschinger effect) for the shakedown pressure to be equal to the plastic collapse pressure for a thick cylindrical tube. Does this depend on the particular distribution of σ_z chosen in the full-plastic condition?

(*Hint.* Sketch stress trajectories on the π-plane.)

3.8.† Solve the compatibility equation (3.32) for a non-zero constant, say $\dot{\epsilon}_z = g$. Show that the resulting mode of deformation is equivalent to a superposition of the modes

$$\begin{aligned} \dot{\epsilon}_\theta &= a\dot{u}_a/r^2 \\ \dot{\epsilon}_r &= -a\dot{u}_a/r^2 \\ \dot{\epsilon}_z &= 0 \end{aligned}$$

and

$$\begin{aligned} \dot{\epsilon}_\theta &= -g/2 \\ \dot{\epsilon}_r &= -g/2 \\ \dot{\epsilon}_z &= g \end{aligned}$$

and that, in particular, the change of internal volume per unit length of tube is *independent of* g. Show that if g has a sufficiently small positive value the algebraic order of the increments

$$\dot{\epsilon}_\theta > \dot{\epsilon}_z > \dot{\epsilon}_r$$

is preserved at all radii. Observe that as none of the principal strain-increments is zero, the stress-point to which the deformation corresponds by the

normality rule is at an edge of the Tresca yield surface (i.e. a corner of the hexagonal C-curve). By using the result of Problem 4.4, show that the work dissipated internally increases as g increases. Similarly, show that the work dissipated increases as g decreases when g is negative.

Hence show that for a given radial expansion rate the pressure derived from the "work" equation is smallest when $\dot{\epsilon}_z = 0$, at least for small values of $\dot{\epsilon}_z$.

3.9. A thick-walled tube of perfectly plastic material sustains the full-plastic internal pressure given by (3.28). Examine the location on the Tresca yield surface of stress points for different radii, apply the normality rule to obtain information about possible plastic deformation, and verify that such deformation is compatible with a mode of collapse for the tube.

3.10. Show that in a graph of σ_θ against σ_r the elastic analysis of a thick tube under internal pressure (equations (3.10), (3.11)) is represented by a straight line, while the yield condition (3.15) is represented by another straight line.

For an initially stress-free tube of given b/a sketch a graph of σ_θ against σ_r (points corresponding to different radii) (a) at first yield, (b) when the elastic–plastic boundary is midway between a and b, and (c) in the full-plastic condition.

3.11. Assuming that the distributions of stress and strain-rate are axisymmetric, find the full-plastic *external* gauge pressure for a thick-walled tube with internal and external radii a and b, respectively, by solving the equilibrium and yield equations together with the stress boundary conditions. Could the result be derived more expeditiously in a different way?

3.12. Make a plastic analysis of a thin-walled cylindrical tube sustaining internal gauge pressure, and reconcile this with a limiting case of the thick-walled tube analysed in the text.

3.13.† Show that for steady radial heat flow in a thick pipe with internal and external radii a and b respectively, the temperature T at any point may be expressed by

$$T = A \ln(b/r) + T_b$$

where
$$A = (T_a - T_b)/\ln(b/a)$$

and T_a, T_b are the temperatures at the inner and outer surfaces, respectively. Assume that the thermal conductivity is independent of temperature.

A thick pipe with closed ends is made of material which may be regarded as a rigid-perfectly plastic Tresca material with a temperature-dependent yield stress Y in pure tension:

$$Y = B e^{-CT}$$

B and C are properties of the material.

Show that the full-plastic gauge pressure p is given by

$$p = \frac{Y_b}{AC}\left\{1 - \left(\frac{a}{b}\right)^{AC}\right\}$$

where Y_b is the value of Y at temperature T_b.

Check that for zero heat-flow formula (3.28) is regained.

(*Hint.* Note that $\lim_{x \to 0} \frac{a^x - 1}{x} = \ln a$ is useful in checking the special case.)

3.14. Derive the following equilibrium equation for a small element of a thick spherical shell with spherically symmetrical distribution of stress (cf. Problem 3.1):

$$\frac{d\sigma_r}{dr} = \frac{2(\sigma_\theta - \sigma_r)}{r}$$

Make a full-plastic stress analysis for a thick-walled spherical shell with internal and external radii a and b respectively, and show that the full-plastic pressure is given by

$$p = 2Y \ln(b/a).$$

Plot stress points for different radii on the π-plane, and compare with the corresponding diagram relating to a cylindrical tube with closed ends under internal pressure. Also compare with your answer to Problem 2.13.

3.15.† A thick cylindrical tube, with internal and external radii a and b, respectively, is closed by matching hemispherical end caps which are fully continuous with the tube. It is decided to remove ambiguity from the determination of σ_z in the full-plastic analysis of the tube by equating σ_z in the tube to σ_θ in the end-caps at their common plane. The stresses in the end-caps are taken to be a scaled-down version of the full-plastic stresses (see Problem 3.14). Verify that σ_z given by this method is everywhere intermediate between σ_r and σ_θ.

3.16. The Tresca yield condition has been used throughout Chapter III. Investigate the effects on the analysis of thick tubes of using the Mises yield condition instead.

Show, in particular, that $\sigma_z = (\sigma_\theta + \sigma_r)/2$ is *necessary* in the plastic zone if the mode of plastic deformation is to involve zero elongation (see equation 2.20). Also show that the full-plastic pressure is given by $p = 2k \ln(b/a)$—where k is the yield stress in pure shear—according to *both* the Tresca and the Mises yield conditions, and explain this in physical terms.

CHAPTER IV

THEOREMS OF PLASTIC THEORY

IN THE previous chapter we saw that it was a relatively simple matter to do a complete study of the elastic-plastic behaviour of a thick tube under varying internal pressure. In our study we made sure of the following four requirements:

(i) That the equilibrium equations were satisfied in both the elastic and plastic zones;

(ii) That the strains and strain increments were geometrically compatible;

(iii) That in the elastic zone the stresses and strains were related by the appropriate form of Hooke's law;

(iv) That in the plastic region the stress points lay on the yield surface while the corresponding plastic strain increment vectors were normal to it.

It is not surprising that it was possible to achieve a complete analysis, since the structure was so simple and symmetrical—indeed it was chosen for this very purpose.

It is plain that most practical engineering structures are a lot more complicated than the simple tube, and we should therefore expect that to do similar sorts of studies on them would be very time-consuming in general. How then can we deal with complicated practical structures, short of doing very elaborate calculations?

One possibility, which results in a considerable saving of effort, is to concentrate on the *collapse* state of the structure and to ignore the elastic and partly-plastic preliminary stages. This is a sound and reasonable step when we realise that, just as in the

previous example, the collapse load is independent of residual stresses and, indeed, of the path by which it was achieved. Of course this step is only justified if we are primarily interested in the *strength* of a structure or the force required to execute a forming process: it would be a quite irrational one if we were mainly concerned about elastic deformation or vibration, etc.—as we have already pointed out.

However, even if we restricted attention only to the collapse state we would find that a complete investigation might be very lengthy for a complicated structure. For example, in the well-developed field of steel-frame building structures, a complete analysis of a one-bay, one-storey frame under combined vertical and sideways load is quite simple, but the corresponding analysis for a two-bay, two-storey frame is much more complicated, even though the structure is still simple in terms of actual steel-frame buildings.

Fortunately, plastic theory provides us with a way of avoiding many of the difficulties arising from the study of complex structures and forming processes by furnishing us with the so-called "*bound*" *theorems*. These theorems are so powerful in the theory of plasticity that it is hardly possible to give, concisely, a reasonably good impression of what they are all about. Indeed, their power will not be fully evident until we have given a wide range of examples of their use; and this, in fact, will occupy a large fraction of the remainder of this book.

4.1. Lower and Upper Bounds on Collapse Loads

Perhaps the best starting-point for a description and explanation of these theorems is the observation made in Chapter III that there are *two* approaches to the problem of calculation of collapse loads, which we can conveniently call the "equilibrium" and "geometry" approaches respectively. We saw in the example that in the "equilibrium" approach we satisfied the equilibrium equations and yield condition, and arrived at an answer for the collapse load without considering the mode of deformation at all.

Conversely, in the "geometry" approach we studied the mode of deformation and an "energy balance" and arrived at an answer without considering the equilibrium equations at all. As we observed then, this "uncoupling" of the equilibrium and geometry aspects of the problem is a direct consequence of the especially simple perfectly-plastic ideal material.

In one important respect, however, this particular example is misleading as a guide to the general situation, for in general the answers given by the two methods are *different* from each other.

As we shall see, this is not so serious a snag as it may appear to be at first sight, because, although *different*, the two answers are often *close*. Further, we shall find that a collapse load predicted by the "equilibrium" method is always on the *low* side of the exact collapse load (if it is not equal to it), and, conversely, the collapse load predicted by the "geometry" approach is always on the *high* side, if not correct. It follows that the "equilibrium" method will always give a "safe" estimate of the strength of a structure—which is often precisely what is needed in structural design—while the "geometry" approach will always give an overestimate of the power needed to execute a forming operation —which again is often precisely what is needed.

When we come to consider specific examples we shall find that in most cases when we are only considering the equilibrium equations and yield condition for a (redundant) structure we shall be free to specify arbitrarily the values of some of the variables. It is this *freedom* which makes the method so valuable as a tool for analysis and design because we can often exploit it to give extremely simple calculations. In an important sense the solution of problems becomes partly an "art", which is a great asset in simple design calculations.

After this general and perhaps rather vague introduction we now give a statement of one of the theorems, followed by an example and then a proof.

4.2. The Lower-bound ("Safe") Theorem

Statement: *If* any *stress distribution throughout the structure can be found which is everywhere in equilibrium internally and balances certain external loads and at the same time does not violate the yield condition, those loads will be carried safely by the structure.*

To illustrate this we consider again the thick-walled tube of the previous chapter, but this time we pretend that we do not know that it is possible very easily to satisfy the equilibrium and yield conditions simultaneously everywhere.

We shall naturally seek a symmetrical stress distribution, so the relevant equilibrium equation, as before, is:

$$\frac{d\sigma_r}{dr} = \frac{\sigma_\theta - \sigma_r}{r} \tag{4.1}$$

The stress boundary conditions are

$$\left.\begin{aligned} \sigma_r &= -p \text{ at } r = a \\ \sigma_r &= 0 \text{ at } r = b \end{aligned}\right\} \tag{4.2}$$

and, in the longitudinal direction,

$$p\pi a^2 = \int_a^b 2\pi\sigma_z r\, dr \tag{4.3}$$

We now seek *any* solution of these four equations, and then find the value of p by putting in the requirement that the yield condition is not violated. Our choice of solution is wide-open because *any* distribution of σ_r which satisfies (4.2) may be substituted in (4.1) to give σ_θ. Perhaps the simplest choice is a linear variation of σ_r with r from $-p$ at $r = a$ to 0 at $r = b$. Putting, therefore,

$$\sigma_r = A + Br$$

and substituting the boundary conditions (4.2) we find

$$\sigma_r = -p\,(b - r)/(b - a) \tag{4.4}$$

Substituting in (4.1) we obtain

$$\sigma_\theta = -p\,(b - 2r)/(b - a) \tag{4.5}$$

As before we note that $\sigma_z = (\sigma_\theta + \sigma_r)/2$ always satisfies (4.3), and since σ_z is intermediate in this solution of the equilibrium equations the relevant form of the Tresca yield condition is

$$|\sigma_\theta - \sigma_r| = Y \tag{4.6}$$

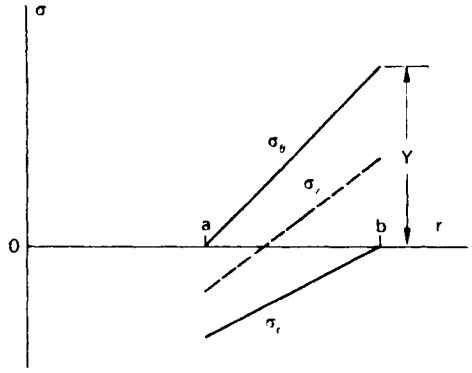

FIG. 4.1. A distribution of stress in a thick tube which satisfies the equilibrium equation and does not violate the yield condition.

From (4.4) and (4.5) (or alternatively from (4.1) and (4.4)) we find

$$\sigma_\theta - \sigma_r = pr/(b - a) \tag{4.7}$$

Clearly $|\sigma_\theta - \sigma_r|$ has its greatest value at $r = b$, so for the yield condition not to be violated anywhere, but just to be reached at $r = b$,

$$p = Y\,(1 - a/b) \tag{4.8}$$

This value of p is easily shown to be always less than that given by the exact solution (equation 3.28) for $b > a$. If $b = 2a$, for example, the value of p is 28 per cent lower than the exact value, p_c, say. The stress distributions worked out above are shown in Fig. 4.1, again for $b/a = 2$. Compare with the curves $c = 2a$ in

Fig. 3.4. Intuitively, the reason why the corresponding value of p is lower than p_c is that the yield point is only reached at $r = b$, whereas in the exact solution the yield condition is satisfied throughout.

There are obviously other possible procedures for satisfying the equilibrium equations; one such would be to specify $\sigma_\theta(r)$ and then to solve (4.1) for σ_r (Problem 4.1).

It is also worth pointing out that the elastic and elastic-plastic stress distributions found in the previous chapter, and viewed simply as stress distributions which in particular satisfy the equilibrium equation, would also obviously give $p < p_c$. Of course there would in general be no point in going through an elastic or elastic-plastic analysis just to find a satisfactory stress distribution, but it is often helpful to be aware that elastic solutions which possibly exist already may be used to give lower bounds on collapse loads.

4.3. Proof of the Lower-bound Theorem

It would be good to prove the theorem once and for all for a general body of unspecified shape supporting a number of arbitrarily placed loads. Here we use the term *body* to include both structures and work-pieces in forming processes. This aim might appear to be rather difficult, particularly when we consider the following point about the yield condition. In general we shall not know the *directions* of the principal axes of stress at a general point in the structure. Use of the three-dimensional yield surface discussed in Chapter II is thus not possible, since this would imply that we already *knew* these directions. We must therefore, in general, think in terms of a *six-dimensional* yield surface in $(\sigma_x, \sigma_y, \sigma_z, \tau_{xy}, \tau_{xz}, \tau_{zx})$ space.

The key to this apparently impossible situation is to use the *theorem of virtual work* in conjunction with some simple symbolic notation.

As far as the six-dimensional yield surface is concerned, we find —from studies which are beyond the scope of this book—that its

crucial property for our present purposes is that it is *convex*, and that the associated plastic flow rule is determined by the *normality* relationship between the direction of the incremental plastic flow vector and the local yield surface.

Now in Chapter II we demonstrated both of these ideas intuitively with respect to the yield surface in principal stress space, but in fact they may both be derived from a single reasonable quasi-thermodynamic *postulate* about the mechanics of elastic-plastic material. It is beyond the scope of this book to describe and discuss this postulate in detail, but as a partial description it

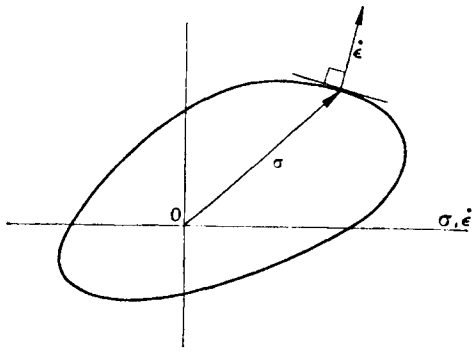

FIG. 4.2. Generalised stress-space, yield surface and strain-increment vector.

may be said that the arguments are of the same *kind* as those used in the theory of elasticity to show, for example, that Poisson's ratio cannot exceed one half. The postulate applies equally for yield conditions in whatever stress space is appropriate: for example, a two-dimensional (σ, τ) space is appropriate for consideration of the results of the experiments of Taylor and Quinney (see Problem 2.7).

In fact the definitions of *convexity* and *normality* in analytical geometry are essentially the same in a space with *any* number of dimensions, and so for present purposes a two-dimensional schematic representation, which is self-explanatory in Fig. 4.2, is

perfectly adequate. This schematic convex yield surface is drawn deliberately non-symmetrical, because neither symmetry nor presence or absence of the Bauschinger effect has any direct relevance to the proof of the bound theorems: the only critical requirements are that the yield surface is convex and that it encloses a simply-connected region which includes the origin. In our proofs the symbols σ and $\dot{\epsilon}$ will stand for a six-dimensional stress-component vector, and the "corresponding" plastic strain increment vector, respectively. As in Chapter III we use the symbol $\dot{\epsilon}$ to denote, conveniently, either a strain increment *or* a strain-rate. In either

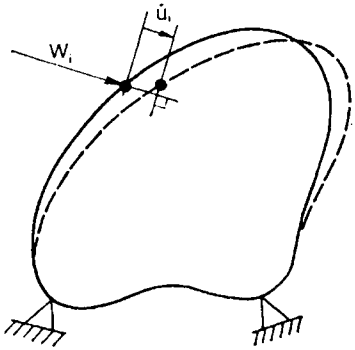

FIG. 4.3. Generalised body and applied loading.

case there is a clear indication that we are dealing with *changes* in strain and not with *absolute* values.

The yield surface shown schematically in Fig. 4.2 is "smooth". The "extreme" possibilities, within the definition of convexity, of "flats" and "corners" will be discussed later.

We denote by W_i, $i = 1 \ldots n$, the n independent loads acting on the body. We shall also need to specify corresponding displacement increments, $\dot{u}_i$, as indicated in the schematic view of the body in Fig. 4.3: $\dot{u}_i$ is the component of the deflection increment undergone by the point of action of W_i in the direction of the line of action of W_i in a typical "collapse" mechanism. The object of this definition is that the product $W_i\dot{u}_i$ represents the *work* done

by W_l during the incremental deformation. Later on we shall widen the scope of the loading to include actions other than "point" forces, but this need not concern us at present.

We are now in a position to prove the theorem.

Let W_l, σ, $\dot{\epsilon}$, $\dot{u}_l$ represent a *complete* plastic collapse solution for the given body, σ and $\dot{\epsilon}$ being functions of position over the entire body. By this we mean that

(i) W_l, σ form an equilibrium set of loads and stresses;

(ii) $\dot{u}_l$, $\dot{\epsilon}$ form a geometrically compatible set of displacement and strain increments;

(iii) In parts of the body where σ is at yield, $\dot{\epsilon}$ is related to it by the normality rule;

(iv) In the remaining parts of the body (where σ is not at yield) $\dot{\epsilon}$ is zero.

This last aspect of the complete solution depends on a result (which we will not prove here or investigate further) in elastic-plastic theory which states that at collapse the stresses, throughout the structure, do not change as the structure deforms. Thus there are no *changes* in strain in the elastic regions at collapse and these regions are thus, in an important sense, *rigid.* We reach the same conclusion intuitively if we regard the elastic strains as negligibly small compared to the plastic strains. We might add in parentheses that we are nevertheless regarding all the deformations as small in proving the theorems; see below.

Further, let W_i^* be a set of loads proportional to W_l, i.e. $W_i^* = \beta W_l$ for all components, where β is a number, and let σ^* be *any* set of stresses (again over the entire structure) which is in equilibrium with W_i^* and also does not violate the yield condition. In other words, W_i^*, σ^* are a schematic representation of the kind of *partial* solution we are dealing with in an "equilibrium" calculation.

As we now have two separate "equilibrium sets" and one "compatible set" we can write the following two virtual work equations (see Appendix II). (This carries the implication, which will hold throughout our work (except for Chapter XI) that all

deflections are sufficiently small for the original undeformed configuration of the structure to be used in setting up the equations of the system.)

$$\sum_n W_i \dot{u}_i = \int_V \sigma \, \dot{\epsilon} \, dV \tag{4.9}$$

$$\sum_n W_i^* \dot{u}_i = \int_V \sigma^* \, \dot{\epsilon} \, dV \tag{4.10}$$

Here, and throughout this chapter, summation is over all n loads and integration is over the whole volume, V, of the structure. At

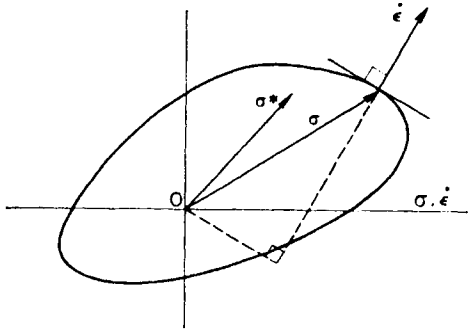

FIG. 4.4. Fundamental inequality in proof of the lower-bound theorem.

all points in the body where the material remains rigid at collapse, the integrand vanishes in both (4.9) and (4.10). At other points there is plastic deformation, and the relationship between $\dot{\epsilon}$ and σ is indicated, schematically, in Fig. 4.2.

Now the product $\sigma \, \dot{\epsilon}$ at a given point in the body is the scalar product of the σ and $\dot{\epsilon}$ vectors, which is represented graphically in two-dimensional space as the product of $\dot{\epsilon}$ and the projection of σ onto the direction of $\dot{\epsilon}$, as shown in Fig. 4.4. At the same point in the body all that we know about σ^* (in addition of course to its forming part of an equilibrium distribution of stress) is that it lies on or within the yield surface, since σ^* does not violate the yield condition, by definition. Although this information seems

somewhat vague, it is in fact sufficient for us to be able to write the following inequality in all circumstances:

$$\sigma \dot{\epsilon} \geqslant \sigma^* \dot{\epsilon} \tag{4.11}$$

As is self-evident from Fig. 4.4, both *convexity* of the yield surface and *normality* of the strain increment vector to it are necessary for this inequality to hold for the entire available range of σ^*. We shall consider the ramifications of the possible equality sign in (4.11) later. It is easy to demonstrate (Problem 4.2) that (4.11) still holds if the yield surface has "flats" or "corners" or both.

Integrating (4.11) over the entire structure and using (4.9) and (4.10) we find

$$\Sigma W_i \dot{u}_i \geqslant \Sigma W_i^* \dot{u}_i \tag{4.12}$$

or simply, since $\Sigma W_i \dot{u}_i$ must be positive,

$$\beta \leqslant 1 \tag{4.13}$$

This proves the theorem.

Note that the equality sign applies in (4.13) only if the equality sign in (4.12) applies everywhere in the plastically deforming parts of the body. For a yield surface without flats this in turn means $\sigma^* = \sigma$ throughout these regions, i.e. the "guessed" σ^* must be the same as the σ of the complete solution in these regions. This restriction does not apply to the non-deforming parts of the body, and the stresses in the rigid regions are therefore not uniquely determined at collapse of the body.

Further, if the yield surface has flats it is possible for the equality sign in (4.11) to hold for σ^* different from σ. In this case therefore some components of stress even in the deforming region may not be uniquely determined at collapse. We have already seen an illustration of this in the case of the thick tube made of Tresca material: σ_z was only determined between limits at collapse. Now while the Tresca yield surface clearly has flats in three-dimensional principal stress space, so also does the Mises condition in the sense (which is not clear in Fig. 4.2) that it is generated by straight lines. Thus, if σ and σ^* in the above analysis differ

by a *hydrostatic* state of stress, the equality sign applies in (4.11).

These possible indeterminacies in stress distribution at collapse are not to be worried about. They do *not* affect the collapse load of the body, which is the quantity of prime importance in plastic theory. They are the finer points which emerge from the analysis and in no way do they affect the practical application of the theorems.

4.4. Loads other than Point Loads

Although we have so far linked the symbol W_i with a point load in the proof of this theorem, we could in fact have linked it with any other form of loading—for example a couple or a pressure—provided that the corresponding deformation increment $\dot{u}_i$ was related to it by the "work" principle (Appendix III). In the present example the corresponding displacement increments are an increment of rotation or an increment of swept volume, respectively.

4.5. The Upper-bound Theorem

Statement: *If an estimate of the plastic collapse load of a body is made by equating internal rate of dissipation of energy to the rate at which external forces do work in* any *postulated mechanism of deformation of the body, the estimate will be either high, or correct.*

This statement, which is oriented to *application*, amounts to the same thing as the more usual statements to be found in other books.

The proof of the theorem runs along similar lines to that of the lower-bound theorem. There is, however, an important difference which is best introduced by means of an example.

When, at the end of Chapter III, we were applying the theorem (although then we regarded the calculation as "intuitive") we

equated the internal dissipation of energy to the work done by the interior pressure p in a postulated mode of deformation. We could have used the same mechanism—and hence the same dissipation calculation—to study the collapse of the tube under *external* pressure q, say, and in this case the L.H.S. of (3.42) would have been $-2\pi b\dot{u}_b q$. We could, moreover, have used the

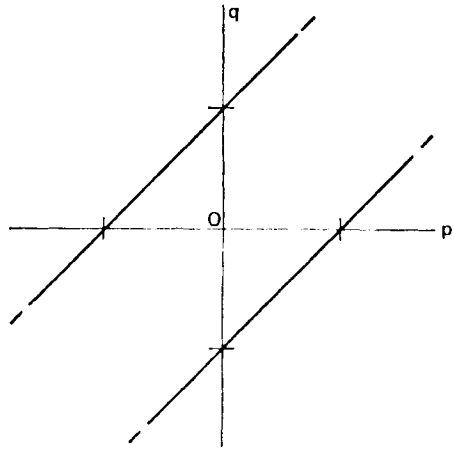

FIG. 4.5. Result of "work" calculation under application of independent internal and external pressures.

same mechanism to study collapse under *combinations* of p and q, in which case the L.H.S. would have been

$$2\pi a\dot{u}_a p - 2\pi b\dot{u}_b q$$

Now in this particular mechanism the product $r\dot{u}$ is independent of r (equation 3.33) so in particular a $\dot{u}_a = b\dot{u}_b$. Consequently a more general upper-bound result than (3.43) is

$$p - q = Y \ln(b/a) \tag{4.14}$$

The important point here is that the same mechanism—and thus the same calculation with trivial extensions—gives a *line* in a p, q load-space, as indicated in Fig. 4.5.

In contrast, a typical lower-bound calculation, being made with a *specific* set of load boundary conditions, provides a *point* in such a load-space.

Now in practice when doing an actual upper-bound calculation, we may be interested only in a *proportional* combination of loads acting on a body, i.e. one in which the component loads are all in fixed proportions (see Appendix IV), in which case the preceding remarks may appear irrelevant. It is, nevertheless, instructive to keep the possibility of the wider interpretation in mind when we prove the theorem.

As before we start our proof by postulating any *complete* plastic collapse solution for the given body; $W_i, \sigma, \dot{\epsilon}, \dot{u}_i$. Also let $\dot{u}_i^*, \dot{\epsilon}^*$ represent *any* compatible set of displacement and strain increments within the body, i.e. a geometrically possible "mechanism" of deformation. The mechanism must be "continuous" in the sense that no gaps or overlaps develop within the body, but mechanisms which, for example, involve rigid-body *sliding* of one part of the body over another, with a narrow zone of intense shearing in between, are not excluded—and are, indeed, very useful, as we shall see. There is no connection between the asterisk notation here and in the proof of the lower-bound theorem except that in both cases it denotes an *incomplete* or partial solution.

Lastly, let W'_i be a set of loads calculated by equating external work to internal dissipation of energy in the postulated mechanism.

First we apply virtual work, once, to the equilibrium set W_i, σ and the compatible set $\dot{u}^*, \dot{\epsilon}^*$:

$$\sum_n W_i \dot{u}_i^* = \int_v \sigma \dot{\epsilon}^* \, dV \tag{4.15}$$

In doing the calculation of internal dissipation we have to find the dissipation which *would* occur in each element of the body *if* the assumed mechanism could be realised. To do this we need to associate a stress vector, σ^*, say, with $\dot{\epsilon}^*$ at each point, because the calculated increment of dissipation of energy per unit volume, $\dot{D}^*$, say, is the scalar product of vectors $\dot{\epsilon}^*$ and σ^*. Now these

vectors are associated via the normality condition, as indicated schematically in Fig. 4.6. In fact (see Problem 4.3) if the yield surface has flats σ^* is not necessarily defined uniquely (as we have noted already) but the relevant scalar product is. Note that in general the stresses σ^* found in this way will *not* be in equilibrium.

At each point in the structure the stress σ in the complete

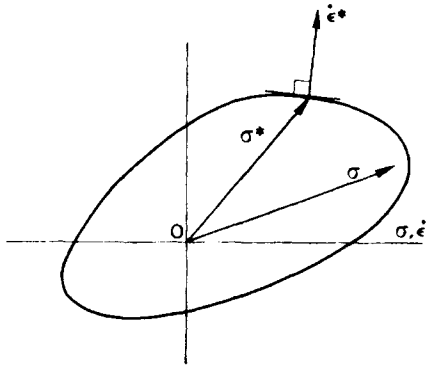

FIG. 4.6. Fundamental inequality in proof of the upper-bound theorem.

solution lies, in particular, on or within the yield surface. Consequently, by an argument similar to that used before, we may write, for all points in the body,

$$\dot{D}^* \geqslant \sigma \dot{\epsilon}^* \tag{4.16}$$

Integrating over the whole body and using (4.15) we have

$$\sum_n W_i \dot{u}_i^* \leqslant \int_V \dot{D}^* \, dV \tag{4.17}$$

Equating the internal dissipation and the external work done by W_i' in the postulated mechanism, i.e. representing schematically our "work" calculation,

$$\Sigma \, W_i' \dot{u}_i^* = \int \dot{D}^* \, dV \tag{4.18}$$

so, combining this with (4.16) we have, finally,

$$\Sigma\, W_i \dot{u}_i^* \leqslant \Sigma\, W_i'\, \dot{u}_i^* \tag{4.19}$$

The meaning of this result is most readily understood with reference to a load space W_i, shown schematically in two dimensions in Fig. 4.7. For a given postulated mode of deformation (4.18) gives a value to the scalar product of W'_i and $\dot{u}_i^*$, thus defining a hyperplane (here a line) in W_i space which is orthogonal to the vector $\dot{u}_i^*$ drawn in a parallel space (see Fig. 4.7). Result

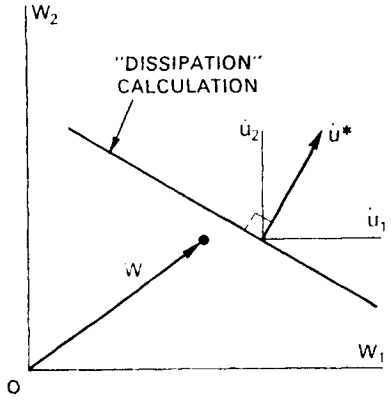

FIG. 4.7. Interpretation of upper-bound theorem in generalised load-space.

(4.19) indicates that the *point* W_i lies on the same side of the hyperplane as the origin. Now W_i represents *any* actual collapse load combination, so (4.19) holds equally for the whole locus of W_i; the hyperplane produced by the work calculation for any postulated mechanism therefore lies outside—or possibly touches —the collapse load surface for the body in W_i space. This is shown schematically in Fig. 4.8, where the work calculation ("upper-bound" calculation) for a few different postulated mechanisms enables us in principle to circumscribe the collapse load locus for an arbitrary body. Figure 4.8 also indicates what happens if we use the upper-bound calculation for a *proportional* set of

loads $W'_i = \beta W_i$. In this case (4.20) becomes simply $\beta \geqslant 1$, and the calculation for each mechanism simply yields a value of β. The relationship between this and the more general interpretation of the theorem is indicated in the diagram.

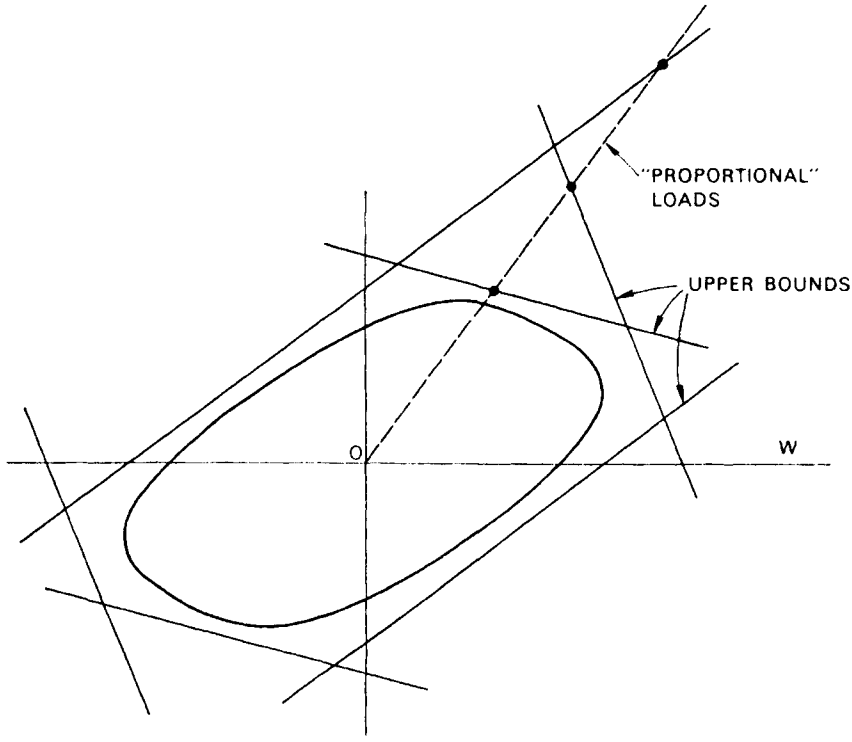

FIG. 4.8. Upper bounds on a collapse load locus, and an indication of the outcome of using the same mechanisms for proportional loads.

4.6. Calculation of Dissipation of Energy

It may appear that the calculation of $\dot{D}^*$ as a function of $\dot{\epsilon}^*$ is rather complicated, both from Fig. 4.2 and from the example at the end of Chapter III. In fact this is not so. For a Tresca perfectly plastic material, for example, we have the simple rule

$$\dot{D}^* = Y \mid \dot{\epsilon}^* \mid_{\max} \tag{4.20}$$

where Y is the yield stress in simple tension and $\mid \dot{\epsilon}^* \mid_{\max}$ is the

greatest principal strain rate magnitude (see Problem 4.4). The analogous expression for a Mises material is also quite simple (Problem 4.5). A special form of equation (4.20) is useful in situations of plane stress, in which one of the principal stresses always has magnitude zero (see Problem 4.6).

4.7. Simpler Form of the Proofs

If the reader finds the above proofs difficult to grasp, he is recommended to work through them again for a general "truss" structure, like that treated in Appendix II, in which yielding of any bar may occur either in tension or compression. All of the steps in the argument are the same, but all of the complications arising from three-dimensional states of stress are avoided.

4.8. Corollaries of the Bound Theorems

We discuss next some results which are of considerable practical importance and which follow almost directly from the theorems we have just proved.

THEOREM. *If in a body we are in a position to investigate all possible distributions of stress which are in equilibrium and do not violate the yield condition, the highest lower-bound load discovered must be equal to the collapse load.*

The proof of this is self-evident. We shall encounter several examples of this situation in the remainder of this book, but in general we should remain aware that the lower-bound theorem is often most rewarding when applied not exhaustively, but intelligently. There is obviously a corresponding theorem relating to exhaustive upper-bound calculations.

THEOREM. *Addition of (weightless) material to a structure without any change in the position of the applied loads cannot result in a lower collapse load.*

Proof. The actual collapse stress distribution for the original structure satisfies the lower-bound requirements for the modified

structure (putting $\sigma^* = \sigma$ throughout the original structure and $\sigma^* = 0$ throughout the added material), so by the lower-bound theorem the modified structure is as strong as, or stronger than, the original structure. Q.E.D.

Note that the "negative" form of the statement of the theorem covers situations where additional material, foolishly placed, does *not* strengthen the structure as well as situations where the reinforcement is beneficial.

This reference to the *weight* of the added material draws attention to an assumption which we have been making implicitly throughout, viz. that the weight of the body is negligible compared to the loads acting on it. The theorems are easily adapted to situations where self-weight is a significant fraction of the applied loads and (see Chapter V) where the primary loads are due to centrifugal effects in rotating bodies.

THEOREM. *The removal of material from a structure cannot strengthen it.*

This (abbreviated) converse of the previous theorem is proved by application of the upper-bound theorem. The actual collapse mechanism for the original structure is used as a postulated mechanism for the modified structure. The internal energy dissipation rate is less than in the original structure (or equal, if all the "cutouts" are made in parts of the structure which are rigid at collapse), so by application of the upper bound theorem the structure is either weaker than or as strong as it was before. Q.E.D.

By similar arguments we may prove the following theorems:

Increasing (decreasing) the yield strength of the material in any region of a body cannot weaken (strengthen) it.

The most useful forms of these theorems, which are of great practical use in calculations, are as follows:

THEOREM. *The (exact) collapse load computed for a (convex) yield locus circumscribing the actual yield locus is an upper*

bound on the actual collapse load. The (exact) collapse load computed for a (convex) yield locus inscribed in the actual yield locus is a lower bound on the actual collapse load.

For example, Fig. 4.9 shows two (similar) Tresca yield surfaces inscribed in and circumscribing, respectively, a Mises yield surface. Any complete solution of a problem for a Tresca material may thus be scaled simply to give close (15 per cent) upper and lower bounds on the actual collapse load for a structure made of a

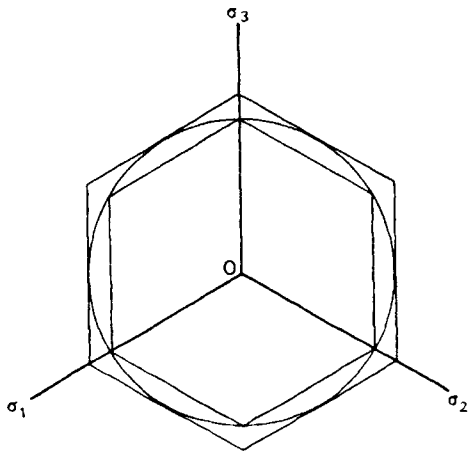

FIG. 4.9. Tresca hexagons inscribing and circumscribing a Mises circle: view of the π-plane.

Mises material. As solutions are often easier to find when the yield surface for the material has flats and corners than when it is "smooth", this result is useful when (as they usually do) experiments on materials show that the Mises yield surface fits the data better than the Tresca.

These last four theorems may well seem to the reader to be intuitively obvious. If so, the reader is in sympathy with the conventional wisdom of structural engineers who in general "thicken up" a structure of a given form, or make it of a stronger material, if they wish to strengthen it.

In view of this we might be tempted to ask if there is any point in going to the trouble of proving theorems which are obvious anyway. The answer to this is twofold.

(i) We may well be able to prove theorems more powerful than those which are obvious; the upper and lower-bound theorems are "revealed" to relatively few engineers, even though some corollaries may be "obvious".

(ii) It may help to know under what precise circumstances the theorems hold. In the present case *perfect plasticity* is a crucial concept, and a parallel possible idea in elasticity theory that "addition of material will always decrease stress concentration factors" is *not* true, as good designers of welded structures are keenly aware.

Two other corollaries of the upper- and lower-bound theorems are useful when the collapse strength of a structure under several independent loads is being studied. They will be stated without proof; suggested outlines for proofs are given in Problems 4.7 and 4.8 respectively.

CONVEXITY THEOREM. *The locus in W_i space of the collapse loads of a structure is convex.*

NORMALITY THEOREM. *The associated collapse velocity vector, $\dot{u}_i$, is normal to the collapse load locus in W_i space at the appropriate point if the axes of the two spaces are parallel* (Fig. 4.10).

These theorems indicate therefore that the convexity and normality properties of the *material* are "reflected" in the behaviour of the *structure* subject to several independent loads. Examples of the use of these theorems are given in Chapter VI.

4.9. Problems solved in Terms of Stress Resultants

So far we have been assuming that in setting up any problem we establish equilibrium equations in terms of stress components, compatibility equations in terms of components of strain increments and yield conditions in terms of stress components. This

obviously *may* be done in general, but whereas it gives simple equations and inequalities in the problem of the thick tube, for example, it would give extremely complicated equations and inequalities for, say, a simply-supported I-beam, since we would have to set up equations for little blocks of material throughout the web and the flanges. What we normally do, of course, when faced with a beam problem, is to use the "strength of materials" approach in which we analyse the behaviour in terms of "bending moment" and "shearing force", these being the relevant integrated "stress resultants" on transverse planes of the beam.

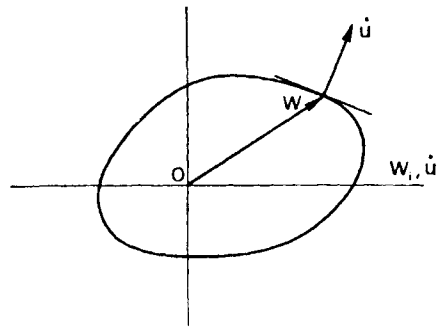

FIG. 4.10. Normality rule in load-space.

In this approach we are, in effect, tackling the problem in two stages:

(i) We study the behaviour of an arbitrary short length of beam, and in particular find its response to bending and shear actions in terms of the yield stress of the material and the dimensions of the cross-section.

(ii) We study the behaviour of the beam regarded as a continuous linear assembly of "sub-structures", whose interactions are bending moments and shearing forces.

It is a simple matter to re-interpret all of our theorems in terms of this approach. Applying the theorems as they stand to the sub-structures loaded by the relevant stress-resultants, we find that the

behaviour of the sub-structures is expressible in terms of a convex "yield locus" in the appropriate stress-resultant space and a normality rule relating the corresponding incremental deformations to this locus. These essential features of convexity and normality enable us to prove the bound theorems for the structure, now regarded as an assembly of sub-structures, simply by letting the symbols σ and $\dot{\epsilon}$ stand for stress-resultants and corresponding incremental deformations of the sub-structures, respectively.

The following six chapters are concerned largely with applications of the lower- and upper-bound theorems, and their corollaries, to a variety of problems. In each case the underlying assumption that the concept of an ideal perfectly plastic material is justified will be implicit, and in each case we must be prepared to submit this and all other assumptions embodied in our conceptual models to the test of experiment.

Problems

4.1. Make a lower-bound analysis of a thick tube under internal pressure by putting σ_θ = constant in the equilibrium equation (4.1) and solving the boundary equations without violating the yield condition.

(*Hint.* Put $\sigma_z = (\sigma_\theta + \sigma_r)/2$, thereby automatically satisfying the axial equilibrium equation. Note that (4.1) may be rearranged as

$$\frac{d}{dr}(r\,\sigma_r) = \sigma_\theta)$$

4.2. Redraw Fig. 4.4 to cover the cases of a yield locus (a) with a corner (b) with a flat, and show that inequality (4.11) is satisfied in all circumstances.

4.3. Redraw Fig. 4.6 to demonstrate that if the yield surface has a flat, σ^* is not necessarily uniquely determined by $\dot{\epsilon}^*$, but that this does not affect the uniqueness of the *scalar product* of σ^* and $\dot{\epsilon}^*$.

4.4. Establish $D^* = Y \mid \dot{\epsilon}^* \mid_{\max}$ (equation (4.20)) for a Tresca material, as follows.

(i) Consider the case in which one of the principal strain increments is zero. The strain-increment vector is then normal to a flat of the Tresca yield surface, and the argument follows that given at the end of Chapter III.

(ii) Now consider the other possibility, that none of the principal strain increments is zero. The strain-increment vector is then normal to an *edge* of the yield surface, or a corner of the C-curve in the π-plane.

By trying several numerical examples show that of the six possibilities the

corner corresponds to the principal strain increment which is of *opposite sign* from the other two.

Note that an edge of the yield surface corresponds to a state of uniaxial tension or compression superposed on a state of hydrostatic stress, and also that the sum of the principal strain increments is zero.

4.5. Show that for a Mises perfectly plastic material

$$D^* = Y\sqrt{\frac{2}{3}}\,(\dot{\epsilon}_1^{*2} + \dot{\epsilon}_2^{*2} + \dot{\epsilon}_3^{*2})^{\frac{1}{2}}$$

(*Hint.* Either use the result of Problem 2.8 or work out the form of the expression from the fact that the strain-increment vector is parallel to the deviatoric stress vector, determining the constant by considering the special case of uniaxial tension.)

4.6. In problems of "plane stress" in which, say, $\sigma_z = 0$, it is convenient to eliminate "z" variables from all equations, etc. Show that for principal strain increments $\dot{\epsilon}_1$, $\dot{\epsilon}_2$ in the x, y plane, the appropriate form of equation (4.20) is:

$$\dot{D} = Y\{\,|\,\dot{\epsilon}_1\,|\,,\ |\,\dot{\epsilon}_2\,|\,,\ |\,\dot{\epsilon}_1 + \dot{\epsilon}_2\,|\,\}_{\max}$$

Here, asterisks have been omitted for convenience.

(*Hint.* Remember that the material is incompressible.)

4.7.† Write out a proof of the Convexity Theorem along the following lines.

Consider any two distinct loading systems, say (a) and (b), under which the body deforms plastically, and the corresponding "exact" stress points in a sufficiently general stress space, for a typical point in the structure. Apply the lower-bound theorem to load and stress combinations which may be described schematically as

$$xa + (1 - x)\,b$$

and find limits on x if the yield condition is *never* to be violated at any point in the structure.

4.8.† Write out a proof of the Normality Theorem along the following lines.

Apply the upper-bound theorem to an "exact" mode of plastic deformation, and bear in mind the interpretation of the theorem indicated in Fig. 4.7.

4.9.† Obtain a "safe" expression for the pressure which may be sustained by a thick tube of perfectly plastic material, of which the outer and inner surfaces are cylinders of radius b and a, respectively, with parallel, but not coincident, axes. The minimum wall thickness is h.

(*Hint.* Think how this tube may be built up from a tube with a concentric bore.)

CHAPTER V

ROTATING DISCS

AN OBVIOUS design requirement for a rotating disc and its attached bladework in a steam- or gas-turbine is that in normal service conditions the blades shall not foul the casing of the turbine, or anything else. At normal running speeds there will inevitably be small radial movements of the tips of the blades due to thermal expansion, elastic strain and, possibly, creep strain.

Another aspect of the behaviour of a rotating turbine disc is that if it is spun at ever-increasing speed in a test rig in which there is no possibility of fouling it will "burst" at a certain speed. Bursting is in fact sudden and catastrophic, and a disc typically breaks into three or four pieces. If the disc is made of a ductile material, bursting must correspond to unconstrained plastic deformation: consequently we would expect that plastic collapse theory should be a useful tool for studying the bursting of discs. This view is supported by the facts that signs of "necking" are often observed at the edges of fragments of burst discs and that predictions of bursting speeds made by setting the yield stress of the idealised material equal to the U.T.S. of the real material usually agree with experiment to within a few per cent.

The designer is interested both in the behaviour of the disc at normal running speeds and in the "overspeed" at which the disc bursts, and he may make an approach to design from either the "normal running" or the "bursting" points of view provided he is prepared subsequently to consider the other aspects of behaviour.

As we shall see, analysis of the bursting of discs by means of plastic theory is particularly simple, and as plastic *design* of discs at the point of bursting turns out to be equally simple, it seems

clear that plastic theory constitutes a useful tool for the design of rotating discs.

As in other design problems plastic theory is inadequate *in itself* to effect a design. In the present case the choice of an overspeed factor is obviously of crucial importance and can only be made after consideration of many different aspects of the performance and operation of the turbine as a whole.

As we have seen, the simple plastic theory is based on a non-hardening idealisation of the material. If the material used is in fact strongly strain-hardening the choice of the "effective" yield stress of the idealised material must be made with care. However, even if it proves necessary to perform more elaborate calculations subsequently to investigate the normal-running behaviour of the disc, the simple plastic theory is still extremely useful in design because it indicates clearly the sorts of disc profile which make efficient use of the material.

In this chapter we shall investigate some aspects of turbine-disc design and, without going into much detail, we shall establish some simple general rules which help to clarify thinking about the problem and which may be particularly useful when disc design is considered in the context not only of structures but also of thermodynamic performance.

Most of the analysis will be based on the lower-bound theorem, but we will make some reference to modes of plastic deformation. We shall assume that the theorem is valid when the loading is due to body forces, although we have not proved this explicitly in Chapter IV.

5.1. The Rotating Hoop

We consider first the behaviour of a thin uniform circular hoop spinning in its own plane about its centre, Fig. 5.1(a). Although this situation would be impossible to realise, and is patently much simpler than a disc, it does nevertheless serve to provide some important insights into the behaviour of the more complicated practical systems.

Let the hoop have radius c and cross-sectional area A; let the material have density ρ and yield stress Y in simple tension, and let the hoop be spinning at the angular velocity, ω_c, at which it is just on the point of collapse.

Figure 5.1(b) indicates the forces acting on a small element of the hoop at an arbitrary angular velocity: D'Alembert's principle has been used and we write down the "equilibrium" equation at the point of collapse

$$c^2\omega_c^2 A\rho\theta = AY\theta \qquad (5.1)\dagger$$

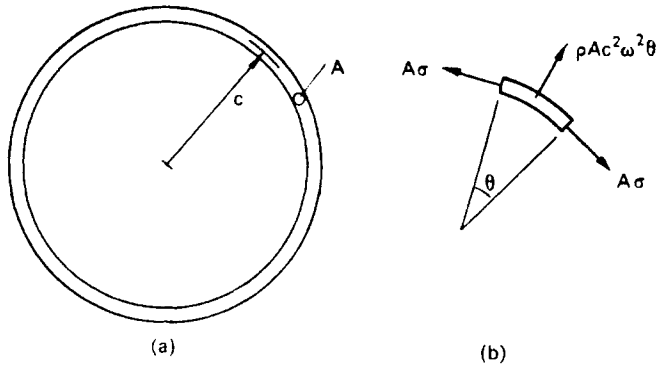

FIG. 5.1. Stresses in a rotating hoop.

Therefore

$$\omega_c^2 = Y/\rho c^2 \qquad (5.2)$$

In the remainder of this chapter the term "equilibrium" will imply prior use of D'Alembert's principle, as in the present example.

Note that in (5.2) the cross-sectional area of the hoop does not appear: just as in the case of the catenary, each "filament" of the hoop carries its own associated loading.

Equation (5.2) gives us the value of ω_c for a given *ring*, but it

† As stress is defined in terms of force on the absolute scale (i.e. force defined in terms of mass and acceleration) the symbol for gravitational acceleration does not occur in this equation (see Appendix VI).

may also be regarded as determining, for a given *material* and *speed* the radius, c, of the hoop which is just at the bursting-point. This "self-supporting radius" as we shall call it, turns out to be a useful concept in the study of more complicated situations, because it is both a sound physical idea and also a means to the reframing of the "disc" equations in a specially simple way.

For the remainder of this chapter the symbol c will have this special meaning, and for ease of reference we rewrite (5.2):

$$c^2 = Y/\rho\omega_c^2 \tag{5.3}$$

In subsequent analysis we shall find it convenient to work in terms of c rather than explicitly in terms of ω_c; at any point in the analysis we can reinterpret equations in terms of ω_c by means of (5.3).

Another interpretation of (5.2) is that at collapse the *peripheral speed* $c\omega_c$ is uniquely determined for a given material. This will also prove to be a useful idea in subsequent discussion.

It is also clear from (5.2) that in the selection of materials for use in turbine and compressor discs, and in the development of new materials, the ratio strength/density is an important parameter (see Problem 5.1).

5.2. The Flat Disc with No Central Hole

To analyse the behaviour of *discs* we need a differential equilibrium equation in place of (5.1). By symmetry the radial, circumferential and axial stress components are the principal stresses, and for a small element dr, θ of a disc of constant thickness (see Fig. 5.2) we have the following equilibrium equation in the radial direction:

$$\frac{d}{dr}(r\sigma_r) = \sigma_\theta - \rho\omega^2 r^2 \tag{5.4}$$

This should be verified by the reader. In all but the "body-force" term this equation is essentially the same as equation (3.2).

For a disc which is thin (i.e. axial dimensions are small compared to the radius) it is reasonable to assume that σ_z is zero everywhere, as the surfaces are unloaded. We shall make this assumption *plane stress* throughout the present chapter, even when we consider, later, discs of variable thickness.

Consider a flat (i.e. constant-thickness), solid (i.e. no central hole) disc of radius b which is stress-free when it is stationary. Elastic analysis, which is analogous to that sketched in Chapter III for thick tubes, gives stress components σ_r, σ_θ which form

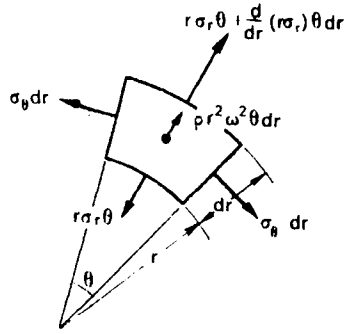

FIG. 5.2. Equilibrium of an element of a rotating disc of constant (unit) thickness.

parabolas if plotted against r, as shown in Fig. 5.3. This analysis is easily checked (Problem 5.2) and it turns out, in contrast to the analysis of thick tubes, that the stresses are not independent of Poisson's ratio, ν.

As the speed increases all stresses within the elastic range increase in proportion to ω^2. To find the speed at which the yield-point is first reached we note that the principal stresses are in the algebraic order $\sigma_\theta \geqslant \sigma_r \geqslant \sigma_z = 0$ (with the equality signs applying at $r = 0$ and $r = b$ respectively); thus σ_r is the intermediate principal stress everywhere and the appropriate version of Tresca's yield condition is therefore

$$\sigma_\theta = Y \tag{5.5}$$

The yield-point is clearly reached first at the centre of the disc at a speed ω_1, say, which is given by (see Fig. 5.3)

$$\omega_1^2 = \frac{8}{(3+\nu)} \frac{Y}{\rho b^2} \tag{5.6}$$

Using (5.3) we find

$$\frac{b}{c} = \sqrt{\frac{8}{3+\nu}} = 1{\cdot}5, \text{ typically} \tag{5.7}$$

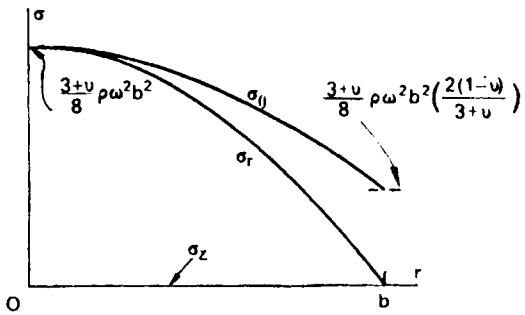

FIG 5.3. Distribution of stress in a flat disc in the elastic range.

In other words, when the yield-point is first reached the angular speed is such that b is about 1·5 times the "self-supporting radius" corresponding to that speed. Alternatively, the peripheral speed of the disc is 1·5 times the critical peripheral speed of a hoop of the same material.

As ω increases further a yield zone, in which $\sigma_\theta = Y$, spreads outwards from the centre. The mode of incremental plastic deformation in this region is such (Problem 5.3) that collapse cannot occur until the surrounding elastic zone has vanished.

To analyse the *full plastic* condition, therefore, we solve the equilibrium equation (5.4) together with the yield condition (5.5). We can see at once that the integration is very simple—but this would not be so if we had used the Mises yield condition instead. The balance of yield stress across a diametral cut with the total centrifugal load of half of the disc at collapse is known as *Robinson's equation* (see Bibliography).

Before solving the equation we shall substitute for c from (5.3) to give:

$$\frac{d}{dr}(r\sigma_r) = Y\left(1 - \frac{r^2}{c^2}\right) \tag{5.8}$$

By making this substitution we are in effect "turning the problem upside-down", so that our aim is now to find the radius b of a solid disc for which the collapse speed is the same as for a hoop of radius c.

Integrating (5.8) we have

$$r\sigma_r = Yc\left(\frac{r}{c} - \frac{1}{3}\left(\frac{r}{c}\right)^3\right) + F \tag{5.9}$$

where F is a constant to be determined. The two boundary conditions may be put

$$r\sigma_r = 0 \text{ at } r = 0 \tag{5.10}$$

—because σ_r is finite at $r = 0$—and

$$r\sigma_r = 0 \text{ at } r = b \tag{5.11}$$

because $\sigma_r = 0$ at the outer edge. The first of these gives $F = 0$, and the second,

$$b = c\sqrt{3}. \tag{5.12}$$

Before accepting this as the solution we must check that σ_r is indeed the intermediate principal stress throughout, to justify use of (5.5). From (5.9)

$$\sigma_r = Y\left(1 - \frac{r^2}{b^2}\right) \tag{5.13}$$

and Fig. 5.4 shows the stress distribution at collapse.

The solution (5.12) can be interpreted in several different ways. It indicates that a flat disc and a hoop of the same material will burst at the same angular speed if their radii are in the ratio $\sqrt{3} : 1$. Alternatively, a flat disc will burst when its peripheral

speed is $\sqrt{3}$ times the critical peripheral speed for a hoop. Or, by substitution in (5.3)

$$\omega_c^2 = 3Y/\rho b^2 \tag{5.14}$$

The speed ratio ω_c/ω_1 necessary to extend the plastic zone from the centre to the periphery is readily found from (5.14) and (5.6). For $\nu = 1/3$, a typical value,

$$\frac{\omega_c}{\omega_1} = \sqrt{\frac{5}{4}} \simeq 1{\cdot}12 \tag{5.15}$$

(see Problem 5.4).

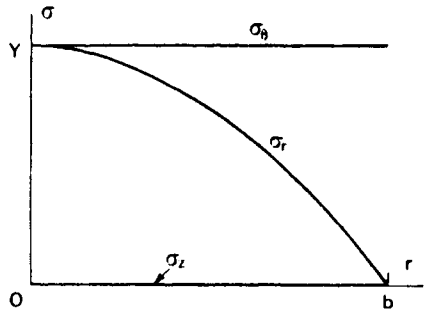

FIG. 5.4. Distribution of stress in a flat disc at the collapse speed.

This is a smaller ratio than typical pressure ratios p_c/p_1 needed to extend the plastic zone in a thick-walled tube from the inner to the outer surface (see Fig. 3.5). The difference between the two cases from this point of view lies in the fact that the elastic and fully-plastic stress distributions are more "similar" for the rotating disc than for the thick-walled tube (compare Figs. 5.3 and 5.4 with 3.4). This in turn arises from the difference between the "plane strain" and "plane stress" boundary conditions which apply, respectively, to the two problems, and the corresponding difference in the yield conditions in σ_r, σ_θ space (see Problem 2.15).

5.3. A Physical Interpretation

The concept of a "self-supporting radius" c is useful in obtaining a "physical" interpretation of the behaviour of the disc at the

collapse speed. A typical "hoop" of material, of which a segment is shown in Fig. 5.2, carries two kinds of loading:

(i) The "centrifugal" load due to its own mass.
(ii) The "applied" load transmitted from the adjacent material: this is proportional to the difference between the product $r\,\sigma_r$ evaluated at the outer and inner edges of the hoop.

A hoop at radius c has, by definition, no carrying capacity for load of type (ii), and so in a graph of $(r\,\sigma_r)$ against r (Fig. 5.5)

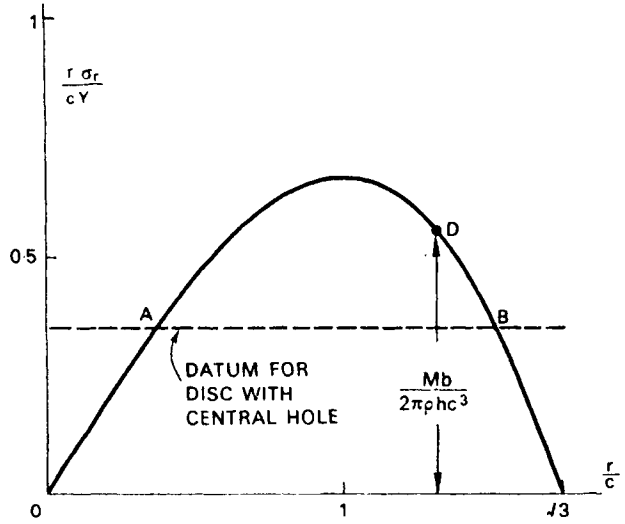

FIG. 5.5. Construction for flat annular discs of equal collapse speed.

there is a horizontal tangent at this point. For $r < c$ a hoop has a positive carrying capacity for this part of the load, which is reflected in the positive slope of the graph in this region. Conversely, for $r > c$ a ring has "negative" carrying capacity; it must be "restrained" if it is to be in equilibrium and the slope of the curve is, correspondingly, negative.

5.4. Discs with Central Holes

Figure 5.5 can also be used conveniently to discuss the *family* of discs with central holes which all collapse at the same angular speed, and of which the solid disc and the hoop are, as we shall see, extreme cases. Suppose that in (5.9) we assigned an arbitrary negative value to F. In terms of Fig. 5.5 the effect would be to lift the "base-line" of the graph, as indicated. At points A and B, both at finite radius, $\sigma_r = 0$, which is the stress boundary condition at a free edge—whether "inner" or "outer"—of a disc. Thus

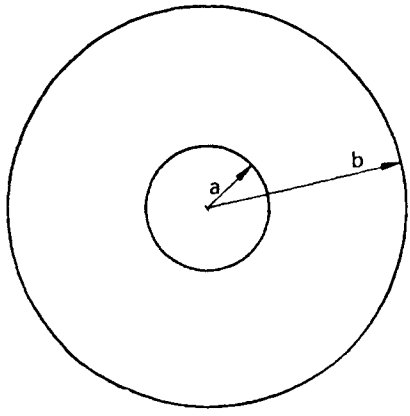

FIG. 5.6. Flat annular disc; definitions.

a disc with inner and outer radii a and b (Fig. 5.6) corresponding to points A and B will satisfy the equilibrium equation (5.8) and the stress boundary conditions. Also $\sigma_\theta > \sigma_r$ everywhere, because the curve between A and B lies wholly below the line corresponding to $\sigma_\theta = Y$; therefore use of the yield condition (5.5) in (5.8) is justified, and we conclude that a disc of these dimensions will have the same bursting speed as the solid disc and the hoop. A family of such discs is thus readily generated by giving the "base line" AB a variety of positions. The whole range of possibilities is shown in Fig. 5.7.

5.5. Mechanisms of Collapse

So far in this chapter we have analysed "collapse" in terms of equilibrium equations and yield conditions. We have thus been using, effectively, a lower-bound approach to the problem and we expect, consequently, that our estimates of collapse speed will be low if they are not correct.

It seems obvious, intuitively, that the collapse speeds which we have worked out are in fact exact, because we have satisfied the

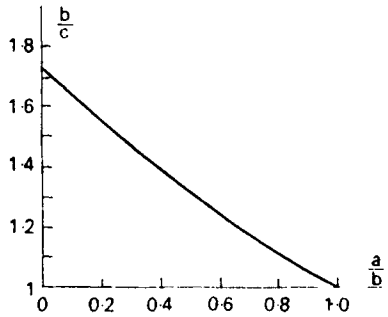

FIG. 5.7. Annular discs having the same collapse speeds, with the solid disc and the thin hoop as special cases.

yield condition everywhere and there is consequently no room for any "improvement".

If our solutions are indeed correct then there will exist mechanisms of plastic deformation which, while satisfying the geometrical compatibility conditions, will also be related to the yield condition via the normality rule. It is instructive to seek these mechanisms.

Consider first the annular disc (Fig. 5.6). We have seen that throughout the material

$$\sigma_\theta > \sigma_r \geqslant \sigma_z = 0 \tag{5.16}$$

with the equality sign applying at $r = a$ and $r = b$. Within the region (5.16) of principal stress space (not admitting the equality sign for the moment) the normality rule gives

$$\dot{\epsilon}_r = 0, \quad \dot{\epsilon}_\theta \geqslant 0, \quad \dot{\epsilon}_z = -\dot{\epsilon}_\theta \tag{5.17}$$

Further, (5.17) does not violate the normality rule in the special case $\sigma_r = \sigma_z$. It is not difficult to visualise a mode of deformation incorporating (5.17). The key is that if $\dot{\epsilon}_r = 0$, equally spaced concentric circles scribed on the disc will remain equally spaced as deformation proceeds; i.e., the radius of each circle will be enlarged by the same amount, say $\dot{u}$.

Thus, from (3.3), (3.4) and (3.31)

$$\left.\begin{aligned} \dot{\epsilon}_\theta &= \dot{u}/r \\ \dot{\epsilon}_z &= -\dot{u}/r \\ \dot{\epsilon}_r &= 0 \end{aligned}\right\} \tag{5.18}$$

By regarding $\dot{u}$ as positive, intuitively, we make (5.18) satisfy (5.17). Thus, as the material moves outwards, the disc becomes thinner, and this decrease in thickness is most pronounced at the inner radius.

It is worth noting that this mechanism of collapse is very different from that of a thick tube (cf. equations (3.34) and (3.35)) in which, of course, plastic straining in the *axial* direction is suppressed, equation (3.30).

For a solid disc the mechanism (5.18) gives singularities in the strain increments at the centre, which can be interpreted as a tendency for the disc to "thin" so much as to produce a small hole very quickly. These singularities are in fact a consequence of the precise angularity of the Tresca yield condition. If a small "rounding" of the edge could be allowed, the singularity would disappear, because in the immediate vicinity of the centre the stress components σ_r and σ_θ are very close. This somewhat curious state of affairs should not be regarded as reflecting discredit on the Tresca condition; it must always be remembered that our main aim here is to predict bursting speeds.

It is interesting to note that we can obtain an extremely simple alternative mechanism of collapse if we allow ourselves to consider the possibility of a mode which is not axisymmetric. In its simplest form this mode consists of an incipient "neck" of

deformation running diametrically across the disc. In this narrow zone the deformation corresponds to

$$\left.\begin{aligned} \dot{\epsilon}_\theta &= \text{constant} \\ \dot{\epsilon}_z &= -\text{constant} \\ \dot{\epsilon}_r &= 0 \end{aligned}\right\} \tag{5.19}$$

The remainder of the disc remains rigid, and the two halves move apart from each other as the neck develops. Another, related, possibility is that a "star" of radial bands of necking develops; this mode is similar to the fracture mode of actual discs.

5.6. Discs with Edge Loading

So far we have considered rotating discs loaded only by body forces due to the mass of the structure itself, whereas the prime function of a turbine disc, of course, is to carry the blades and their means of attachment at the periphery. For a given disc it is clear, intuitively, that the attachment of peripheral mass must lower the bursting speed.

To gain insight into the problem without going into details of attachment of blades, etc., which are beyond the scope of this book, we consider only the simplified situation of a disc carrying a *total* mass M uniformly distributed around the periphery, as shown in Fig. 5.8. In an actual disc the centre of mass of the attached blades, etc., is further from the axis than the "edge" of the disc, so the same total mass of blades, etc., would, at a given speed, exert more radial pull than mass M situated at the outer radius. However, for a given blade layout the "equivalent" mass M can be worked out without difficulty.

First we consider the case of a flat disc of thickness h, with no central hole, supporting a total mass M. The only difference from the point of view of analysis between this situation and the one we have studied already is in the boundary condition at the periphery. The equilibrium of a small sector of the attached mass

is shown in Fig. 5.9. If σ_r represents the radial stress at the edge of the disc, and the disc is rotating at the collapse speed, we have

$$M = 2\pi h\sigma_r/\omega_c^2 = 2\pi\rho hc^2\sigma_r/Y \tag{5.20}$$

using (5.2).

The semi-graphical approach to the boundary conditions which we used earlier is easily adapted to solution of the present problem. In general the boundary condition at the outer edge of the

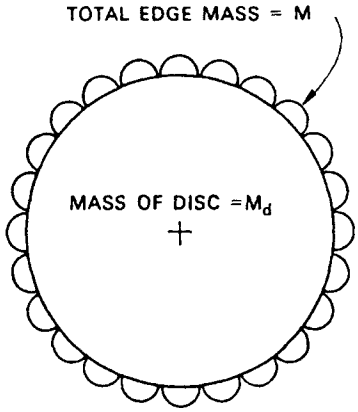

FIG. 5.8. Rotating disc supporting an edge mass.

disc will correspond to a point such as D, Fig. 5.5. For a disc with no central hole we already know that $F = 0$; the ordinate of D is thus a measure of σ_r at the outer edge and it may be used in (5.20) to give the corresponding edge mass. We find

$$M = 2\pi phc^2\left(1 - \frac{1}{3}\left(\frac{b}{c}\right)^2\right) \tag{5.21}$$

where b is the radius of the disc.

5.7. Analysis of Mass

Now one obvious question in the design of discs is: what is the total mass of a disc which will carry a given peripheral mass?

To answer this question in the present case (i.e. a flat disc with no central hole) we evaluate the ratio M_d/M, where M_d is the mass of the disc:

$$M_d = \pi b^2 h \rho \tag{5.22}$$

From (5.21) and (5.22) we find

$$\frac{M_d}{M} = 1.5 \Big/ \left(3\left(\frac{c}{b}\right)^2 - 1\right) \tag{5.23}$$

This simple result shows that the "mass ratio" is a function only of the ratio (b/c); which is perhaps not surprising in view of

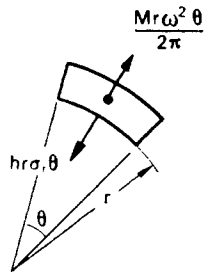

FIG. 5.9. Equilibrium of edge mass.

our previous results. We have already given a physical interpretation of the ratio (b/c). Equation (5.23) is plotted in Fig. 5.10 (full curve). The curve rises steeply above $b/c = 1$, and M_d/M becomes infinite at $b/c = \sqrt{3}$, as it obviously should from our previous analysis of a flat disc with zero peripheral mass.

In aero engines it is obviously desirable to reduce mass wherever possible, so from this simple point of view b/c should be kept as *low* as possible. As we have seen already, for a given material b/c is a measure of the peripheral burst speed of the wheel. But from the point of view of raising the power output of an engine the peripheral speed should be as *high* as possible. These conflicting requirements of weight and power suggest that there is an optimum peripheral speed from the point of view of obtaining the best "power/weight" ratio.

However complicated the actual process of producing a design of a gas turbine, one factor is clear; if it is possible to reduce M_d/M for a given b/c by varying the thickness of the disc with the radius, this will almost certainly be advantageous.

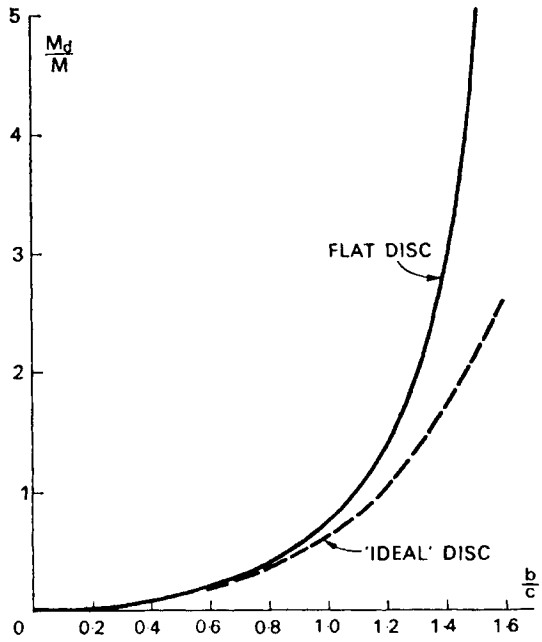

FIG. 5.10. "Mass ratios" for a solid flat disc and a profiled disc.

5.8. Discs of Variable Thickness

A clue to a possible line of attack on the problem of determining an "optimum" profile for a disc may be obtained from Fig. 5.4. Here we see that when a *flat* disc bursts the radial stress is lower than the circumferential stress except at the centre of the disc. According to the Tresca yield condition in plane stress—see Fig. 5.11—there is a "reserve" of strength in the radial component of stress.

It thus seems likely that we shall be able to reduce the mass of the disc by making use of this reserve of strength. As the stress

distribution of Fig. 5.4 is statically determinate, the only way of making use of this reserve is to vary the thickness of the disc.

It is not difficult to rewrite the equilibrium equation (5.4) including the thickness h as a variable: see Fig. 5.12 and Problem 5.5.

$$\frac{d}{dr}(hr\sigma_r) = h\sigma_\theta - h\,Y\frac{r^2}{c^2} \tag{5.24}$$

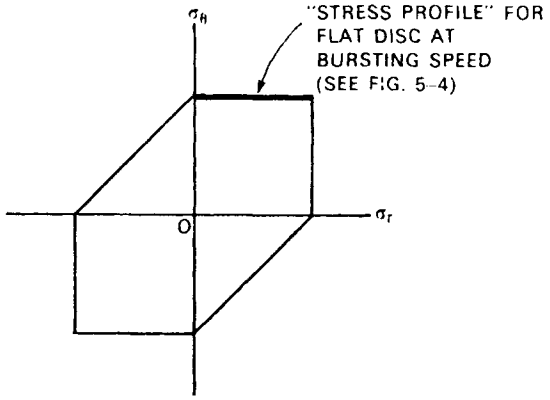

FIG. 5.11. Tresca yield condition in principal stress space under conditions of plane stress (see Problem 2.15).

We assume here that the change of h with r is sufficiently gradual for our "plane stress" assumption to be justified. We have also expressed the inertia loading in terms of radius c.

For any specified $h(r)$ we can, in principle, solve (5.24) subject to an appropriate yield condition. We can, inversely, specify the stresses and solve the resulting equation in h. This is a simple procedure if we put

$$\sigma_\theta = \sigma_r = Y \tag{5.25}$$

in an attempt to make full use of the "biaxial" strength of the material; (5.24) then becomes, simply:

$$\frac{dh}{h} = -\frac{rdr}{c^2} \tag{5.26}$$

Solving this and putting $h = h_0$ (say) at $r = 0$, we have

$$h = h_0 \exp(-r^2/2c^2) \tag{5.27}$$

This "profile" is plotted in Fig. 5.13. It is in fact the "normal distribution curve" of statistical analysis. At the special point $r = c$ there is a *point of inflection* in the profile, and in this region therefore the form of the disc approximates a double cone.

The disc given by (5.27) extends to infinity. We can make practical use of it very simply, however, by "cutting out" a disc

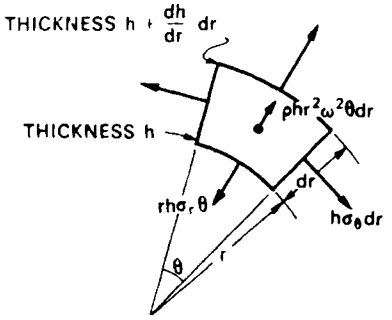

FIG. 5.12. Element of a variable-thickness disc (see Problem 5.5).

at any radius and providing the necessary radial stress by attaching appropriate peripheral mass. We have already studied the equilibrium of the peripheral mass: putting $\sigma_r = Y$ in (5.20) we obtain

$$M = 2\pi\rho c^2 h_b \tag{5.28}$$

where h_b is the thickness of the disc at the outer edge, $r = b$. Note that b does not appear explicitly in this formula.

Thus for a disc of given radius, supporting given peripheral mass, made of given material and required to burst at a given angular speed, the design is fixed. To determine the disc, first we find c from (5.3), then h_b from (5.28) and finally $h(r)$, from (5.27). In particular $h_0 = h_b \exp(b^2/2c^2)$, and the ratio h_0/h_b is thus a steeply-rising function of b/c.

The total mass of the disc is readily found by integration:

$$M_d = \rho \int_0^b 2\pi hr \, dr = \pi\rho h_o \int_0^b \exp(-r^2/2c^2) 2r \, dr = 2\pi\rho c^2(h_o - h_b) \tag{5.29}$$

For a disc of this particular profile there is thus a specially simple relationship between the mass of the disc and the difference in thickness between the centre and the outer edge.

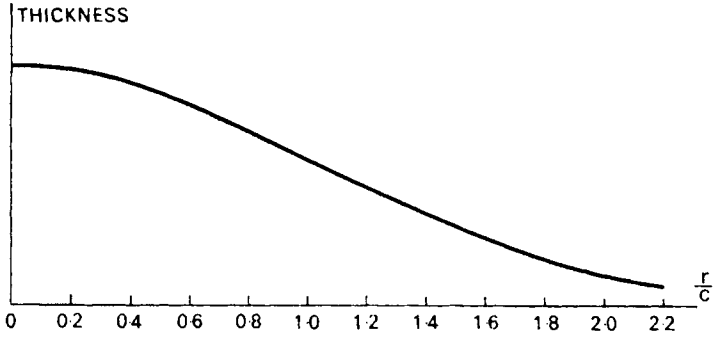

FIG. 5.13. Profile of an ideal disc.

Using (5.28), (5.29) and (5.27) we have

$$\frac{M_d}{M} = \frac{h_o - h_b}{h_b} = \exp(b^2/2c^2) - 1 \tag{5.30}$$

This curve is also plotted in Fig. 5.10 (broken curve), and we see clearly that although the profiled disc is not much more "efficient" for $b/c < 1$ there is a substantial saving in mass at higher values. Nevertheless, the mass ratio is a steeply-rising function of b/c.

5.9. Reinforcement of Central Holes

An obvious disadvantage of the variable-thickness ideal disc developed in the preceding section is that it lacks the central hole necessary if the disc is to be mounted on a shaft, or which may be

desirable for any other reason—such as to remove an "unreliable" central core from a forging.

Fortunately it is not difficult to modify the design (5.27)—or indeed any other design—by "cutting out" a hole at radius a and arranging for the radial stress in the disc at $r = a$ to be carried by a "compact" ring designed for the purpose. In an actual design the reinforcing ring may prove to be too diffuse for the compact-ring idealisation to be justified (see Problem 5.6); an initial study of the compact ring is, nevertheless, illuminating. A reinforcing

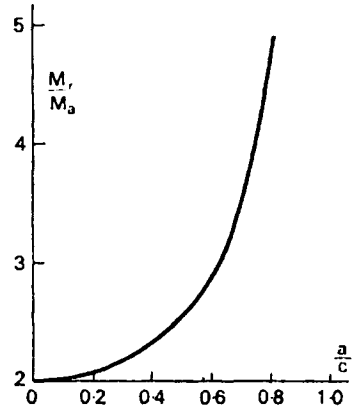

FIG. 5.14. Mass-ratios for a ring-reinforced central hole in an "ideal" disc.

ring of this sort would, of course, be made integral with the disc in practice.

It is a straightforward matter to design a ring of given radius a to carry its own centrifugal load in addition to a radial stress applied by the remainder of the disc (Problem 5.7). As might be expected, the necessary cross-sectional area is a function of a/c. In terms of mass (or volume), we find that if M_a is the mass of material removed by the cut at $r = a$, and M_r is the total mass of the "equivalent" reinforcing ring for a central hole in an "ideal" disc,

$$M_r/M_a = 1/(\exp(a^2/2c^2) - 1)(c^2/a^2 - 1) \qquad (5.31)$$

This ratio is plotted as a function of a/c in Fig. 5.14. Although the

ratio becomes infinite as a approaches c (as it obviously should) it is practically constant for $a/c < 0{\cdot}5$, tending to 2 as a/c tends to zero. This limiting value is readily checked from first principles (Problem 5.8).

We are therefore justified in making the apparently paradoxical statement that an adequately reinforced hole in the centre of a turbine disc weighs at least twice as much as the material removed.

Problems

5.1. Equation (5.2) concerns a *hoop* of material, but the remark on p. 120 about strength/density being an important material parameter was made with reference to *discs*. On what grounds may this generalisation be justified?

Calculate the critical peripheral speeds for rotating hoops made of some or all of the materials listed in Table 2.1, p. 58.

5.2. Verify the "elastic" distribution of stress in a flat disc indicated in Fig. 5.3. (Check that the stresses satisfy the equilibrium equation (5.4). Evaluate the corresponding strains from the elastic stress/strain relations (3.1) and check that these are geometrically compatible by substitution in (3.9)).

5.3. Show that the increment of plastic strain in a region of a disc for which $\sigma_\theta = Y > \sigma_r > \sigma_z = 0$ involves, in particular—according to the Tresca flow rule—$\dot{\epsilon}_r = 0$, and that consequently, by geometry, a surrounding ring of elastic material prohibits unconstrained plastic flow in the region.

5.4. Examine the overall "equilibrium" of half of a rotating flat disc with no central hole (i.e. the balance of the "centrifugal" forces for a semicircle and integrated hoop stress on the diametral "cut") and establish equation (5.15) by using data in Figs. 5.3 and 5.4.

5.5. Figure 5.12 shows a small element of a variable-thickness disc. Complete the labelling of the arrows (cf. Fig. 5.2) and hence obtain equation (5.24) by consideration of equilibrium.

(Note that it is simplest to regard $(hr\sigma_r)$ as a composite variable; cf. Fig. 5.2.)

5.6.† Study, for example, collapse of a flat disc carrying no peripheral mass but having a central hole reinforced by a flat annulus ("hub") of thickness (say) three times that of the disc. Assume plane stress conditions throughout.

(*Hint.* Observe (i) that (for the same material) c is the same for both annuli; (ii) that Fig. 5.5 applies to both regions (with different constants F in the two regions); and (iii) there is a factor 3 between the radial stress (averaged through the thickness) at the interface between the two annuli.

Evaluate a few possible designs by measurement from Fig. 5.5 and compare the excess mass (over that of a disc without a hole) to that for a "compact" reinforcement designed by the formula given in Problem 5.9.

5.7. Obtain a formula for the cross-section area, A, of a hoop of radius a which will just sustain at angular velocity ω_c a radial pull $h\sigma_r$ per unit circumference in addition to the centrifugal effects of its own mass. Work from first principles and express the result in terms of the "self-supporting radius" c, of the material at ω_c.

5.8. From the result of Problem 5.7 show that for $a \ll c$ the centrifugal effect of the mass of the ring is negligible and that, consequently, the problem of design of the ring reduces in effect to one of static equilibrium. Consider a compact ring reinforcing a hole in a plate with, locally, $\sigma_r = \sigma_\theta = Y$ and show that the mass of the compact ring is twice that of the equivalent portion of the plate.

5.9. A flat disc of thickness h and radius b, supporting no peripheral mass, is to be modified by the cutting of a central hole of radius a reinforced by a compact hoop of cross-section area A, so arranged that the bursting speed is unaltered. Show that

$$A = \frac{ha(1 - a^2/b^2)}{(1 - 3a^2/b^2)}$$

(*Hint.* Use the solution of Problem 5.7.)

CHAPTER VI

TORSION

THE basic questions in the theory of torsion which can be answered by simple plastic theory are: what is the full plastic torque of a given prismatic member? and: how can we design a prismatic member to withstand a given torque?

These questions are obviously important in the analysis and design of some simple structures and machines. However, in practice, except in some specially simple situations, torsion in a member is usually accompanied by tension or bending or both. It will be of much more practical use therefore to study torsion in combination with tension and bending rather than simply by itself. This we shall do later in the chapter, making free use of the lower-bound theorem in conjunction with the "pure torque" analysis of the first part of the chapter, to provide "safe" estimates of the carrying-capacity of prismatic bars of arbitrary cross-section.

In fact we shall use the lower-bound theorem throughout the present chapter both because it is "safe" and also because it provides an extremely simple and direct approach to the problem.

In this respect the present chapter differs substantially from chapters on plastic torsion in other textbooks. The more usual approach is via elastic analysis and Prandtl's so-called "membrane" analogy. As we shall see, the approach of the present chapter is much more direct, and although it avoids elastic and elastic–plastic analysis entirely (and therefore, *ipso facto*, cannot deal with certain important practical questions) it has the advantage of not demanding of the reader a prior knowledge of a particular region of elasticity theory.

For those readers who are familiar with the membrane analogy and wish to establish a connection between it and the present approach, an extra Problem (6.4) is provided.

6.1. Torsion of Thin-walled Tubes of Arbitrary Cross-section

In Chapter V it turned out to be a useful first step to consider the simplest conceivable rotating "disc", viz. a rotating hoop. Likewise in the present chapter we shall find it advantageous to begin by considering the problem of torsion in the specially simple

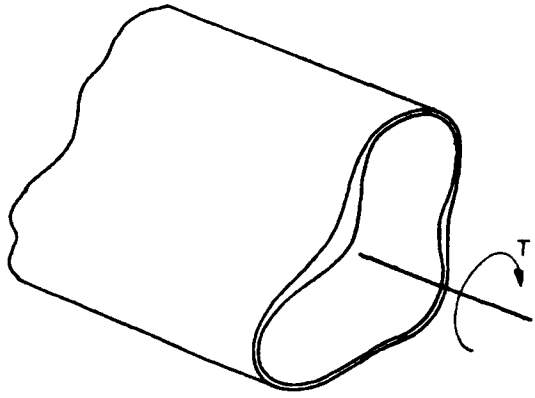

FIG. 6.1. Torsion of a thin-walled tube of irregular cross-section.

thin-walled tube. Rather surprisingly we can analyse easily the torsion of a thin-walled tube of *arbitrary cross-section*, shown schematically in Fig. 6.1. The tube is loaded by a torque T, i.e. by equal and opposite couples applied at the ends about an axis parallel to the tube. The tube is uniform in the sense that it is generated by sliding a cross-section in a direction perpendicular to its plane. The cross-section is simply-connected, of any arbitrary shape, and the thickness t—which is small compared to the overall dimensions of the cross-section—is a variable function of the distance, s, measured around the periphery from an arbitrary datum (see Fig. 6.2). As the tube is *thin* there is no significant difference in s measured around the inside or the outside surface.

In specifying torque T we do not specify the *details* of the way in which it is supplied; instead we suppose that end-fittings are provided which "diffuse" the torque into the tube. We therefore appeal to the principle of St. Venant and consider a representative cross-section sufficiently remote from the ends for the stresses to be uniform along the tube.

In order to describe adequately the state of stress in the thin wall of the tube we need to specify a coordinate system. The

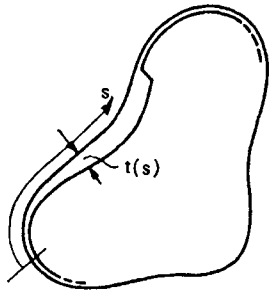

FIG. 6.2. Cross-section of an irregular thin-walled tube.

obvious one to choose is (s, z) in the thin wall, z being measured axially from an arbitrary datum. We also use the symbol n to describe the direction of the local normal to the tube wall, and thus to complete the *local* set of three mutually perpendicular axes.

The notation for stress referred to this set of axes is that given in Appendix V.

The first steps in the analysis of stress are to observe that it is safe to assume that the stress system does not vary through the (thin) wall of the tube and that several components of the stress on a typical small element, shown in Fig. 6.3(a), vanish:

(i) $\sigma_s = 0$ because there is no difference in pressure between the inside and outside of the tube,

(ii) $\sigma_z = 0$ because there is no axial pull (also assuming the tube to be initially stress-free),

(iii) $\left.\begin{aligned} \sigma_n &= 0 \\ \tau_{nz} &= 0 \\ \tau_{ns} &= 0 \end{aligned}\right\}$ because the surfaces of the tube are unloaded.

This leaves τ_{sz} and τ_{zs} as the only non-zero stress components, and by "complementary shear" (see Appendices I and V) they are equal—and opposite in this notation.

The stress system at any point in the thin wall is thus a very simple one, viz. a state of pure shear referred to the s, z directions.

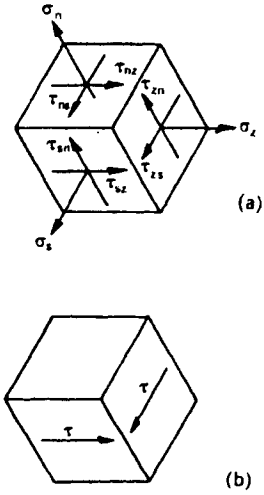

FIG. 6.3. State of stress in an element of the tube wall.

To simplify the notation we shall henceforth use the symbol τ for this shear stress: see Fig. 6.3(b).

To analyse the stresses in the tube we first consider the equilibrium of a finite portion of the wall between two arbitrary generators at $s = s_1$ and $s = s_2$, say, and two arbitrary cross-sections distance l apart, as shown in Fig. 6.4.

Let the thickness of the wall be t_1 and t_2 respectively at s_1 and s_2, and the corresponding shear stresses τ_1 and τ_2.

In the z-direction, equilibrium requires

$$l\,\tau_1 t_1 = l\tau_2\, t_2 \tag{6.1}$$

Therefore, since s_1 and s_2 were chosen arbitrarily, we may write

$$\tau t = \text{constant} = q, \text{ say} \tag{6.2}$$

around the circumference. The value of q obviously depends on the dimensions of the cross-section and the applied torque. The quantity q is sometimes known as the "shear flow" in the wall of the tube; it is the shear *force* per unit peripheral length. We can readily check that the other equilibrium conditions for the segment are satisfied.

To find the relationship between T and q we work out the

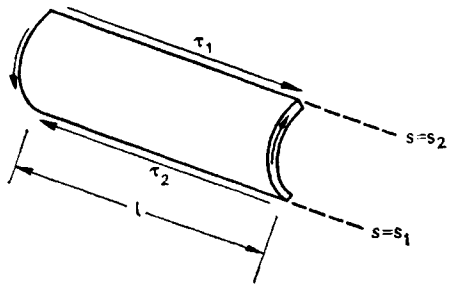

FIG. 6.4. Equilibrium of part of the tube wall.

resultant of the shear stresses acting on any cross-section, and identify it with T. In general the resultant of a set of forces in a plane is a couple together with a force. In the present case we expect the resultant to be a pure couple, so we must show that we obtain the *same* quantity by taking moments about an *arbitrary* point in the cross-section.

First we take moments about an arbitrary point within the tube, such as D in Fig. 6.5. A small element of wall, BC, of length δs has an associated force

$$\tau t \delta s = q \delta s$$

and a moment about D of

$$DFq\delta s$$

when DF is the perpendicular from D to BC (produced). But $DF\delta s$ is twice the area of the narrow triangle BCD; therefore, as q is a constant, we have on integration around the circumference

$$T = 2Aq \tag{6.3}$$

where A is the total area enclosed by the cross-section. (Note that A is *not* the cross-sectional area of the tube wall.)

This result is indeed independent of the position of D within the tube, and also outside the tube if some areas are reckoned, appropriately, as negative.

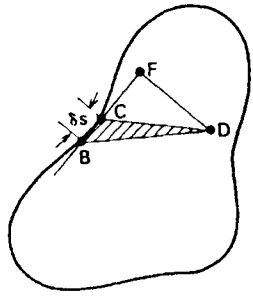

FIG. 6.5. Taking moments about a point.

From (6.2) and (6.3) we have, at any point in the cross-section

$$\tau = T/2At \tag{6.4}$$

As we have completed the analysis of stress by the use of equilibrium considerations alone, we note that the tube is *statically determinate.*

From (6.4) we obtain directly a lower bound on the full plastic torque, T_p, for such a tube made of perfectly plastic material with yield stress k in pure shear. The shearing stress is largest where the thickness has its smallest value, say t_{min}, so, setting this stress equal to the yield stress we have

$$T_p = 2Akt_{min} \tag{6.5}$$

When we consider plastic *design* of a thin-walled tube we can

see immediately that as far as economy of material is concerned it is always best to have a *constant* wall thickness, for then the shearing stress is constant also. However, even if we decide to have constant wall thickness we still have great freedom in design because only the enclosed *area* of the cross-section, and not its shape, is determined by (6.5).

The shape which gives minimum volume of material for a given torque is that for which the circumference is least for a given area, i.e. the circle; but a square tube of the same enclosed cross-section area has a perimeter only 13 per cent larger (see Problem 6.1).

Considerations of economy must not be pressed too far, however. In general the above analysis shows that for a required full plastic torque the amount of material needed diminishes as the wall thickness decreases and the enclosed cross-sectional area increases. Quite apart from the fact that *compactness* is often desirable in structural components from the point of view of space, there is a tendency for thin-walled structures of all kinds to become unserviceable through *buckling*. The designer must be aware of this possibility when designing unstiffened thin-walled tubes.

However, as our prime concern in the present chapter is the torsion of bars of compact cross-sections, we shall not need to investigate this aspect of the behaviour of tubes; as we have already pointed out, our analysis of thin-walled tubes serves primarily as a stepping-stone to the analysis and design of more useful cross-sectional shapes.

6.2. Lower-bound Analysis of Thick-walled Tubes and Solid Cross-sections

We first recall that a lower-bound analysis consists of finding *any* distribution of stress which is in equilibrium and does not violate the yield condition: then the corresponding external loads will be carried safely.

As an example, let us try to obtain a lower-bound on the full

plastic torque of a hollow square tube with the cross-section shown in Fig. 6.6(a).

Now in general the more "solid" a body is, the more freedom there is in satisfying the equilibrium equations alone. Our aim in applying the lower-bound theorem is to exploit this freedom and produce relatively simple solutions of the equilibrium equations. In the present case the key to the situation is the physical idea of "slitting" the tube, conceptually, into a set of nesting thin-walled tubes, as in Fig. 6.6(b), which we now know we can analyse. A "slit" in a body has completely stress-free faces, so by thus

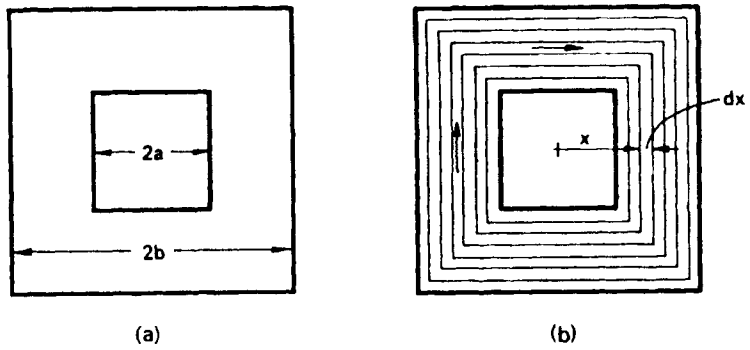

FIG. 6.6. Hollow square tube and its conceptual subdivision into nesting thin-walled tubes.

cutting a body up we are in effect specifying that certain stress components on certain planes have certain values. If we make *enough* slits we can make the resulting structure or component statically determinate, and thus end up with a set of simple equilibrium problems to solve. On the other hand, if we make *too many* slits we may render the structure unserviceable.

Figure 6.6(b) shows an "obvious" way of breaking down the thick tube into a nest of thin ones. It is worth while, however, to establish at this point a general procedure which will apply equally whatever the shape of the cross-section. Our object is simply to obtain the highest possible value of T for the given cross-section. We shall clearly aim to have $\tau = k$ everywhere,

and we must therefore make each thin tube have *constant thickness*. Moreover, if we intend to "cut up" the whole cross-section into thin rings, it is clear that the torque will be largest if each ring encloses the largest possible area.

Our strategy is therefore clear. Starting from the outer edge of the cross-section we cut off complete, simply-connected thin shells of constant thickness; and we repeat the process until the whole cross-section area is used up. We then sum up the torques provided by the nesting tubes to give our lower-bound on the full plastic torque T_p, to which we shall give the symbol T_p^l—the superscript reminding us that we have calculated a lower bound.

We might call this the *spring onion* analogy of torsion.

In the chosen example Fig. 6.6, the procedure results in a set of nesting square tubes, and we can easily sum up the torques by using calculus, for it is clear that the torque is largest when the tubes are vanishingly thin. Let a typical elementary tube have side $2x$ and thickness dx as shown in Fig. 6.6(b). Using (6.5)

$$dT = 2Ak\,dx = 8x^2k\,dx \tag{6.6}$$

Therefore

$$T_p^l = 8k\int_a^b x^2dx = \frac{8}{3}k(b^3 - a^3) \tag{6.7}$$

The direction of the arrows in Fig. 6.6(b) shows the direction of the shearing stress on a cross-section for a "right-hand" torque; we clearly want all the elementary tubes to provide components of torque of the same sign.

For some further simple examples see Problem 6.2.

A second example is shown in Fig. 6.7. In this case the inner and outer boundaries of the cross-section are concentric but dissimilar, so a purely repetitive procedure will not "cover" the whole cross-section. Starting from the outside by removing concentric circular shells we are left with three zones of irregular shape, Fig. 6.7(b). Now our "stripping" process must always produce *complete* simply-connected tubes, so the only rational procedure open to us is to treat each of the three remaining areas

separately, as shown in Fig. 6.7(c), with the shear directions as shown. It is clear that the enclosed areas of these irregular tubes are considerably smaller than those of the circular tubes, so for a rough (but quite good) lower bound we might well ignore the contribution of the irregular areas and simply integrate over the circular tubes. This gives

$$T_p^l = \frac{2\pi}{3} k(b^3 - a^3) \tag{6.8}$$

Another interpretation of this calculation is that we are doing a lower-bound calculation by assigning zero stress to all material

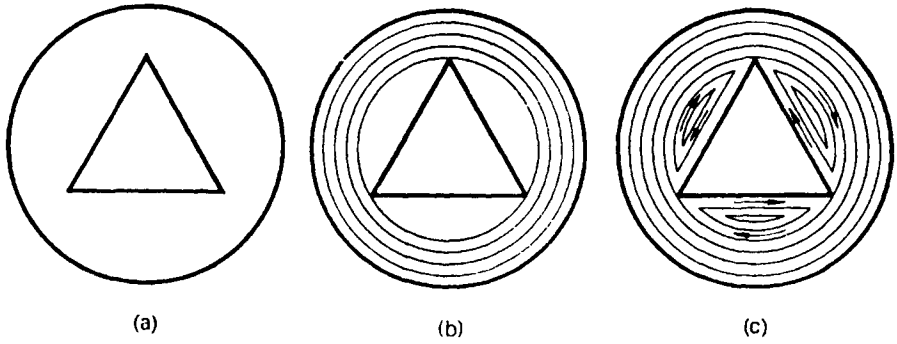

FIG. 6.7. Irregular thick tube and its subdivision into nesting thin-walled tubes.

not in a simple symmetrical area. The same sort of technique is useful in obtaining lower bounds on the bursting pressure of thick pipes of irregular cross-section (see Problem 4.9).

The "stripping" procedure can be used to compute a lower bound on the full plastic torque for a prismatic bar of any arbitrary cross-section, however complicated. Rings of constant thickness are removed inexorably from the cross-section, working always from the outside of whatever remains of the cross-section, and treating separately any areas which may become detached in the process. Figure 6.8 shows an example. The evaluation of areas of irregular shape will not be simple, of course: *ad hoc* approximations and planimeters may be useful in practice.

6.3. The Sand-hill Analogy

It is sometimes helpful to attach a geometrical meaning to the integration of the torques corresponding to our nesting thin tubes of thickness dt, say:

$$T = \int dT = 2\int Akdt \tag{6.9}$$

If we regard (kdt) as a thickness, the integrand is the *volume* of a "slice" of thickness kdt. These slices, piled on top of each other,

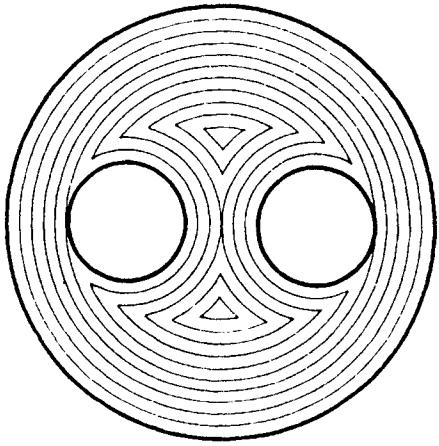

FIG. 6.8. Subdivision of a double tube into nesting thin-walled tubes.

form a solid with sides having a common slope k. On this interpretation the "slits" between successive tubes, as shown for example in Figs. 6.6 to 6.8, become *contours* of the solid figure. It is important to note that when the cross-section has a *hole*, there is no corresponding hole in the "slices", and the outline of the hole simply indicates a "plateau" of the solid figure.

We may summarise this interpretation by stating that the lower-bound torque is equal to twice the volume of the solid erected over the cross-section with slope k above the "material" parts of the cross-section and zero slope above any holes.

This is in fact the celebrated "sand-hill" analogy for plastic torsion first put forward by Nadai. It is so called because dry sand has a definite "angle of repose" and the "volume" corresponding to any cross-section (without holes) may be generated automatically—to within a vertical scale factor—by pouring sand onto a flat horizontal board cut out to the shape of the cross-section.

For torsion of a *tube* (or in general any multiply-connected cross-section) the sand-hill analogy is not nearly so satisfactory as our "spring onion" analogy, because the special devices which are necessary to realise the sand-hill have no direct physical significance. With the nesting-tube method contours of the volume are built up one at a time until the whole area is covered: the only problem then remaining is the purely geometrical one of integration. See, for some examples, Problem 6.3.

Another analog of the volume to be evaluated is a *roof* with sloping sides. This is a natural analogy to use when discussing the transition from elastic to plastic torsion (see Problem 6.4). Obviously the two analogies produce volumes which have identical contours.

6.4. Re-entrant Corners

The nesting thin-tube procedure for finding lower-bound full plastic torques for prismatic bars of *any* (simply or multiply-connected) cross-section is bound to work in all cases. There is a pitfall for the unwary, however, when the cross-section has a sharp re-entrant corner. We illustrate this by considering plastic torsion of an L-shaped cross-section shown in Fig. 6.9.

The *roof* of an L-shaped house would have contours as shown in Fig. 6.9(a), while our stripping process would provide contours as shown in Fig. 6.9(b). In particular, in the region of the re-entrant corner the second procedure generates a conical surface of slope k. Each thin tube in (b) has a greater enclosed area than the corresponding one in (a) and so the corresponding torque is higher.

However, there is no doubt that (a) represents a perfectly satisfactory way—from the present lower-bound point of view—of dividing up the bar into thin tubes, and it is clear that the volume calculation would be easier than for (b). The question of which approach to use—(a) or (b)—is thus very largely a question of taste. If, as is often the case in engineering, speed and ease of calculation are of more importance than extreme accuracy, (a) will be the better method. If a check on the difference between the two corresponding torques is required, this can be made, roughly,

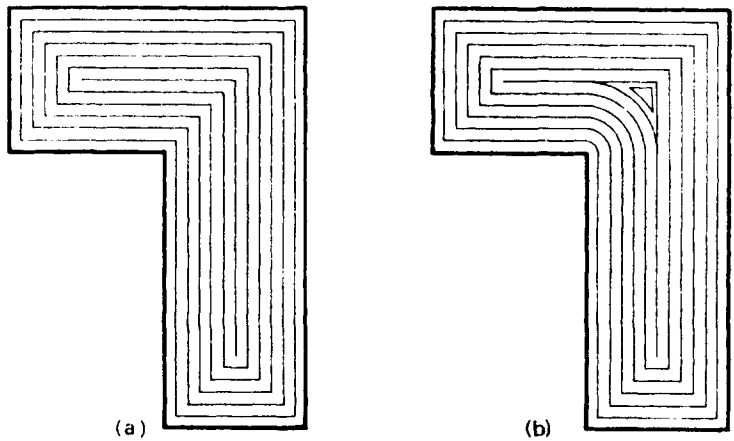

FIG. 6.9. The problem of the re-entrant corner.

by neglecting the small, awkwardly-shaped volume, but including the "conical" part: see Problem 6.5.

In an important practical problem like that of estimating the reduction in torque carrying-capacity of a shaft when a keyway is cut into it (Fig. 6.10) the calculation of volumes is obviously more complicated. For a simpler "keyway" situation see Problem 6.6.

6.5. Other Aspects of Plastic Torsion

If a lower-bound on the full plastic torque T_p is obtained by use of the "spring onion" method or, equivalently, the sandhill

analogy, with all details of the volume carefully accounted for, it is clear that no higher lower bound on T_p can possibly be obtained.

If we have thus arrived at the "exact" stress distribution, it follows that a mechanism of collapse must exist in which the incremental strains at each point are associated with the stresses by means of the normality rule.

It is not difficult to determine the pattern of deformation in plastic torsion. We shall not go into details here (we refer the reader who is interested to the book by Hill listed in the Biblio-

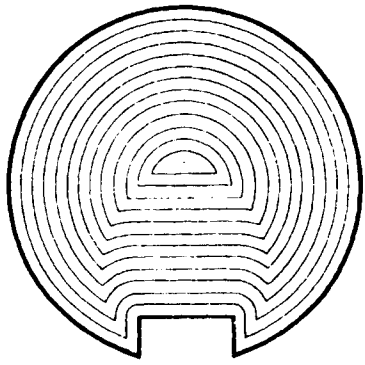

FIG. 6.10. Shaft with a keyway.

graphy) except to point out that in general the deformation involves *warping* of the cross-section, i.e. non-uniform displacements in the axial direction over the cross-section.

Now we have assumed throughout our analysis that the bar being twisted is sufficiently long for end-effects to be negligible. The above remarks about warping serve to reinforce the necessity for an assumption of this sort, because warping according to the same pattern at all cross-sections of a bar would require, in particular, warping at the ends of the bar, which might be incompatible with, say, massive enlarged end-pieces.

In general the effect of restraint of warping at the ends of a twisted bar is to increase the torsional strength of the bar. It is well known, for example, that in the twisting of relatively short

relatively thin-walled "angles" with encastered ends the torque-carrying capacity determined by experiment may be considerably larger than that according to our simple theory.

While this has important implications for combined flexural-torsional buckling in frameworks it is not so significant in the torsion of members of more "compact" cross-section, and in any case our lower-bound technique is intended to provide "safe" estimates of torque-carrying capacity.

Useful estimates of the effect of "end-restraint" on the torque-carrying capacity of very short members may be made by using an upper-bound approach; see Problem 6.7.

6.6. Combined Torsion and Tension

The lower-bound approach enables us to make safe estimates of the strength of prismatic members subject simultaneously to tension and torsion, at the expense of very little further effort.

Let T and P represent the applied torque and longitudinal tension carried by the member. We seek, then, information about the collapse load locus in T, P space. A pure torsion analysis furnishes two points in this space, $(\pm T_o, O)$, say, while a pure tension analysis furnishes the point (O, P_o). $P_o = AY$, where A is (now) the total cross-section area of material and Y is the yield stress in pure tension. If we suppose that there is no buckling in compression, and no Bauschinger effect, as usual, we also have a fourth point, $(O, -P_o)$. These four points, Fig. 6.11(a), all lie on or within the collapse load locus.

The convexity theorem, p. 113 indicates that the locus formed by joining the four points by straight lines is "safe", see Fig. 6.11(a); this is because the quadrilateral shown is the curve which comes as close to the origin as possible without being concave anywhere. The quadrilateral thus represents an "inner" bound on the true T, P collapse load locus. Note that this applies *whatever* the cross-section shape of the bar.

It is a simple matter to improve on this lower bound, and enlarge the "safe" area of P, T space, as follows.

We know from the "spring onion" analogy that shearing stresses of magnitude k over the cross-section are in equilibrium with torque T_o; therefore proportional stresses of magnitude λk are in equilibrium with torque λT_o. Similarly, tensile stresses μY are in equilibrium with axial tension μP_o. Thus, provided the combined stresses λk, μY—properly added—do not exceed yield,

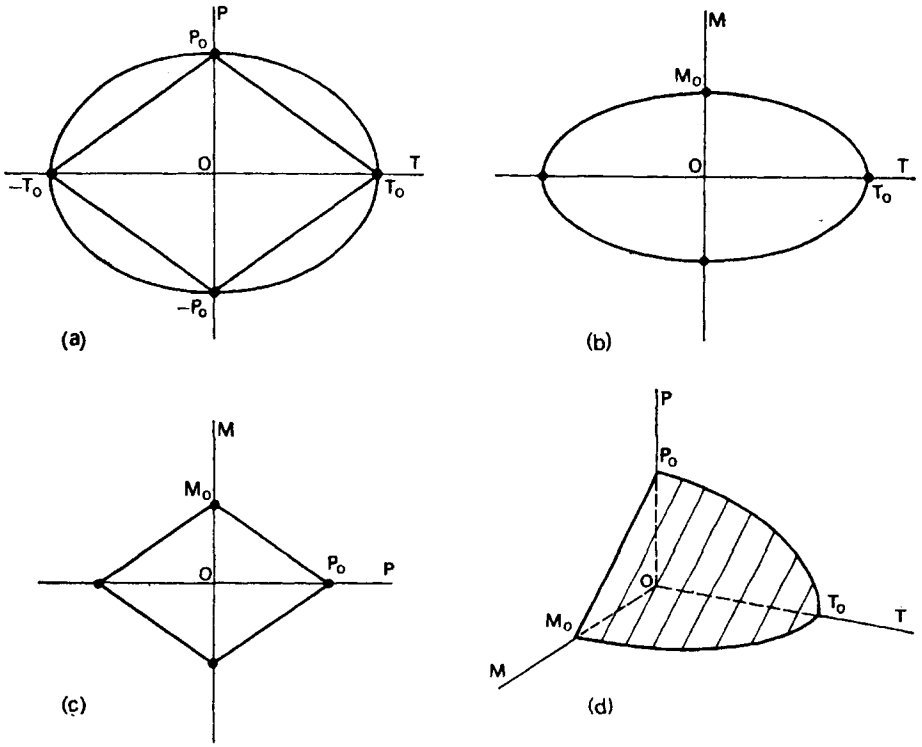

FIG. 6.11. Combinations of tension (P), torsion (T) and bending (M).

the loads (λT_o, μP_o) will be "safe". Figure 6.12(a) shows the combined stresses acting on an elementary cube "cut" with one face parallel to the tangent-plane to the local thin tube, and another perpendicular to the axis. We have already studied yielding under this particular combination of stresses in Chapter II with the result that for *either* the Tresca *or* the Mises yield condition

$$\left(\frac{\tau}{k}\right)^2 + \left(\frac{\sigma}{Y}\right)^2 = 1 \qquad (6.10)$$

as shown in Fig. 6.12(b); $k = Y/2$ (Tresca) or $Y/\sqrt{3}$ (Mises). Here $\tau = \lambda k$ and $\sigma = \mu Y$ so (6.10) gives

$$\lambda^2 + \mu^2 = 1$$

and it follows that

$$\left(\frac{T}{T_0}\right)^2 + \left(\frac{P}{P_0}\right)^2 = 1 \tag{6.11}$$

represents safe combinations of load.

The corresponding ellipse is shown in Fig. 6.11(a); it obviously encloses considerably more space than the quadrilateral.

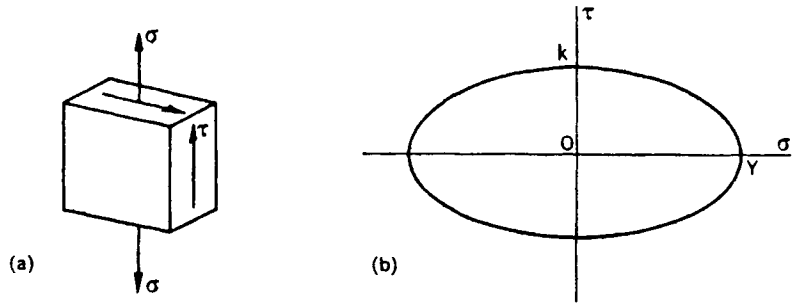

FIG. 6.12. Yield locus for combined tension and shear.

In this analysis we have been able to find safe combinations of T and P without reference to the cross-sectional shape beyond the fact that values of T_0 and P_0 depend on it. Any further extension of the safe zone can only be done with reference to a particular cross-section geometry. In fact, for the simple cross-sectional shapes which are fully analysed in the literature under combined tension and torsion the elliptical locus is a very close lower bound. We conclude then that further detailed analysis of this problem would have little practical value.

6.7. Combined Torsion, Bending and Tension

It is easy to show, by a simple extension of the arguments of the previous section, that if M_0 is the full-plastic (pure) bending

moment of a prismatic member about a "natural" axis, the ellipse

$$\left(\frac{T}{T_o}\right)^2 + \left(\frac{M}{M_o}\right)^2 = 1 \tag{6.12}$$

in (T, M) space, as shown in Fig. 6.11(b), represents safe combinations of torque and bending moment.

The same approach can obviously be applied to combined torsion, tension and bending. For combined bending and tension (with no torsion) we cannot, unfortunately, improve on the quadrilateral joining the points $(\pm P_o, O)$, $(O, \pm M_o)$ in P, M space, Fig. 6.11(c), as a locus of safe loads without taking into account details of the cross-section geometry: consequently in T, P, M space our best general safe load locus is made up of two intersecting surfaces:

$$\left(\frac{P}{P_o} \pm \frac{M}{M_o}\right)^2 + \left(\frac{T}{T_o}\right)^2 = 1 \tag{6.13}$$

One octant of this surface is shown in Fig. 6.11(d). The surface may be derived from the three two-dimensional loci (Fig. 6.11(a), (b) and (c)) by application of the *convexity* theorem. It is not difficult to extend the "safe" region of T, M, P space in specific simple cases; see Problem 6.8.

It should be pointed out that considerable care is necessary in the discussion of plastic bending of members of arbitrary cross-section, due to the presence of "preferred" or "natural" axes of bending within the section, somewhat analogous to principal axes in the theory of elastic bending.

Problems

6.1. Compare the full plastic torques for several thin-walled tubes all having the same thickness and perimeter, but different shapes. (For example, circle, square, rectangle, triangle.)

6.2. Sketch nesting thin-walled tubes which "fill" some simple solid cross-sections. (For example, circle, square, rectangle, triangle.)

6.3. Evaluate, by determining the appropriate volume, T_p for the cross-sections studied in Problem 6.2.

6.4.† Show that in the "membrane" analogy for elastic torsion (see a textbook on elasticity or one on plasticity which covers elastic–plastic torsion) the contours of the relevant stress function correspond to slits in a decomposition of the cross-section into a set of nesting tubes of variable thickness; and hence that the torque is directly related to the volume enclosed by the "membrane".

6.5. Find the volume indicated by the contours shown in Fig. 6.9(a), and make an estimate of the percentage increase in volume resulting from adoption of the alternative contours shown in Fig. 6.9(b).

(*Hint.* Use an *ad hoc* approximation to the awkwardly-shaped volume.)

6.6. A square shaft with a "keyway" has a cross-section consisting of a square of side $5a$ with a square of side a removed from the middle of one side. Make a safe estimate of the full plastic torque of the shaft, and an (over-)esti-

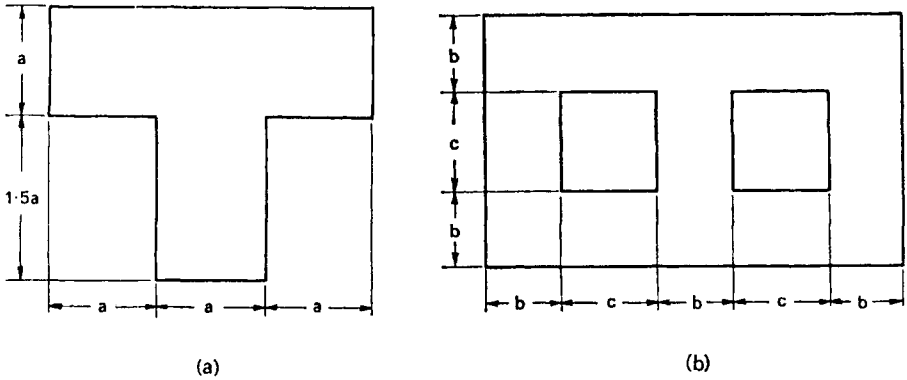

FIG. 6.13. Examples.

mate of the reduction of full plastic torque of a square shaft due to the cutting of the keyway.

6.7.† A short shaft with massive end fittings is subjected to a pure torque. An upper-bound on the full plastic torque may be obtained by considering the simple mechanism in which originally plane sections of the shaft remain plane, and simply rotate relative to each other with no change in axial separation. Apply this calculation to (a) a solid circular shaft and (b) a solid square shaft, and compare the results with the corresponding lower-bound values.

6.8. Consider combined tension (P) and bending (M) of a prismatic member of *rectangular* cross-section, with the axis of the bending moment parallel to one of the edges of the cross-section, and show that a more extensive "safe" region of P, M space than the simple quadrilateral may be obtained. Sketch the corresponding surface in T,P,M space, as in Fig. 6.11(d).

(*Hint.* In pure bending the border between areas of compressive and tensile yield bisects the rectangle. Examine the effect of moving this border parallel to itself.)

6.9. Find a lower bound on T_p for the T-section shown in Fig. 6.13(a).

6.10. Find T_p for the doubly-connected cross-section shown in Fig. 6.13(b), and assess the contribution of the "bridge" to the total.

6.11. Find "safe" combinations of P, T in combined tension and torsion of a square shaft by dividing the shaft into a square inner region sustaining only tension, and an outer square tube sustaining only torsion. Show that this lower-bound approach produces points lying *within* the ellipse of Fig. 6.11(a).

CHAPTER VII

INDENTATION PROBLEMS

IN ITS simplest form the problem studied in the present chapter is: what force applied to a hard die is necessary to form a permanent indentation in the flat surface of a large block of perfectly plastic material?

There are many practical applications of this problem, and we list four important ones below:

(i) In a sense the operation of indenting a surface is a primitive *forming process*, and some practical—but obviously more complicated—forming processes are closely related, in terms of mechanics, to indentation.
(ii) The problem is relevant in a broad sense to the design of foundations in civil engineering.
(iii) The problem forms the basis of the theory of the *hardness* test whereby the yield stress of a material may be determined by making and measuring a microscopic indentation in its surface.
(iv) The analysis is relevant to studies of friction and wear on a microscopic scale.

Supposing we were free to choose a single form of indenter for our study, we would probably select one *circular* in plan, because this would combine a broad similarity to most of the practical situations listed above with a high degree of symmetry.

It turns out, however, somewhat surprisingly, that this sort of (axial) symmetry does not lead to a particularly simple mathematical treatment. On the other hand the mathematical aspects are specially simple when the conditions of deformation are those

of *plane strain*; that is, when the flow of the plastic material is confined, so to speak, between smooth rigid parallel plates which prevent straining in a particular direction. In consequence of these mathematical aspects, most studies of indentation problems have been made in terms of plane strain, and we shall follow suit here. In physical terms the plane strain situation corresponds to indentation by an infinitely long strip punch, something like a long blunt knife.

Although we are persuaded into a study of this somewhat untypical situation by mathematical considerations, it seems reasonable to suppose that the indentation pressures found for problems of plane flow will be broadly similar to those which would occur in the corresponding axisymmetric problems.

Plane plastic flow is in fact one of the most highly developed branches of plasticity theory, largely as a result of the work of Hill in developing and applying the theory of the "slip-line field", a theory whose simplicity is derived largely from the restrictions imposed by plane strain conditions. We shall give a brief outline of this theory in the next chapter, but for the present we shall concentrate on application of the lower- and upper-bound theorems: for engineering purposes the former is appropriate for the safe design of foundations, etc., while the latter is relevant to forming processes.

In fact, arguments which predispose to the study of problems in plane plastic strain on the grounds of mathematical convenience are not nearly so strong when we turn from the derivation of complete solutions to applications of the bound theorems. In the present chapter we consider only "plane strain" problems, but in Chapter X we shall extend application of the upper-bound theorem to axisymmetrical forming processes without much difficulty.

7.1. Upper-bound Approach

First let us attempt an upper-bound solution of our plane-strain indentation problem, shown schematically in Fig. 7.1. The

diagram shows a cross-section of a long "rigid" indenter A being pressed by a force F per unit length into a large block of perfectly plastic material.

The first step in our analysis must be to postulate a geometrically satisfactory mode of deformation of the plastic material. Since movements out of the plane of the paper are ruled out by our assumption of plane strain, we must construct a pattern of deformation in the plane. Evidently if the indenter is to descend and the material is incompressible there must be a gross "sideways and upwards" movement of material.

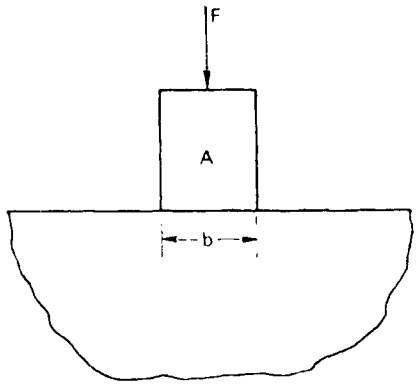

FIG. 7.1. Basic configuration of the indentation problem.

Perhaps the most obvious simple mode is that shown in Fig. 7.2, which is geometrically permissible if there are no external constraints to hold the indenter vertical. The block of material B rotates with angular velocity $\dot{\theta}$ as a rigid body, and there is a semicircular zone of "intense shear" between it and the remainder of the body. The mode is certainly simple, but are we justified in postulating a mechanism with, effectively, a "jump" in tangential velocity across an interface?

To answer this question we consider the "unit" mechanism shown in Fig. 7.3. The rigid top part of this block is moving to the right with velocity v relative to the rigid bottom part, and the

two parts are separated by a zone of plastic deformation of unit area and thickness h, in which the shearing strain rate is uniform. Here, and throughout this chapter, we shall consider unit thickness (perpendicular to the plane of the diagram) of material.

Let us evaluate the rate of dissipation of energy, $\dot{D}$, in this zone of plastic deformation. The mode of deformation is instantaneously one of pure shear; the shear strain rate $\dot{\gamma}$ in the zone is equal to v/h, so the rate of dissipation of energy is equal to

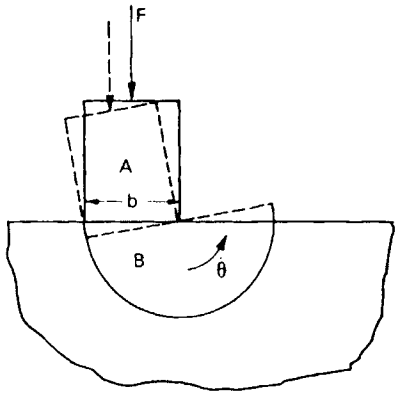

FIG. 7.2. Simple postulated mode of deformation.

kv/h per unit volume, k being the yield stress in pure shear. The volume of the zone is numerically equal to h, so

$$\dot{D} = (kv/h)h = kv \tag{7.1}$$

This equation states that the rate of dissipation of energy per unit area of interface of the narrow zone is the product of the yield stress in pure shear and the relative velocity of the two rigid blocks. Note that, in particular, the expression is independent of the thickness h, so h may be as small as we please, including zero. True, if h is zero $\dot{\gamma}$ will be infinite, but this is quite satisfactory for perfectly plastic (non-hardening) material, which is, of course, the idealised material we must use when we apply the bound theorems. The conceptual advantage of a zone of zero

thickness is that it enables us to consider simple mechanisms consisting of rigid blocks sliding over each other.

The question of whether velocity discontinuities occur in complete solutions, or in reality, is irrelevant in the present context; we are at present simply using a postulated mechanism which is *geometrically* satisfactory (although it may be somewhat *implausible* as a real mode) to obtain an upper bound on an indentation *load.*

Another possible objection to the mode of Fig. 7.2 is that it creates "steps" in the surface of the plastic material. As we shall see, the upper-bound load is independent of the magnitude of the

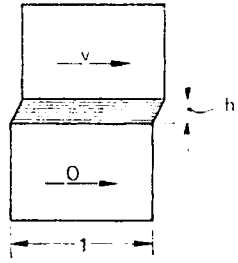

FIG. 7.3. Narrow band of intense shearing.

angular velocity $\dot{\theta}$, so we can regard θ as sufficiently small not to disturb the overall geometry. But by regarding the surface as flat we shall, of course, restrict the scope of our study to the *initial* indentation problem. If we wished to study the forces required to advance the indentation after there had occurred a considerable "pile-up" of material on either side of the indenter, we should have to take into account the shape of the surface.

The upper-bound "work" calculation gives:

$$F^u b\dot{\theta}/2 = kb\dot{\theta}\pi b \tag{7.2}$$

where b is the width of the indenter, Fig. 7.2. The superscript reminds us that we are finding an upper bound on F. From (7.2)

$$F^u = 2\pi kb = 6{\cdot}29kb \tag{7.3}$$

We have thus obtained, very simply, an upper bound on the indentation force per unit length of indenter.

Now the mechanism of Fig. 7.2 may easily be generalised by regarding the radius and position of the centre of the circle as variables; and we could try out several possibilities in the hope of finding a lower, and therefore better, upper bound; see Problem 7.1.

Before we move on to consider other modes which do not involve rotation of the indenter we note that "slip circle" failures of this sort—in which whole buildings, docks, embankments or hillsides tilt and descend—have occurred on soft clays in many parts of the world. In using upper-bound methods to study problems of this sort we must be aware that the *self-weight* of the soil may play an important part (see Problem 7.2). In the present book we ignore the self-weight of the material in comparison with the indentation forces, which is almost always justified in mechanical engineering situations.

The next simple mode of deformation we use is shown in Fig. 7.4. As in the previous mode all the internal dissipation of energy takes place at *interfaces* between rigid blocks, but now there are several blocks, and all of the interfaces are plane. In Fig. 7.4(a) all of the blocks are shown equilateral, for convenience of calculation, but they could obviously have been drawn in many different ways.

To evaluate the dissipation of energy we need to know the relative (sliding) velocities between adjacent blocks. The most direct way of determining these is by means of a velocity diagram (or hodograph), as shown in Fig. 7.4(b).

Each of the blocks in Fig. 7.4(a) is labelled with a capital letter, and the zone which remains stationary is labelled O. In the velocity diagram, Fig. 7.4(b), the velocity of each block is represented by a single point (as the blocks do not rotate) which is labelled with the corresponding lower-case letter. The velocity diagram has the general property that the vector joining two points represents the *relative* velocity of the corresponding blocks.

We construct the diagram as follows. The velocity of the in-

denter is first drawn as *oa* to a convenient arbitrary scale, and in the correct orientation with respect to the layout of Fig. 7.4(a). There is no *need* in the present example for the velocity of the punch to be vertical, but by making *oa* vertical we impart a simplifying symmetry to the velocity diagram. Relative to *A*, block *B* may only move horizontally, because otherwise a gap would open between *A* and *B*. Again for simplicity we assume

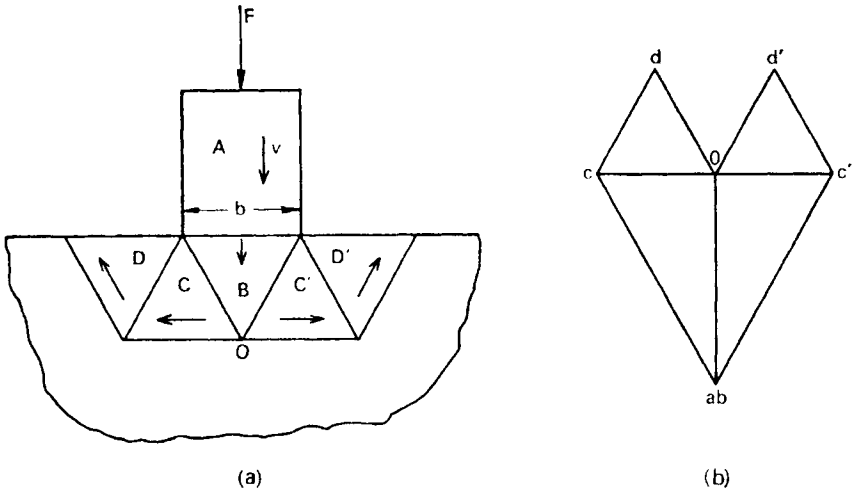

FIG. 7.4. Simple "rigid-block" mode of deformation and associated velocity diagram.

that *B* descends vertically—in effect as an "extension" of the indenter. Thus in the velocity diagram points *a* and *b* coincide. We next fix point *c*. The directions of the velocity of *C* relative to *B* and *O* are the same as the directions of the corresponding interfaces—since our mechanism involves only sliding, with no *separation* of the blocks—so the position of *c* is determined uniquely from *b* and *o*, as shown. Similarly *d* is located from *c* and *o*. The points *c'*, *d'* are located either by symmetry or by direct construction.

Using the notation l_{BC} for the length of the interface between

blocks B and C, etc., we write down the work equation for unit thickness of material, making use of symmetry:

$$F^u\, oa = 2k\{bc.l_{BC} + co.l_{CO} + cd.l_{CD} + do.l_{DO}\} \qquad (7.4)$$

Each of the terms on the R.H.S. is positive, so there is no occasion for difficulty over signs when the expression comes to be evaluated.

Clearly the absolute size of the velocity diagram, and indeed the magnitude of the indentation velocity, are immaterial.

In the present case the trigonometry of the velocity diagram is especially simple, and we write down by inspection

$$oc/oa = 1/\sqrt{3}, \text{ etc.} \qquad (7.5)$$

Also
$$l_{BC} = l_{CO} = \ldots = b \qquad (7.6)$$

so

$$F^u = 2kb(2/\sqrt{3} + 1/\sqrt{3} + 1/\sqrt{3} + 1/\sqrt{3})$$

$$= (10/\sqrt{3})kb = 5{\cdot}76\, kb \qquad (7.7)$$

This bound is about 8 per cent lower than the one corresponding to the simple "slip circle".

A possible objection to the mechanism of Fig. 7.4(a) is that the block B cannot descend, since its lower edge is already in contact with region O. The answer to this is that the contradiction disappears if the interfaces are given small but finite widths (Problem 7.3). The magnitude of the incremental motion of the mechanism is in any case irrelevant to the calculation.

It is clear that if these calculations were repeated (a drawing board would be useful) for mechanisms of the same family, but with the interfaces at various different inclinations, a minimum value of F^u could, in principle, be found. A partial minimisation may easily be accomplished analytically (Problem 7.4) by keeping all the triangles congruent but varying their depth. The value of

F^u may be decreased by only 2 per cent in this way, but the depth of the triangles in the corresponding mode is about 20 per cent less than that of equilateral triangles. In other words the minimum is a "flat" one, and a wide variety of geometries within the same family would be expected to yield only slightly different upper bounds.

Now the least value of F^u for *all possible* mechanisms will be the exact value of F, and in particular the corresponding distribution of stress will be in equilibrium. It is clear that equilibrium cannot possibly be satisfied in the neighbourhood of the intersection of three slip planes in Fig. 7.4(a), because this would require maximum shearing stress to occur on planes not mutually perpendicular, which is impossible by the Mohr circle construction (Appendix I). Thus, however hard we try to find the optimum layout in this family of modes, we know that we shall never achieve the *exact* value of F. This, of course, is not particularly disconcerting if, as engineers, we are not primarily interested in accuracy for its own sake.

7.2. Lower-bound Approach

Let us now attempt a lower-bound solution of the same indentation problem, by constructing simple equilibrium distributions of stress which do not violate the yield condition. We shall use the idea of "blocks" over which the stress does not vary—which are therefore automatically in equilibrium internally (in the absence of self-weight of the material)—and exploit the possibility of *discontinuity* of stress between adjacent blocks.

First we consider the possibility that the stress systems on two sides of a plane may be different, but yet in equilibrium. Fig. 7.5(a) represents such a boundary plane and the states of stress on either side, which are referred to t, n axes, tangential and normal to the boundary, respectively. In plane strain the direction normal to the paper is a principal direction of stress, so to study equilibrium across the boundary we only need to consider equilibrium in the plane of the paper.

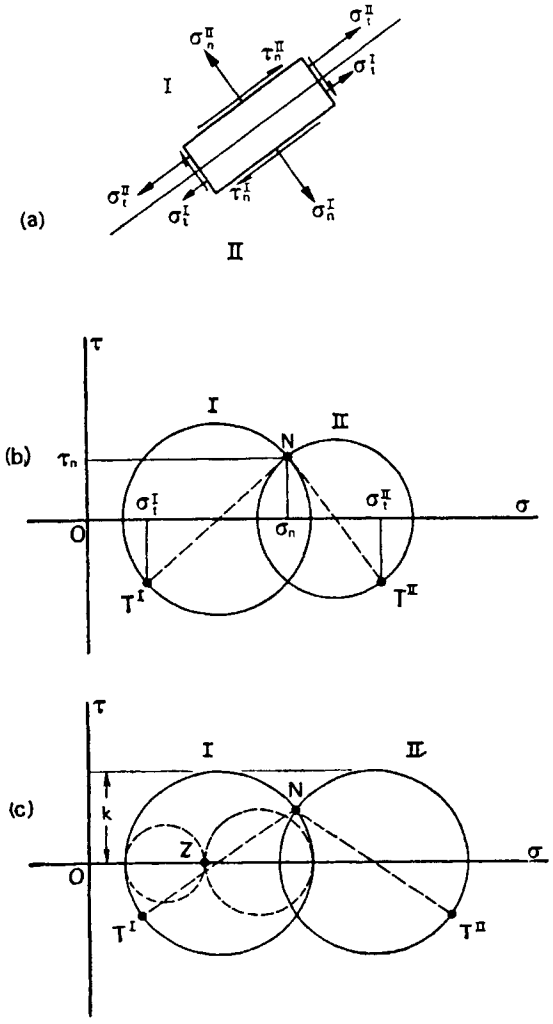

FIG. 7.5. Discontinuity of stress across an interface.

Resolving in the n and t directions for a small block as shown we have

$$\sigma_n^{\mathrm{I}} = \sigma_n^{\mathrm{II}} \tag{7.8}$$

and

$$\tau_n^{\mathrm{I}} = \tau_n^{\mathrm{II}} \tag{7.9}$$

where the superscripts denote the zones. By taking moments about any point we simply obtain the "complementary shear" relationship (Appendix I).

Note that the stress components σ_t cannot be brought—in a non-trivial way—into these equations. We must conclude therefore that as far as *equilibrium* is concerned we may have a *discontinuity* in the σ_t component across the boundary, although the other components of stress, σ_n and τ_n, must be continuous across the boundary, from (7.8) and (7.9).

The situation is illustrated clearly by the Mohr circle diagram for stress, Fig. 7.5(b): the two stress components σ_n, τ_n coincide at the interface, but the two states of stress, represented by circles I and II, may nevertheless be different.

On the whole in applying the lower-bound theorem it will be advantageous if the material is at the yield point on both sides of a boundary of this sort, in which case the two Mohr circles will have the same radius, k, as shown in Fig. 7.5(c). In this case, by simple geometry applied to the circles, the axes of principal stress in the two regions form mirror images of each other in the boundary (see Problem 7.5).

It is important to realise that this diagram applies only to the *plane strain* situation we are discussing. Because there is no possibility of straining in the z direction, perpendicular to the plane of the diagram, σ_z is always the *intermediate* principal stress (on Tresca's criterion: see (2.12) on p. 42), so the Mohr circles shown are in fact always the *largest* of the three circles needed to describe the state of stress completely; see Appendix I. The dotted circles corresponding to region I are included in Fig. 7.5(c) as a reminder. If we were dealing with a state of *plane stress*, in which $\sigma_z = 0$, then it would not be true, necessarily, that σ_z was the intermediate principal stress, and the lower-bound analysis in the present chapter would not be correct in general; see Problem 2.15.

Diagram 7.5(c)—and consequently the whole of the remainder of the present analysis—is also valid (with a small modification; see Problem 7.6) for the Mises yield condition.

7.3. A Simpler Problem

Consider for the moment the simpler problem of a flat surface of infinite extent, loaded by pressure q extending indefinitely in one direction, as shown in Fig. 7.6(a). The simplest possible equilibrium distribution of stress is found by having a vertical plane of discontinuity between zones I and II, and postulating zone I to be stress-free. In this case the Mohr circles are as shown in Fig. 7.6(b), circle II having been drawn as large as possible (radius k)

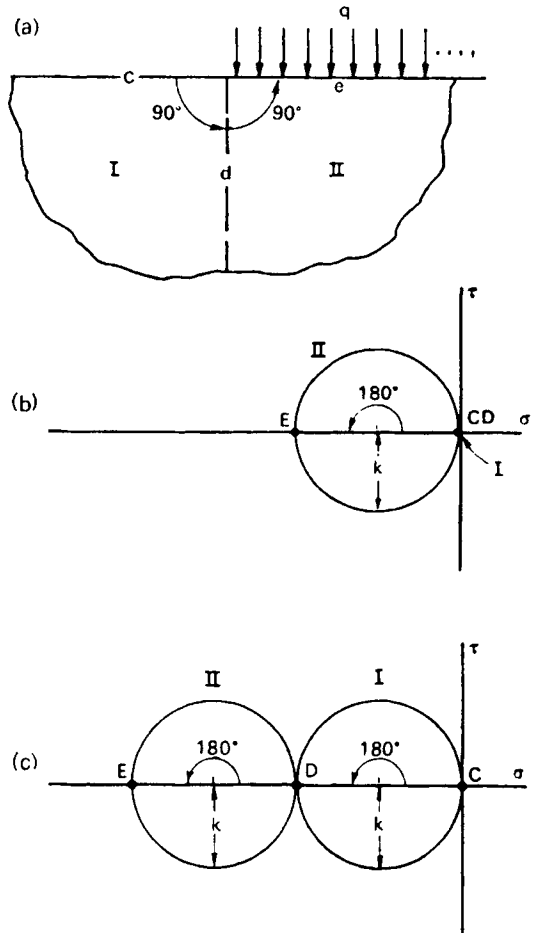

FIG. 7.6. Lower-bound stress field for a partly-loaded surface.

and circle I vanishingly small. Note the correspondence between the points on the circles and the planes to which they refer (see Appendix I). The diagram is thus a special case of Fig. 7.5(b), and we find

$$q^{\prime} = 2k \tag{7.10}$$

by reading off from Fig. 7.6(b) the state of stress on plane e of Fig. 7.6(a).

This result obviously corresponds to an effective "removal" of zone I, and pure uniaxial compression of zone II.

We can very easily obtain a better lower bound by setting the stress in zone I at yield, as shown in Fig. 7.6(c). Here the stress-free surface c fixes the point C on circle I. For the lower bound of Fig. 7.6(b) to be improved, E must move to the left in diagram, so it is clear that circle I should extend to the left rather than the right. The reader should indicate the stress systems in the two regions by sketching a small principal stress element in each.

The result

$$q^{\prime} = 4k \tag{7.11}$$

is an obvious improvement on the previous one, but it does of course assume that the body of plastic material is so large that the stress components in the horizontal direction can be sustained. This solution can clearly be adapted to the problem of a finite indenter by having a zone II "sandwiched" between two zones I. As the indenter is supposed to be rigid, or at least to have a yield stress much higher than that of the material beneath it, equilibrium of the punch gives

$$F^{\prime} = 4kb \tag{7.12}$$

This load is only about 2/3 of the upper-bound loads already calculated, which is perhaps a little disappointing.

Let us therefore explore the possibility of improving the lower bound $q^{\prime}$ by using *more than one* plane of discontinuity of tangential stress. Tentatively we replace plane d, Fig. 7.6(a), by two planes equally inclined to the vertical at a small angle ϕ, and

thus enclosing a third zone, as shown in Fig. 7.7(a). By using the "double angle" rule (see Appendix I) on Fig. 7.7(a) we obtain the Mohr circles of Fig. 7.7(b). In fact we need not have drawn the diagram symmetrically, but by putting the centre of circle II in any other place we would have found that point F was off the σ

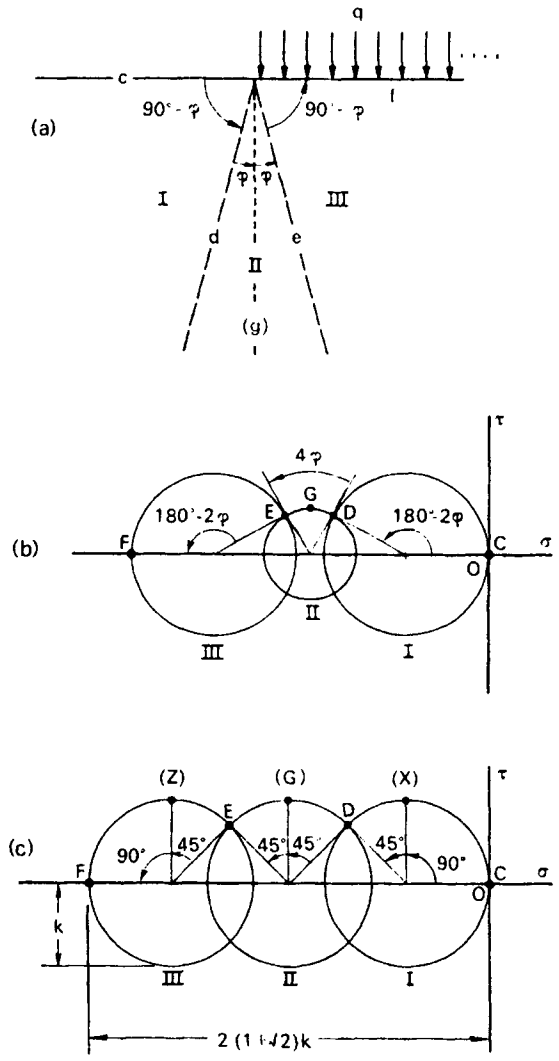

FIG. 7.7. A stress field with two planes of discontinuity.

axis, which would have violated the stress boundary condition on plane *f*. Note that the angle subtended by *DG* at the centre of circle II (*g* being the vertical plane in Fig. 7.7(a), and not a plane of discontinuity) is 2ϕ, and so, by simple geometry, the angle subtended at *D* by the centres of circles I and II is a right-angle, as indicated: this gives a way of locating the centre of circle II for any value of ϕ.

Clearly two planes of discontinuity are better than one from the present point of view because the two "original" circles are "pushed apart" by the circle corresponding to the newly-formed zone. As ϕ increases the new circle becomes larger, and clearly when $\phi = 22{\cdot}5°$ the new circle has grown to its largest allowable radius, *k*, as shown in Fig. 7.7(c). This gives

$$q' = (2 + 2\sqrt{2})k = 4{\cdot}83\,k \tag{7.13}$$

which is a substantial (20 per cent) increase on the previous value.

Holding in abeyance the question of whether this solution can be adapted to the problem of the finite indenter, let us see whether a further improvement may be made by having *three* planes of stress discontinuity, as shown in Fig. 7.8(a). The Mohr diagram will now have four circles, disposed as in Fig. 7.8(b), but not necessarily touching. The location of the circles and the corresponding planes is most easily done by making use of the two auxiliary planes *x* and *z* inclined at 45° to the horizontal and the corresponding points on the circle diagram, as shown. The angle between planes *x* and *z* is 90°, so the *total* angle subtended by the arcs *XD*, *DE*, *EF* and *FZ* at the centres of their respective circles must be 180°. With the circles equally spaced all six angles marked with a cross in Fig. 7.8(b) are equal, and therefore equal to 30°; thus the angles between planes *d*, *e* and *f* must be 30°, by inspection. The circles therefore touch in pairs, as shown, and in particular

$$q' = 5k \tag{7.14}$$

which is a further improvement of about 3 per cent on the previous lower bound.

We now investigate whether the two previous solutions are adaptable to the problem of the finite indenter. Figure 7.9(a) shows the obvious "overlapping" arrangement of planes corresponding to Fig. 7.7, and the reader should check that it does

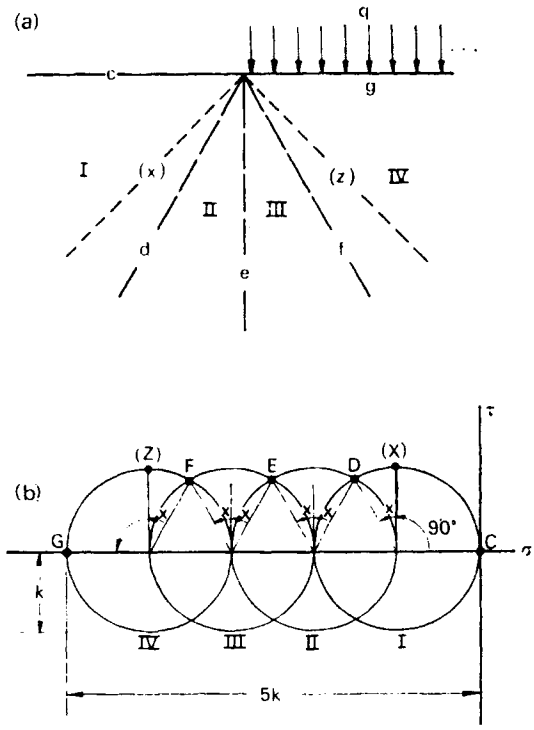

FIG. 7.8. A stress field with three planes of discontinuity.

indeed satisfy all the inter-region boundary conditions. Note that the planes *g* and *d*, which are *geometrically* the same, have different stresses acting across them.

The corresponding check for Fig. 7.8(a) is also satisfactory, but it is more complicated, Fig. 7.9(b). In this case we find that there is a zone of hydrostatic compression beneath the indenter, represented by a *point* in the Mohr circle diagram.

As both solutions are thus adaptable to the indenter we have

$$\left.\begin{aligned} F^{I} &= 4{\cdot}83kb \\ F^{I} &= 5kb \end{aligned}\right\} \qquad (7.15)$$

Taken together with the result (7.12) corresponding to a single plane of discontinuity we detect a strong law of "diminishing returns" as the number of planes of discontinuity is increased: progressively smaller increases in the lower-bound load are made at the expense of progressively more labour.

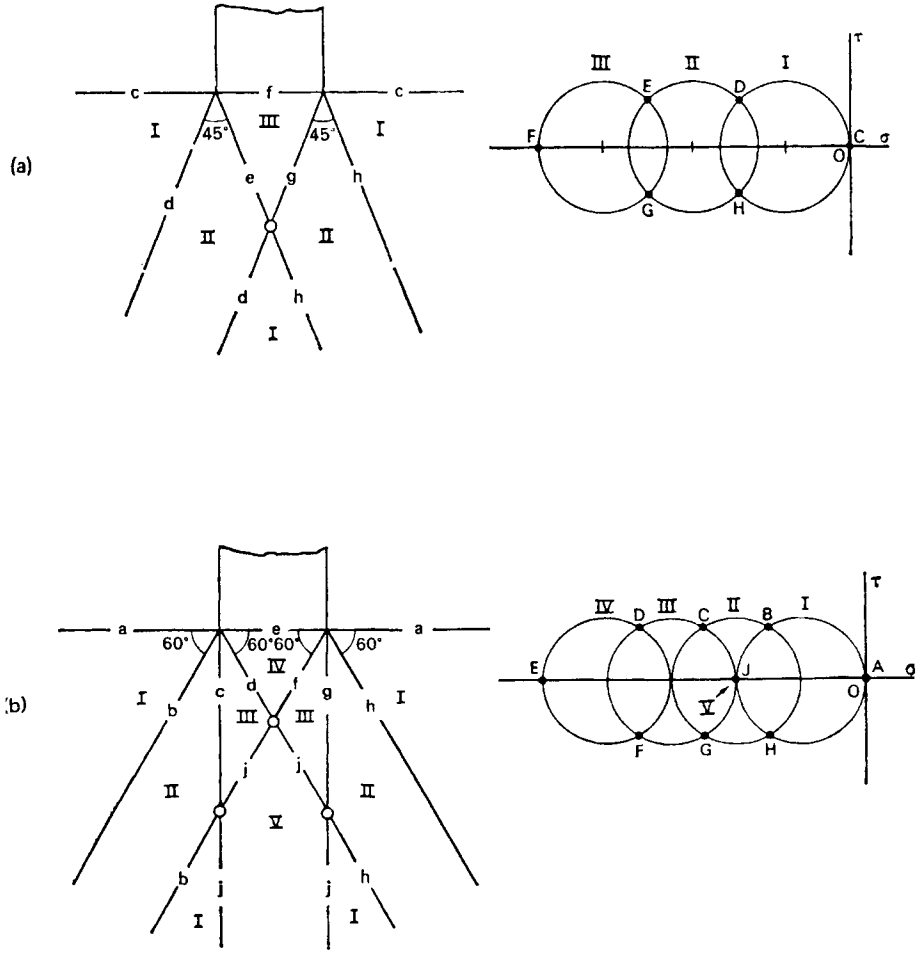

FIG. 7.9. Stress fields for the indentation problem.

At what stage an engineer would "stick" in this succession of lower-bound calculations depends to some extent on how busy he is and how much he enjoys doing calculations. A good case may be made for stopping after the *first* attempt if a quick estimate only is required.

7.4. Experimental Confirmation: the Hardness Test

In hardness testing a strong indenter, usually in the form of a wide-angled pyramid or a sphere, is pressed into the surface of a specimen by a known force, and the force divided by the area of the resulting impression is taken to be a measure of the hardness of the material. The indenter is usually small, and the size of the impression is measured microscopically.

Now in spite of obvious points of difference, there is a broad similarity between this sort of test and the problem we have been studying Fig. 7.1. The convexity of the indenter—which ensures that the effective width automatically adjusts itself to the applied force—should not make too much difference to the behaviour, provided the indenter may be classified as "blunt".

Experimental studies of the hardness test applied to a wide range of materials have shown that there is indeed a simple relation between the average pressure on the indenter and the yield stress of the material as measured in the tensile or compression test: see the book by Bowden and Tabor listed in the Bibliography. The ratio of indentation pressure to tensile yield stress is rather insensitive to the pyramid angle (in the "blunt" region) and to the degree of lubrication (or friction), and is generally in the region 2·5 to 3, corresponding to a ratio of indentation pressure to yield stress in pure shear in the region 4·5 to 6 (depending on whether $Y = 2k$ (Tresca), or $Y = \sqrt{3}k$ (Mises)). In the case of a rapidly strain-hardening material (like annealed copper at small strain) an "equivalent" yield stress must be estimated with regard to the average amount of strain occurring under the indenter. When this has been done the ratio defined above is found to be insensitive to the degree of strain hardening.

This provides a major justification for the use of a perfectly plastic (i.e. non-hardening) idealisation of strongly strain-hardening material, provided the yield stress is chosen intelligently.

In spite of the fact that our studies have been in terms of plane strain, we can regard them as agreeing broadly with a substantial amount of experimental evidence from hardness testing.

7.5. Indentation of Finite Blocks of Plastic Material

A feature of the plane-strain indentation problem we have been studying so far is that the dimensions of the block of plastic material, both in width and depth, are large compared to the width of the indenter. While this feature applies to micro-hardness testing, it is clear that in many other situations we are interested in the indentation of blocks whose dimensions are of the same order of magnitude as those of the indenter.

It is clear from one of the corollaries of the lower-bound theorem (p. 111) that for a given size of indenter the indentation load can only decrease as the size of the block decreases: but it also seems clear, intuitively, that the rate of decrease of load with dimensions is probably small when the block is large.

When the block is the *same* width as the indenter, the indentation pressure is clearly equal to the (plane-strain) yield stress of the material, so the total range of indentation pressure as the size of the block is reduced is about a factor of 3.

For the sake of simplicity we shall study only two finite-block geometries: compression of a sheet between equal and opposite dies (Fig. 7.10(a)) and indentation of a narrow block (Fig. 7.10(b)). Both of these will again be treated as problems in plane strain.

From the lower-bound point of view we solve both problems by using the "compact" discontinuous stress field shown in Fig. 7.11. In zones I, edge c is stress-free, so the Mohr circle at yield is fixed. Because c and e are planes of principal stress the discontinuity plane d must bisect the angle between them; similarly, f bisects the angle between c and g. But the enclosed angles between planes e, c and c, g add up to 180°, so $\theta + \phi = 90°$ in Fig.7.11(a);

consequently planes d and f are mutually perpendicular. This property imparts some symmetry to the Mohr circle diagram, Fig. 7.11(b), and we readily find that

$$\left.\begin{aligned}\sigma_x &= 4k \sin^2\phi \\ \sigma_y &= 4k \cos^2\phi\end{aligned}\right\} \tag{7.16}$$

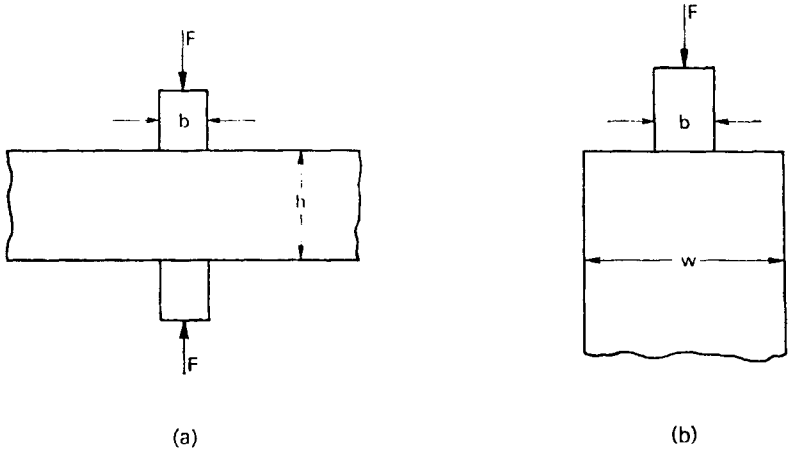

FIG. 7.10. Indentation of a sheet and of a narrow block of plastic material.

It should be noted that

$$45° \leqslant \phi \leqslant 90° \tag{7.17}$$

so that $$\sin\phi \geqslant \cos\phi$$

The trigonometry of Fig. 7.11(a) is simple, and the dimensions indicated are readily worked out in terms of b and ϕ. It is instructive to make several simple checks on this diagram: see Problem 7.7.

Two such stress fields back-to-back (i.e. mirror images in plane g) are suitable for a study of the sheet problem, Fig. 7.10(a), the remainder of the sheet being regarded as stress-free. If h is the

thickness of the sheet, comparison of Figs. 7.11(a) and 7.10(a) gives

$$\tan \phi = h/2b \tag{7.18}$$

so, using Pythagoras' theorem and substituting in (7.16) we have

$$F^l = 4kb \Big/ \left(1 + \left(\frac{2b}{h}\right)^2\right) \tag{7.19}$$

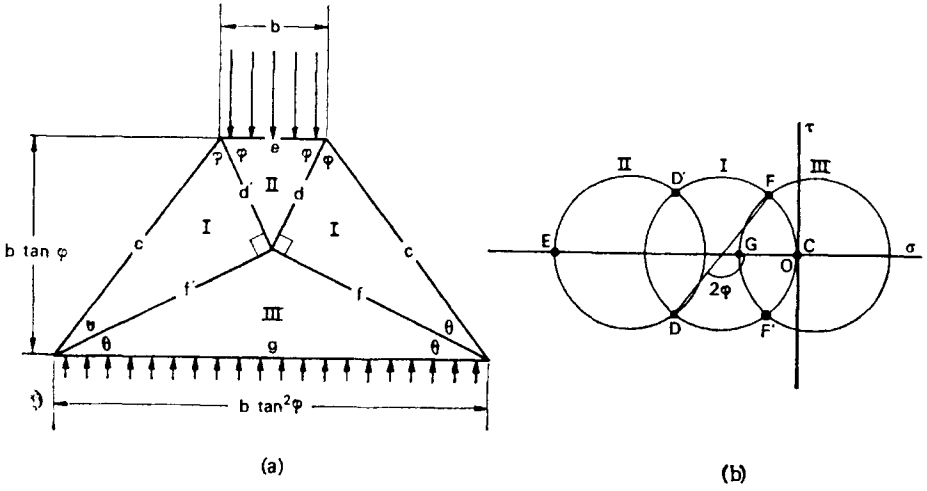

FIG. 7.11. A simple "compact" stress field.

Similarly, fitting the field 7.11(a) into the top of the narrow block, Fig. 7.10(b), and supporting it on a uniformly stressed rectangular section—which is "safe" because $\sigma_g \leqslant 2k$, from (7.16) and (7.17)—we find

$$F^l = 4kb \Big/ \left(1 + \left(\frac{b}{w}\right)\right) \tag{7.20}$$

When the block is large in either direction, both of these formulas indicate

$$F^l \to 4kb \tag{7.21}$$

which is the same as the *lowest* of our earlier lower bounds.

We turn now to upper-bound calculations, and first consider compression of a sheet between dies, Fig. 7.10(a). In contrast to the situation of Fig. 7.1 there is now the possibility of the halves of the sheet moving apart, bodily, and the mechanism of Fig.

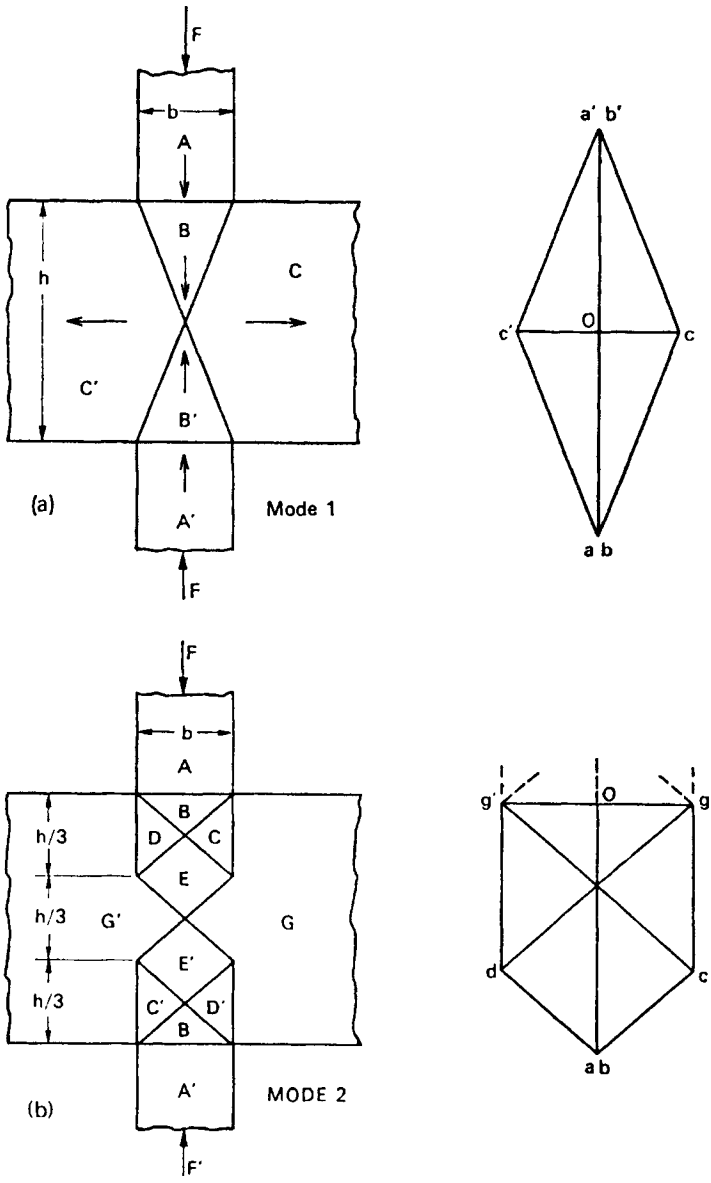

FIG. 7.12. Upper-bound modes for indentation of a sheet.

7.12(a) almost suggests itself. The velocity diagram is as shown and we find, after a simple calculation,

$$F^u = kb\,(b/h + h/b) \tag{7.22}$$

This mode has no "degrees of freedom" and it becomes somewhat implausible for larger values of h/b. A simple alternative is shown in Fig. 7.12(b), and the corresponding calculation (Problem 7.8) gives

$$F^u = kb\left(3\,b/h + \frac{7}{9}h/b\right) \tag{7.23}$$

which furnishes a lower upper-bound than (7.22) for $h/b > 3$.

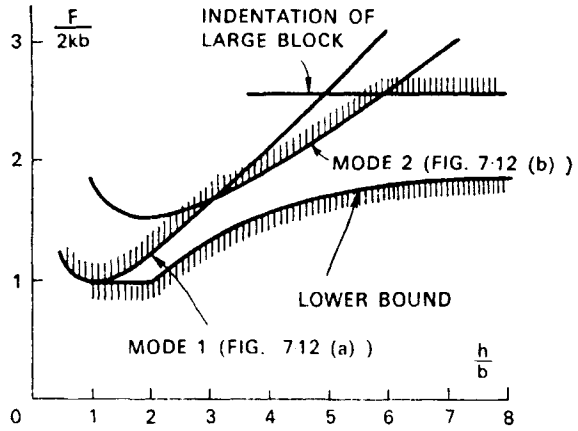

FIG. 7.13. Indentation of a sheet: results (see Fig. 7.10 (a)).

These two results, together with the lower bound (7.19), are plotted in Fig. 7.13, together with the optimised result (Problem 7.4) from the mode of Fig. 7.4(a). The upper and lower bounds are not particularly close in general, but the diagram gives, nevertheless, a fairly clear impression of the part played by the thickness of the sheet in the indentation behaviour.

The method of the slip line field, described in the next chapter, gives the "exact" indentation force for the semi-infinite block:

$$F = kb\,(2 + \pi) \simeq 5{\cdot}14\,kb \tag{7.24}$$

The upper-bound calculation is fairly close to this, and we have

already observed that the lower bound (7.19) is not particularly good when $h/b \to \infty$. It seems probable therefore that the exact result lies closer to the upper bound in Fig. 7.13 than to the lower bound, and indeed this is precisely what is found when the slip-line method is applied to the general problem.

Turning now to the problem of indentation of a narrow block, Fig. 7.10(b) we postulate the two simple mechanisms shown in

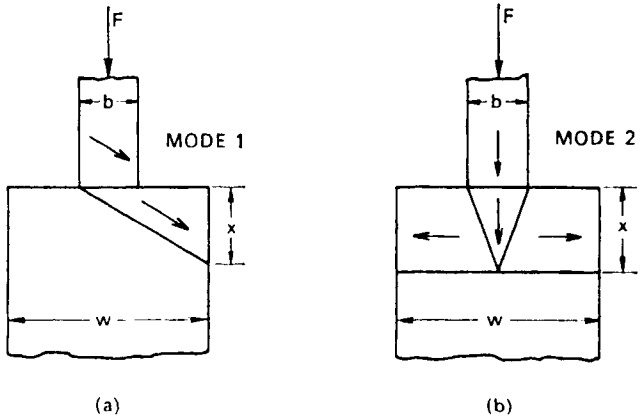

FIG. 7.14. Upper-bound modes for indentation of a narrow block.

Fig. 7.14 (see also Problem 7.9), each having a single degree of freedom, as indicated.

In calculations of this sort it is usually most convenient (as pointed out in Problem 7.4) to take a *length* (in these cases x) as the variable parameter, rather than an *angle*, because the final expression turns out to be simple by virtue of Pythagoras' theorem. The optimisation is then correspondingly easy.

The following results are obtained:

$$\left.\begin{aligned} F^u &= kb\,(1 + w/b), && \text{mode 1} \\ F^u &= 2kb\,(1 + w/b)^{\frac{1}{2}}, && \text{mode 2} \end{aligned}\right\} \qquad (7.25)$$

These are plotted in Fig. 7.15, and the same general remarks apply as to Fig. 7.13.

7.6 The Effects of Friction

So far in this chapter we have not mentioned, except in passing, the effect on indentation of friction between the die and the plastic material.

We are in fact at a disadvantage in applying the bound theorems to situations where friction plays an important part, because these theorems cannot normally be applied in the presence of friction. We shall examine briefly the reason for this, and then go

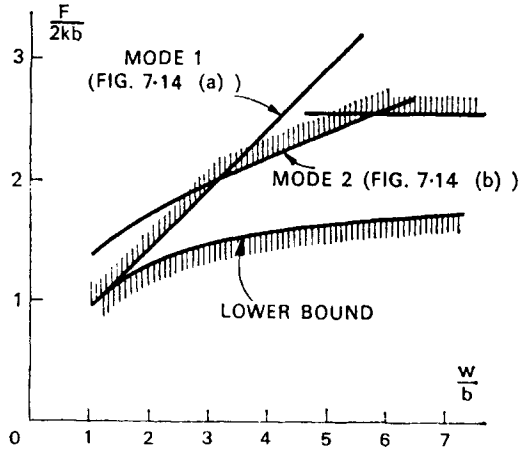

FIG. 7.15. Indentation of a narrow block: results (see Fig. 7.10 (b)).

on to see how we can, nevertheless, obtain a limited amount of useful information about friction effects by use of the theorems.

An essential point in the proofs of the bound theorems (Chapter IV) is the *normality* relationship between yield stress and plastic strain increment; without this condition the theorems cannot be proved in general. Now a block sliding on a rough plane, Fig. 7.16(a), bears a superficial resemblance to a block on a plastically deforming interface, as in Fig. 7.3. There is an important difference, however, between the two situations in that the critical shearing stress for a *plastic* material is independent of the hydrostatic pressure, whereas in *friction* the shearing force, Q,

is a function of the normal force P. The functional relationship may usually be idealised as $Q = \mu P$, where μ is the *coefficient of friction*. This line in P, Q space, in so far as it is the boundary of a zone in which no motion takes place, and beyond which a load point (P, Q) cannot pass, is analogous to a *yield* surface for a perfectly plastic material. Any sliding of the block along the plane gives a corresponding increment of irreversible deformation, but as the block slides *along* the plane there is no component of deformation in the direction corresponding to P, as indicated in Fig. 7.16(b). The "displacement" vector is thus *not* normal to the

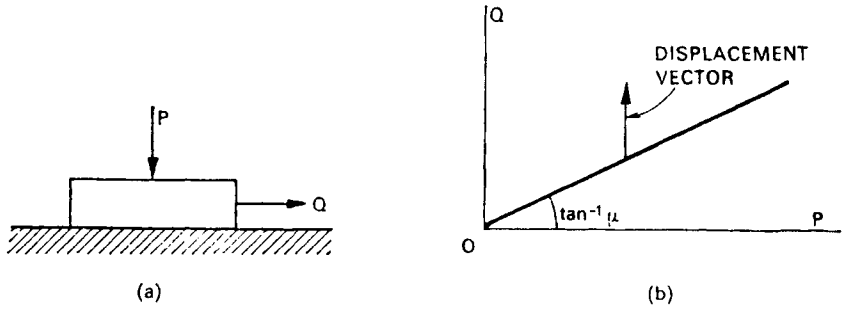

FIG. 7.16. Friction between a block and a plane.

"yield curve" for friction, except in the special case $\mu = 0$, i.e. frictionless sliding.

This lack of normality frustrates any attempt to extend the bound theorems to systems in which there are frictional elements, and so, consequently, such systems are not susceptible to analysis by the limit theorems.

There is—fortunately—an easy and relatively satisfactory way out of this difficulty, because the special values zero and infinity of the coefficient of friction are in fact within the scope of the theorems: zero because—as we have seen—normality does apply as a special case, and infinity because it corresponds to a "bonding" or "welding" of the interface, and any "sliding" must therefore be

of the plastic kind. For simplicity we shall call these two conditions "smooth" and "rough", respectively.

It seems clear that the actual behaviour in the presence of a finite coefficient of friction will lie between the behaviour corresponding to these "extreme" conditions. If, then, we can show in any particular case that the range between upper and lower bounds is not affected much by the question of whether the die is rough or smooth, it is likely that friction is of only secondary importance in the determination of the behaviour of the system. On the other hand, if we find that there *is* a large difference between the bounds corresponding to rough and smooth dies, this will indicate that friction plays an important part, and it may then be necessary to use approximate intuitive methods for assessing the effect of any particular coefficient of friction.

The corollaries of the bound theorems given on p. 111 may be applied to directly the present situation as follows:

A lower bound for "smooth" dies will also be a lower bound for "rough" dies.

An upper bound for "rough" dies will also be an upper bound for "smooth" dies.

Examination of the calculations done so far in this chapter reveals that in all lower-bound calculations we have taken the die face to be a plane of principal stress; consequently our calculations are "safe" for smooth dies and hence also for "rough" dies. Further in all our postulated mechanisms for upper-bound calculations we have not had any *sliding* of material over the die face. These calculations apply equally therefore to rough and smooth dies. (It is not difficult to devise simple mechanisms which do involve sliding on the die face, and some are suggested in Problem 7.10.)

In all of the situations we have considered, therefore, it seems fairly clear that, since our upper- and lower-bound indentation loads have all been fairly "close", the effect of friction on the indentation force is of secondary importance.

7.7. Compression of a Thin Sheet between Broad Dies

We now consider a problem in which, as we shall see, friction is of primary importance. A thin plate is compressed in plane strain between broad dies, as indicated in Fig. 7.17. As in Fig. 7.10(a) h is the thickness of the plate and b the breadth of the dies, but now $b/h > 1$.

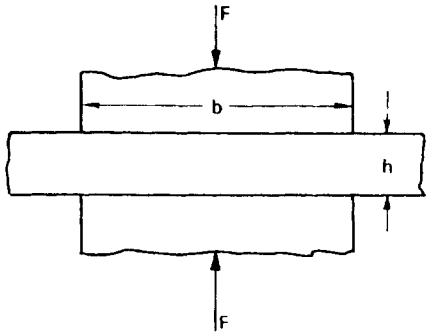

FIG. 7.17. Compression of a sheet between smooth dies.

First let us study the smooth-die case. The mode already studied in Fig. 7.12(a) applies, of course, to all values of b/h, and the corresponding upper-bound, given by (7.22), is plotted in Fig. 7.18. The same calculation also applies to a "double" mode,

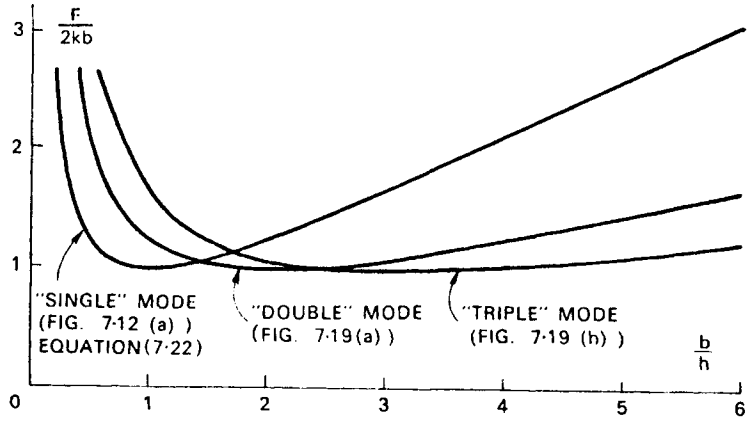

FIG. 7.18. Compression of a sheet between smooth dies: envelope of upper-bound calculations.

as in Fig. 7.19(a), because the lateral displacements of zones *B*—which are necessary for compatibility—do not involve any additional dissipation of energy if the dies are smooth. Equation (7.22), with $b/2$ substituted for b is thus also an upper bound; and indeed the same argument applies for any integral number of elementary modes (see, for example, Fig. 7.19(b)) as indicated in Fig. 7.18.

The most striking feature of this combined upper-bound—i.e.

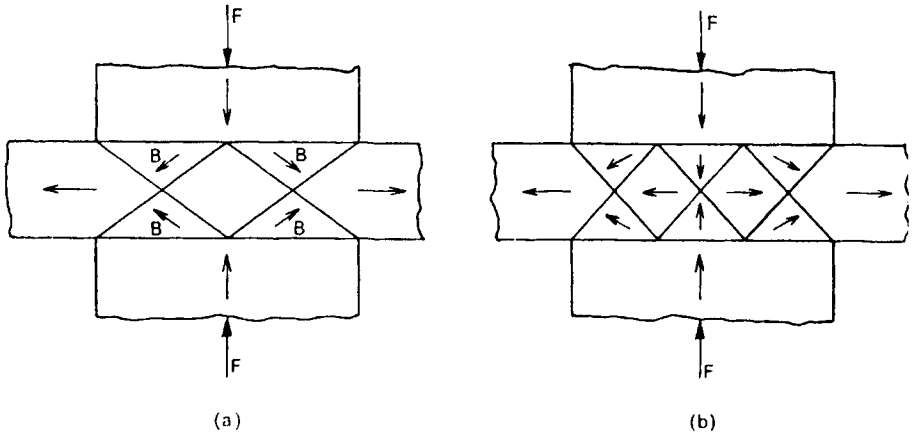

FIG. 7.19. Upper-bound modes for compression of a sheet between rough dies.

the *lowest* of the three curves at any b/h—is that it differs by very little from a *constant* value for the whole range $b > h$. At integral values of b/h, with the interfaces inclined at 45° to the die faces, we have, simply,

$$F^u = 2kb \tag{7.26}$$

A lower-bound solution is exceptionally simple: a constant stress in the part of the sheet between the dies gives, trivially,

$$F^l = 2kb \tag{7.27a}$$

Thus, for smooth dies there is very little difference between the upper- and lower-bound loads, and the "squeezing" load per unit area is practically independent of the ratio b/h.

For rough dies the situation is very different. For upper-bound calculations the multiple modes of Fig. 7.19 may be used, but terms corresponding to sliding at the die surface must be included in the calculation of dissipation of energy. For simplicity we shall investigate only *integral* values of b/h, and modes involving slip planes inclined at 45° to the die faces; more general forms of the modes may readily be studied, and a family of overlapping curves like that of Fig. 7.18 found.

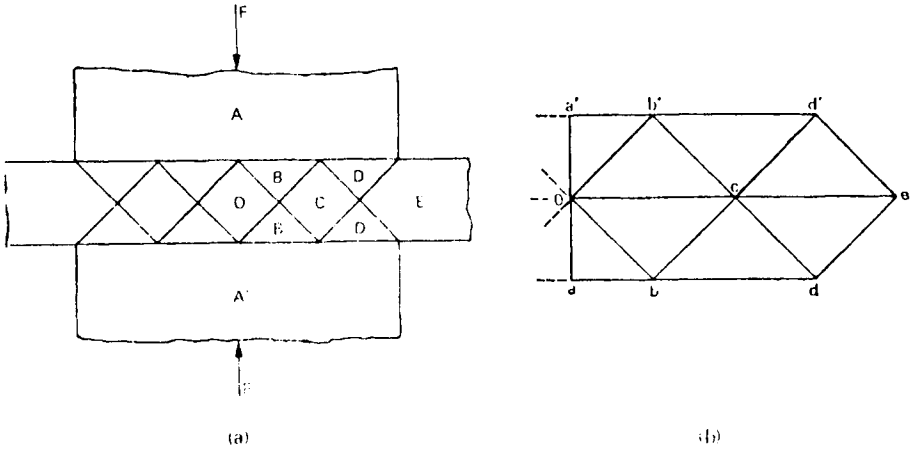

(a) (b)

FIG. 7.20. Compression of a sheet between rough dies: an "even" mode and the corresponding velocity diagram.

For example, Fig. 7.20 shows the mode for $b = 4h$ and the associated velocity diagram. An upper-bound calculation gives

$$F^u = 4kb \tag{7.27b}$$

It is clearly not difficult to generalise this calculation to situations where $b/h = 2n$ (n an integer): the dissipation at the face of the die involves summation of an arithmetic progression and the result is

$$F^u = 2kb\,(1 + b/4h), \qquad b/h = 2n \tag{7.28a}$$

When b/h is an odd integer, another calculation on similar lines gives

$$F^u = 2kb\,(1 + b/4h - h/4b) \tag{7.28b}$$

These two results are plotted in Fig. 7.21, and in spite of the fact that our upper bound is not a continuous function of b/h a clear picture emerges.

We now seek a lower-bound solution of the same problem, as shown in Fig. 7.22. Supposing the material beyond the edges of the die to be stress-free, we have plane c as a plane of principal stress in particular. On planes d and e we shall make full use of the "rough" boundary condition and have maximum shearing

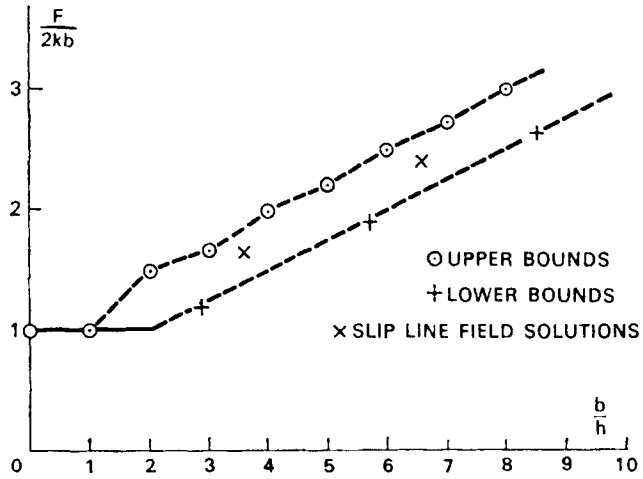

FIG. 7.21. Compression of a sheet between rough dies: results (see Fig. 7.17).

stress. The planes of stress discontinuity f and g must therefore intervene, and as the total angle subtended by arcs CG and GE at the centres of the respective Mohr circles must be 180°, we find that the planes f and g must be inclined at $22\frac{1}{2}°$ to the die faces, as shown. The normal pressure on the die faces given by the analysis so far is thus $k(1 + \sqrt{2})$, by inspection. We hope to increase the die pressure towards the centre of the dies, so we try to terminate zones II in as small a distance as possible. This is done by having planes of stress discontinuity j and l orthogonal to planes f and g respectively. These in turn define region III, which

has axes of principal stress parallel and perpendicular to the die faces. The whole construction may now be begun afresh, in effect by translating the circles I and II until C coincides with M.

The length of zone II along the die face is readily shown to be equal to $h\sqrt{2}$, so in the special case when b is an even integral multiple of this distance the stress pattern of Fig. 7.22 just "fits" the available space. The total compression on the die is found by summing an arithmetic progression, and we find, simply,

$$F' = kb\left(1 + \frac{b}{2h}\right), \qquad \frac{b}{h} = 2n\sqrt{2}, \qquad n \text{ an integer} \tag{7.29}$$

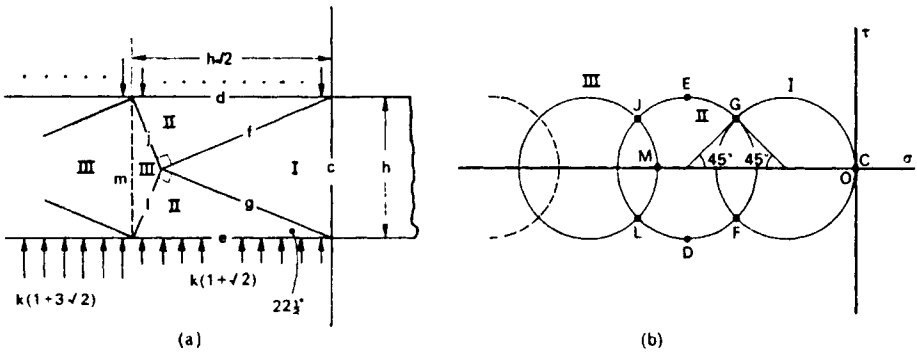

FIG. 7.22. Compression of a sheet between rough dies: lower-bound stress field.

This is also shown in Fig. 7.21, and although the analysis is not complete (but see Problem 7.11) it is clear that as b/h becomes large the difference between lower and upper bounds becomes comparatively small.

Comparing Figs. 7.18 and 7.21 we see that the larger b/h becomes the more is the divergence between the "smooth" and the "rough" situations, and we would therefore in general expect the actual compressive forces on the dies to depend critically on the coefficient of friction between the dies and the sheet of plastic material.

The above analysis for compression between rough dies may be applied, by reversing signs, to the tension of soldered and brazed

butt joints. In such joints the joining material is often intrinsically much weaker than that of the components being joined, but provided the layer of joining material is sufficiently *thin* its effective strength may be almost as great as of the other material.

A more complicated version of the same phenomenon is found in the small-scale structure of composite materials such as those used in tungsten carbide cutting tools. Here the extremely hard particles of tungsten carbide are separated from each other by relatively thin layers of cobalt which is, by comparison, much softer, but ductile. The strength of the composite is much larger than that of the "bonding" material, largely because the layers are thin compared to the dimensions of the hard particles.

Problems

7.1. Consider a family of mechanisms involving a circular band of intense shear—of which that shown in Fig. 7.2 is a member—and find the lowest corresponding upper-bound on the indentation force. (The problem of *Fellenius*.)

(*Hint*. First show that if the centre of the circle is *on* the surface the lowest upper-bound is found when the centre is at one edge of the die and the circle passes through the other edge (as in Fig. 7.2). Extend this result to cases where the centre of the circle is not on the surface, and hence study a family of mechanisms with a single degree of freedom.)

7.2. Show that if the (uniform) self-weight of the plastic material is taken into account in the upper-bound calculation corresponding to Fig. 7.2, it makes no difference to the result. Try and think of situations in which the self-weight would have an effect.

(*Hint*. Investigate similar modes for non-horizontal surfaces.)

7.3.† In order to resolve the paradox that in Fig. 7.4(a) zone *B* cannot descend because it is already in contact with zone *O*, examine the pattern of deformation in finite-thickness bands of shearing between the rigid blocks.

(*Hint*. First examine two bands of deformation which intersect at right-angles.)

7.4. Find the lowest upper-bound for a family of modes of deformation like that of Fig. 7.4 but with all vertical dimensions in Fig. 7.4(a) altered by a variable factor.

(*Hint*. Take a *length* rather than an *angle* as the variable parameter and work algebraically, making use of Pythagoras' theorem.)

7.5. Show on a diagram like Fig. 7.5(a) the principal axes in the two zones on either side of the discontinuity plane corresponding to the states of stress indicated in Fig. 7.5(c). Label the major and minor axes of principal stress. As an example consider the plane of discontinuity between the tensile and

compressive zones in pure plastic bending of a beam of rectangular cross-section.

7.6. Show from the flow conditions and the normality rule that for plane plastic strain according to the Mises yield condition, the "intermediate" principal stress is the *mean* of the other two (see section 2.13).

7.7. In Fig. 7.11(a) check the trigonometry, and then check that the quadrilateral as a whole is in equilibrium in the vertical direction under the external stresses indicated by the Mohr circles. Also check the equilibrium of half of the quadrilateral formed by a central vertical cut.

7.8. Perform the upper-bound calculation corresponding to the mechanism of deformation shown in Fig. 7.12(b). Work out lengths and velocities in terms of h and b, using Pythagoras' theorem.

7.9. Make an upper-bound analysis of the problem shown in Fig. 7.14, using a symmetrical version of the mode of Fig. 7.14(a), (i.e. one with two equally-inclined bands of intense shear and the zone immediately under the indenter descending vertically. Compare your result with equation (7.25).

7.10.† Use the mechanisms shown in Fig. 7.23 to obtain upper bounds on the force required for plane-strain indentation for "rough" and "smooth" dies.

Note that in Fig. 7.23(b) zone B is one of homogeneous deformation, while zones C slide as rigid blocks. Be careful when integrating the dissipation at the interfaces surrounding zone B.

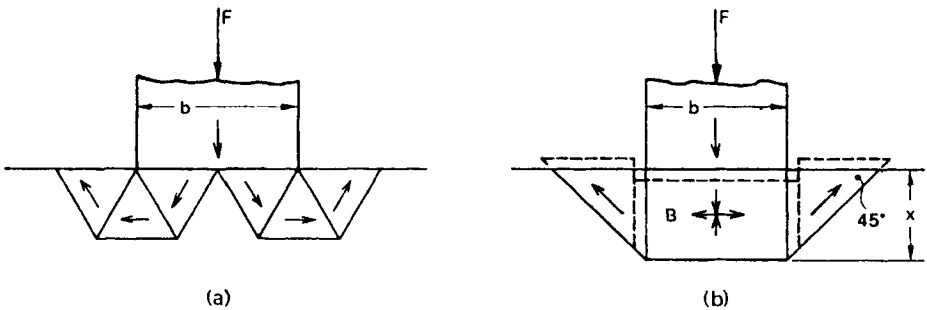

FIG. 7.23. Upper-bound modes involving sliding on the face of the indenter.

7.11.† Complete the lower-bound analysis indicated in Fig. 7.22 for general values of b/h between any two "special" values.

(*Hint.* Observe that the principal axes of stress in zone III, etc., are parallel and perpendicular to the die faces, and hence that such zones may be extended to fill a central zone of any extent.)

7.12.† Investigate a mode of deformation for compression of a sheet between rigid dies in which the criss-cross pattern of bands of intense shear in Fig. 7.12(b) is replaced by a rectangular zone of homogeneous deformation,

as in Fig. 7.23(b). Compute upper-bound loads in terms of h/b and plot the results on Fig. 7.13.

7.13.† A well-lubricated knife consisting of a rigid long wedge of included angle 20° is pressed normally into the flat surface of an infinite block of incompressible perfectly plastic material. By using an upper-bound method find an expression for the force needed per unit length of knife, F, in terms of the penetration of the edge beneath the original surface, y.

(*Hint.* First treat the deformed surface as if it were flat, and then introduce the condition of constant volume together with that of *similarity* of deformation at all stages of penetration.)

CHAPTER VIII

INTRODUCTION TO SLIP-LINE FIELDS

WE HAVE already made, in passing, several references to the theory of the *slip-line field* in problems of plane plastic flow. The present chapter is not necessary to the main theme of this book; but because the literature on slip-line fields is so large, and in many ways important, it seems worth while to give a brief introduction to the theory here.

We take as our starting point the sequence of lower-bound solutions to the problem of the loaded half-space represented in Figs. 7.6, 7.7 and 7.8, in which there are, as we know, successively more planes of discontinuity of stress. It is not difficult to see from Fig. 7.8 that if a *large* number of such planes is postulated, as indicated in Fig. 8.1, the separation of the centres of the "first" and "last" circles approaches πk, because the sum of the angles subtended by all the little arcs $DE \ldots PQ$ must be equal to 180°. It follows that the highest possible lower bound on q according to this family is

$$q' = k(2 + \pi) \tag{8.1}$$

We shall leave until later the question of whether or not this solution may be adapted to the problem of a *finite* indenter. The main point at this stage is that our initial idea of a small number of zones of constant stress has led naturally to the concept of a *continuously variable* distribution of stress which satisfies the yield condition throughout a region.

Now the techniques we have developed for dealing with discontinuities of stress will not necessarily be—and indeed probably

will not be—the most suitable for dealing with continuously variable states of stress. The key to the analysis of varying states of stress lies in the choice of *reference axes* for stress. It turns out to be easily the best plan for equilibrium analysis of continuous states of stress which also satisfy the plane-strain yield condition

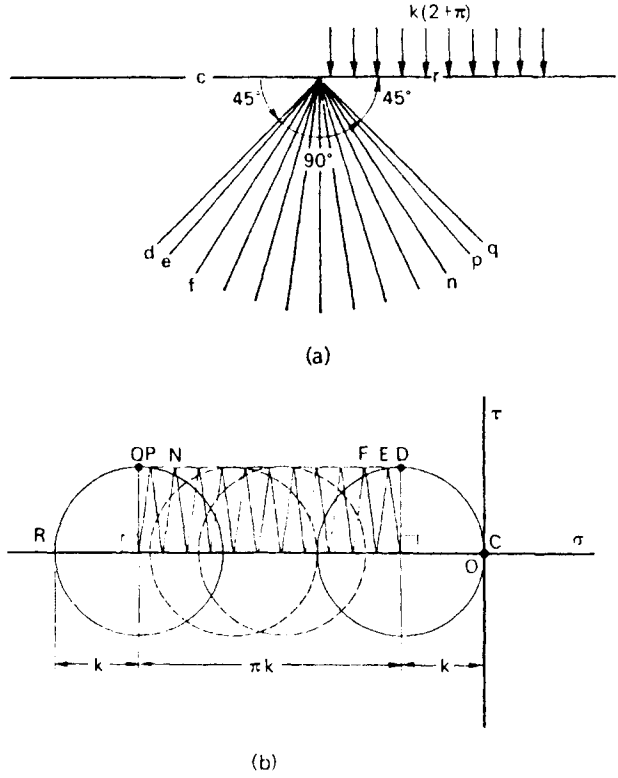

FIG. 8.1. A "fan" of planes of stress discontinuity.

to take as coordinate system not a fixed cartesian one, but a *curvilinear* one in which the axes are always inclined, locally, in the directions of maximum *shearing* stress.

A typical elementary block of material at the yield-point in plane strain is shown in Fig. 8.2(a), and the corresponding Mohr circle in 8.2(b). We adopt the sign convention set out in Appendix I and *define* points A and B on the Mohr circle as the "lowest"

and "highest" points, respectively. As the material is at the yield-point, by hypothesis, we have

$$\left.\begin{aligned} \tau_\alpha &\equiv -k \\ \tau_\beta &\equiv +k \end{aligned}\right\} \tag{8.2}$$

where the α- and β-axes correspond to points A and B. The state of stress on the block is thus as shown, in general, in Fig. 8.2(a). In particular, because points A and B correspond to the same value of σ, say t, we see that the state of stress on the block with

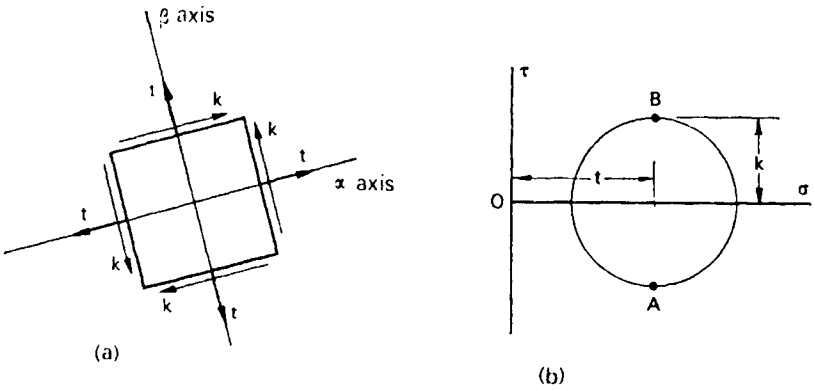

FIG. 8.2. The yield-point in plane strain: an element oriented in the directions of maximum shearing stress.

reference to *this* set of axes is an equal biaxial tension t superimposed on a pure shear. According to the Mises yield condition for plane strain (Problem 2.15) the stress on planes parallel to the paper—which are principal planes—is also equal to t; thus we may conveniently regard t as a *hydrostatic* (equal all-around) tension. For the Tresca yield condition this third principal stress need only be *intermediate* between the other two, but it may certainly be set equal to t if we so wish.

The state of stress at yield in the block is thus *completely* defined by two parameters, viz. the hydrostatic tension, t, and the inclination, ϕ, of the α-axis to an arbitrary datum axis. Let ϕ be measured in the anticlockwise direction.

In principle therefore a variable state of plastic stress over a region constrained to deform in plane strain may be specified by a network of curved, orthogonal α, β-lines, in which the inclination of the lines at any point is known by inspection and the hydrostatic tension is specified.

Now we have not yet introduced the condition that equilibrium is satisfied throughout our plastic region. When we do so we shall expect to find some sort of relationship between our two variables t and ϕ.

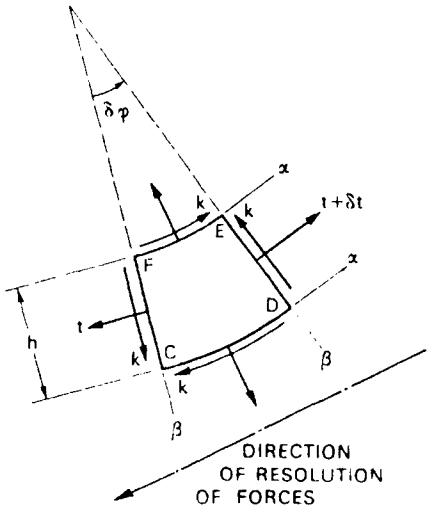

FIG. 8.3. Stresses acting on a slightly curved element.

8.1. Equilibrium Equations

To find this relationship we must consider in general the equilibrium of a small block with curved faces cut out by adjacent α- and β-lines. Figure 8.3 shows a slightly less general block defined by curved α-lines but straight β-lines. By definition the shearing stress on all four faces of the block has magnitude k, but the normal stress will in general differ slightly from one side of the block to the other. If t is the normal stress on face FC we may write the normal stress on face ED as $t + \delta t$, as shown. These two faces include the small angle $\delta\phi$, measured anticlockwise.

We now consider equilibrium of the block in the direction perpendicular to the internal bisector of CF and DE, as indicated. The block has unit thickness, and the distance between the α-lines is h. In considering equilibrium in this direction we see that the normal stresses on faces CD and EF do not enter into the equation, which is why we have not given them symbols. The normal stresses on faces FC and DE almost cancel (taking $\cos(\delta\phi) \simeq 1$) but there is a small imbalance, of magnitude $h\delta t$. Again, the shear forces on faces CD and EF almost cancel, but as CD is longer than EF by an amount $h\ \delta\phi$ there is a small imbalance of magnitude $kh\delta\phi$. The shearing stress on faces DE and CF have resultants of the same sign, and the sum of their effects also has magnitude $kh\delta\phi$. Our equilibrium equation is thus

$$h\delta t = 2kh\delta\phi \tag{8.3}$$

So, in the limit $\delta\phi \to 0$,

$$dt/d\phi = 2k \qquad \text{in the } \alpha\text{-direction} \tag{8.4}$$

It is not difficult to check that this result is unchanged if the β-lines defining the element are curved.

This result is remarkable because we have a *complete* derivative and not, as we might have expected—bearing in mind the form of the equilibrium equations referred to cartesian coordinates—a *partial* derivative. We can therefore integrate (8.4) along an α-line to give the result

$$t = \text{constant} + 2k\phi \qquad \text{along an } \alpha\text{-line} \tag{8.5}$$

In this equation each α-line is associated with a constant of particular value. Thus if the value of t is known at *any* point on a given α line, values of t can be computed at *all other* points on the same α-line. The change in value of t from point to point depends only on the change of *inclination* of the α-line between points: it does not depend, for instance, on the distance measured along the α-line.

Similarly, by considering the equilibrium of a small block in the β direction we find

$$t = \text{constant} - 2k\phi \qquad \text{along a } \beta\text{-line} \tag{8.6}$$

Note the difference in sign between (8.5) and (8.6).

Developing the previous result we can now see that if we are given an arbitrary orthogonal network of α- and β-lines, and the value of t at *one* point in the network, we can immediately work

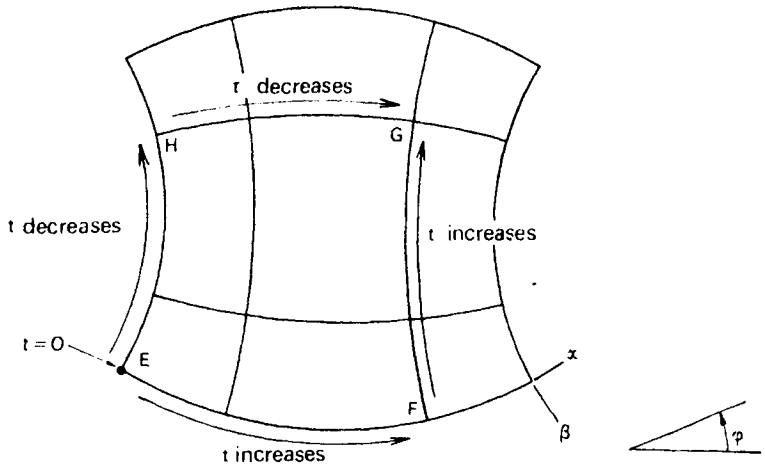

FIG. 8.4. An inadmissible α, β net.

out the value of t at all other points of the network by use of (8.5) and (8.6) along α- and β-lines.

Suppose we try out this exercise on the arbitrary orthogonal grid of curved lines shown in Fig. 8.4, and calculate the value of t at G, given $t = 0$ (for convenience) at E. Without doing any numerical calculations we can see that the value of t depends on the path taken between the points in this case. For example, t increases steadily along EFG but decreases steadily along EHG. (The reader should check these statements carefully.) Now in general it is meaningless, see Fig. 8.2, for t to have more than one

value at any point, so we must conclude that although the network shown in Fig. 8.4 is orthogonal, yet it does not correspond to a state of equilibrium of material at the yield-point.

8.2. Geometry of α, β nets

Clearly, then, equations (8.5) and (8.6) must impose geometrical conditions on the α, β net. In fact these conditions are simple ones, and may readily be determined with the aid of Fig. 8.5. Let us write down the requirement, in terms of the angles ϕ at

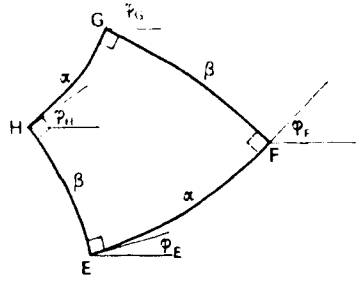

FIG. 8.5. Interrelation of angles in an α, β net.

the nodes, that the change in value of t around a closed circuit (say *EFGHE*) is zero—which must be so if t has a unique value at any point. Applying (8.5) and (8.6) we find

$$0 = +2k(\phi_F - \phi_E) - 2k(\phi_G - \phi_F) + 2k(\phi_H - \phi_G) - 2k(\phi_E - \phi_H) \tag{8.7}$$

which simplifies to

$$-\phi_E + \phi_F - \phi_G + \phi_H = 0 \tag{8.8}$$

If we rewrite this as

$$\phi_H - \phi_E = \phi_G - \phi_F \tag{8.9}$$

we obtain the geometrical result (Hencky's first theorem) that the angle subtended by two α-lines at points where they are cut by a

given β-line is the same as the angle subtended by the two α-lines where they are cut by *any other* β-line (see Fig. 8.6). The net shown in Fig. 8.4 clearly does *not* satisfy this geometrical condition. The above theorem also holds, of course, if the symbols α and β are interchanged.

Another geometrical interpretation is found by rearranging (8.8) as

$$\phi_F - \phi_E = \phi_G - \phi_H \tag{8.10}$$

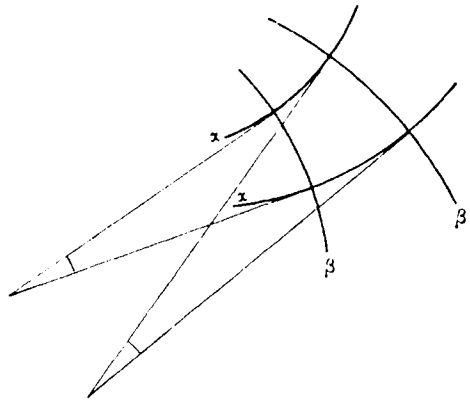

FIG. 8.6. Hencky's first theorem.

This states that the change of inclination of all α-lines between intersections with any two β-lines is the same. In particular, if an α-line is *straight* between two β-lines, *all* α-lines are straight between the same two β-lines.

Our study has thus shown that the problem of satisfying simultaneously the equilibrium equations and the plane-strain yield condition may be transformed into a purely *geometrical* problem of establishing a net of α, β-lines subject to certain restrictions. The method thus constitutes a powerful tool for setting up lower-bound distributions of stress within a body, and we shall investigate later some of the trial-and-error procedures which are useful.

8.3. Hyperbolic Equations

Without going into the theory of partial differential equations we can say that since there exist—as we have just demonstrated—trajectories along which *complete* derivatives of the relevant variables may be computed, then the governing partial differential equations are members of the general class of differential equations known as *hyperbolic*. The α- and β-directions are known as the *characteristic* directions, the essence of a characteristic direction being that along it a *complete* derivative may be evaluated. (For a clear account of the theory of characteristics see the book by Abbott listed in the Bibliography.) This fortunate circumstance is by no means universal; for so-called *elliptic* partial differential equations the characteristic directions are not real, and cannot be used as a computational aid. The equations of the theory of elasticity are of this second sort, and, except where solutions may be obtained in terms of known functions, procedures of successive adjustment must be used over the whole area of interest until a satisfactory solution has been obtained. In contrast, the equations of the present solution can be handled by the much simpler procedure of "marching out" the solution from a known region.

In our present treatment of the equations we have simply *verified* that the α, β-directions are the characteristics of stress; by appropriate rigorous analysis we could have derived the result that the characteristic directions are real and are in fact the α- and β-directions.

8.4. Extension of α, β nets

In the construction of an α, β net as a step in the solution of a problem one of the important questions is how to *extend* the net from an existing region in which it has already been established. This basic problem is illustrated in Fig. 8.7. The points 1 and 2 are close to each other on the edge of an α, β net which, we suppose, has already been established to the left of these points.

In particular the value of t and the inclination of the α- and β-lines are known at the two points. We ask the question: what is involved in extending the α-line through 1 to meet the β-line through 2? In general the short extensions of the lines are curved, and they must intersect orthogonally. This, however does not define the extensions uniquely, and three possibilities are sketched in Fig. 8.7. There is, however, only *one* solution which gives *a unique value of* t at the new point, according to (8.5) and (8.6). Thus, provided all distances are sufficiently small for curvatures to be practically constant along the short arcs, the new point is located uniquely in space.

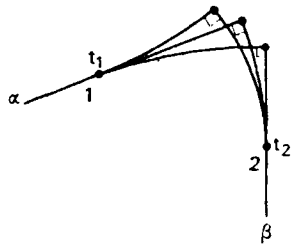

FIG. 8.7. Continuation of α- and β-lines through two known points.

A specially simple example is shown in Fig. 8.8, in which points 1 and 2 are on a plane free surface of the material. If both points are in a plastic zone, we know from the Mohr circle that the α- and β-lines are inclined at 45° to the edge at 1 and 2, and that $t_1 = t_2$. Application of (8.5) and (8.6) indicates that the lines which meet at point 12 must be straight. This should be verified in detail by the reader. If, instead, the free boundary had been curved (so that $\phi_1 \neq \phi_2$) the intersecting lines would also have been curved (see Problem 8.1).

Returning to Fig. 8.7 we can see that if we know the values of t and ϕ at a finite *sequence* of points along the (current) boundary of a known α, β net, we can repeat the unit step procedure between each adjacent pair of points, and then repeat the exercise with the newly-generated set of points. At each "pass" we would

generate one less point than the starting number, so the process would eventually have to stop for lack of information. We can thus see that the area which can be "covered" in this way is bounded by the α- and β-lines passing through the end-points of the sequence, as shown in Fig. 8.9(a). In principle the sequence of known points may lie on curves crossing the net diagonally, as shown, but a common special case is as shown in Fig. 8.9(b) where segments of two intersecting α- and β-lines are known. The corresponding area which is uniquely determined from this information is also shown. In fact the particular region shown is

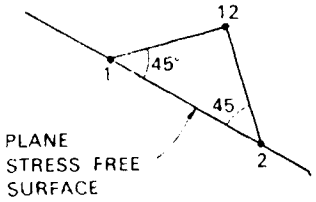

FIG. 8.8. α- and β-lines extending from a plane, stress-free surface.

generated from two equal circular arcs, which turns out to be a useful special case.

Graphical methods are convenient for making constructions of this sort. Without going into details it is not difficult to see that practical procedures based on quadrilaterals consisting of chords between points on α- and β-curves may be devised.

Returning to Fig. 8.9(b), it is clear that *no* extension is possible from a known portion of an α- or β-line *alone*.

8.5. The Indentation Problem

To illustrate these ideas and some of their consequences let us return to the plane-strain indentation problem, and try and construct the appropriate α, β net, shown in Fig. 8.10. The steps in the trial-and-error method are as follows.

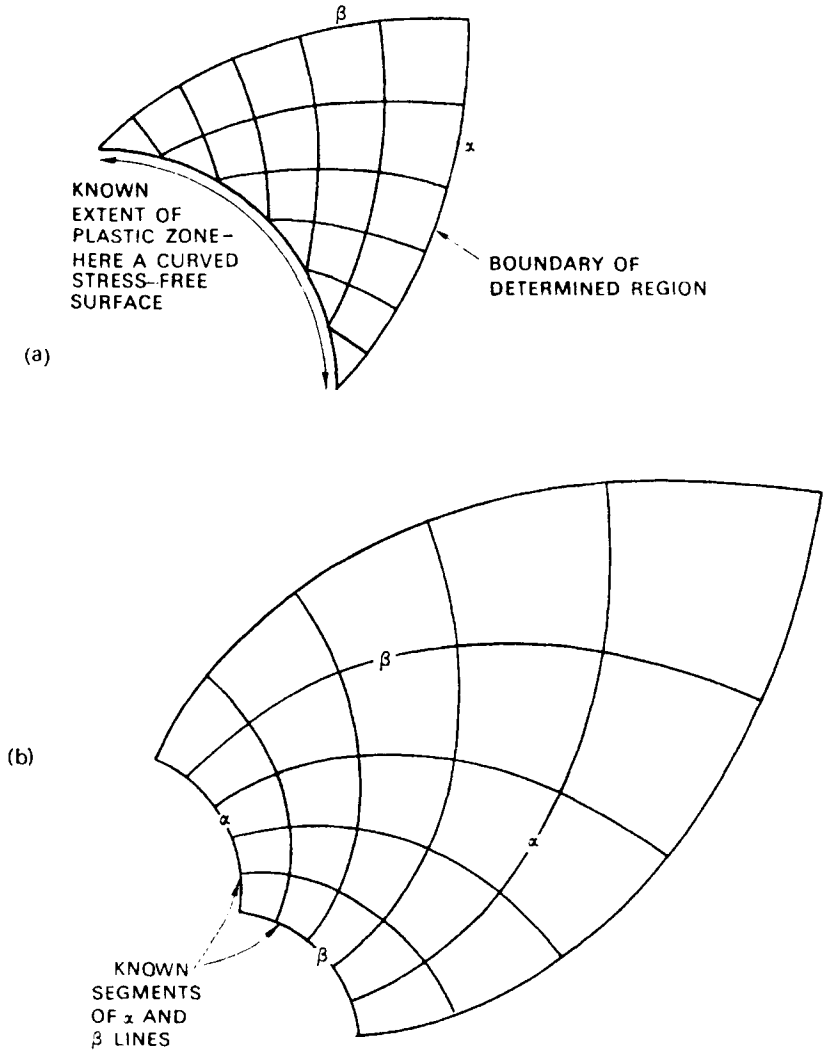

FIG. 8.9. α- and β-lines extending (a) from a curved stress-free surface, (b) from two known α- and β-lines.

First, the portions CD and EF of the flat surface are unloaded, so the α- and β-lines (within the plastic zones) intersect the surface at 45°. It is clear intuitively that material in these regions will be in compression laterally, so the Mohr circle at the surface will be as shown in Fig. 8.10(b). In particular, from this diagram

we are able to label the α- and β-directions as shown. The reader should check this step carefully.

Under DE we have a somewhat similar state of affairs (the indenter being assumed frictionless), but here it is clear that the greatest compressive stress is in the vertical direction, so by the Mohr circle the α- and β-directions are opposite from those in the outer regions.

From edges CD, DE and DF the α, β nets may be extended (see Figs. 8.8 and 8.9(a)), but the separate regimes cannot be

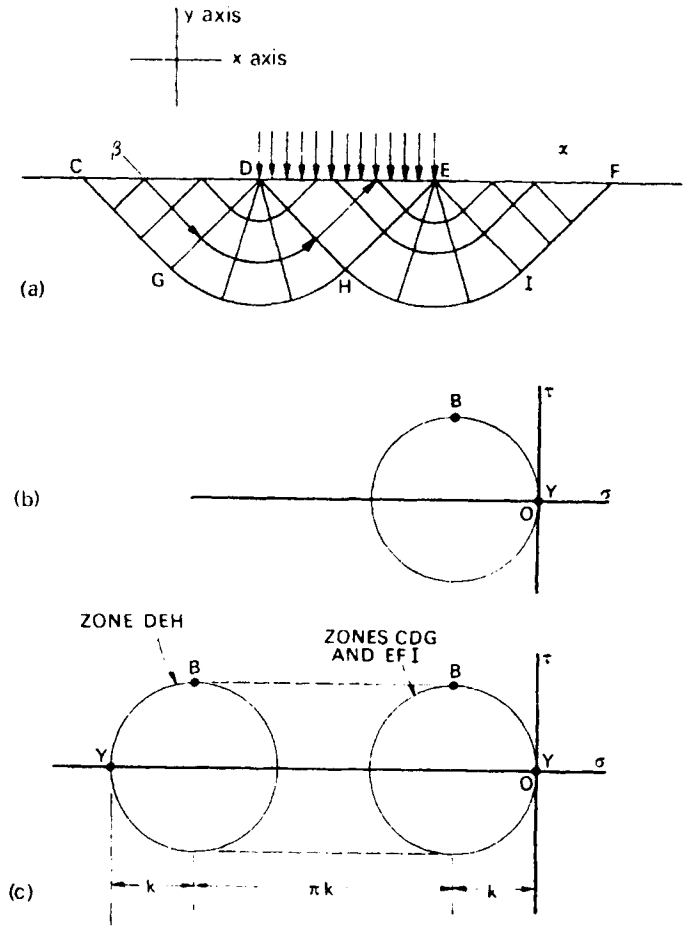

FIG. 8.10. α, β net for the indentation problem and the corresponding Mohr circles.

merged directly because this would involve an α-line turning into a β-line which is not possible if discontinuities in stress are to be avoided. We must therefore join the separate zones with "fans" as shown, centred at D and E respectively. In this way the triangular zones are connected without discontinuity of stress, and the correct size of regions CD and EF is determined.

We are now in a position to evaluate the indentation pressure along DE, by following a typical β-line from the free surface CD to the loaded surface DE. First, from the Mohr circle for region CDG (Fig. 8.10(b)) we have $t = -k$ throughout this region. As we cross GD and move towards DH a tangent to the β-line turns anticlockwise, through $\pi/2$ altogether. Therefore, by (8.6), t must decrease by $k\pi$ altogether as we travel along any β-line from CD to DE. This locates the centre of the Mohr circle for region DEH (see Fig. 8.10(c)); hence we readily find that the normal pressure, q, on face DE is given by

$$q = k(2 + \pi) \tag{8.11}$$

The pressure under the indenter is uniform, because the above calculation applies equally for a β-line starting at any point in DE. The reader should check that exactly the same result is obtained by following any α-line from EF to DE.

Several points emerge from this example, as follows.

(i) At points D and E in the circular fans the hydrostatic tension t is *multivalued*. That there should be such singularities in stress is not surprising when we note that there are abrupt changes of surface loading at these points.

(ii) Having established an α, β net over only *part* of the plane we cannot strictly claim that the above constitutes a lower-bound analysis. We should really establish that a permissible distribution of stress exists in the remainder of the body also. This can be done by extending the net downwards from the β- and α-lines CGH and HIF respectively, as far as it will go (cf. Fig. 8.9(b)), and then extending the net sideways from the boundaries of this field, introducing curved "free" surfaces which start at C and F and extend sideways and downwards. In this way the

size of the *smallest* block for which the analysis is valid may be found, and the result holds also for larger blocks, by one of the theorems on p. 110.

(iii) So far we have discussed α, β nets only in terms of *stress*, but in the complete "slip-line" theory we consider plastic *deformation* as well. The α- and β-lines are also in fact the characteristic directions for *velocities*, and in consequence velocity calculations are best done with reference to these lines. Without going into any details here it is not difficult to see that, because the plastic deformation must be one of pure shear referred to the local α, β-axes, the α- and β-lines do not change in length during deformation. The net may therefore be regarded for present purposes as a rather elaborate "lazy-tongs" of small bars hinged to each other at their ends. This analogy is not quite perfect, however, because there exists also the possibility of interfaces of intense slip.

For an α, β net to represent a *complete* solution within the plastically deforming region three conditions must be satisfied

(i) The geometrical conditions on the α, β net equivalent to the equilibrium equations must be met.
(ii) There must exist a mode of deformation which satisfies the velocity requirements noted above.
(iii) The shear strain increments in this mode of deformation must have the same "sign" as the shear stresses within the net.

The second and third conditions sometimes indicate clearly that a particular postulated α, β net does not correspond to a complete solution, although it may well represent in part a satisfactory lower-bound stress field. We will not go into details of examples here: for further reading and a complete treatment of the subject see the book by Hill listed in the Bibliography.

Nevertheless, to provide an illustration of mechanisms of deformation in a simple problem we indicate in Fig. 8.11 three possible modes corresponding to the α, β net of Fig. 8.10(a). The mode of Fig. 8.11(a) includes a rigid zone *DEH* which descends vertically,

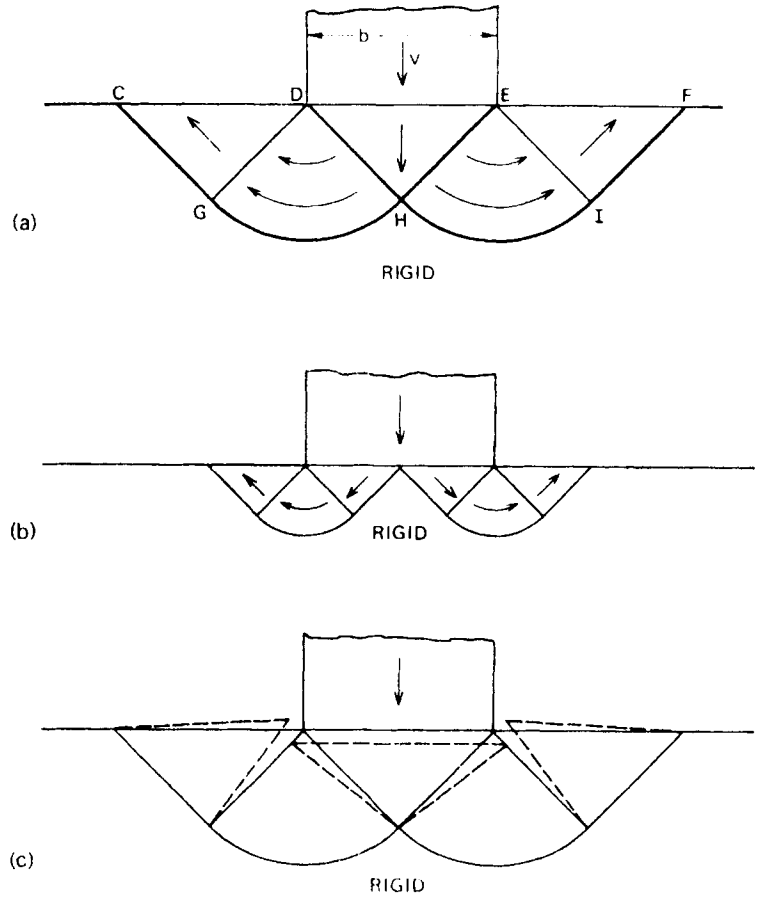

FIG. 8.11. Modes of deformation compatible with the α, β net of Fig. 8.10(a).

in effect as an extension of the indenter. Surfaces of intense shear are indicated by bold lines, and the reader should verify by means of a velocity diagram that in the regions *DGH* and *EIH* each particle has the same peripheral velocity. Thus, in particular—in contrast with the mode postulated in Fig. 7.2—there is continuous shearing over these regions in addition to the intense shear on the surfaces *CGHE* and *FIHD* (see Problem 8.2). The reader should also check that the signs of shearing stress and shearing strain increment correspond. The other two mechanisms shown are

intended to be self-explanatory: they both involve sliding of material over the surface of the indenter and can thus be considered only for well-lubricated indenters (see Problem 8.3). Mode (b) is in many respects similar to mode (a), but mode (c) is rather different in that all zones are undergoing continuous shearing and there are no interfaces of intense shear. All three modes in fact satisfy all the necessary conditions, and are hence equally satisfactory solutions. The theory cannot distinguish between them (and in fact an indefinite number of others), so all are equally correct. Such non-uniqueness of modes of deformation is not uncommon in plasticity theory, and we have already seen several examples of this (see Problem 8.4).

Ambiguity of this sort must not be regarded as a disadvantage; it is often easy to decide which mode is most likely to occur when the real features of friction, strain-hardening, etc., are contemplated. But in any case there is no ambiguity about the *load* at which deformation takes place, according to the theory.

8.6. Choice of Approach: Slip Lines or Bound Theorems?

In analysing a problem in plane plastic strain, the engineer must decide either to seek a slip-line solution or to apply the bound theorems. Which method is most expeditious depends to a large extent on the worker's confidence in his ability to apply successfully the slip-line theory to a new situation, which in turn hinges largely on his previous experience. Both approaches are satisfactory from the point of view of answering significant engineering questions, and both are intellectually satisfying in their different ways. The choice thus depends ultimately on the temperament of the engineer, and little more can be said in general, except, obviously, that if the deformation is not one of *plane* strain the possibility of choice does not exist.

8.7. Notation

The slip line field is often used in problems where there is predominantly a state of hydrostatic compression. Most textbooks use the symbol p $(= -t)$ for hydrostatic *compression*, and the relations (8.5) and (8.6) are correspondingly different (Problem 8.5). This is simply a matter of definition, and the answers to problems are of course identical whichever notation is used.

Problems

8.1. A thick-walled tube has inner and outer radii a and b respectively. It is subject to internal pressure and is constrained to deform without elongation. By considering an appropriate α, β net and drawing Mohr circles find the value of the gauge pressure at which unrestricted plastic deformation of the tube occurs.

(*Hint.* Establish, from conditions of symmetry and orthogonality of the α, β net, an equation for a typical α-line, and apply (8.5).)

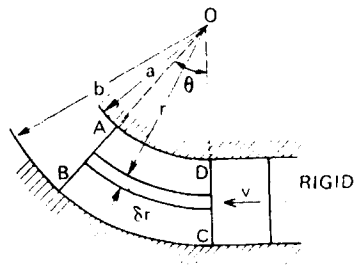

FIG. 8.12. Shearing deformation within a circular fan.

8.2. Figure 8.12 shows part of a circular "fan" of material which is being constrained to deform in plane strain and is being pushed by a rigid plunger which is moving *without rotation* with velocity v. The edges of the deforming material remain in contact with the rigid boundaries and edge DC and all lines originally radial remain straight.

Consider the deformation of the slice r, δr in two parts:

(i) a rigid-body motion about O, the centre of the fan;

(ii) uniform shear with reference to radial and circumferential axes, with strain rate $\dot{\gamma}$.

Obtain an expression for $\dot{\gamma}$ and evaluate the rate of dissipation of energy

(for yield stress k in pure shear) per unit thickness perpendicular to the paper of sector $ABCD$.

8.3.† Construct velocity diagrams for the modes of deformation shown in Fig. 8.11 (a) and (b) (devise a suitable notation for use within the "fans") and evaluate corresponding *upper-bound* indentation loads.

(*Hint*. Make a careful tabulation of all energy dissipated.)

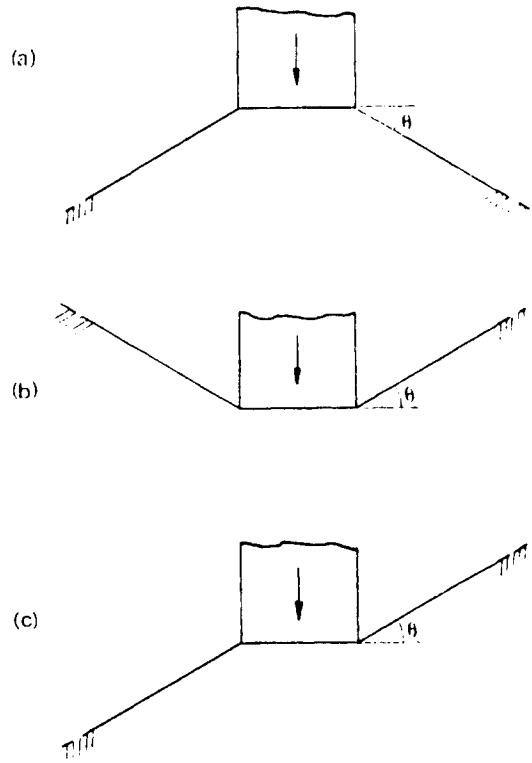

FIG. 8.13. Variants of the indentation problem.

8.4.† Draw up a list of all situations given so far in the book in which the mode of plastic deformation is non-unique.

(*Hint*. Pay particular attention to yield loci with corners.)

8.5. Redraw Fig. 8.3 and re-derive equations (8.5) and (8.6) when the symbol p is used (in place of t) to denote a hydrostatic *compression*.

8.6. Assuming conditions of plane plastic strain, construct α, β nets in the vicinity of the indenters shown in Fig. 8.13, and derive the corresponding indentation pressures q.

8.7. A block of perfectly plastic material has two slots machined in it as shown in Fig. 8.14. Assuming conditions of plane plastic strain construct an

α, β net in the central region and thus obtain an expression for the full-plastic tension F per unit thickness perpendicular to the paper.

(*Hint.* Compare Figs. 8.13 and 8.14.)

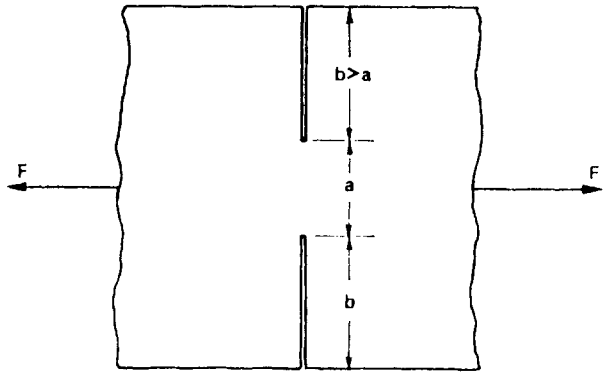

FIG. 8.14. Tension in a slotted block.

8.8.† Investigate the mode of deformation indicated in Fig. 8.11(c) and obtain the corresponding upper-bound indentation load. Compare your answer with those to Problem 8.3.

(*Hint.* Use an analysis along the lines of—but different from—Problem 8.2 to find the dissipation of energy in the "fans".)

CHAPTER IX

CIRCULAR PLATES UNDER TRANSVERSE LOADING

FLAT plates form important structural elements in many branches of engineering. In some cases their prime function is to sustain loads acting in their own plane, for example the webs of I-beams. In the present chapter, however, we shall be concerned only with the other main class of plate problems in which loads are applied *transversely*, i.e. the forces (both "loads" and "support reactions") act in directions *perpendicular* to the plane of the plate. It is clear at the outset that we shall be interested in *bending* action, as we are of course in the simpler analogous situation of transversely loaded beams; and indeed we may think of plates as beams somehow "generalised" into two dimensions.

Now for many flat structures under transverse loading a simple uniform plate of constant thickness is not the most economical design. For example, in lightly-loaded domestic flooring a common scheme is to have wooden joists spanning the width of a room, with floorboards spanning the spaces between the joists. A "single-stage" floor made simply by placing joists in contact with each other would be an order of magnitude more expensive and heavy. Another example is found in bridge construction, in which the actual roadway is often supported on several "stages" of beams, each set of beams having a larger span than that of the set it supports.

Plates of constant thickness are desirable, however, where *continuity* is important. A good example is the plating on a ship's hull, which is the last "stage" in a complex structure of bulkheads, ribs, etc. The outer skin must support, across relatively

short spans, forces arising from the buffeting of waves, water pressure below the water-line and a variety of loads which may be applied to the decks. Another example is the construction of large multi-storey buildings, where it is sometimes convenient from the construction and soundproofing points of view to make the floors by casting them as continuous slabs of concrete, reinforced by steel bars. For column spacing up to about 6 m this is a competitive procedure, but for larger spans it may be more economical to have a beam-slab composite structure or to use some sort of *cellular* slab.

In the present chapter we shall consider only the simplest of all possible plate problems, viz., the uniform circular plate carrying uniformly distributed transverse load, i.e. pressure loading. We make this restriction both for the sake of brevity and also to avoid a discussion of the highly-developed subject of "yield-line theory" which is used widely for the design of concrete slabs in building construction.

We shall, however, discuss some of the similarities and differences between the analysis of metal *plates* (strictly, plates of Tresca perfectly plastic material) and concrete *slabs*; and to facilitate discussion we shall adopt this terminology throughout the present chapter.

Some of the problems at the end of the chapter will indicate ways in which the theory may be extended to more complicated situations.

9.1. Validity of the Simple Plastic Theory

As the simple plastic theory is known to give a good account of the behaviour of beams and frameworks made of steel and reinforced concrete, it seems reasonable to suppose that it will be applicable equally to the behaviour of plates and slabs.

However, a closer examination of the behaviour of plates and slabs indicates that in fact the situation is somewhat more complicated, because in plates and slabs there are geometrical constraints of a kind not normally present in beams and frameworks.

Broadly, when a plate or slab deforms it turns into a shallow three-dimensional *shell* which is capable of acting to some extent as a *membrane*. The effect of this transformation is, usually, to increase the strength of the structure, so the simple plastic theory (which ignores such changes in geometry) is likely to be conservative in the context of design.

In the present chapter we shall *assume* that the simple theory is valid, and apply the bound theorems to obtain estimates of collapse loads. In Chapter XI we shall examine briefly some of the consequences of the changes in geometry which occur when structures deform, although we shall not study plates and slabs as such.

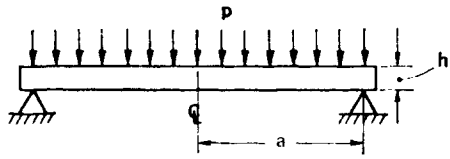

FIG. 9.1. A simply supported circular plate carrying a uniformly distributed transverse load (p per unit area).

9.2. Collapse of a Simply Supported Circular Plate under Uniform Transverse Pressure

We consider first the behaviour of a circular plate, radius a and thickness h, resting on a continuous simple support around its edge and sustaining a uniformly distributed transverse load of intensity p per unit area, as shown in section in Fig. 9.1.

The plate is a three-dimensional body, and it is fairly clear that the loading sets up a variety of stresses within the body which, by virtue of the manifest symmetry of the situation, may be classified broadly as follows:

(i) Shearing stresses on concentric circular cylindrical "cuts".
(ii) Compressive stresses in the direction of the axis of rotational symmetry.

(iii) "In-plane" stresses, compressive at the upper surface and tensile at the lower surface of the plate.

Following traditional plate theory we immediately seek ways of avoiding analysis of a fully three-dimensional situation. The key to the desired simplifications is the observation that for sufficiently *thin* plates (i.e. thickness/diameter sufficiently small) stresses in classes (i) and (ii) are negligible compared to the in-plane stresses (iii). This enables us to assume that the *bending* strength of elements of the plate is unaffected by the small shear

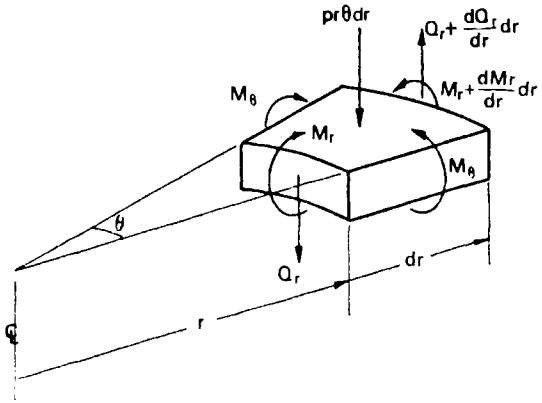

FIG. 9.2. Equilibrium of a small element of plate.

(i) and pressure (ii) effects, and hence to set up the problem as a two-dimensional one in terms of the variation of *bending moments* over a surface.

When we have solved the problem in these terms we shall be able to check our initial assumptions *a posteriori*, and establish limits, if any, on the range of geometrical parameters of the plate for which our solution is valid.

9.3. Yield Locus for an Element of Plate

One of our preliminary tasks is to set up a "yield locus" in a suitable bending-moment space.

Figure 9.2 shows a typical element of the plate (defined by

radial and circumferential cuts) and the stress resultants which act upon it: those which vanish by virtue of symmetry are not indicated. The bending moments M_r and M_θ per unit length (which have the dimensions of *force*) are, by symmetry, *principal* bending moments. The shearing stress resultant Q_r is necessary

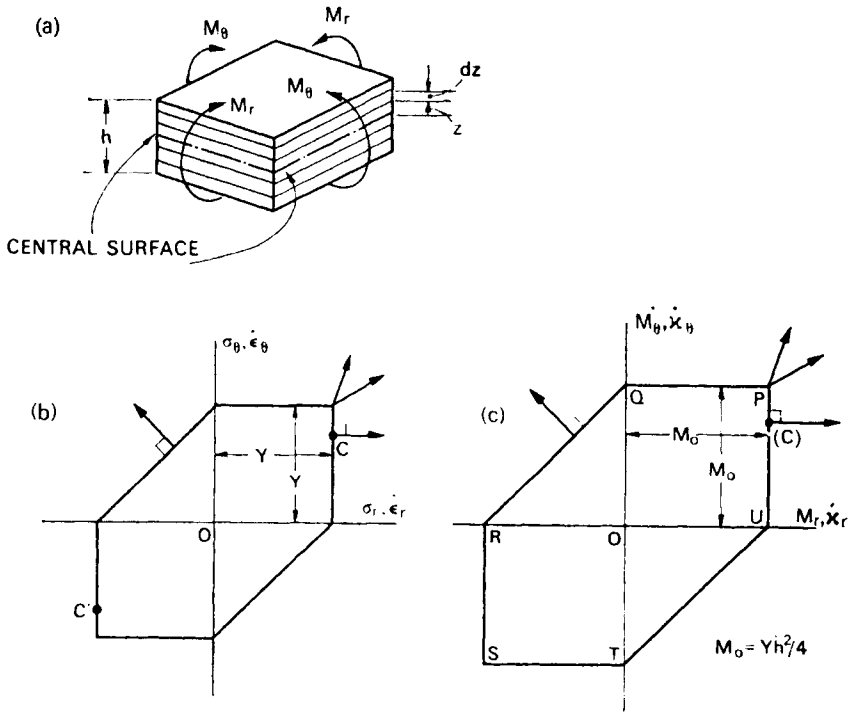

FIG. 9.3. Biaxial plastic bending of an element of plate.

for equilibrium but, as we have argued, it does not enter the yield condition. In Fig. 9.2 all the stress resultants are shown in their positive senses.

To establish the required yield locus in M_r, M_θ space we investigate by a lower-bound technique the strength of an element in pure biaxial bending, as shown in Fig. 9.3(a). It is convenient for this purpose to imagine the element slit into a number of parallel thin layers, symmetrically disposed about the central

surface. We can easily achieve a state of full-plastic pure biaxial bending in a pair of layers by setting the σ_r, σ_θ stress points for the two layers at diametrically opposite points on the relevant biaxial yield locus, for example C and C' in Fig. 9.3(b).† If the distance of the two layers from the central surface is $\pm z$ and the thickness of the layers is δz, we have the following expressions for the corresponding contributions of bending moment:

$$\left.\begin{aligned} \delta M_r &= 2z\sigma_r{}^c\delta z \\ \delta M_\theta &= 2z\sigma_\theta{}^c\delta z \end{aligned}\right\} \tag{9.1}$$

where $\sigma_r{}^c$, $\sigma_\theta{}^c$ are the coordinates of point C.

If we now assign the stress state C to *all* layers above the centre surface and state C' to all layers below, we can integrate through the thickness to give the following "safe" pure bending moments:

$$\left.\begin{aligned} M_r &= \sigma_r{}^c h^2/4 \\ M_\theta &= \sigma_\theta{}^c h^2/4 \end{aligned}\right\} \tag{9.2}$$

This provides a lower-bound point in M_r, M_θ space corresponding to any point C; thus the lower-bound locus in this space, shown in Fig. 9.3(c) is *similar* to the yield locus in σ_r, σ_θ space. The leading dimension is M_o:

$$M_o = Yh^2/4 \tag{9.3}$$

where, as usual, Y represents the yield stress of the material in simple tension (see Fig. 9.3(b)).

It is not possible to enlarge the locus of Fig. 9.3(c) by any other choice of distribution of stress through the thickness of the element, so the locus must in fact be exact. It follows therefore that the corresponding deformation of the element, consisting of incremental changes in curvature, $\dot{\kappa}_r$, $\dot{\kappa}_\theta$, is related to the M_r, M_θ locus by the normality rule. (For an alternative approach, see Problem 9.1.) When we come to do upper-bound calculations we shall need to evaluate the dissipation of energy per unit area of

† See Fig. 5.11, p. 133.

the plate: by analogy with the plane stress expression (Problem 4.6) we find

$$\dot{D} = M_0 (\text{max of } | \dot{\kappa}_r |, | \dot{\kappa}_\theta |, | \dot{\kappa}_r + \dot{\kappa}_\theta |) \tag{9.5}$$

(see also Problem 9.2).

For most of the remainder of the chapter we shall discuss the plate problem in terms of the distribution of bending moment with radius: the *thickness* of the plate will only enter the equations through the "composite" parameter M_0.

9.4. Lower-bound Analysis

We obtain the necessary equilibrium equations for the plate by considering the equilibrium of the small element shown in Fig. 9.2. Two non-trivial relations are found by taking moments about a local circumferential axis and resolving in the direction perpendicular to the plate, respectively:

$$\frac{d}{dr}(rM_r) = M_\theta - rQ_r \tag{9.6}$$

$$\frac{d}{dr}(rQ_r) = pr \tag{9.7}$$

In the present problem (9.7) may be integrated to give

$$Q_r = pr/2 \tag{9.8}$$

This equation may also be obtained by considering the equilibrium of a disc "cut out" at radius r. Substituting for Q_r in (9.6) (to eliminate the stress resultant which does not appear in the yield condition) we obtain

$$\frac{d}{dr}(rM_r) = M_\theta - \frac{pr^2}{2} \tag{9.9}$$

To find a lower bound on the collapse pressure p we must satisfy the equilibrium equation (9.9) without violating the yield con-

dition, Fig. 9.3(c), as well as the boundary condition corresponding to the simple support which is, evidently,

$$M_r = 0 \text{ at } r = a \tag{9.10}$$

It seems clear—intuitively—in the present problem that both M_θ and M_r will be positive throughout, and so we might guess that the M_r, M_θ "trajectory" will lie on either PQ or PU in Fig. 9.3(c). If we put $M_r = M_o$ (corresponding to PU) in (9.9) we find $M_\theta > M_o$ for positive values of p, which violates the

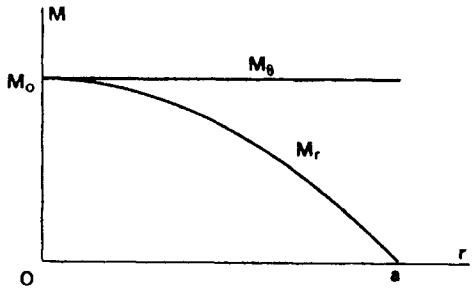

FIG. 9.4. Radial distribution of bending moments at collapse of a simply supported plate under uniform pressure.

yield condition. We therefore try the alternative, $M_\theta = M_o$ in (9.9) and integrate to give:

$$M_r = M_o - \frac{pr^2}{6} + \frac{C}{r} \tag{9.11}$$

C is a constant of integration. According to this equation M_r is infinite at the centre of the plate if C is finite; we conclude from this that C must be zero, so

$$M_r = M_o - \frac{pr^2}{6} \tag{9.12}$$

Finally, using the boundary condition (9.10) we obtain

$$p_l = 6M_o/a^2 \tag{9.13}$$

after checking that the M_r, M_θ trajectory (see Fig. 9.4) does not indeed extend beyond the postulated segment PQ.

It is interesting to note the direct analogy between (9.9) and the equilibrium equation on p. 120, for the rotating flat disc, and the analogy between the corresponding solutions (compare Figs. 9.4 and 5.4). The analogy is not as helpful as it might appear, however, because the practically important boundary condition for a *clamped* edge of the plate, which we shall study later, would correspond in the rotating disc to negative peripheral mass.

It is also instructive to note that (9.13) may be obtained very simply by considering the equilibrium of *half* of the plate about a

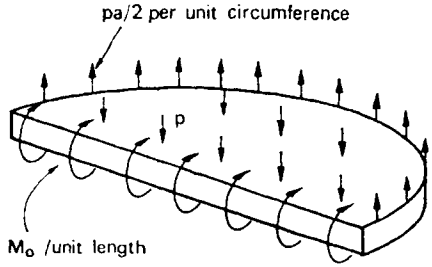

FIG. 9.5. Equilibrium of half of a circular plate.

diameter, Fig. 9.5 (see Problem 9.3). Although this does not constitute a proper lower-bound analysis (as we have not investigated the variation of M_r with r) it is nevertheless an illuminating exercise.

Equation (9.13) implies that the *total* collapse load (i.e. pressure $\times$ area) is equal to $6\pi M_o$ which is, in particular, independent of the radius of the plate. This last observation is readily obtained from *dimensional analysis* (see Problem 9.4).

We are now in a position to check our starting assumptions that certain stress components are negligible compared to the in-plane stresses, which we now see have magnitude Y. To justify the neglect of class (i) stresses (p. 216) we must work out the shearing stress on a typical cylindrical cut. Q_r is greatest at $r = a$, by (9.8), and the *average* shearing stress, τ, on a cylindrical

surface at this radius is equal to Q_r/h. Using (9.13) and (9.3) we find

$$\frac{\tau}{Y} = \frac{3}{4}\left(\frac{h}{a}\right) \tag{9.14}$$

Allowing for the fact that the maximum shearing stress will be larger than this average value, we can see that if h/a is less than, say, 1/5 our initial assumption is justified.

Similarly, from (9.13) and (9.3) we have

$$\frac{p}{Y} = \frac{3}{2}\left(\frac{h}{a}\right)^2 \tag{9.15}$$

so the same limit on h/a certainly justifies neglect of class (ii) stresses.

It is in fact impossible to improve on (9.13) as a lower bound, and so our result must be exact, subject to the assumptions made. We shall find when we do an upper-bound analysis of the same problem later that upper and lower bounds do in fact *coincide* for this problem and they are therefore *both* correct.

9.5. A Clamped Circular Plate: Lower-bound Analysis

It is a relatively simple exercise to extend the analysis above to deal with a circular plate which is supported by a fully-clamped edge. It is intuitively obvious that M_r will be negative at and near the clamped edge, so the M_r, M_θ trajectory PQ, Fig. 9.3(c), will be inadequate by itself. Now M_r must be a continuous function of r (Problem 9.5) and so there must exist a radius within the clamped plate at which $M_r = 0$. Within this radius conditions are *exactly* as for a simply supported plate of a smaller radius. Our best strategy therefore is to build on our previous work, using the value of p given by (9.13) and regarding a as the radius at which the M_r, M_θ trajectory changes from one edge to another of the yield locus: we shall seek a larger radius b for the clamped edge, and having found it we shall be able to express the safe pressure in terms of this radius.

Substituting for p from (9.13), equilibrium equation (9.9) becomes

$$\frac{d}{dr}(r\,M_r) = M_\theta - \frac{3M_o r^2}{a^2} \tag{9.16}$$

It seems clear that for $r > a$ we shall be in the second quadrant of M_r, M_θ space, for which the equation of the yield condition is (Fig. 9.3(c))

$$M_\theta - M_r = M_o \tag{9.17}$$

To solve these two equations simultaneously we first differentiate the product in (9.16) (following our treatment of the thick tube in Chapter III) and obtain

$$\frac{dM_r}{dr} = \frac{M_\theta - M_r}{r} - \frac{3M_o r}{a^2} \tag{9.18}$$

Using (9.17) and integrating we have

$$M_r = M_o \ln r - \frac{3}{2}\frac{M_o r^2}{a^2} + C \tag{9.19}$$

The constant of integration, C, is determined by the fact that $M_r = 0$ at $r = a$; this gives us

$$M_r = M_o \ln(r/a) - \frac{3}{2} M_o \left[\left(\frac{r}{a}\right)^2 - 1\right] \tag{9.20}$$

This equation is valid only if the M_r, M_θ trajectory is on QR, Fig. 9.3(c). It is not possible to extend the trajectory into RS—the reader should check this—and so point R must correspond (in this lower-bound analysis) to the clamped edge, $r = b$.

Plotting out (9.20) as in Fig. 9.6 we find that the clamped edge is reached at $b/a \simeq 1{\cdot}37$. As the pressure $p = 6M_o/a^2$ is a safe pressure for a clamped plate of radius b, we obtain, finally,

$$p^l \simeq 11{\cdot}3\, M_o/b^2 \tag{9.21}$$

As with the previous solution there is no way of improving on this lower bound, and the result is therefore exact.

Comparing (9.13) and (9.21) we see that by *clamping* the edge of a uniform circular plate we almost double its load-carrying capacity (see Problem 9.6).

9.6. Upper-bound Calculations

As we have seen already, our lower-bound analyses of the simply supported and clamped circular plates under uniform

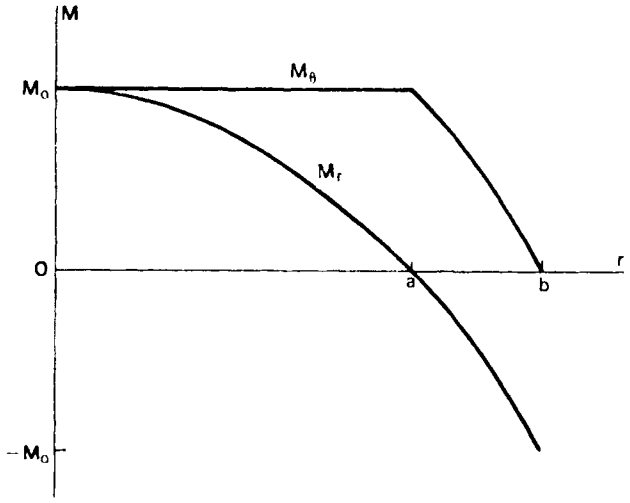

FIG. 9.6. Radial distribution of bending moments at collapse in a plate with a built-in edge.

transverse load left no room for improvement; the corresponding collapse pressures are therefore exact, and consequently no further useful information about carrying capacity can be gained from any upper-bound calculations.

Although the above argument is incontrovertible *in the present context of circular plates* we would be unwise to apply it in general. Indeed, it turns out on the whole that for plates of other shapes, both regular and irregular, it is much easier to obtain "good" upper bounds on collapse loads and pressures than it is to obtain "good" lower bounds.

Thus, although upper-bound methods—which include the celebrated "yield-line" theory due to Johansen—are always "unsafe" they are much more widely used in practice than simple lower-bound methods which are generally not only safe but also over-conservative.

It should be remarked that many experiments have shown that yield-line theory is a satisfactory design procedure. This is probably due, to some extent, to the strengthening effects of geometry changes already referred to. The upper-bound approach to design is not entirely satisfactory, however, because it is, of course, quite possible for an inexperienced or unimaginative designer when using an upper-bound method to "miss" the mechanism corresponding to the lowest load in his necessarily incomplete search.

One promising feature of lower-bound methods which has not yet been fully exploited in the field of slab design is the possibility of designing *variable* reinforcement. In contrast, the upper-bound methods (yield-line theory) work most easily when the reinforcement is *uniform*.

The aim of the present section is twofold: first to give an impression of the ease and brevity of upper-bound calculations, and second to demonstrate the close agreement between the upper bounds so obtained and the exact results for uniformly loaded circular slabs.

9.7. Modes of Deformation

Our first task is to envisage a likely mechanism of deformation. Two obvious ones are indicated in Fig. 9.7(a) and (b): the initially flat surface deforms into shallow spherical and conical surfaces respectively. It turns out that the *conical* mode gives the lower upper bound, so, as the spherical mode is very simple to analyse (Problem 9.7) we shall not study it further.

There are various ways of tackling the geometrical analysis of the shallow cone. Perhaps the simplest is as follows—but see Problem 9.8.

Radial lines on the surface remain straight, so (except in a vanishingly small region at the centre) we shall be interested only in changes in curvature, $\dot{\kappa}_\theta$, in the circumferential direction. Suppose we wish to find the change in curvature at radius r when the apex of the cone descends a small distance δ, as shown in Fig. 9.7(c). Curvature κ_θ is defined as the relative inclination in the vertical plane of two tangents to the surface in the circumferential direction, at points unit distance apart around a circle of radius

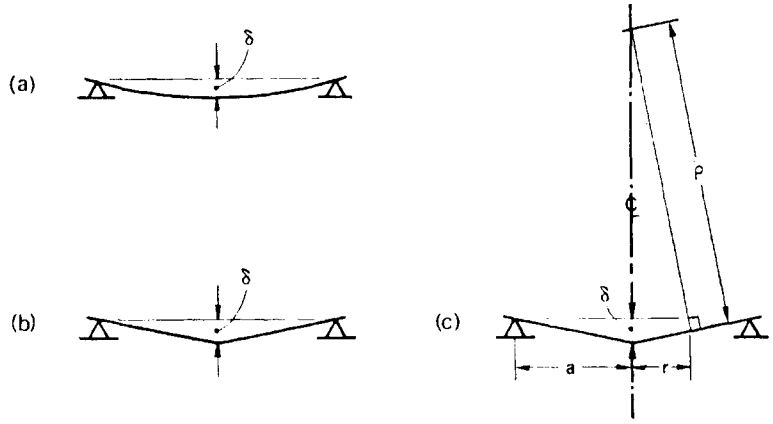

FIG. 9.7. (a) "Spherical" and (b) "conical" modes of deformation of a plate: (c) geometry of a shallow cone.

r. This is equal to the relative inclination of two *normals* to the surface at the same two points. Suppose two normals were attached, physically, to the initially flat surface, unit distance apart around the circle of radius r. In the deformed position shown, Fig. 9.7(c), these two normals would *intersect* at the axis of the cone, so the required change of curvature is simply equal to the reciprocal of the distance ρ indicated, since the two points are unit distance apart.

By similar, narrow, triangles,

$$\delta/a = r/\rho$$

so

$$\kappa_\theta = \frac{1}{\rho} = \frac{\delta'}{ra}$$

Therefore $$\dot{\kappa}_\theta = \dot{\delta}/ra \tag{9.22}$$

As $\dot{\kappa}_r = 0$ over the whole surface, the total rate of dissipation of energy over the surface is given by

$$\int_A M_0 \dot{\kappa}_\theta \, dA \tag{9.23}$$

where dA represents an elementary area: see (9.5). Taking a ring element of area between radii r and $r + dr$ we obtain, using (9.22)

$$2\pi M_0 \int_0^a r\dot{\kappa}_\theta \, dr = 2\pi M_0 \int_0^a \frac{\dot{\delta}}{a} dr = 2\pi M_0 \, \dot{\delta} \tag{9.24}$$

The rate at which pressure p does work in this postulated mechanism is simply equal to p times the rate of increase of volume under the shallow cone, i.e.

$$p \, \pi \, a^2 \dot{\delta}/3 \tag{9.25}$$

Equating the internal dissipation and external work we have, finally,

$$p^u = 6M_0/a^2$$

which is identical with our previous lower bound. It may seem surprising that a conical mode should be "preferred" to a spherical one; but if we examine it in relation to the bending-moment distribution of Fig. 9.4 and the normality rule of Fig. 9.3(c) we can see the explanation.

The analysis is readily extended to a plate with a clamped edge. In this case we have a term in addition to expression (9.24) corresponding to the dissipation of energy around the edge. At the edge $\dot{\kappa}_r$ is infinite if there is no transition zone between the cone and the support; this presents no difficulty in the evaluation of dissipation, however, because the dissipation of energy per unit length of such a plastic *hinge* is simply M_0 times the rate of change of hinge angle (see Problem 9.9). In the present example

the rate of rotation of the hinge is δ/a, so the additional dissipation term is, simply,

$$2\pi a M_0 \, \delta/a = 2\pi M_0 \, \delta \tag{9.26}$$

It is useful to remember that this is *exactly* the same as the dissipation term for the continuous deformation of the conical surface itself.

Thus, for a clamped plate,

$$p^u = 12 M_0/a^2 \tag{9.27}$$

which is about 6 per cent higher than the corresponding lower bound.

It is not difficult to see that the conical mode is not "compatible"—via the normality rule—with the lower-bound bending-moment trajectory: this accounts for the non-coincidence of the two bounds in this case.

9.8. Reinforced Concrete Slabs

A proper discussion of the subject of reinforced concrete and the relevance of plastic theory to it is beyond the scope of this book, since it would require consideration of a large amount of special technology. A reader who is interested in this branch of civil engineering should consult one of the books listed under "Reinforced concrete and yield-line theory" in the Bibliography.

However, it does seem worth while to make a small connection with the yield-line theory of reinforced concrete slabs at this point by noting that the only essential way in which metal plates and reinforced concrete slabs differ, as far as plastic theory is concerned, is in their respective yield loci: compare Fig. 9.3(c) with Fig. 9.8, which corresponds to a uniformly reinforced concrete slab with different amounts of "top" and "bottom" steel. The theoretical and experimental justification of a yield locus of this sort would occupy a considerable space, but if we can accept Fig. 9.8 as valid we can see immediately that practically all of our

results so far may be adapted readily to concrete slab construction; see Problem 9.10. In fact the absence of "inclined cut-offs" in Fig. 9.8 makes lower-bound analysis somewhat easier in the case of a clamped circular slab, and in these circumstances the upper and lower bounds coincide.

9.9. Point Loads

In many situations plates and slabs are loaded by forces which may be described as "concentrated" in so far as their area of

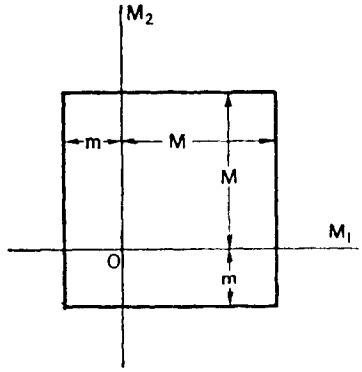

FIG. 9.8. Biaxial plastic bending of an element of a concrete slab with unequal "top" and "bottom" isotropic reinforcement.

application is small compared to the area of the plate or slab as a whole. For example, a ship may accidentally run into an angular projection on a jetty; or a compact, heavy piece of equipment may rest on a floor slab; or a continuous floor slab may be supported on a set of columns.

An obvious way of idealising such loads is as *point* forces. This idealisation, which is obviously a very useful one in some branches of mechanics, must nevertheless be regarded with particular caution in the context of the behaviour of plates and slabs. The difficulty is that our assumptions about the negligibility of certain components of stress (see pp. 216–217) may not be justified in the

vicinity of a concentrated load; and if this is so, then the basis of our theory is undermined.

To illustrate the dangers consider a simply supported circular plate, radius a and thickness h, loaded by a uniform pressure p applied over a small central circular area of radius c, as shown in Fig. 9.9.

An upper-bound analysis (which we may assume will give a "close" bound) based on a mechanism which consists of a rigid central area surrounded by a "conical" zone indicates (see Problem 9.11) that the total load P which can be sustained is:

$$P^u = 2\pi M_o/(1 - c/a). \tag{9.28}$$

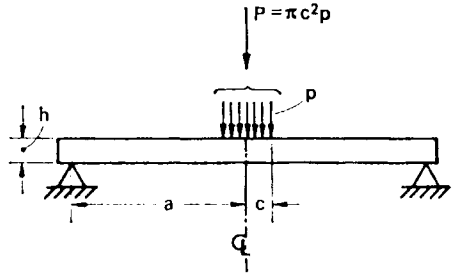

Fig. 9.9. A simply supported plate with a central loaded area.

An alternative mechanism, in which a central "plug" slides downwards on a cylindrical interface of intense shear, and the outer zone remains rigid, gives

$$P^u = 2\pi chk \tag{9.29}$$

Putting $M_o = Yh^2/4$ and $k = Y/2$ we can see by comparing (9.28) and (9.29) that the "local" mode is "preferred" if $c < h/2$, $c/a \ll 1$.

Although we do not know how "close" the bound (9.29) is, it seems clear that if the load is applied over an area whose diameter is not more than the thickness of the plate there may be a possibility of failure by "punching through".

This suggests that continuous floor slabs may fail locally where they are supported on columns. Indeed, it is well known that

special precautions have to be taken to avoid this sort of failure in reinforced concrete structures. There are, fortunately, several possible remedies including the use of "mushroom-headed" columns and the incorporation of heavy steel reinforcement.

Provided we are fully conscious of the possibility of local failure, it is instructive to study the effects of transverse point loads on plates and slabs. Several simple and interesting results are found in Problems 9.12 and 9.13.

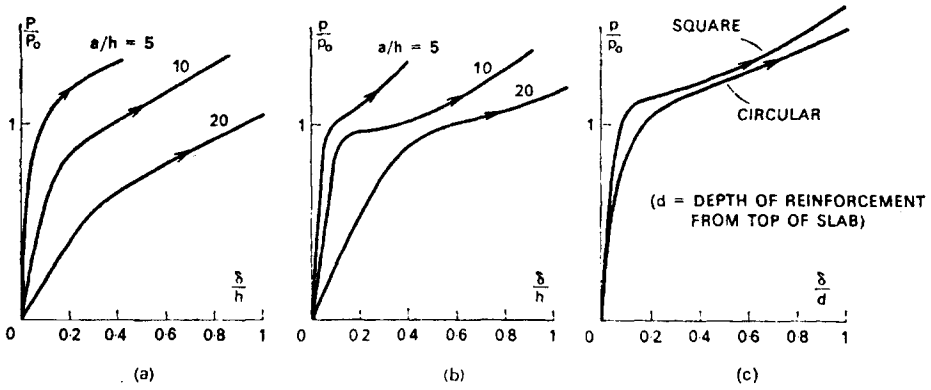

FIG. 9.10. Plates and slabs: experimental behaviour. (a) Mild-steel plate, simply supported, central "point" load applied through boss. (b) Mild-steel plate, built-in edge, pressure load. (c) Reinforced-concrete slab, simply supported, pressure load. Subscript 0 refers to collapse load/pressure according to the simple plastic theory of the present chapter.

9.10. Experimental Behaviour

We pointed out at the beginning of this chapter that it was reasonable to suppose that when plates and slabs deflected under transverse loading they would tend to become stronger. Therefore the "plateau" in the load-deflection curve predicted by simple plastic theory and observed in tests on beams and frames might, perhaps, not be so conspicuous in tests on plates and slabs.

Figure 9.10 shows some typical results of laboratory tests of simple plate and slab structures. Although the "geometry change" effects are clearly discernable it is nevertheless plain that the

collapse loads predicted by the theory we have developed in this chapter are strongly relevant to engineering design studies.

Problems

9.1. Show that the "safe" distribution of stress in an element of plate indicated in Fig. 9.3 is in fact compatible (via the normality rule) with a mode of deformation in which the central surface does not extend and "plane sections remain plane"—and hence that the "safe" locus of Fig. 9.3(c) is in fact exact for a Tresca material.

9.2. Assuming modes of deformation as in Problem 9.1, obtain an upper bound on the yield locus in M_r, M_θ space for an element of a symmetrically loaded circular plate.

9.3. Obtain an estimate of the load-carrying capacity of a simply supported circular plate by considering the overall equilibrium of a semicircular sector (see Fig. 9.5).

(*Hint.* First find the resultants (magnitude and position) of the "support" and "pressure" forces, respectively.)

9.4. Assume that the total transverse load which can be supported by a plate is a simple function of the full plastic moment per unit length of plate and a typical linear dimension in the plan view, and study the relationship from the point of view of dimensional analysis.

9.5. By studying the equilibrium equations for a circular plate symmetrically loaded, show that if the transverse loading consists only of pressure and forces there can be no "jumps" in the value of M_r. Similarly, show that there *may* be jumps in the value of M_θ.

9.6. A uniform beam of full plastic moment M_p is simply supported over a span l, and it carries a uniformly distributed load. Show that if the ends are subsequently "built in", the carrying capacity of the beam is thereby doubled. Make the usual assumptions of plastic theory about the bending of beams.

9.7. Make an upper-bound analysis of the simply supported circular plate under pressure loading, based on the "spherical" mode of collapse shown in Fig. 9.7(a).

(*Hint.* Consider the deflected profile to be a shallow parabola. Express curvature and "swept volume" in terms of the central deflection and radius.)

9.8.† Consider a plate which is a regular polygon in plan and which is deforming into a shallow regular pyramid. By using elementary solid geometry find an expression for the (small) angle of inclination between adjacent faces in terms of the height of the apex, the length of the edges and the number of faces of the pyramid. Show that the sum of all the small angles occurring in an annular region surrounding the apex tends to a constant value as the number of faces increases, and that the dissipation of energy within such a many-faced pyramid tends to expression (9.24) for a cone.

9.9. Examine the statement in the text (p. 228) about work dissipated at a *hinge* in terms of curvature-rate and normality rule: see equation (9.5).

9.10. Work through the chapter using the principal bending-moment yield

locus of Fig. 9.8 in place of that of Fig. 9.3(c), and make a table comparing your results with ones derived in the text. Use the symbols M, m to define the dimensions of the yield locus, as in Fig. 9.8.

9.11. Make an upper-bound analysis of the plate shown in Fig. 9.9. Try a mode consisting of an outer "conical" zone connected to an inner "flat" zone by a circumferential hinge, and express the dissipation quantities in terms of the velocity of the "virtual" apex of the cone and the ratio of the radius of the hinge circle to the radius of the plate.

(*Hint.* Check that the optimum position for the circumferential hinge is at radius c.)

9.12. Make lower- and upper-bound analyses of a uniform simply supported circular plate carrying a central "point" load P (say). Note that equilibrium equations (9.7) and (9.8) need modification.

(*Hint.* Be especially careful in the lower-bound analysis, and make checks like re-plotting Fig. 9.4.)

9.13.† Show that the upper-bound analysis of a uniform clamped plate under a central point load gives the same collapse load irrespective of the radius of the circumferential hinge—i.e. irrespective of the "size" of the deforming region. Show that, consequently, the same upper-bound load applies to a point load *anywhere* on the plate, and, indeed to a point load applied anywhere over a uniform plate of arbitrary plan, clamped around its edge.

Further, see if you can establish a result applying to several point loads placed arbitrarily on such a plate.

(*Hint.* Use the convexity theorem, as at the end of Chapter VI.)

9.14. In Fig. 9.8 the values of M and m may be identified with uniform isotropic "bottom" and "top" steel reinforcement, respectively. By making a lower-bound analysis of a uniformly loaded clamped circular slab (see Problem 9.10) and drawing the equivalent of Fig. 9.6, see if there is any region of the slab over which either "top" or "bottom" reinforcement may be omitted altogether without a corresponding reduction of carrying capacity.

9.15.† A uniform circular concrete slab of radius b with equal uniform isotropic top and bottom steel reinforcement (i.e. $m = M$, Fig. 9.8) rests on a concentric simple circular support of radius $a < b$. Find the value of a/b for which the plate can support the most load, uniformly distributed.

(*Hint.* Consider separately collapse of the outer and inner regions.)

CHAPTER X

METAL-FORMING PROCESSES: WIRE-DRAWING AND EXTRUSION

As WE pointed out in Chapter I, a large number of metal-forming processes are possible by virtue of the capacity of metals to undergo large-scale plastic deformation.

The most primitive of these processes is *forging*, in which the workpiece is deformed by successive hammer blows. The hammer may range in size from the kind wielded by a blacksmith to a large mechanical hammer capable of forging workpieces weighing tens of tons. Shafts, wheels, turbine discs and many other parts may be shaped in this way, and there are many variants of the process.

A short list of industrially important *continuous* metal-forming processes would include *rolling* of steel sections and sheet—usually in a large number of related operations from billet to finished product, *drawing* of wire through a sequence of tapered dies to reduce its diameter, *extrusion* of billets through orifices to many and various cross-sections, and *spinning* of sheet into parts of vessels, etc.

Non-continuous processes include, besides forging, *pressing* of sheet or plate into pressure-vessel ends or car-body panels, etc.

There are of course many important *technical* aspects of all these processes which are beyond the scope of a book on plasticity; for example there are metallurgical problems, including the question of the temperature of the workpiece; questions of lubrication, wear, surface finish, the maintenance of dimensional tolerances, control and many others.

Plasticity theory is relevant to questions of evaluation of power requirements, of loading on the dies, etc., and consequently of the design of details of forming processes. Not surprisingly most progress has been made in the application of plasticity theory to steady-state forming processes, although a large number of analyses have now been made on other processes. It might be added that plasticity theory has also been useful in analysing some *machining* processes.

In the present chapter we shall consider, briefly, the steady-state processes of *drawing* and *extrusion*, which are very different from each other technologically but nevertheless somewhat similar from the point of view of mechanics.

It may not be at all obvious why plasticity theory, which regards the mechanical deformation of materials as essentially time-independent, should be relevant to, say, the extrusion of a billet of metal at a temperature at which the mechanical response of the material is a continuing deformation with time—i.e. so-called "creep" deformation. Experiments indicate that the stress-dependence of creep rate at these temperatures is strongly non-linear, so that above a relatively narrow range of stress creep is "rapid", while below, creep is "slow". Under these circumstances the material may be idealised as rigid-perfectly plastic in situations where the load is applied to the workpiece at a prescribed speed; for example by a hydraulically operated ram in an extrusion machine. On the other hand, in the case of creep in structures at elevated temperatures under constant load, where the engineer needs to know the rate of deformation of the structure, plasticity theory is clearly incapable of answering the relevant questions.

Major advances in the application of plastic theory to the analysis of metal-working processes were made by Hill (see Bibliography) in the late 1940's and early 1950's; in particular Hill developed the use of slip-line fields for problems in plane strain. In the present chapter, however, we shall be concerned mainly with upper-bound calculations. As we have pointed out already, these are particularly appropriate in calculation of the power requirements of forming processes. Further, as we shall

see, they provide a ready access to the analysis of axisymmetric processes, to which nothing comparable is afforded by slip-line theory.

It may seem paradoxical that, having proved the bound theorems by means of virtual work—which is only applicable when geometry changes are negligible—we should apply one of the theorems to a situation where there are gross deformations.

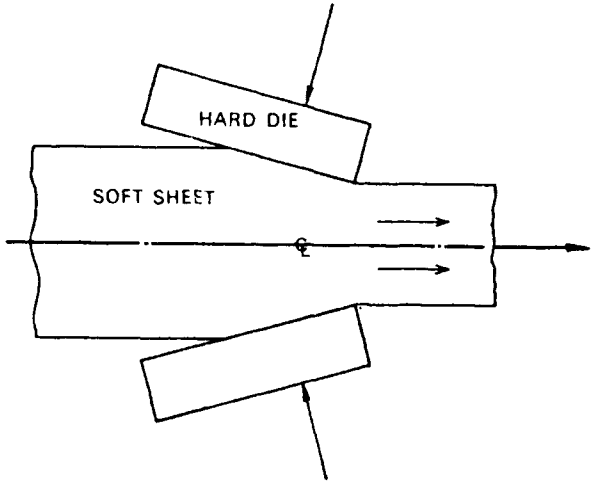

FIG. 10.1. Sheet drawing.

The paradox is resolved by noting that when a steady state has been reached the geometry is self-reproducing; it is therefore legitimate to consider small deformations at any point in time.

10.1. Sheet Drawing

For the sake of simplicity we begin our study with an analysis of sheet drawing, in which a metal sheet is reduced in thickness by being drawn through a pair of long dies, as shown schematically in section in Fig. 10.1. The width of the sheet (i.e. the dimension perpendicular to the section shown) is taken to be large compared

to the thickness, so that the process may justifiably be regarded as one of plane strain.

The process may be regarded as a continuous version of a *pressing* operation in which the sheet is made thinner, step by step, by being compressed between dies as shown in Fig. 10.2(a). This comparison is instructive in several ways (see below) but here we are concerned with only one aspect of it, namely that if the tools are too narrow, as in Fig. 10.2(b), the plastic deformation will be confined to shallow regions in the sheet (see Chapter

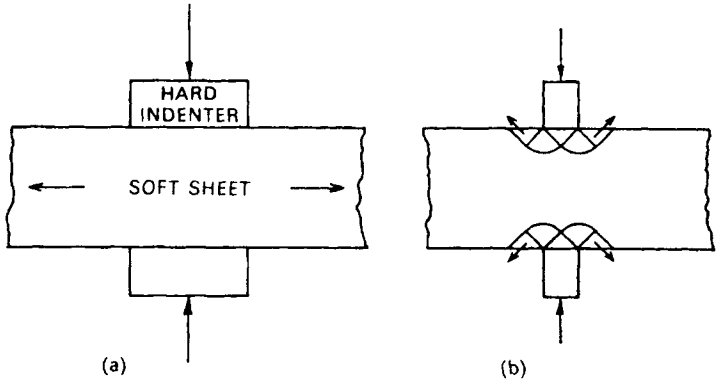

FIG. 10.2. Pressing of a sheet between (a) wide and (b) narrow dies.

VII). In this case the thickness of the sheet will be reduced locally, but a repetition of the process cannot produce a thinner sheet because the length of the central plane of the sheet remains unchanged. We see that a necessary condition for the effectiveness of the processes indicated in Figs. 10.1 and 10.2(a) is that the zone of plastic deformation should extend *through* the sheet.

10.2. A Simple Mode of Deformation

By analogy with Fig. 7.12(a), the upper-bound mode of deformation shown in Fig. 10.3(a) almost suggests itself for sheet drawing. The blocks B, B' slide along the faces of the die—assumed perfectly smooth at present—and they are separated from the

material approaching and leaving the dies (blocks A and C, respectively) by interfaces of intense shearing. These interfaces remain stationary with respect to the dies, and the only deformation undergone by an element in the sheet as it passes through the constriction occurs when it traverses these planes of discontinuity. The interfaces of intense shear must intersect the surface of the material at the points where there is a discontinuity in slope of the surface.

The position of point F is arbitrary, but if we assume that F is on the centre-line, for reasons of symmetry, we conveniently limit our family of modes to one with a single degree of freedom.

In Fig. 10.3(a) we denote the half-angle of the die by α, and the average drawing stress acting on the emerging sheet by t. It is convenient to take the half-thickness of sheet entering the die as the unit of length, and to denote the half-thickness of the sheet emerging by s, as indicated.

The corresponding velocity diagram is shown in Fig. 10.3(c): it is drawn and labelled as in Chapter VII. For reasons of continuity we expect

$$oc = oa/s \tag{10.1}$$

and we can check that this is so for all positions of F by analysing the trigonometry of the velocity diagram.

Using the notation l_{AB}, v_{AB}, etc., for lengths and relative velocities as in Chapter VII, and defining the approach velocity of A as unit velocity, for convenience, we write down the upper-bound equation for unit width (perpendicular to the plane of the diagram) for half the sheet:

$$t''s\ (oc) = k(l_{AB}\, v_{AB} + l_{BC}\, v_{BC}) \tag{10.2}$$

Here, as usual, k is the yield stress of the material in pure shear. Note that, by (10.1), s cancels from the L.H.S., thus giving a direct expression for the drawing stress. Note also that precisely the same expression would be obtained if we used the same mode to study *extrusion* of the material through the same dies; the extrusion pressure and drawing stress would thus be identical—

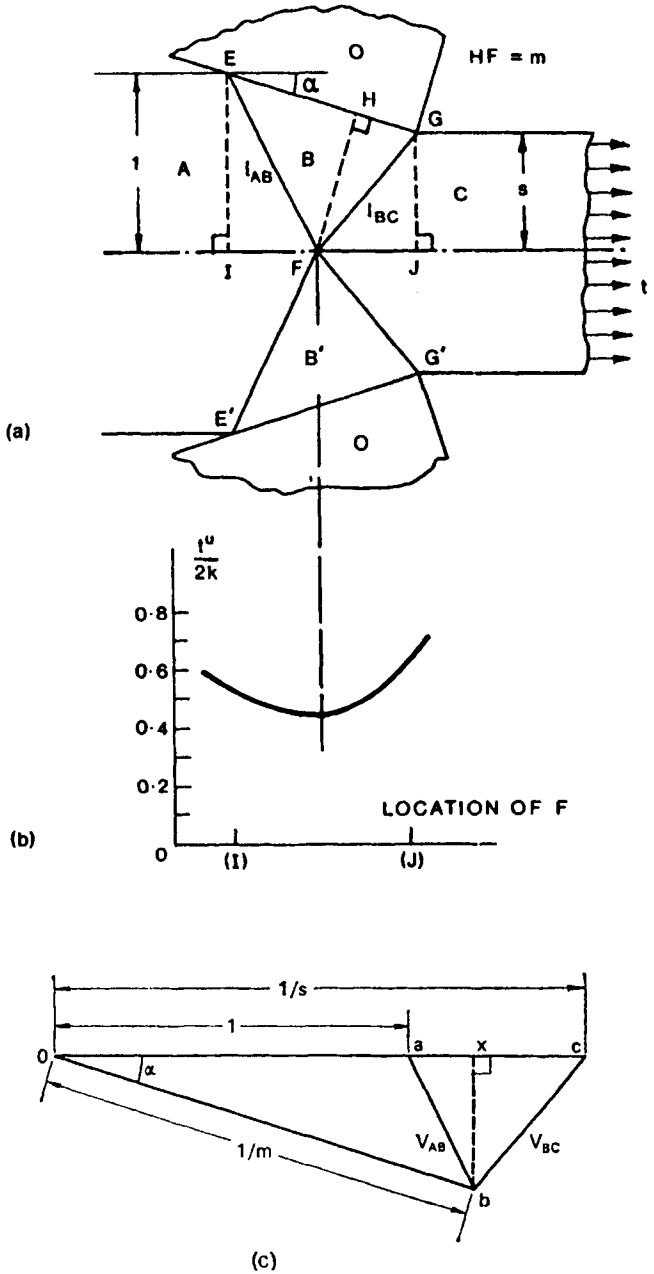

FIG. 10.3. A postulated "rigid-block" mode of deformation for sheet drawing.

in this upper-bound calculation—but the *force* required for extrusion would be greater, of course.

For given values of α and s the calculation of (10.2) is readily accomplished, by means of measurement from scale drawings, for any postulated position of F. Some results are shown in Fig. 10.3(b); against the position of F (projected from Fig. 10.3(a)) is shown the value of $t/2k$, i.e. the ratio of t to the yield stress of the material in pure tension, according to Tresca. The curve has a "flat minimum", so a good estimate of the minimum value of $t/2k$ could be found in this case with little labour.

In fact it is not difficult, with a little ingenuity, to evaluate the R.H.S. of (10.2) algebraically. Following hints obtained from Chapter VII we seek a suitable *length* variable to define the mode. The most convenient variable turns out to be the length of the perpendicular FH from F to EG, Fig. 10.3(a), say m. As the rate of flow of volume past FH is the same as that across EI (or GJ), we see in Fig. 10.3(c) that $ob = 1/m$. Using the auxiliary point x in the velocity diagram, applying Pythagoras' theorem and tidying up we obtain general expressions (which the reader should check for himself):

$$v_{AB} = \left(\frac{1}{m^2} - \frac{2\cos\alpha}{m} + 1\right)^{\frac{1}{2}} \tag{10.3}$$

$$v_{BC} = \left(\frac{1}{m^2} - \frac{2\cos\alpha}{sm} + \frac{1}{s^2}\right)^{\frac{1}{2}} \tag{10.4}$$

The lengths l_{AB}, l_{BC} could be evaluated similarly from the geometry of Fig. 10.3(a), but it is quicker to observe that triangles EIF and bxa are similar, and hence

$$l_{AB} = v_{AB}/xb$$

In terms of m and α, therefore

$$l_{AB} = v_{AB}\, m/\sin\alpha \tag{10.5}$$

Similarly

$$l_{BC} = v_{BC}\, ms/\sin\alpha \tag{10.6}$$

Substituting in (10.2) and tidying up we have, finally,

$$\frac{t^u}{2k} = \frac{1 + s}{2 \sin \alpha}\left(\frac{1}{m} + \frac{m}{s}\right) - 2 \cot \alpha \tag{10.7}$$

This has a minimum value with respect to our independent variable m when

$$m = \sqrt{s} \tag{10.8}$$

Our lowest upper-bound is thus

$$\frac{t^u}{2k} = \frac{1}{\sin \alpha}(s^{\frac{1}{2}} + s^{-\frac{1}{2}}) - 2 \cot \alpha \tag{10.9}$$

It is interesting to note that the optimum value of m for a given reduction of thickness is thus independent of the die angle. There are several other interesting aspects of this solution, which are indicated in Problem 10.1.

10.3. Ideal Drawing

Before we explore in detail the implications of (10.9) it is useful to establish some general considerations relating to frictionless drawing of non-hardening plastic material.

First we observe that the upper-bound analysis we perform involves the calculation of dissipation of energy by the material in the zone of deformation per unit time. The same calculation could equally be said to apply to unit volume of material *passing through* the die, and it is easy to verify that the average upper-bound drawing stress is numerically equal to the work dissipated per unit volume "throughput". This statement applies not only to the simple modes of deformation which we are considering but also to any geometrically compatible mode, including in particular the "correct" one.

It is sometimes instructive to approach upper-bound calculations from this point of view. However, our main purpose in making this observation is to lead to the question: what is the

least amount of energy necessary to change the thickness of unit volume of material by a factor s? The answer to this question will indicate the least possible drawing stress required to execute a drawing process for a given reduction. We may call this the "ideal" drawing stress, and use it as a basis of comparison, from the point of view of *efficiency*, for any given drawing process.

It is easy to show (Problem 10.2) that in homogeneous plane strain deformation of a block of perfectly plastic material to a fraction s of the original thickness the work required is $2k \ln(1/s)$ per unit volume; and in fact this is the required minimum. It follows that $t/2k = \ln(1/s)$ is the minimum drawing stress for a plane-strain reduction in thickness from 1 to s in an "ideal" drawing process.

In discussing the efficiency of a drawing process it is natural to refer to the work done per unit volume throughput in excess of this ideal work as the *redundant work*.

It is also useful when presenting information about drawing stresses to use the parameter $\ln(1/s) = \xi$, say, as a measure of the reduction of thickness. The more conventional measure, defined as the decrease in thickness per unit original thickness, is known as the "reduction", r. Here we shall use the symbol r_t to denote reduction of *thickness*; it will be useful in later discussion to have a different subscript for reductions of *area* in axisymmetric processes. In the present notation, $r_t = 1 - s$, so

$$\xi = \ln(1/s) = \ln(1/(1 - r_t)) \tag{10.10}$$

For sufficiently small reductions, $r_t \simeq \xi$.

Although we shall regard ξ as the "natural" measure of reduction, we shall always indicate some values of r_t on the ξ-axis of our graphs, for convenience of comparison with other work.

The notion of an ideal process provides, then, a rational basis for assessment of actual processes. As we shall see, some drawing processes with dies of small inclination come close to the ideal as far as drawing stress is concerned, but extrusion through "square" (i.e. $\alpha = 90°$) dies will turn out in general to be considerably less efficient.

If instead of analysing given die geometries we were to set out to *design* dies, it would obviously be a useful aim to try and realise an ideal process. Hill and others have recently studied this problem, and have produced relatively simple procedures for generating efficient die profiles with curved flanks. It remains to be seen

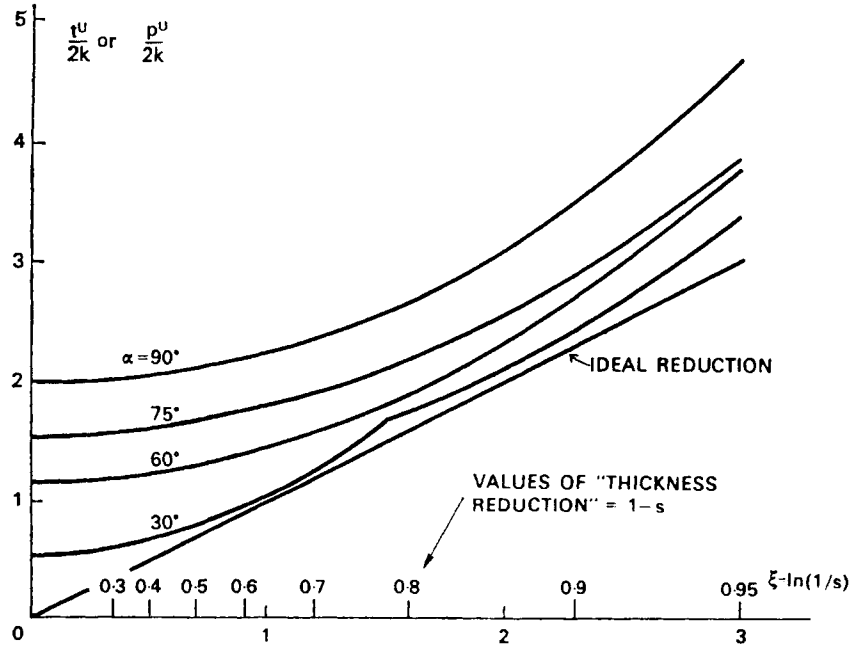

FIG. 10.4. Upper bounds on the sheet drawing stress for various die-angles: smooth dies.

whether widespread use will be made of dies of this sort, and we shall not study the problem further in this book.

10.4. Presentation of Results

Returning to our general upper-bound result (10.9) and observing that $s^{\frac{1}{2}} + s^{-\frac{1}{2}} = 2\cosh(\xi/2)$ we may write

$$\frac{t^u}{2k} = \frac{2}{\sin\alpha}\left(\cosh\left(\frac{\xi}{2}\right) - \cos\alpha\right) \tag{10.11}$$

This is plotted in Fig. 10.4 for several values of α ranging from 30° to 90°.

Now it is clearly not possible to sustain in the drawn sheet a tensile stress larger than the yield stress for the material, so in the graph configurations for which $t^u/2k > 1$ are of no practical interest for drawing—assuming, of course, that our upper-bound results are not much too "high". In particular, we shall not be

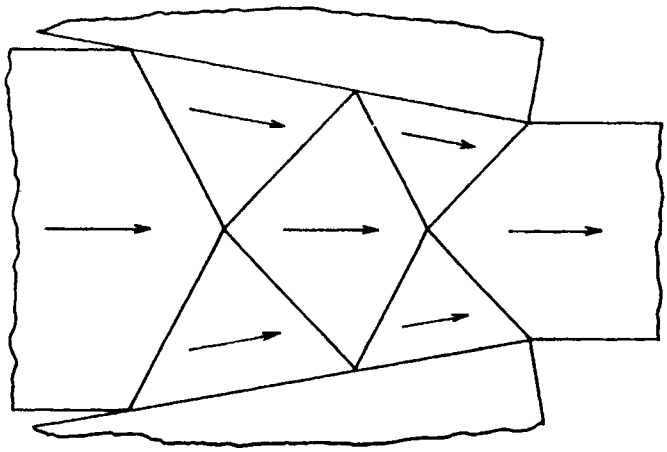

FIG. 10.5. An alternative "double" mode.

able to use large die angles for drawing. Such die angles will, however, be relevant to extrusion processes.

Before we restrict attention to small values of α it is worth while making several points with reference to Fig. 10.4.

(i) The curve for $\alpha = 30°$ is shown with a kink. This is because a lower upper-bound is found, for $\xi > 1 \cdot 5$, by considering two modes like Fig. 10.3 "end-to-end", as shown in Fig. 10.5. If the (proportional) reduction is the same for the two sub-modes, we can easily adapt equation (10.11) to the "double" mechanism. For larger overall reductions a larger number of sub-modes may give lower upper-bounds (see Problem 10.3).

(ii) All of the curves are nearly parabolic in the range plotted (up to $r_t = 95$ per cent). The explanation of this is that the first two terms of the power series

$$\cosh(\xi/2) = 1 + \xi^2/8 + \xi^4/384 + \ldots \quad (10.12)$$

underestimate the value of $\cosh(\xi/2)$ by relatively small amounts in the relevant range of ξ.

(iii) The curve for $\alpha = 30°$ approaches quite closely the "ideal" line $p/2k = \xi$, at about $\xi = 1$. From (10.11) we find that for a given ξ, $t^u/2k$ is minimum when

$$\sin\alpha = \tanh(\xi/2) = (1-s)/(1+s) \quad (10.13)$$

(see Problem 10.4) and the minimum is given by

$$(t^u/2k)_{min} = 2\tan\alpha = 2\sinh(\xi/2) \quad (10.14)$$

Thus the ratio of the minimum upper-bound value of $t/2k$ for a given ξ (obtained by using the optimum value of α indicated by (10.13)) to the ideal value is:

$$\frac{(t^u/2k)_{min}}{(t/2k)_{ideal}} = \frac{2\sinh(\xi/2)}{\xi} = 1 + \frac{\xi^2}{24} + \frac{\xi^4}{1920} + \ldots \quad (10.15)$$

For small values of ξ, therefore, the optimum smooth wedge-shaped die gives very nearly ideal drawing stresses.

10.5. Drawing with Small Die Angles

For sufficiently small angles α we may use the approximations

$$\sin\alpha = \alpha \quad \text{and} \quad \cos\alpha = 1 - \alpha^2/2$$

Using also the quadratic approximation for $\cosh(\xi/2)$ (10.12), equation (10.11) becomes

$$\frac{t^u}{2k} = \alpha + \frac{\xi^2}{4\alpha} \quad (10.16)$$

This approximate formula is represented, universally, in Fig. 10.6.

The curve touches the "ideal" line $t/2k = \xi$ at $t/2k = 2\alpha$ (Problem 10.5), and the changeover from one to two effective reductions (see Fig. 10.5) takes place at $\xi = 2\sqrt{2\alpha}$ (see Problem 10.6).

Now equation (10.11) and the approximation (10.16) give the physically unrealistic result that for zero reduction a finite drawing stress is required. These equations, of course, only represent *upper bounds* on drawing stress, so we suspect that the mode we have used, Fig. 10.3, is probably not really appropriate for small

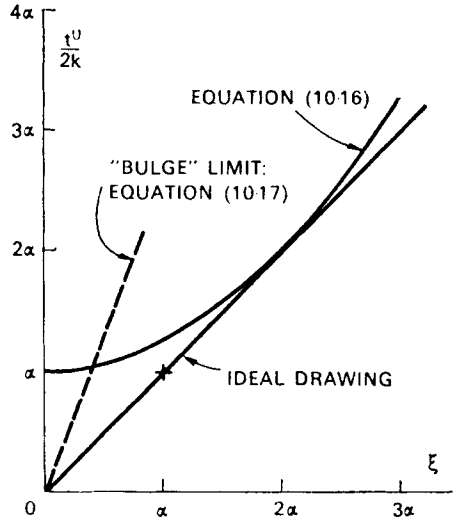

FIG. 10.6. Upper bounds on drawing stress: smooth dies and small angles of inclination.

reductions. Figure 10.7 shows an alternative mode suggested by the "pressing" analogy, Fig. 10.2(b), in which the sheet "bulges" instead of being reduced in thickness. Analysis shows (Problem 10.7) that for this mode

$$t/2k = (2{\cdot}57 - \alpha)\,\xi \simeq 2{\cdot}57\,\xi \qquad (10.17)$$

for sufficiently small values of ξ and α. This equation is also shown in Fig. 10.6, which suggests that the required drawing operation will not be accomplished unless

$$\xi > 0{\cdot}4\,\alpha$$

or, equivalently, unless the *length of contact* with the die is more than about 0·4 times the half-thickness of the entering sheet. (It is interesting to examine equation (10.13) from the point of view of length of contact with the die.)

10.6. Sheet Drawing in the Presence of Friction

As we observed in Chapter VII the bound theorems do not apply in the presence of friction, but we can nevertheless make a rough estimate of the effect of friction by considering the two extreme cases of perfectly smooth and perfectly rough dies, for which the theorems are valid.

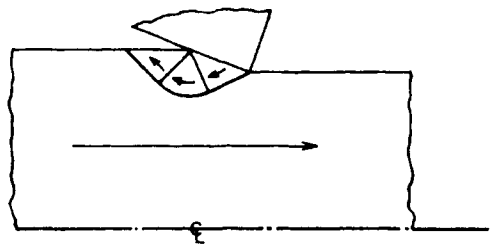

FIG. 10.7. A "bulging" mode.

In good wire-drawing practice the coefficient of friction between the wire and the dies is less than 0·1, so it seems clear that the actual situation is nearer the "smooth" than the "rough" extreme. It is not difficult to justify this by comparing the drawing stress in the smooth and rough conditions, respectively: see Problem 10.8, which makes use of results obtained in a later section. Even so, friction can have a pronounced effect on the drawing stress. Therefore, it seems appropriate to make a temporary departure from strict use of the bound theorems and seek an *approximate* way of investigating the effects of given coefficients of friction. The key is provided by slip-line theory, which is in fact immune from these difficulties over friction, since the inclination of α- and β-lines to a rough surface can be made to

correspond with a given coefficient of friction. Slip-line studies have shown that for practical purposes the *normal pressure* on dies is unaffected by friction provided the coefficient μ is small. If this is so, we find from simple statics

$$\left(\frac{t}{2k}\right)_\mu = \left(\frac{t}{2k}\right)_{\mu=0} (1 + \mu \cot \alpha) \tag{10.18}$$

We may now apply this correction to the results we have obtained so far. In particular, we may investigate the dependence of the optimum value of α on ξ and μ.

Combining (10.11) and (10.18) we have an expression which we can minimise with respect to α. Not surprisingly, small coefficients of friction do not change the optimum value of α much from the value (equation (10.13)) for zero friction, and an approximate analysis indicates that the optimum angle is increased by the addition of:

$$\frac{\mu}{1 + \dfrac{3\mu}{\sinh(\xi/2)}} \tag{10.19}$$

in the presence of a small coefficient of friction.

A rough empirical rule is that the optimum angle for zero friction is given by $\alpha_{opt} = 2{\cdot}8\ \xi$ (for $r_t < 0{\cdot}5$) and that this is increased by a factor of approximately $(1 + 2\mu)$ for a small coefficient of friction. This analysis agrees closely with the results of Hill's slip-line analysis.

We shall see later that the relationship between optimum die angle and coefficient of friction is rather different in the case of axisymmetric drawing.

10.7. Extrusion through Square Dies

The methods of the previous section can be extended readily to a study of plane-strain extrusion through a smooth square (i.e. $\alpha = 90°$) die from a smooth container.

As we have already observed, extrusion pressures are numerically equal to drawing stresses and there is no reason why extrusion pressures should not exceed the yield stress of the material; thus we may simply interpret the curve for $\alpha = 90°$ in Fig. 10.4 as a graph of $p''/2k$, where p is the extrusion pressure, against ξ. The corresponding mode is shown in Fig. 10.8(a), and the curve is replotted in Fig. 10.9. For small reductions we must also consider a "bulging mode" analogous to that of Fig. 10.7, but now a *forward* bulging as shown in Fig. 10.8(b) since the possibility of

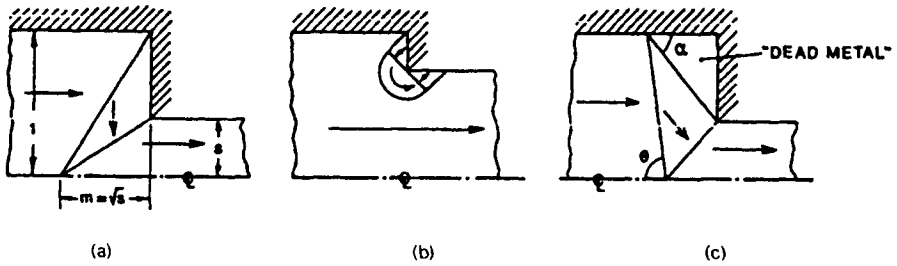

FIG. 10.8. Plane-strain extrusion through square (i.e. $\alpha = 90°$) dies: three possible modes.

backwards flow is precluded by the presence of the container. This mode gives (cf. Problem 10.7)

$$\frac{p''}{2k} = 4{\cdot}14\,(1 - s) \tag{10.20}$$

which is indicated in Fig. 10.9. The upper-bound curves corresponding to the modes of Fig. 10.8(a) and (b) intersect at a reduction of r_t of about 0·5. On this basis a proper extrusion would not be expected for reductions of less than 0·5.

However, experiments indicate that in some circumstances "dead zones" of metal are formed behind the die, somewhat as indicated in Fig. 10.8(c), which shows a general possible "rigid block" mechanism. The upper-bound calculation for this mechanism is of course very similar to that for the mechanism of

Fig. 10.3(a), the only difference being that EG is now an interface of intense shear instead of a smooth surface. To the R.H.S. of equation (10.2) must be added an extra term $kl_{OB}v_{OB}$. Now

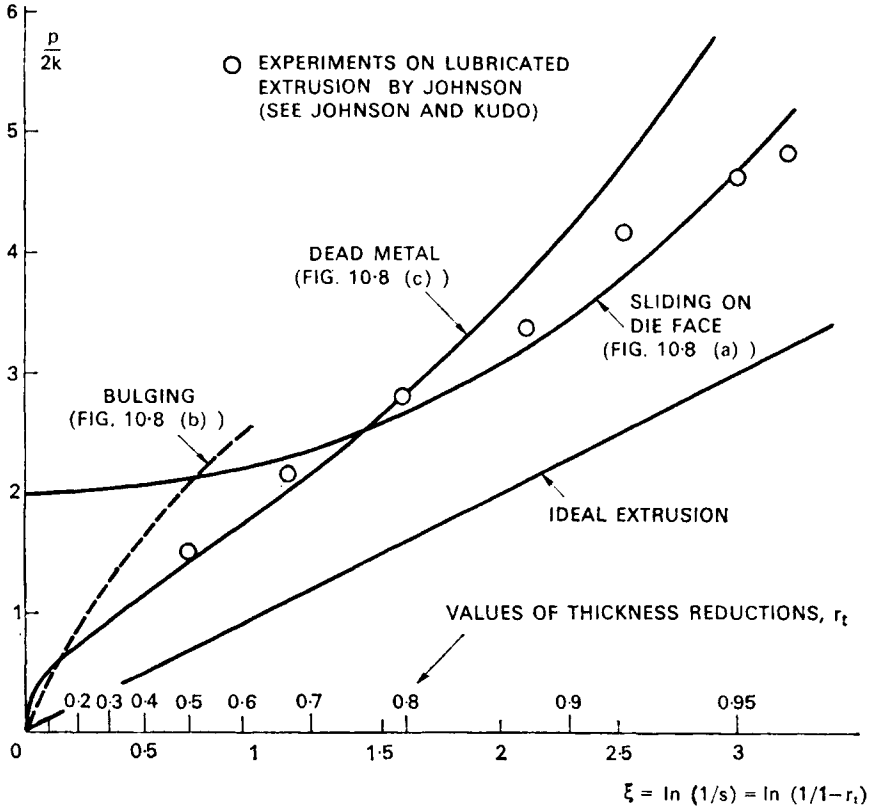

Fig. 10.9. Plane-strain extrusion through square dies: upper bounds on extrusion stress and experimental points.

$l_{OB} = (1-s)/\sin\alpha$, by simple geometry, and $v_{OB} = 1/m$. Hence, instead of equation (10.7) we now have

$$\frac{p''}{2k} = \frac{1}{2\sin\alpha}\left[\frac{2}{m} + \left(\frac{1+s}{s}\right)m\right] - 2\cot\alpha \qquad (10.21)$$

This expression is a minimum with respect to m when

$$m = \sqrt{2s/(1+s)} \qquad (10.22)$$

and thus for a given value of α the minimum upper bound is

$$\frac{p^u}{2k} = \frac{1}{\sin\alpha}\sqrt{\frac{2(1+s)}{s}} - 2\cot\alpha \qquad (10.23)$$

The angle α defining the dead-metal zone is a variable, and so expression (10.23) may be minimised w.r.t. α. We find that for $p^u/2k$ to be a minimum,

$$\sin\alpha = \sqrt{(1-s)/(1+s)} \qquad (10.24)$$

This corresponds to $\theta = 90°$ in Fig. 10.8(c). Hence the best upper bound is

$$\frac{p^u}{2k} = \sqrt{\left(\frac{2(1-s)}{s}\right)} \qquad (10.25)$$

This is also plotted in Fig. 10.9. It is lower than the two previous bounds over a range of thickness reductions from 0·15 to 0·8 approximately.

In drawing processes the question of efficiency is very important because drawing is impossible if $t > 2k$. The same restriction does not apply to extrusion, because the container walls prevent thickening of the original sheet when $p > 2k$, and this of course makes possible larger reductions in extrusion than in drawing. The penalty paid for inefficiency in extrusion is that the internal pressure tending to burst the container, the frictional drag between the billet and the container, and the total load on the die all increase as extrusion pressure increases. This, in turn, makes for greater difficulty in designing the various components of the extrusion machine against fatigue damage due to repeated loading.

From our analysis, roughness of the die face in extrusion of this sort does not seem to make much difference to the overall efficiency of the process: if a "dead metal" zone forms over the whole face the upper bound calculation just given applies whatever the coefficient of friction (see Fig. 10.9).

In real extrusion the force/distance relationship for the ram is typically somewhat as indicated in Fig. 10.10. The initial portion

of the curve may be irregular while the steady-state is being established. The steady drop of extrusion force is due to the progressive shortening of the billet and consequent reduction of the surface available for frictional action. The final part of the curve relates to the so-called "post-steady" state when the billet becomes so short that it is possible for plastic deformation to extend to its back face. The steady-state conditions assumed in our analysis may be expected to approximate the actual conditions at about point *B*.

Figure 10.9 also shows some experimental results, due to W. Johnson, for lubricated plane-strain extrusion of tellurium

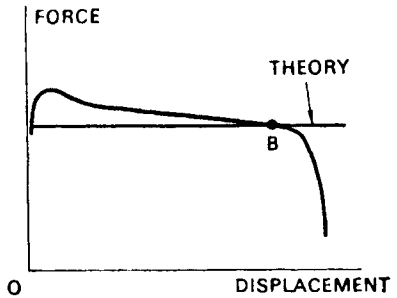

FIG. 10.10. Force–distance relationship in extrusion.

lead through square dies (*Journal of the Mechanics and Physics of Solids*, vol. 4, 1954, p. 264). In each case the force corresponds to point *B*, Fig. 10.10. Tellurium lead has a low yield stress and exhibits practically no work hardening over a large range of strain, and is thus a suitable material for simple experiments. Agreement between theory and experiment is very good, and although the experimental points lie up to 10 per cent higher than what are supposed to be upper-bound curves, they were plotted on the (Tresca) assumption that $k = Y/2$, Y having been measured experimentally. If the Mises hypothesis had been used instead, all of the points would have been lowered by about 15 per cent. We conclude therefore that the upper-bound calculation gives results which agree very well with experiments in this case.

10.8. Hydrostatic Extrusion

There are economic and commercial advantages to be gained from the extrusion of stronger materials, and extrusion with larger reductions, both of which require higher extrusion pressures and forces.

A stringent limit is usually set on the operating conditions of an extrusion press by the desirability of avoiding fatigue damage after repeated operation of the press, which in turn limits the extrusion pressures and forces which can be allowed in a given press.

A relatively new variant of conventional extrusion procedures is *hydrostatic extrusion* in which the billet is surrounded by a lubricant at a pressure of the same order of magnitude as the extrusion pressure. Among the advantages claimed are substantially less frictional drag between the billet and the container, and better lubrication of the die, resulting in a better finish on the extruded product.

10.9. Allowance for Work-hardening

So far in this chapter we have assumed that the material being drawn or extruded is perfectly plastic, i.e. non-hardening; and indeed this is a necessary assumption whenever we apply the upper- or lower-bound theorems. It is obviously desirable to be able to make a rough assessment of the effects of work-hardening on drawing and extrusion stresses, and it would be pleasant if we could somehow adapt the results of the preceding analysis for this purpose.

Hill has given an elegant argument leading to a simple calculation, which applies equally to drawing and extrusion. In the drawing of a perfectly plastic material through frictionless dies the drawing stress t is equal to the mean plastic work done per unit volume throughput, as we have seen. Since the yield stress is constant, the quantity $t/2k$ represents (for a Tresca material) the equivalent (true) strain imparted on average to the material in the

process. Let us assume that, to a first approximation, the same mean equivalent strain is imparted by the die *whatever* the strain-hardening characteristics of the material. The work done per unit volume of material taken to this strain level is simply equal to the area beneath the true stress–true strain curve in pure tension or compression up to strain $t/2k$, and this is therefore equal to the drawing stress in the presence of strain-hardening. Applying this idea to a linear strain-hardening material with

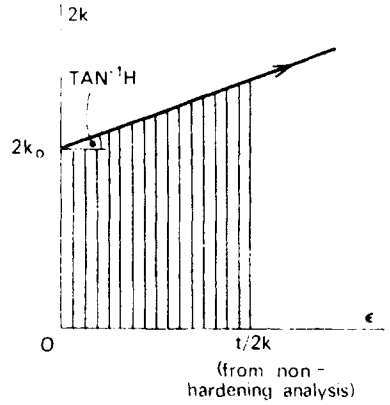

FIG. 10.11. Effect of linear strain-hardening.

initial yield stress $2k_0$ in tension and a strain-hardening coefficient H, see Fig. 10.11, we find

$$t = \left(\frac{t}{2k}\right) \cdot 2k_0 + \left(\frac{t}{2k}\right)^2 \cdot \frac{H}{2} \qquad (10.26)$$

Note that in this calculation we are regarding $(t/2k)$, read from a graph such as Figs. 10.4, 10.6 or 10.9, as a *geometrical* quantity.

Formula (10.26) is tantamount, for linear strain-hardening, to using graphs such as Fig. 10.4, etc., in conjunction with the *mean* yield stress of the material before and after drawing. This procedure for "allowing" for strain-hardening was used by Wistreich in the interpretation of his wire-drawing experiments, which we shall consider later.

10.10. Axisymmetric Wire-drawing

The deliberate redundancy in the above heading emphasises that so far, by considering plane-strain drawing and extrusion, we have avoided a proper consideration of the practically more important axisymmetric problems.

One result in the theory of axisymmetric plastic flow is easily established. It is that in "ideal" processes the drawing or extrusion stress is given by

$$\frac{t}{Y} = \frac{p}{Y} = \ln\left(\frac{1}{s^2}\right) = \ln\left(\frac{1}{1 - r_a}\right) \tag{10.27}$$

where s is the radius emerging per unit radius entering, and r_a is the reduction in cross-sectional area per unit cross-sectional area entering. This result is obtained by considering the work done in homogeneous axisymmetric deformation, and, in contrast to the equivalent plane-strain calculation, Y is the appropriate measure of the yield stress (see Problem 10.2).

If we adopt the Tresca hypothesis $Y = 2k$ we see that the ideal drawing stress is given by the same formula in both plane-strain and axisymmetric flow, provided the reduction is expressed as a reduction in *area*, since in plane strain $r_a = r_t$. This suggests that any comparison between the two kinds of process should be on a basis of reduction of cross-sectional area rather than, say, reduction of linear dimensions.

It would be unwise, however, to take this idea further at this stage, and regard our plane strain results in Figs. 10.4, 10.6 and 10.9 as applying directly to axisymmetric processes, because the manner of deformation of material is quite different in the two processes. In axisymmetric processes the circumference of a "hoop" entering the die is reduced, so the circumferential stress, which is a principal stress by symmetry, is necessarily *non-intermediate*. In contrast, in plane strain the principal stress perpendicular to the plane *is* intermediate. It is not clear *a priori* whether this difference will produce markedly different relation-

ships in general between extrusion pressure and reduction in area for the two kinds of process.

To investigate this question let us begin by seeking an upper-bound solution for drawing or extrusion through a smooth conical die.

The most obvious postulated mode of deformation includes a zone of pure radial flow towards the virtual apex of the cone, as shown in Fig. 10.12. This radial flow is "ideal", so the work dissipated at the spherical interfaces at entry to and exit from this

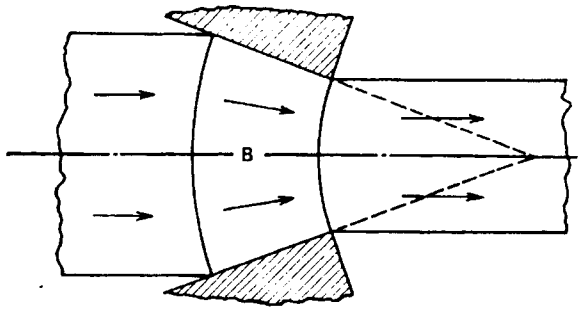

FIG. 10.12. A simple mode involving a region of radial flow: plane-strain or axisymmetric conditions.

zone is all "redundant" (see section 10.3). For small die angles α at least this redundant work is proportional to α (see Problem 10.9), so this upper-bound analysis does not indicate, in particular, a finite optimum value of α for any given reduction. Much the same conclusions are drawn from an upper-bound analysis in plane strain based on a *cylindrical* flow pattern, Fig. 10.12, and as these are at variance with those already made, it seems clear that the "radial flow" mode is too unrealistic to be useful.

As Fig. 10.12 serves to define *either* a plane-strain flow *or* an axisymmetric one, it seems plausible that an axisymmetric analog of the plane-strain mode of Fig. 10.3 might furnish good upper bounds on drawing stress. Let us therefore investigate the geometry of axisymmetric flow corresponding to Fig. 10.13(a).

Zones A and C are moving as rigid bodies along the centre

line. *EF* and *FG* represent *conical* interfaces of intense shear defining the zone *B*. If we postulate that the path of any particle in zone *B* is parallel to *EG* in the section shown, the flow in zone *B* is uniquely determined for an incompressible material. The flow in zone *B* is thus as if between a set of nesting *equi-angular* conical surfaces, in contrast to the flow in zone *B* of Fig. 10.12 which is effectively between a set of cones of different angle but common *apex*. As the perpendicular distance between two nearby "virtual" cones is everywhere the same, it follows that the speed of any element is inversely proportional to its distance from the axis as it travels through the zone.

In each of these elementary thin conical "flow tubes" the material undergoes a circumferential compression accompanied by an extension along the flow line, but no change of thickness perpendicular to the surface of the tube. The deformation is therefore tantamount to an "ideal" plane-strain flow, and as the flow tube emerges at radius s times its initial radius the work dissipated per unit volume of material in region *B* is simply equal to $2k \ln(1/s)$ (see Problem 10.2).

We shall need to look more closely at the flow pattern in region *B* later on, but let us next investigate the work dissipated at the conical interfaces of tangential velocity discontinuity *EF* and *FG*. Consider a small stream-tube of flow through the die, of cross-sectional area Δ at entry, Fig. 10.13(a). The velocity diagram for the interface *EF*, for unit entry velocity, is exactly the same as *oab*, Fig. 10.3(b). The area of intersection of the stream tube with interface *EF* depends only on Δ and the cosine of the angle between *EF* and the axis, and is equal to $l_{AB}\Delta$, see Fig. 10.3. The rate of dissipation of energy at this interface is therefore equal to $kl_{AB}v_{AB}\Delta$.

The cross-section of the same stream tube emerging from the die is equal to $s^2\Delta$, since in this mode of deformation all stream tubes undergo geometrically similar flow. The area of intersection of the tube with interface *FG* is therefore $s^2(l_{BC}/s)\Delta = sl_{BC}\Delta$. The velocity diagram for this interface is *similar* to *obc*, Fig. 10.3(b), but enlarged by a factor $(1/s)$ on account of the accelera-

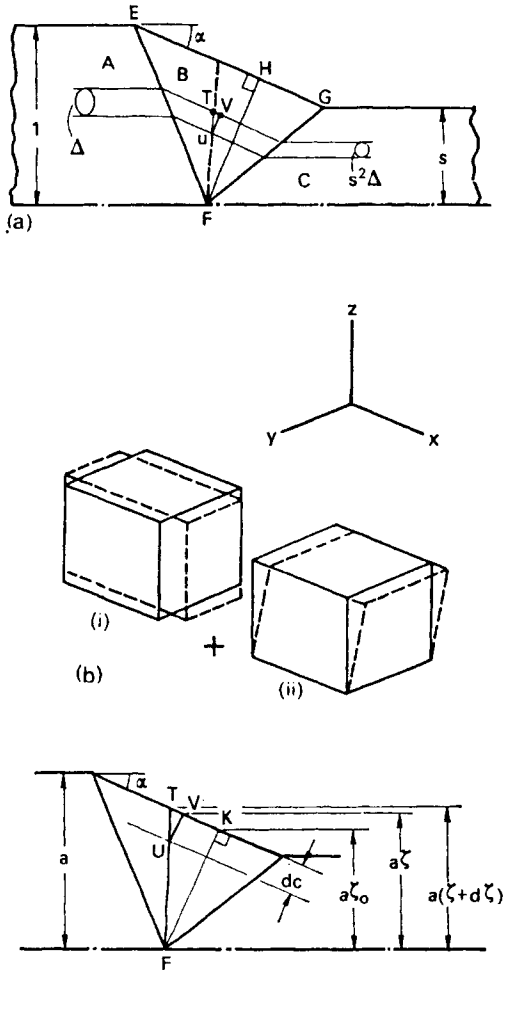

FIG. 10.13. Deformation within zone B in the axisymmetric version of the mode shown in Fig. 10.3(a).

tion of flow in zone B as the radius decreases. The rate of dissipation of energy at this interface is therefore equal to $ksl_{BC}v_{BC}\Delta/s = kl_{BC}v_{BC}\Delta$.

In other words the rate of dissipation of energy at the discontinuity surfaces per unit volume entering the die is *exactly* the same as in plane strain flow, for the same angles of inclination of the discontinuity interfaces to the axis. We may reach the same

conclusion in another way by observing that the work dissipated in unit volume throughput across an interface of discontinuous tangential velocity is a function only of k and the angles between the flow directions and the interface.

It thus seems that our calculation of energy dissipated in the axisymmetric mode of Fig. 10.13 is very simple: we add to the dissipation per unit volume throughput in the plane-strain flow having the same cross-section, a term corresponding to the ideal deformation in zone B. There is, unfortunately, a flaw in this argument, arising from the fact that we have not yet made a sufficiently thorough analysis of the flow in zone B. We now seek to rectify this omission.

10.11. Diffuse Shear in Region B

The velocities of all points in zone B which coincide with EF, Fig. 10.13(a), at a given instant are equal, by virtue of the velocity diagram at the interface. The velocity of a point on any streamline is inversely proportional to the distance from the axis, and it follows, by simple geometry, that the velocities of all points in region B lying on any straight line through F are equal. Thus the velocities of points such as T and U are equal along their respective streamlines. It follows in general that the velocities of points such as U and V, where UV is perpendicular to the flow direction, are *not* equal and that there is consequently a shearing action in the meridional plane in so far as the right-angle between UV and the streamlines is not preserved as flow proceeds.

A typical small element in the conical stream tube is thus subject to two kinds of deformation, as shown diagrammatically in Fig. 10.13(b). Note that the shearing strain rate (mode (ii)) is zero on FH, perpendicular to EG or EG produced, and that FH may be either inside or outside zone B, depending on the position of F.

Calculation of the energy dissipation rate in a block such as that shown in Fig. 10.13(b) requires an investigation of the principal strain rate magnitudes in the combined mode of deforma-

tion. The labour of this calculation can be avoided, however, at the cost of a probably small overestimation of the dissipation rate if it is noted that the dissipation rate for the combined deformation is less than or equal to the sum of the dissipation rates for the two kinds of deformation considered separately. This result is readily established in the present case as follows, but it may also

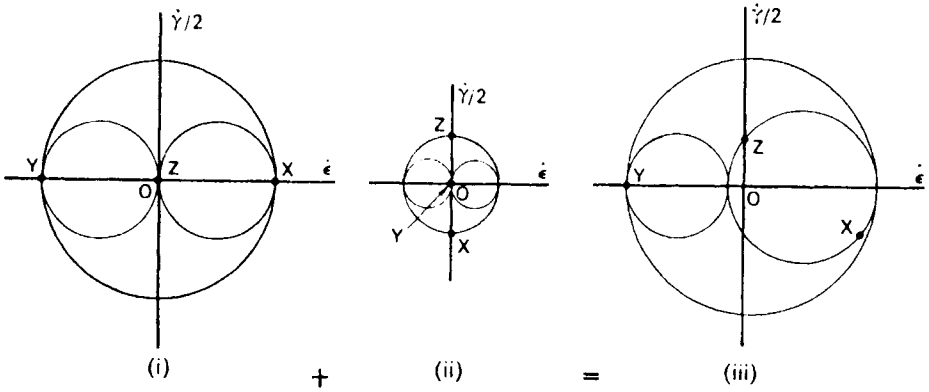

FIG. 10.14. Analysis of strain increments in the postulated axisymmetric mode.

be shown to be generally true, as a simple consequence of convexity and normality (Problem 10.10). Figure 10.14 shows the Mohr circles of strain rate for the modes (i) and (ii) separately and together. Since the rate of dissipation of energy is equal to $2k$ times the largest principal strain rate modulus (see equation (4.21)) the result is obtained by inspection. In fact the estimate of dissipation rate made in this simple way cannot be more than 25 per cent high in the present case.

We can summarise our upper-bound analysis of axisymmetric flow so far by stating that an over-estimate of the dissipation of energy is composed of three parts:

(a) "Intense" shear at the interfaces *EF* and *FG*.
(b) "Ideal" circumferential compression in zone *B*.
(c) "Diffuse" shear in zone *B*.

Of these, only component (c) requires further analysis.

10.12. Evaluation of "Diffuse Shear" Work

To find the work dissipated in diffuse shear in zone B we must first obtain an expression for the shear strain rate $\dot{\gamma}$ at a typical point in B, i.e. the angular velocity of an infinitesimal line segment such as UV in Fig. 10.13(a). This is readily determined with the aid of Fig. 10.13(c), which shows a streamline originally distance a from the axis. At any point on the streamline in region B the distance from the axis is defined by the dimensionless parameter ζ, as shown. The perpendicular distance from F to the streamline is ma, where m has the same meaning as before (Fig. 10.3(a)). At the foot, K, of the perpendicular from F to the streamline let

$$\zeta = \zeta_0 = m \cos \alpha. \tag{10.28}$$

As we have shown already, the velocity of point V (and indeed of all points on FV) is $1/m\zeta$ for unit approach velocity. The velocity at point T, where T is defined by $(\zeta + d\zeta)$ differs from the velocity of V by

$$\frac{d}{d\zeta}\left(\frac{1}{m\zeta}\right)d\zeta = \frac{-d\zeta}{m\zeta^2}$$

The point U, on the perpendicular to the streamline through V, has the same velocity, so the numerical value of the angular velocity of the short segment UV, which is by definition $\dot{\gamma}$ at U, is $\frac{1}{m\zeta^2}\frac{d\zeta}{dc}\,dc$ being the small distance UV.

Now triangles TUV and TFK are similar, so

$$\frac{d\zeta}{dc} = \frac{\zeta - \zeta_0}{ma}$$

Hence

$$|\dot{\gamma}| = (\zeta - \zeta_0)/m^2 a\zeta^2 \tag{10.29}$$

To evaluate the corresponding rate of dissipation of energy we have to integrate $k\,|\dot{\gamma}|$ per unit volume over the whole volume B. This may be turned into an integration over the meridional

section area of B by associating with each elementary area dB, say, of the meridional plane a volume $2\pi a\zeta\, dB$. The integration thus becomes

$$\frac{2\pi k}{m^2}\int_B \left|\frac{\zeta - \zeta_0}{\zeta}\right| dB \tag{10.30}$$

Now since the product of velocity and cross-sectional area of block C (or, indeed, block A) is π, the contribution of this part (c) of the energy dissipation to the value of $t^u/2k$ (or $p^u/2k$) is found by dividing expression (10.30) by $2\pi k$.

The integration is most conveniently done over elementary triangular areas of common height m (= FH, Fig. 10.13(a)) and base $d\zeta/\sin\alpha$. The contribution to $t^u/2k$ is thus, using (10.30),

$$I = \frac{1}{2\sin\alpha}\int_s^1 \left|\frac{1}{m} - \frac{\cos\alpha}{\zeta}\right| d\zeta \tag{10.31}$$

In performing this integration we have to consider two cases, depending on whether or not H lies within EG.

If H is within EG, i.e.

$$1 > m\cos\alpha > s \tag{10.32}$$

we find

$$I = \frac{1}{2\sin\alpha}\left\{\frac{1+s}{m} - 2\cos\alpha + \cos\alpha\,\ln(m^2\cos^2\alpha/s)\right\} \tag{10.33}$$

It is useful later to note that this integral is a minimum with respect to the position of F when H bisects EG, i.e.

$$m\cos\alpha = (1+s)/2 \tag{10.34}$$

We are now in a position to sum the contributions (a), (b) and (c) to the drawing stress. We find

$$\frac{t^u}{2k} = \frac{1+s}{2\sin\alpha}\left(\frac{1}{m} + \frac{m}{s}\right) - 2\cot\alpha + \ln(1/s) + \frac{1}{2\sin\alpha}\left\{\frac{1+s}{m} + 2\cos\alpha\,\ln\left(\frac{m\cos\alpha}{\sqrt{s}}\right)\right\} - \cot\alpha \tag{10.35}$$

For any given α and s this expression can be evaluated for any assumed value of m, i.e. any assumed position of F, Fig. 10.13(a). In principle, we could find the optimum value of m, but without going into details we can see that the optimum lies between the values which minimise contributions (a) and (c) respectively, which are given by (10.8) and (10.34). For small reductions and small values of α these values are close to each other, so by putting $m = \sqrt{s}$ in (10.35) we should obtain a good estimate for the least upper bound—provided, of course, (10.32) is satisfied. We have, on substitution,

$$\frac{t''}{2k} = \frac{3}{\sin\alpha}\left(\cosh\left(\frac{\xi}{2}\right) - \cos\alpha\right) + \cot\alpha\,\ln(\cos\alpha) + \xi \tag{10.36}$$

This expression bears a striking resemblance to the corresponding expression for plane strain, equation (10.11), p. 244.

Making the same approximations as before when ξ and α are small we find

$$\frac{t''}{2k} = \frac{3}{8}\frac{\xi^2}{\alpha} + \alpha + \xi \tag{10.37}$$

In these circumstances (10.32) is satisfied provided $\xi > \alpha^2$: whether or not this is so may be checked in any particular case.

To make a comparison of expressions (10.37) and (10.16) on a basis of reduction of area, let us define $\eta = \ln$ (area entering/area leaving) $= 2\xi$, by (10.10). We obtain, finally,

$$\frac{t''}{2k} = \alpha + \frac{3}{32}\frac{\eta^2}{\alpha} + \frac{\eta}{2} \quad \text{(axisymmetric)} \tag{10.38}$$

$$\frac{t''}{2k} = \alpha + \frac{1}{4}\frac{\eta^2}{\alpha} \quad \text{(plane strain)} \tag{10.39}$$

These formulas are compared, universally, in Fig. 10.15.

Although we have not evaluated a "bulge limit" for axisymmetric drawing, it will presumably not differ much from that in plane strain drawing.

Also plotted in Fig. 10.15 are some test results from wire-drawing experiments performed by Wistreich (see Bibliography). In these experiments light-drawn copper wire, well lubricated with sodium stearate, was drawn through a set of dies with semi die-angle α ranging from 3° to 15°. The dies were made in two halves, and by measuring the force required to hold the halves together the coefficient of friction could be determined (see Problem 10.11). On average the coefficient of friction was about

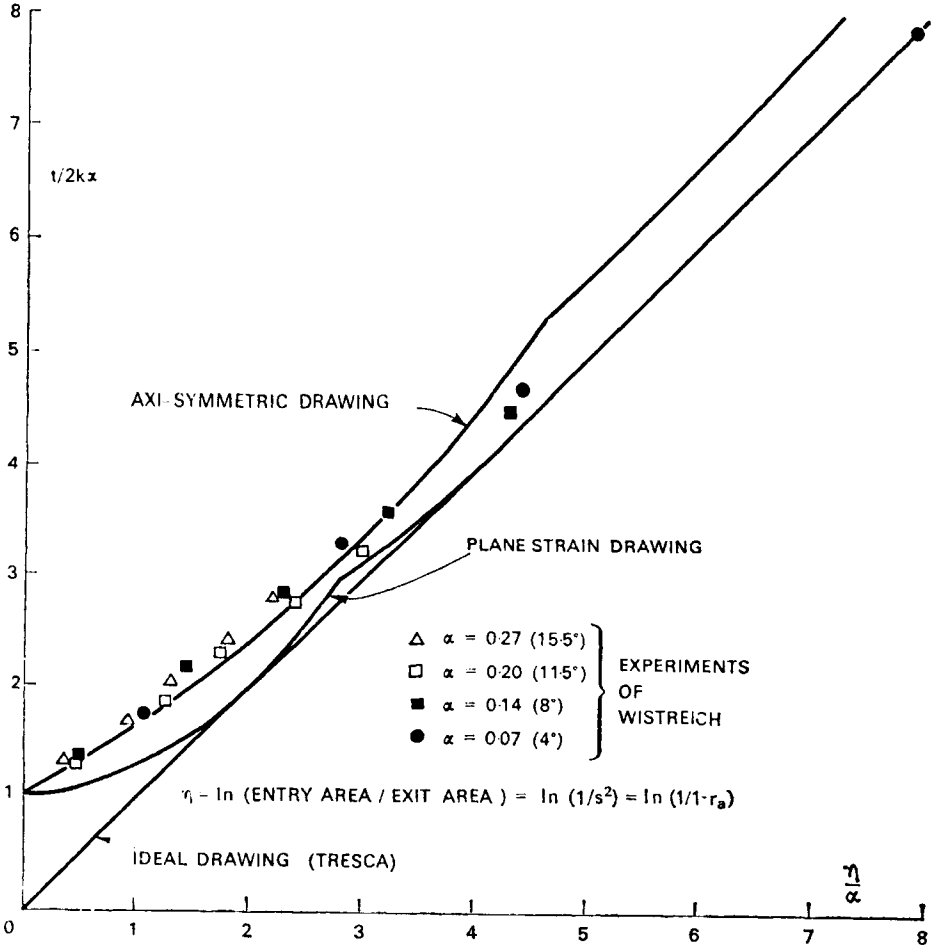

FIG. 10.15. Axisymmetric drawing through smooth conical dies: upper bounds on drawing stress, and experimental points.

0·03. In the graph from which the data were taken Wistreich plotted as ordinate $t/Y(1 + \mu \cot \alpha)$, where Y is the mean of the yield stress of the wire in tension before and after drawing, to "correct" for the effects of friction and strain-hardening. There was relatively little strain-hardening, so this probably provides a good estimate of the "effective" yield stress, as we have argued already.

The experimental points all lie close to the curve (10.38) for the whole range of values of α tested, thus giving general confirmation to the preceding analysis. Most of the experimental points in fact lie above the curve, whereas they should lie below a true upper-bound. As in the case of the plane-strain extrusion experiments, this discrepancy, 10 per cent at most, is removed if the Mises hypothesis $Y = k\sqrt{3}$ is used instead of $Y = 2k$. However, it should be re-emphasised that in applying our calculation to a strain-hardening material by means of an *average* yield stress we cannot strictly claim that our calculation is an upper-bound one, because the relevant theorem is known to be valid only for non-hardening material.

10.13. Optimum Die Angles

The experiments of Wistreich show that for a given reduction there is, in the presence of friction, an optimum die semi-angle α_{opt} for which the drawing stress is minimum. In the neighbourhood of α_{opt} the drawing stress is insensitive to α: typically the drawing stress is not more than about 5 per cent above its minimum value over the range $0{\cdot}5\alpha_{opt} < \alpha < 1{\cdot}5\alpha_{opt}$. Consequently, as differentiation is involved, estimation of optimum die angles is essentially more difficult than prediction of drawing stress. From the preceding analysis (without friction) the optimum value of α is readily found by differentiation of (10.38) and (10.39):

$$\left.\begin{aligned} \alpha_{opt} &= 0{\cdot}5\eta, \quad \text{plane strain} \\ \alpha_{opt} &\simeq 0{\cdot}3\eta, \quad \text{axisymmetric} \end{aligned}\right\} \tag{10.40}$$

The effect of friction can be taken into account, approximately, by multiplying the expression for drawing stress in the absence of friction by $(1 + \mu \cot \alpha) \simeq 1 + \mu/\alpha$. Again the minimum is readily found, but the relationship between α, η and μ is not explicit. In general the effect on α_{opt} of μ is much more pronounced for axisymmetric drawing than for plane strain drawing; typically $\mu = 0{\cdot}05$ raises α_{opt} by the order of 50 per cent, compared with the order of 10 per cent in plane strain drawing, as we have seen already. For this value of μ, therefore, the predictions of α_{opt} for the two situations are about the same. Numerical estimates of α_{opt} agree fairly well with experimental observations for reductions up to about $r_a = 0{\cdot}25$, but are found to be as much as 50 per cent high for reductions $r_a = 0{\cdot}5$. In terms of drawing stress, however, this difference is not too important.

A simple, explicit formula for α_{opt}, which agrees well with experimental observations, may be made by fitting a straight line

$$\frac{t}{2k} = \alpha + c\eta \tag{10.41}$$

to the points on the left in Fig. 10.15. Evidently the value of c lies between about $0{\cdot}6$ and $0{\cdot}9$, depending on the number of points taken. Putting in the factor accounting for friction we have

$$\frac{t}{2k} = (\alpha + c\eta)(1 + \mu/\alpha)$$

and we find, simply,

$$\alpha_{opt} = \sqrt{c\,\mu\,\eta} \tag{10.42}$$

This formula is similar to one proposed by Wistreich, also based on data-fitting:

$$\alpha_{opt} = \sqrt{0{\cdot}87\,\mu r_a/(1 - r_a)} \tag{10.43}$$

These formulas are not valid for $\mu = 0$, or for very small values of μ, because (10.41) is then not appropriate; but they work well in the range of μ of practical interest, say $0{\cdot}02 < \mu < 0{\cdot}07$.

10.14. Axisymmetric Extrusion for $\alpha = 90°$

It is relatively simple to extend our analysis to cover axisymmetric extrusion through square (i.e. $\alpha = 90°$) dies both when there is sliding over the face of the die (cf. Fig. 10.8(a)) and when a dead-metal zone occurs (cf. Fig. 10.8(c)).

The *sliding* mechanism is particularly straightforward to calculate, because the integration of the "shearing" work (c) in zone B is specially simple when $\alpha = 90°$. From (10.31)

$$I = \frac{1}{2}\int_s^1 \frac{d\zeta}{m} = \frac{1-s}{2m}$$

The effect of the "intense shear" deformation is given by (10.7), so adding together the three components we have—now regarding m as a variable, because the expression is so simple—

$$\frac{p^u}{2k} = \frac{1+s}{2}\left(\frac{1}{m} + \frac{m}{s}\right) + \frac{1-s}{2}\left(\frac{1}{m}\right) + \ln\left(\frac{1}{s}\right) \qquad (10.44)$$

This is minimum w.r.t. m when $m = \sqrt{2s\,(1-s)}$, so for this optimum value

$$\frac{p^u}{2k} = (2(1+s)/s)^{\frac{1}{2}} + \ln\left(\frac{1}{s}\right) \qquad (10.45)$$

This is plotted in Fig. 10.16. It is interesting to note that if instead of a proper minimisation the value $m = \sqrt{s}$ (corresponding to the plane-strain minimum) had been used, the results would have differed by less than about 1 per cent for $r_a < 0{\cdot}9$, and about 4 per cent as $r_a \to 1$.

Next we investigate the mechanism involving a dead-metal zone, cf. Fig. 10.8(c). We already know that the dissipation of energy at the interfaces of intense shear which intersect at the axis is precisely the same, per unit volume throughput, as in the corresponding plane strain flow. The dissipation of energy at the interface between zone B and the dead-metal zone is exactly *twice* as much, per unit volume throughput, as in plane strain (see

Problem 10.12). Thus we can readily adapt our previous work (see (10.7) and (10.21)) to give the contribution of work dissipated in intense shear to the extrusion pressure:

$$\frac{p^*}{2k} = \frac{1}{2\sin\alpha}\left(\frac{3-s}{m} + m\left(\frac{1+s}{s}\right)\right) - 2\cot\alpha \qquad (10.46)$$

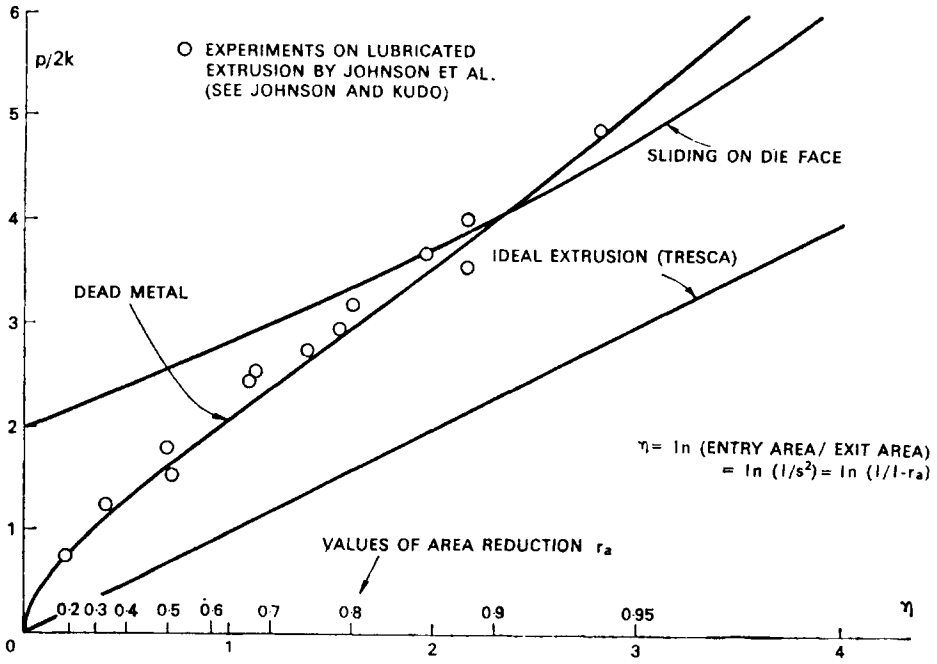

FIG. 10.16. Axisymmetric extrusion through square dies: upper bounds on extrusion stress and experimental points.

For a given value of s this expression is minimum when

$$m = \sqrt{\frac{(3-s)s}{1+s}} \quad \text{and} \quad \cos\alpha = \frac{2\sqrt{s}}{\sqrt{3-s}\,\sqrt{1+s}} \qquad (10.47)$$

and the minimum value is

$$\frac{p^*}{2k} = \frac{\sqrt{3+s}\,\sqrt{1-s}}{\sqrt{s}} \qquad (10.48)$$

Integration of the "diffuse shear" work in region B is precisely the same as for drawing. As in the previous calculations, we use values of m and α which minimise the "intense shear" component of work, to avoid a messy minimisation. For these values (10.47) we have

$$\zeta_0 = m \cos \alpha = 2s/(1+s) \tag{10.49}$$

which always lies between 1 and s. Hence we may use (10.33) directly to give

$$I = \frac{(1-s)^{3/2}}{2\sqrt{3+s}\ \sqrt{s}} + \frac{2\sqrt{s}}{\sqrt{3+s}\ \sqrt{1-s}} \ln\left(\frac{2\sqrt{s}}{1+s}\right) \tag{10.50}$$

Our upper-bound on $p/2k$ is found by adding together the R.H.S. of (10.48) and (10.50) and $\ln(1/s)$. The resulting calculation is shown graphically in Fig. 10.16, and we see that over almost all of the practical range of reductions of area this "dead metal" upper bound is lower than the "sliding" one. Therefore, over the relevant range of reductions, this upper bound is valid *whatever* the value of the coefficient of friction.

Experimental observations made by Johnson and Kudo (see Bibliography) on axisymmetric extrusion of lead and tellurium lead are again in excellent agreement with our upper-bound calculations.

Over practically its whole range the "dead metal" upper-bound curve is fitted well by the simple formula

$$\frac{p^u}{2k} = 0{\cdot}5 + 1{\cdot}5 \ln\left(\frac{1}{1-r_a}\right) \tag{10.51}$$

and this agrees well with the formula quoted by Johnson and Mellor as the "best fit" of a wide range of experimental results.

Problems

10.1. Show that in the mode of plane plastic flow of Fig. 10.3(a) the rates of dissipation of energy at interfaces EF and FG are equal when F is in its optimum position, given by (10.8).

Show also that in the optimum configuration for given α and s the flow in half of the sheet may be considered as two identical "single bend" reductions (each to $1/\sqrt{s}$ of the original thickness) in series. In particular show that the quadrilaterals *IEHF* and *HFJG* are similar.

10.2.(a) A unit cube of perfectly plastic (non-hardening) material undergoes a plane-strain deformation in which it remains a rectangular parallelopiped and finishes up with dimensions s, $1/s$, 1. Show that the total work necessary to accomplish this deformation is $2k \ln (1/s)$, where k is the (constant) true yield stress in pure shear.

(*Hint.* Express the yield condition in terms of the greatest and least principal stresses, and integrate the work done by these stresses. Remember that the volume of the cube remains constant.)

(b) A cylinder of unit length and unit cross-sectional area and made of perfectly plastic material undergoes an axisymmetric plastic deformation in which it remains cylindrical and finishes up with length s and cross-sectional area $1/s$. Show that the total work necessary to accomplish this deformation is $Y \ln (1/s)$, where Y is the (constant) true yield stress in pure tension or compression.

(*Hint.* Recall that yielding is unaffected by the addition of a hydrostatic component of stress, and that the volume of the cylinder remains constant.)

Compare results (a) and (b).

10.3. A "combined" mode of deformation analogous to that shown in Fig. 10.5 consists of n similar sub-modes, all with the same fractional reduction of thickness, arranged end-to-end. Express the value of ξ for each sub-mode in terms of the overall value of ξ and n, and obtain a formula for drawing stress. Give a geometrical interpretation of your result on a graph of $t''/2k$ against ξ.

(*Hint.* First demonstrate that the dissipation of energy per unit volume throughput is independent of the *size* of the sub-mechanism.)

10.4. Use small-angle approximations to trigonometrical and hyperbolic functions in equation (10.13) to obtain a simple approximate formula for the optimum value of α (degrees) for frictionless sheet-drawing in terms of the reduction parameter ξ.

10.5. Verify that the approximate curve (10.16), plotted on a graph of $t/2k$ against ξ, touches the "ideal" line. Compare Figs. 10.6 and 10.4 and explain the discrepancies in terms of the approximations on which equation (10.16) is based.

10.6. Re-work Problem 10.3 in terms of the approximate relationship (10.16) and find the value of ξ beyond which a mode comprising $n + 1$ sub-modes gives a lower upper-bound than one of n sub-modes.

10.7.† From considerations of overall equilibrium obtain an expression for the mean normal pressure on the die faces in frictionless sheet-drawing in terms of the drawing stress and the reduction. Hence, by inserting the limiting die-pressure indicated by "indentation" analysis (see Problem 8.6) obtain the "bulge limit" formula (10.17) for small reductions and small die angles.

(*Hint.* Remember $r_t \doteq \xi$ for small reductions.)

10.8.† Equation (10.23) (with p replaced by t) may be regarded as an upper-bound solution for plane-strain drawing through perfectly rough dies—cf. equation (10.9) for perfectly smooth dies. By substituting typical values, or

by making approximations for small values of α and ξ, show that the roughness of the die contributes markedly to the drawing stress.

(*Hint*. For small ξ use the approximation $s = 1 - \xi$, and then apply the binomial theorem.)

10.9.† (a) Consider a plane-strain mode for sheet drawing, Fig. 10.12, in which there is a region B of radial flow (towards the intersection of the die faces, produced) separated by cylindrical interfaces from the material approaching and leaving the die. Sketch velocity diagrams for several points on the interfaces and show that for small values of α the sliding velocity at the interface is proportional to distance from the centre-line. Hence, by integration, determine the upper-bound expression for drawing stress, for small die angles:

$$\frac{t^u}{2k} = \ln\left(\frac{1}{s}\right) + \frac{\alpha}{2} = \xi + \frac{\alpha}{2}$$

Plot this relationship on Fig. 10.6, and show that this mode gives a better upper-bound than the two studied in the text over only a very small range of reductions.

(b) Repeat the analysis for an axisymmetric mode of the same general character and obtain the upper-bound result (assuming $Y = 2k$):

$$\frac{t^u}{2k} = \ln\left(\frac{1}{s^2}\right) + \frac{2}{3}\alpha = 2\xi + \frac{2}{3}\alpha.$$

10.10.† A body of perfectly plastic material is constrained to undergo deformation in a mechanism (a). An identical block is then constrained to deform in a different mechanism (b), and a third block is constrained to deform in a combined mechanism (a) and (b) together. Here "mechanism" implies not only a *mode* but also a scalar *magnitude* of deformation rate. Show that the sum of the work dissipated separately in modes (a) and (b) is at least as large as the work dissipated in the combined mode.

(*Hint*. Work graphically in a schematic two-dimensional load space in which the behaviour of the body is represented by a convex yield locus enclosing the origin, related to incremental deformation by the normality rule.)

10.11.† In an experiment a sheet is drawn between two flat dies, each inclined at angle α to the central plane. The steady-state drawing force per unit width of sheet is P and the "splitting" force, perpendicular to the mid-plane of the sheet, required to hold the dies in position is S. It is assumed that the normal pressure q on the dies is uniform, and that the coefficient of friction between the dies and the sheet is μ. The forces and pressures acting on a die are thus as shown in Fig. 10.17.

By considering the equilibrium of the die show that the value of μ may be deduced from the measurements by use of the following formula:

$$\mu = \tan\left(\tan^{-1}\left(P/2S\right) - \alpha\right)$$

If P and S are now the drawing and splitting forces respectively in an experiment on wire drawing through a conical die of semi-angle α, show that the corresponding relationship is

$$\mu = \tan(\tan^{-1}(P/\pi S) - \alpha)$$

(*Hint.* Consider the inclination of the resultant pressure and shear stress on a narrow frustum of the cone; resolve the resultant along and perpendicular to the axis and integrate around a semicircle.)

10.12.† In Fig. 10.13 let EG be the interface between moving material in zone B and a stationary dead-metal zone. Let A approach the die at unit velocity, and let v^* be the velocity magnitude of the material immediately beyond interface EF. Derive the upper-bound equation for the dissipation at

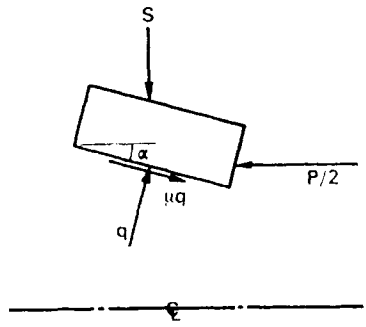

FIG. 10.17. Pressures and resultant forces on a die in sheet drawing.

the interface EG alone (a) for plane strain and (*b*) for axisymmetric flow in terms of v^* (which is the same, as defined, in both cases) and suitable dimensions. Hence show that the dissipation of energy per unit volume throughput is exactly twice as much in (b) as in (a).

(*Hint.* Start by showing that the rate of dissipation per unit *axial* length of the conical surface is constant.)

10.13. Compare Figs. 10.9 and 10.16, and the two curves of Fig. 10.15, and comment on the proposition that in practice there is little difference in average drawing or extrusion stress—expressed as a function of reduction of area—between plane-strain and axisymmetric flow conditions, respectively.

10.14.† Make a lower-bound analysis of sheet drawing between smooth plane dies by using a sector of the stress field derived for thick cylinders in Chapter III in conjunction with an odd-shaped region of hydrostatic stress. Similarly, make a lower-bound analysis of axisymmetric drawing through a smooth conical die, using the stress field derived in Problem 3.14.

Further, show that these lower bounds also hold for plane-strain drawing through dies with convex flanks and axisymmetric drawing through "trumpet-shaped" dies.

10.15.† Investigate an upper-bound solution of the sheet-drawing problem using the special (no-degree-of-freedom) case of the mode of Fig. 10.3(a) in which GFE' is straight. (In a sense this is more directly related to the mode of Fig. 7.12(a) than the general mode of Fig. 10.3(a).)

Derive a general formula and make spot comparisons with Fig. 10.4.

10.16†. (a) In a proposed "single bend" thickness-reducing operation a sheet is drawn between two smooth flat dies arranged as shown in Fig. 10.18(a). The corresponding velocity diagram for an upper-bound analysis is shown in Fig. 10.18(b), q being an auxiliary point.

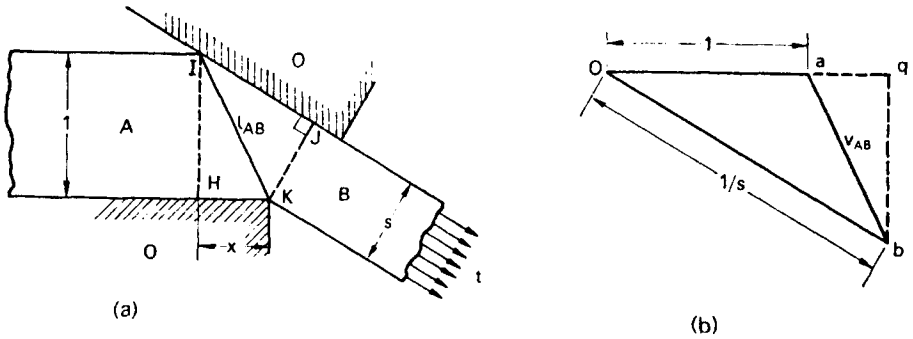

FIG. 10.18. A "single bend" reduction process.

For a given reduction $1 : s$ find the optimum layout of the dies and the corresponding drawing stress.

(*Hint.* Use x as the independent variable (Fig. 10.18(a)) and solve a quadratic equation to obtain an expression for v_{AB}.)

(b) Examine the relationship between this "unit" of deformation and the more complex mode of Fig. 10.3(a). Check that the optimum drawing stress, equation (10.14), may be obtained by suitable adaptation of the result of (a).

(*Hint.* Note that $2 \sinh(\xi/2) = 1/\sqrt{s} - \sqrt{s}$.)

(c) Verify that in the optimum configuration of Fig. 10.18(a) the postulated mechanism is such that an orthogonal plane in the entering sheet (such as HI) emerges as an orthogonal plane (such as JK). Also show that this is *not* so if the configuration is *not* optimum.

CHAPTER XI

EFFECTS OF CHANGES IN GEOMETRY

IN CHAPTER III we analysed the behaviour, under steadily increasing pressure, of a thick-walled tube made of ideal elastic-perfectly plastic material, and we came to the conclusion that the "collapse pressure" calculated on the assumption that the material was rigid-perfectly plastic was a good approximation to the maximum pressure which a real tube could sustain. In the subsequent chapters we *assumed* that the same was true for other kinds of structures also, and set out to calculate—or estimate, by means of the upper- and lower-bound theorems—the collapse loads of several kinds of structures, and the forces required to execute certain metal-forming processes.

The idea of a "plateau" in the generalised load-deflection behaviour of a structure, Fig. 11.1(a), depends, in fact, not only on the non-hardening property of the ideal material, Fig. 11.1(b), but also on the *assumption* that during collapse it is still reasonable to write down the relevant equations as if the structure were actually *undeformed.* This assumption is a feature of the virtual work equations (Appendix II); consequently it is built into the lower- and upper-bound methods.

Now in some situations the assumption is reasonable. For example, in steady-state wire drawing there are considerable changes in geometry in the wire as it passes through the die, but, as we observed in Chapter X, the geometry is "self-reproducing" in the sense that the disposition of the material in the immediate neighbourhood of the die is always the same in steady flow.

It is not difficult, however, to think of simple situations in which changes in geometry during collapse have a significant

effect on the subsequent behaviour of the structure. For example, consider two uniform non-horizontal cantilevers, Fig. 11.2(a), loaded vertically by forces W at their tips. The cantilevers are made of perfectly plastic material, and we shall discuss their behaviour, appropriately, in terms of bending moments. The bending-moment/curvature relation for an element of the beam is as shown in Fig. 11.2(b), and the shape of this curve indicates that plastic deformation will occur by formation of a *plastic hinge* when the bending moment reaches the "full-plastic" value M_o. The largest bending moments in the cantilevers occur at the

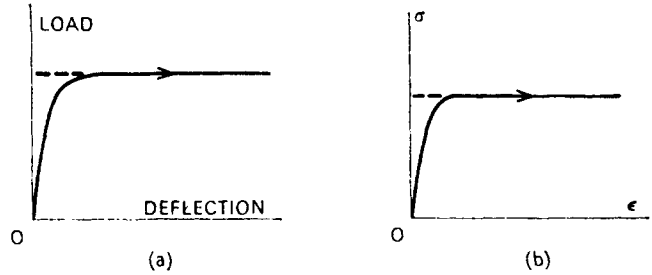

FIG. 11.1. Idealised plastic load-deflection and stress-strain relations.

roots, and so the simple plastic theory indicates that collapse occurs in both cases when

$$Wl_h = M_o \tag{11.1}$$

where l_h is the horizontal projection of the length of the cantilever. However, the value of l_h changes when the inclination of the cantilever changes, as it must if a hinge forms at the root; consequently the value of W must change as the cantilever deforms plastically if equilibrium is still to be preserved. The relationship between W and the vertical deflection, y, at the tips is easily derived (see Problem 11.1) and is indicated in Fig. 11.2(c).

From this example we see that geometry changes may work either for or against the strength of the structure—or they may, presumably, be "neutral" in effect in some circumstances.

If the load-deflection curve rises—as for cantilever 1—the deformation is *stable* under steadily increasing dead load. On the other hand a falling load-deflection curve—as for cantilever 2—indicates an *unstable* situation under dead loading, because once the maximum load has been reached any further deformation renders the structure incapable of sustaining the applied load, and inequality of the forces accelerates the collapse of the structure. When we consider that there will in general be some *elastic*

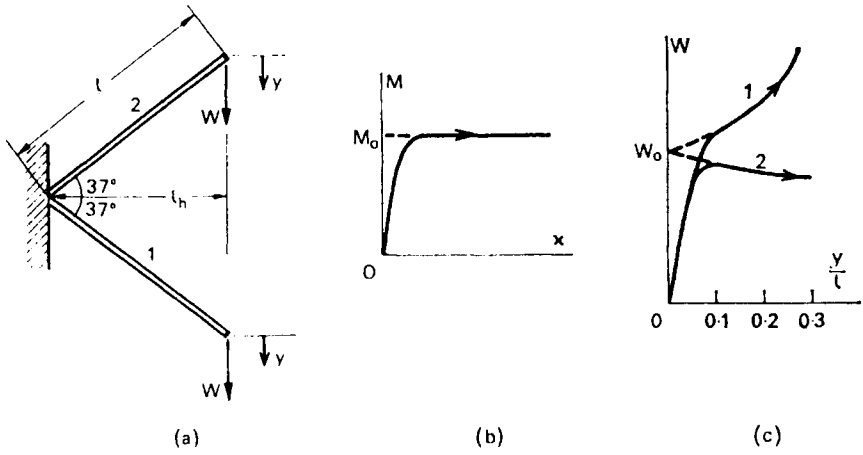

FIG. 11.2. Load-deflection behaviour of inclined cantilevers.

deformation of the structure before M_o is reached at the root (see Fig. 11.2(b) and (c)) we can appreciate that the collapse load indicated by simple plastic theory will not in fact be reached by cantilever 2; the actual maximum load will depend to some extent on the elastic properties of the structure.

The fact that "adverse" geometry-change effects can reduce the carrying capacity of structures to *below* that indicated by simple plastic theory is obviously one which must be taken seriously in structural design. On the other hand, "beneficial" geometry-change effects provide an additional margin of safety when simple plastic design methods are used. In the remainder of this chapter

we shall be concerned mainly with situations in which the geometry-change effects are "adverse".

11.1. Three Broad Classes of Structural Behaviour

If we now consider the whole field of engineering structures—in only part of which plastic theory is an appropriate conceptual tool—we find that the engineer often encounters situations in which the load-deflection curve first rises and then falls, as shown

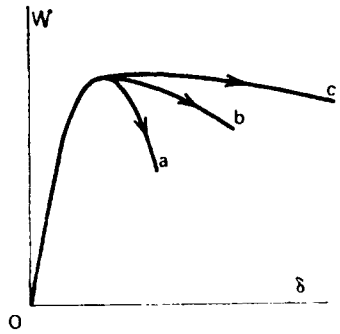

FIG. 11.3. Schematic load-deflection curves for different kinds of structure.

schematically in Fig. 11.3. On the whole his approach to structural design is conditioned largely by how "peaky" the load-deflection curve is in any particular case; clearly a structure with load-deflection characteristics like (a) would collapse, under dead loading, much more suddenly and catastrophically than one corresponding to (c), and it would therefore be wise to allow a wider margin between the "working" load of the structure and the maximum load the structure could support; in other words, to assign a higher "load factor".

The question of how to choose a suitable load factor in any given situation is beyond the scope of this book; we refer the interested reader to the work of Pugsley (see Bibliography). It is

perfectly plain, however, that before *any* rational design method can be devised it is necessary to have information from loading tests on real structures and from carefully planned experiments performed in the laboratory, as well as information about the statistical nature of actual loading.

Let us now consider in more detail the three broad classes of structural behaviour indicated in Fig. 11.3.

When we point out that structures of type (a) tend to have maximum loads which are *sensitive to initial imperfections of geometry* in the structure, it is easy to see that the design of such structures is in general a difficult and worrying business. For example, curve (a) is broadly similar to the pressure–volume relation for a closed thin-walled vessel under external pressure—such as the pressure hull of a submarine. Although pressures below the surface of the sea are a well known function of depth in still water, it is of course very difficult to estimate the additional impulsive pressures which may be set up by explosions nearby, and which may clearly initiate catastrophic failure.

Curve (b) may be taken to represent, schematically, the behaviour of axially compressed columns in the elastic-plastic range; here again special care is necessary in design to avoid catastrophic failures. The buckling load of columns in the elastic-plastic range in fact depends critically on the strain-hardening characteristics of the material. This also is beyond the scope of the present book, and for a concise introduction to the subject we refer the reader to Chapter 16 of the book by Drucker listed in the Bibliography.

Curve (c) represents, schematically, the behaviour of a steel arch under the action of a downward-directed point load. The carrying-capacity of the arch might fall to, say, 5 per cent below the maximum load when the distortion of the arch was conspicuous. Under these circumstances the simple plastic theory—used perhaps with a slightly augmented load factor—would appear to constitute a rational basis of design.

In contrast, the behaviour of a steel *dome* under the action of an inward-directed point load would correspond more closely to

curve (a); the carrying capacity might fall to about half of the maximum value for a deflection equal to the thickness of the shell. Clearly in this case the simple plastic theory would *not* constitute a rational basis of design.

11.2. An Approach to Geometry-change Effects in Plastic Deformation

The list of effects which would need to be taken into account in a detailed calculation of the load-deflection behaviour of a structure is a long one: it includes elastic deformation, elastic-plastic deformation, residual stresses, geometry changes, strain-hardening and many other effects.

The approach of the simple plastic theory to this situation is, as we have seen, a simple and radical one: we consider the material to be rigid-perfectly plastic and calculate—or find bounds on—the "collapse" load of the structure on the assumption that geometry changes are unimportant.

Suppose, however, that for a particular type of structure made of a ductile material the load-deflection curve is found by experiment to fall after a peak load has been reached. Clearly our simple plastic theory is not fully justified—although as we have pointed out above it may still be useful for design in some circumstances. What approach should we take to obtain a more realistic plastic theory?

In some very simple cases—like pure tension of a bar—it is not particularly difficult, as we saw in Chapter II, to devise an analysis which takes into account changes in geometry *and* arbitrary strain-hardening. Most practical structures are, however, much more complicated than this and it is not clear that these two aspects of structural behaviour, which are deliberately excluded from the simple plastic theory, could be comprehended within a general theory which did not rely very heavily on the assistance of high-speed computers.

In view of the widespread success of the simple plastic theory, let us enquire into the possibility of modifying the theory in some

relatively simple way to take account of the changes in geometry which occur when the structure deforms—for this appears to be, *prima facie*, the most obvious unaccounted feature of the behaviour, since it is unlikely that strain hardening would ever weaken a structure.

The obvious approach, suggested by the example of Fig. 11.2, is to compute, in effect, a *sequence* of collapse loads according to the simple plastic theory, but with each based on a geometrical configuration of the structure differing from the previous one by a small amount corresponding to the collapse mode of the previous structure. Apart from difficulties arising from *alternative* modes of deformation (where the collapse locus has a pointed vertex) this procedure is straightforward—in principle, at least.

Now if we are doing a sequence of calculations of this sort, we will probably be most keenly interested in the difference between the first collapse load calculated for the deformed structure and the *initial* collapse load, since this will enable us to obtain the initial *slope* of the load-deflection curve, which in turn will give an impression of the probable subsequent course of the curve. If the slope is positive, it will be reasonable to suppose that the actual structure will undergo a *stable* deformation at about the collapse load according to the simple theory for the initial geometry. If, on the other hand, the slope is negative—indicating *unstable* behaviour—we shall be keenly interested in the *magnitude* of the slope.

Let us, therefore, concentrate on the problem of determining the initial slope of the load-deflection curve.

11.3. The Rate-problem

The labour which must be invested in the calculation of the initial slope of the load-deflection curve when a structure of rigid-perfectly plastic material deforms, obviously depends largely on the simplicity, or otherwise, of the structure and its loading. For example, the inclined cantilever, Fig. 11.2, presents little difficulty to a complete analysis; and for other structures, as we

shall see, approximate intuitive methods are not difficult to devise.

Although such methods may be useful in practice it is nevertheless instructive to study, briefly, the nature of the general problem. In general we are concerned with small *changes* in the external and internal forces which are a consequence of small *changes* in geometry of the structure when plastic deformation takes place. Investigation of the relationship between these small quantities constitutes the so-called *rate-problem.*

The best way of appreciating the important ingredients of the problem, without going into unnecessary detail, is to study a deliberately simple example such as that shown in Fig. 11.4. A pin-jointed structure ABC is constrained to lie in a plane. The equal members, AB and BC, of length L, have the rigid-perfectly plastic load-extension characteristics shown in Fig. 11.4(b). (The example is thus somewhat artificial as buckling of the members, which would normally be an important consideration, is excluded.) A load P hangs under gravity from joint B.

Our first step is to find the "collapse" load P_0, say, of the structure according to simple plastic theory. This is done most conveniently for this simple statically-determinate structure by drawing the triangle of forces for joint B, as shown in Fig. 11.4(c). As P increases steadily, member AB is the first to reach the yield tension T_0; the corresponding value of P is P_0. When member AB extends plastically the structure becomes a mechanism with one degree of freedom. A small displacement of the mechanism, involving in particular a vertical component δy of the small displacement of joint B, gives the modified geometrical layout indicated by dotted lines. Consequently the triangle of forces is also modified, as indicated. In particular the force P will change by a small amount δP. However, it is not clear from the sketch whether the increment is a positive or a negative one. As we are primarily interested in the slope $\delta P/\delta y$ it seems clear that we must study carefully the *changes* in the triangle of forces which occur when the mechanism undergoes a small displacement.

The most convenient way of finding the small changes of in-

clination of the members is by means of a displacement diagram, shown in Fig. 11.4(d). This is self-explanatory, the construction being similar to that of the velocity diagrams in Chapter VII. In particular, the incremental rotations of AB and BC, θ_{AB} and θ_{BC}, are given, to within an arbitrary multiplier, by ab'/L and bc/L respectively.

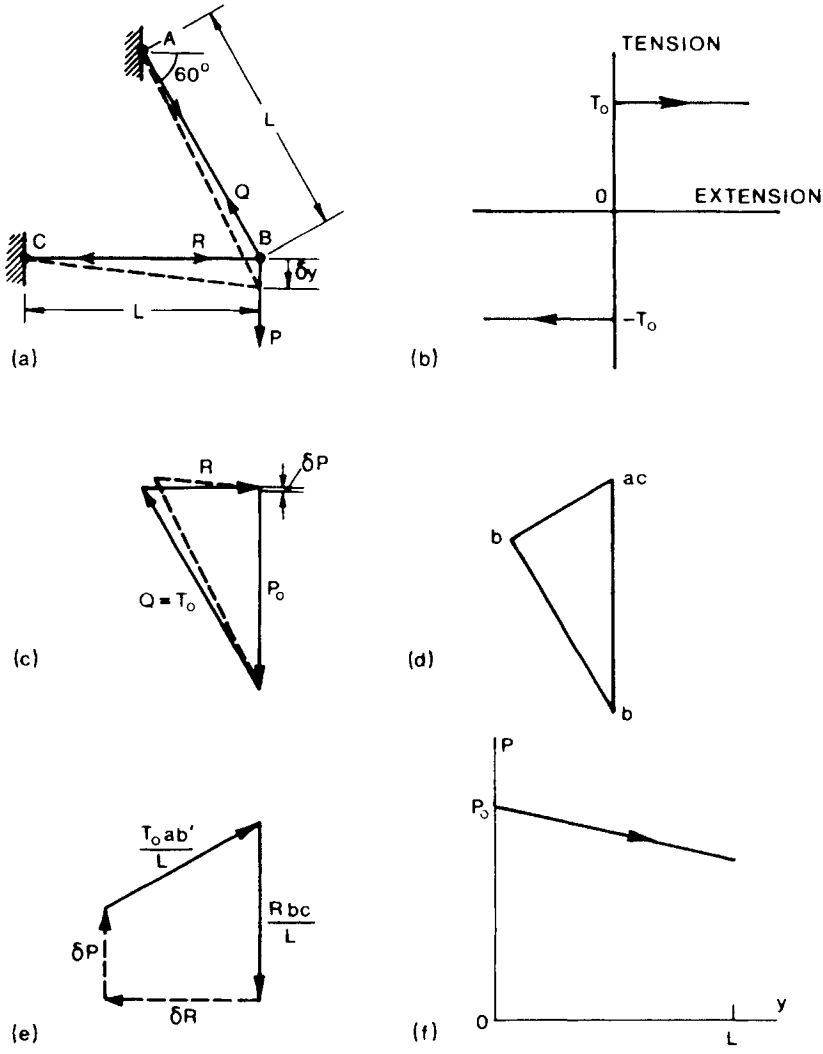

FIG. 11.4. Graphical "rate-problem" analysis of a simple structure.

The "change of force" diagram, Fig. 11.4(e) is constructed as follows. The magnitude of the tension in AB remains constant as the mechanism deforms (see Fig. 11.4(b)), so the change of tension is represented, vectorially, by a vector $T_0\theta_{AB}$, perpendicular to vector T_0 in Fig. 11.4(c). The change of force from CB consists of two parts, due to a change in *direction* of the bar (analogous to the change in AB) and a change in *tension*, δR, respectively. These two force increments are shown in Fig. 11.4(e), and the magnitudes of δR and δP are determined by the fact that the diagram must close. It is clear from the sketch that δP acts upwards, indicating that P must *decrease* as deformation proceeds if the joint B is to remain in equilibrium.

With the geometry shown,

$$\delta P = -\frac{R}{2} \cdot \frac{bc}{L} = -\frac{P_0}{2\sqrt{3}} \cdot \frac{\delta y}{L}$$

Therefore

$$\left(\frac{dP}{dy}\right)_0 = -\frac{P_0}{2\sqrt{3}L} \tag{11.2}$$

This result is indicated in Fig. 11.4(f).

It is interesting to note that a *complete* description of the "collapse" state of the initial structure—involving both forces and displacements—is both necessary and sufficient for the calculation of the initial slope $(dP/dy)_0$; and indeed this is true in general. In particular, neither an upper-bound nor a lower-bound calculation is sufficient in itself. In essence what we have done is to apply the simple plastic theory to a slightly different structure, and it is obviously important in doing this to know the *exact* configuration of the modified structure and the *exact* collapse loads, in order to be able to assess the slope $(dP/dy)_0$ accurately.

In principle the process can be repeated again and again to follow the complete relationship between load and deflection: however, the contention of the present argument is that the *initial*

slope is the single most valuable piece of information, and this, as we have shown, may be derived by applying relatively straightforward procedures to information available from a plastic analysis of the structure in its initial configuration.

Returning to the present example we can readily see (Problem 11.2) that by keeping the initial inclination of the members the same but varying the length of BC and the position of C we can alter the value of $dP/dy)_0$ and, indeed, change its sign. In this example it is, plainly, not simply a matter of *inspection* to decide whether the initial slope $dP/dy)_0$ is positive or negative in any given case.

11.4. Geometry-change Effects in Simple Structures

For some other structures, however, it is fairly clear by inspection whether the sign of $dP/dy)_0$—or the appropriate corresponding quantity—is positive or negative. Indeed, the structures we have been considering in this book furnish several examples.

Simple intuitive arguments (see Problems 3.5 and 11.3) lead us to expect *negative* slopes to the load-deflection curves for thick tubes under internal pressure and rotating discs, both being made of rigid-perfectly plastic material; and this does indeed correspond to the catastrophic bursting of such structures under "dead" loading in practice.

We also expect a negative slope in the simple tension test (Problem 11.4) and it is instructive to recall (Chapter I) that the onset of instability in a tension test of a real material is determined largely by the *strain-hardening* characteristics of the material. We would expect a somewhat similar state of affairs in the behaviour of tubes and rotating discs made of real strain-hardening materials: although failure will be catastrophic the maximum load may not be reached until relatively large deformations have occurred (see Problem 11.5).

We have already observed, in Chapter IX, that geometry changes tend to enhance the carrying-capacity of plates under

transverse loading, by virtue of the possibility of a kind of membrane action. In fact the large-deflection analysis of rigid-perfectly plastic plates typically gives a load-deflection curve like that of Fig. 11.5 (cf. the experimental curves of Fig. 9.10) which rises after an initial slope of zero. In this case the *initial* rate-problem would not, by itself, indicate the strengthening effect of subsequent changes in geometry. Although the large-deflection analysis of plates is beyond the scope of the book, it is instructive

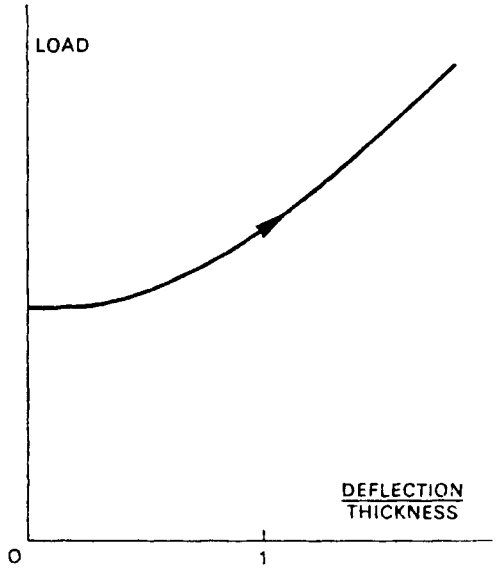

FIG. 11.5. Typical theoretical pressure-deflection curve for a plate of rigid-perfectly plastic material for steadily increasing pressure.

to study by approximate methods the large-deflection behaviour of beams with full end fixity: see Problem 11.6.

11.5. Summary and Concluding Remarks

The "plateau" in the predicted load-deflection curve for a structure made of perfectly plastic material depends not only on the non-hardening nature of the material but also on the *assump-*

tion that the effect of geometry changes on the collapse load is negligible. In general the initial (post-yield) slope of the load-deflection curve may be either positive or negative, according to circumstances. A negative slope suggests that the real structure may collapse catastrophically—under dead loading—at a load below that indicated by the simple plastic theory, provided the effect of strain-hardening is not strong. The seriousness of this state of affairs depends strongly on the magnitude of the initial negative slope of the load-deflection curve. This slope represents the change in the collapse load according to the simple theory as the geometry changes a small amount at collapse, and all the information necessary for its determination is contained in a "complete" plastic analysis of the original structure. In some important practical cases, however, an estimate of the slope—and particularly its *sign*—may be made on an *ad hoc* intuitive basis.

There are several points arising from a full consideration of the "rate-problem" which we have not touched upon. A proper analysis enables us to shed light on the questions of uniqueness of deformation of a body at the yield-point state and its relation to the stability of ensuing deformation.

Problems

11.1. Calculate the curves of Fig. 11.2(c) for, say, $\theta_0 = \sin^{-1} 0{\cdot}6 \simeq 37°$.

Also find the initial *slope* of the load-displacement curve for an arbitrary initial inclination of the cantilever by drawing a displacement diagram corresponding to a small rotation and evaluating the corresponding small changes in W and y.

11.2. (a) Find the initial slope of the load-deflection curve for the structure of Fig. 11.4(a), but with the load at joint B applied vertically *upward*.

(b) Find the initial slope of the load-deflection curve for a structure like that of Fig. 11.4(a), carrying a downward load, but with abutment C moved horizontally so that the length of CB equals αL, the inclination of AB remaining unchanged.

11.3. A rotating disc is made of rigid-perfectly plastic material. Starting from the assumption that in any deformation of the disc no particle will move towards the centre, and regarding an "overall" analysis of the equilibrium of half of the disc as adequate (see Problem 5.4), argue that the deformation of the disc will be unstable under steadily increasing speed.

(*Hint*. Examine qualitatively the effect of the first assumption on (a) the inertia loading on half of the disc (b) the diametral cross-sectional area of the deformed disc. Remember that the material is incompressible.)

11.4. Assuming that the deformation is homogeneous, determine the initial slope of the nominal stress–strain curve for a tension test on a bar of rigid-perfectly plastic material with (true) yield stress Y in uniaxial tension.

Determine the initial slope (i.e. strain-hardening coefficient) of the true stress–strain curve if the initial slope of the nominal stress–strain curve is to be zero. Verify that your answer agrees with the Considère construction (Fig. 2.7, p. 25).

11.5.† A complete analysis of the stable part of a simple tension test on a material with arbitrary strain-hardening characteristics may be made by means of the generalised Considère construction, Fig. 2.7. Make a corresponding analysis of a rotating hoop of the same material, which is constrained to remain symmetrically disposed about the axis of rotation, and devise an appropriate construction for the "nominal" bursting stress, i.e. the bursting stress based on the bursting speed and the *original* dimensions of the hoop.

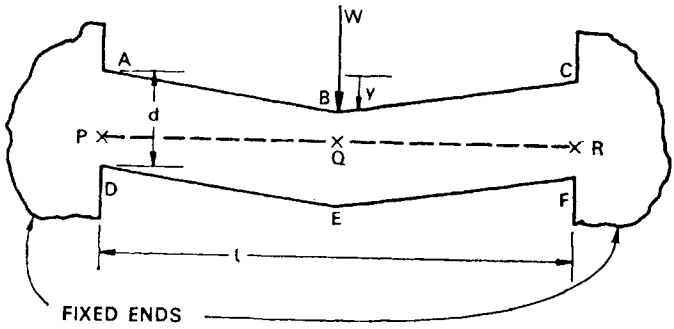

FIG. 11.6. Large-deflection analysis of a beam with fully restrained ends.

11.6.† Make an upper-bound analysis of the collapse load of the deflected beam shown in Fig. 11.6. The beam has a rectangular cross-section and the ends are built into supports which prevent not only rotation but also translation of the ends of the beam. As a mode of deformation consider rigid-body rotations of the blocks $ABED$ and $CBFG$ about points P and R, and evaluate the dissipation of energy at the planes AD, BE and CF. Note that for geometric reasons point Q, which is on line PR, divides the plane BE into zones of compressive and tensile dissipation. For a given configuration optimise the "level" of PQR.

Hence construct a curve showing, approximately, the relationship between W and y as deformation proceeds.

CHAPTER XII

THE WIDER SCOPE OF PLASTIC THEORY AND DESIGN

THE examples of application of plastic theory given in Chapters V to X were intended to serve two main purposes. First, in making predictions about the behaviour of actual structures and the operation of forming processes they make possible the experimental justification of the theory—and particularly the idealisations which are involved in it—over a wide range of situations. Second, in demonstrating the power and flexibility of the theory in application to a wide spectrum of problems, they may give the reader some confidence in tackling other problems which he may encounter in the course of his engineering career. In a sense this book is like a manual on "how to play tennis", which aims to improve the reader's performance at the game, but which can only do so if the reader is prepared to read the book in conjunction with practice sessions on the court. Similarly the present book can only succeed in its ultimate objectives if the student is prepared to practise the theory not only on the problems provided in the book, but also on other engineering problems which he may encounter in the future.

In order to correct any misleading impressions about the scope of application of plastic theory which may have been obtained from a study of the restricted and somewhat arbitrarily chosen list of examples in Chapters V to X, we give below a list of other fields in which plastic theory has made considerable contributions or in which it appears to be capable of making contributions in the future.

Plastic theory is a well-developed tool in the design of *beams*

and *framed structures* in steel and reinforced concrete and, more recently, in "composite" construction using both of these materials. The theory is a tool not only for design of the overall dimensions of the members of these structures but also for design of the *details* of connections, etc. For an authoritative treatment of this subject see the book by Baker, Horne and Heyman listed in the Bibliography.

In the field of *pressure vessel engineering*, and particularly in the design of reinforcement of openings and junctions, plastic theory appears to form a sound basis for rational design. The widely-used "area replacement rule" is indeed a simple, intuitive application of a lower-bound idea, but it seems that careful and sophisticated application of the theorem to more complex junction geometries will be rewarding. Plastic theory should find increasing application also in the design of reinforcement around cut-outs in complex cellular structures such as the hulls of ships.

Another large area in which plastic theory seems capable of making a significant contribution is the field of *micro-mechanics* of composite materials. An obvious example was mentioned in Chapter VII, but many other materials may usefully be idealised as simple composite materials on a microscopic scale. This field shows promise as a way of bridging the enormous gap between atomic-scale studies on the one hand and "continuum" studies on the other, and producing meaningful interpretations of phenomena which have so far eluded description in conventional terms.

Plastic theory has proved to be a useful tool in several aspects of *soil mechanics*. Although saturated clays have strong time-dependent components of behaviour it is nevertheless justifiable in some circumstances to regard the material as basically time-independent. Here, a plastic theory generalised to account of plastic volume changes has played an important part in the conceptual development of the subject in recent times; see the book by Schofield and Wroth listed in the Bibliography. It also seems likely that application of plastic theory to clay materials on the micro-scale will be rewarding. Also, in broad terms the "mature

view" of structural behaviour afforded by plastic theory has helped to put some simple conventional soil-mechanics calculations into a proper perspective of mechanics.

12.1. Interrelation with Other Aspects of Design

At several points in the book we have made the observation that plastic theory is specially appropriate for design of structures of various kinds and for optimisation of various forming processes. Once we are satisfied that conditions are appropriate, we can apply the theory, and in many cases we obtain a clear view of the mechanics of the situation which points directly to a relatively simple design procedure.

We must recognise, however, that structural design cannot be carried out in isolation from the many other aspects of engineering design. For example, in the design of a complex piece of machinery such as a gas turbine there are obviously very many technical problems which must be solved in the fields of aerodynamics, combustion, lubrication, heat transfer, vibration, etc., besides those concerning materials and structures; and obviously all of these problems impinge on each other to a greater or lesser degree. Similarly, in the design of a large multi-storey building, many of the overall dimensions of the structure will be determined by such considerations as the use to which the building is to be put, local building regulations, aesthetic aspects, and so on.

In situations of this sort the structural engineer must be in continuous communication with many other workers, and it is especially valuable for him to appreciate concepts which give him the ability to make clear statements about the effects on the structural aspects of the design of, say, changes in dimensions which may be desirable from other points of view. The ideas of plastic theory, and particularly those which derive from the lower-bound theorem, are very useful in this respect, because anyone who understands the main points of the theory can often make particularly valuable rapid and incisive structural analyses.

12.2. The Role of Computers in Structural Design

All the examples we have considered so far have been sufficiently simple for the relevant plastic-theory calculations to be done "by hand". In the age of the high-speed computer and of more and more complex machines it would be exceedingly naïve to suppose that *all* problems of structural analysis and design could be solved at the expense of small amounts of computational labour. On the other hand it would be even more naïve to think that the mere power of the computer could in any way enable us to dispense with the conceptual framework within which all meaningful calculations are necessarily made. There can never be a substitute in structural design for clear thinking and the application of powerful proven concepts: and, indeed, the need for conscious thought about presuppositions and idealisations becomes more acute if effective use is to be made of the ever-increasing power of high-speed computers.

Several computer packages for comprehensive structural analysis have recently become widely available. These can perform static and dynamic analyses of structures and continua in the course of geometrically non-linear deformation, and with a variety of optional non-linear formulations of irreversible material behaviour. Experience with these packages shows that simple hand-calculations done by thoughtful engineers on the basis of well-chosen idealisations are very helpful in making preliminary design decisions and in suggesting suitable parameters for use in the main computations. Moreover, simple studies of this sort are also indispensable in finding the key dimensionless groups which characterise the behaviour of structures and which thus provide a rational scheme for thinking about structural problems and interpreting the computer output.

The modern, comprehensive computer packages mentioned above are all descendants of schemes of linear-elastic analysis which were set up in the early days of high-speed computation. Successive features such as geometric and material non-linearity have all been provided by means of an accretion of schemes of

iteration and successive approximation. A radically different route of structural computation has been taken by a group of workers who have aimed at adapting the techniques of Operational Research to the direct *design* of engineering structures. The earliest example of this *genre* of structural computation was the application of the technique of linear programming to the plastic design of framed structures under conditions of minimum weight. Much progress has been made over recent years in the deployment of other methods of operational research in the field of structural optimisation. The volumes listed under that heading in the Bibliography are representative of work in this area.

12.3. Application of Plastic Theory to Other Fields of Design

Throughout the book we have been at pains to emphasise that plastic theory is only relevant to the analysis and design of structures and forming processes within a certain well-defined region of structural mechanics. Nevertheless, as we pointed out in Chapter I, plastic theory is a *mature* subject, and one of the by-products of this maturity is that some of the insights into structural action afforded by the theory are relevant to structures falling strictly outside the scope of the theory. An example which has already been cited is masonry construction: see pp. 10–11.

Provided we are cautious, and fully conscious of what we are doing, it is reasonable to seek to apply some of the benefits of plastic theory in an intuitive way to other aspects of structural design which are beyond the scope of plastic theory as such.

Two fields in which plastic theory has limited application of this sort are the design of structures to avoid failure by fatigue, and the design of structures which must operate in creep conditions.

In spite of the fact that fatigue damage is likely to be initiated in local regions of high concentration of stress in the *elastic* range, it is nevertheless useful in the design of structures which must

sustain many repeated loadings to have a clear qualitative idea of the overall way in which the structure acts to carry the applied loads. A little thought along "lower-bound" lines often indicates clearly the parts of the structure which need reinforcement, and by putting reinforcing ribs, etc., in *other* places the designer may well exacerbate the fatigue problem.

In the field of design against creep one of the important observations on the creep of metals at elevated temperature is that the creep strain-rate in a specimen is highly sensitive to the stress level. Therefore a relatively low *stress* concentration factor in a creeping structure may be associated with a high *strain* concentration factor, which should be avoided if at all possible since the occurrence of rupture in creep conditions appears to depend largely on the creep strain which has accumulated locally. The lower-bound approach of plastic theory envisages equilibrium distributions of *uniform* stress, and is likely therefore, in design, to indicate the regions in any given structure which need reinforcement if the stress levels are to be kept satisfactorily low.

The question of creep in structures is complicated by the fact that if parts of the structure are at elevated temperature there are likely to be other parts at lower temperature, and therefore *thermal stresses* due to self-restraint of differential expansion may be present. Whether or not such thermal stresses may be ignored for some purposes—as they are in plastic theory with reference to collapse—remains to be investigated.

BIBLIOGRAPHY

THE following short list is intended to provide additional reading over a wide field for the interested student. All but a few of the works cited are books, and most of these contain detailed references to original papers.

The first book in the list is an especially valuable collection of papers which survey the literature over a wide field up to 1960.

Current work may be followed through papers in such periodicals as *Journal of the Mechanics and Physics of Solids*, *Proceedings of the Institution of Mechanical Engineers*, *Journal of Applied Mechanics*, *International Journal of Mechanical Sciences*, *International Journal of Solids and Structures* and *International Journal of Plasticity*. Abstracts of papers are presented regularly in *Applied Mechanics Reviews*.

PLASTICITY

Plasticity. Proceedings of the Second Symposium on Naval Structural Mechanics, Brown University, 1960. Pergamon 1960.

R. HILL, *The Mathematical Theory of Plasticity*. Oxford University Press, 1950.

A. NADAI, *Theory of Flow and Fracture of Solids*, vol. I. McGraw-Hill, 1950.

W. PRAGER and P. G. HODGE, *Theory of Perfectly Plastic Solids*. John Wiley, 1951.

P. G. HODGE, *Plastic Analysis of Structures*. McGraw-Hill, 1959.

J. HEYMAN and F. A. LECKIE (editors), *Engineering Plasticity*. Cambridge University Press, 1968.

J. B. MARTIN, *Plasticity: fundamentals and general results*. MIT Press, 1975.

W. JOHNSON and P. B. MELLOR, *Engineering Plasticity*. Ellis Horwood, 1983.

STRUCTURAL MECHANICS

W. FLÜGGE (editor), *Handbook of Engineering Mechanics*. McGraw-Hill, 1962.

D. C. DRUCKER, *Introduction to Mechanics of Deformable Solids*. McGraw-Hill, 1967.

B. G. NEAL, *Structural Theorems and their Applications*. Pergamon, 1964.

T. H. LIN, *Theory of Inelastic Structures*. John Wiley, 1968.

Mechanical Properties of Materials

A. H. Cottrell, *The Mechanical Properties of Matter*. John Wiley, 1964.
F. P. Bowden and D. Tabor, *Friction and Lubrication*. Methuen, 1956.
M. F. Ashby and D. R. H. Jones, *Engineering Materials*. Pergamon, 1980.

Fracture

S. Nemat-Nasser (editor), *Three-dimensional Constitutive Relations and Ductile Fracture* (IUTAM Symposium). North-Holland, 1981.
D. Broek, *Elementary Engineering Fracture Mechanics*. Martinus Nijhoff, 1982.
R. W. Hertzberg, *Deformation and Fracture Mechanics of Engineering Materials*. Wiley, 1983.
A. G. Atkins and Y. W. Mai, *Elastic and Plastic Fracture*. Ellis Horwood, 1985.

Beams and Framed Structures

J. F. Baker, M. R. Horne and J. Heyman, *The Steel Skeleton*, vol. II. Cambridge University Press, 1956.
B. G. Neal, *The Plastic Methods of Structural Analysis*. Chapman & Hall, 1956.
L. S. Beedle, *Plastic Design of Steel Frames*. John Wiley, 1958.
J. F. Baker and J. Heyman, *Plastic Design of Frames* 1: *Fundamentals*. Cambridge University Press, 1969.
J. Heyman, *Plastic Design of Frames* 2: *Applications*. Cambridge University Press, 1971.

Rotating Discs

E. L. Robinson, Bursting tests on steam-turbine disk wheels, *Transactions of A.S.M.E.*, vol. 66, 1944, pp. 373–380.
J. Heyman, Plastic design of rotating discs, *Proceedings of the Institution of Mechanical Engineers*, vol. 172, 1958, pp. 531–541 (Discussion pp. 542–547).
V. Tvergaard, On the burst strength and necking behaviour of rotating discs, *International Journal of Mechanical Sciences*, vol. 20, 1978, pp. 109–120.
D. Durban and V. Birman, Elasto-plastic analysis of an anisotropic rotating disc, *Acta Mechanica*, vol. 49, 1983, pp. 1–10.

Metal-forming

R. Hill, *The Mathematical Theory of Plasticity*. Oxford University Press, 1950.
J. G. Wistreich, Investigation of the mechanics of wire drawing, *Proceedings of the Institution of Mechanical Engineers*, vol. 169, 1955, pp. 655–665.
C. E. Pearson and R. N. Parkins, *The Extrusion of Metals*. Chapman & Hall, 1960.
W. Johnson and H. Kudo, *The Mechanics of Metal Extrusion*. Manchester University Press, 1962.

H. LIPPMAN (editor), *Engineering Plasticity: theory of metal-forming processes* (CISM Lectures 139). Springer-Verlag, 1977.
W. SZCZEPINSKI, *Introduction to the Mechanics of Plastic Forming of Metals.* Sijthoff and Noordhoff, 1979.
W. JOHNSON and P. B. MELLOR, *Engineering Plasticity.* Ellis Horwood, 1983.

SOIL MECHANICS

A. N. SCHOFIELD and C. P. WROTH, *Critical-state Soil Mechanics.* McGraw-Hill, 1968.
J. SALENCON, *Applications of the Theory of Plasticity in Soil Mechanics.* (Translated R. W. Lewis *et al.*) Wiley, 1977.

REINFORCED CONCRETE AND YIELD-LINE THEORY

R. H. WOOD, *Plastic and Elastic Design of Slabs and Plates.* Thames & Hudson, 1961.
R. P. JOHNSON, *Structural Concrete.* McGraw-Hill, 1967.
W. F. CHEN, *Plasticity in Reinforced Concrete.* McGraw-Hill, 1982.
M. P. NIELSEN, *Limit Analysis and Concrete Plasticity.* Prentice-Hall, 1984.

SHELL STRUCTURES

P. G. HODGE, *Limit Analysis of Rotationally Symmetric Plates and Shells.* Prentice-Hall, 1963.
C. R. CALLADINE, *Theory of Shell Structures* (Chapter 18). Cambridge University Press, 1983.

STRUCTURAL SAFETY

A. G. PUGSLEY, *The Safety of Structures.* Edward Arnold, 1965.

THEORY OF CHARACTERISTICS

M. B. ABBOTT, *An Introduction to the Method of Characteristics.* Thames & Hudson, 1966.

STRUCTURAL OPTIMISATION

R. H. GALLAGHER and O. C. ZIENKIEWICZ (editors), *Optimum Structural Design: Theory and applications.* Wiley, 1973.
M. Z. COHN, G. MAIER and D. E. GRIERSON (editors), *Engineering Plasticity by Mathematical Programming.* Pergamon Press, 1979.

MASONRY CONSTRUCTION

J. HEYMAN, *The Masonry Arch.* Ellis Horwood, 1982.

APPENDIX I

THE MOHR CIRCLE OF STRESS

IN ORDER to discuss in a meaningful way the idea of "state of stress" at a point within a body it is necessary to be able to describe a given state of stress with respect to an arbitrary set of local orthogonal axes. A fairly complete picture of what is involved in transformations of this sort may be obtained from a study of *two-dimensional* states of stress.

Consider a sheet of material subject to loading in its own plane. At any point in the sheet we may define an axis u in the plane of the sheet, and we may examine the tractions transmitted over a "slit" perpendicular to the u-axis, which we call the u-plane. The tractions may conveniently be separated into two components, a normal stress σ_u and a shearing stress τ_u, as indicated in Fig. A.1(a), acting normal to and tangential to the slit plane, respectively. σ and τ are forces per unit area of slit, in the limit as the area tends to zero. We attach subscript u to the components of stress acting on the u plane. In Fig. A.1(a) σ and τ are shown in their positive sense: σ is positive when the arrow is directed *out* of the material, and τ is positive when the arrow is directed to the *right* with reference to a vantage point within the material.

It is clear that with this convention of sign the stress components σ_u and τ_u have the same values with reference to the material on *both* sides of the slit.

We now enquire how the values of σ_u and τ_u vary at a given point in the sheet when the inclination of the u-axis changes.

To do this we consider the equilibrium of a little block of material detached from the body by a *set* of slits. The simplest small block is a triangle, and we choose to make two of the slits perpendicular to arbitrary orthogonal x-, y-axes fixed in the sheet, as shown in Fig. A.1(b). The geometry of the wedge thus formed is defined by the angle α, measured clockwise from the x-axis to the u-axis.

Equilibrium of the block requires satisfaction of three equations. One is, simply,

$$\tau_y = -\tau_x \qquad \text{(A.1}$$

and the others give relationships between the variables σ_u, τ_u, the given values of σ_x, σ_y, τ_x, τ_y $(= -\tau_x)$ and the variable α.

The result expressed by (A.1), viz. that shearing stresses on perpendicular planes have the same magnitude (and opposite sign with the present notation), is known as "complementary shear". It applies to *all* mutually perpendicular

planes in states of two-dimensional stress and it has its counterpart in three-dimensional stress systems (see Appendix V).

It is a matter of straightforward manipulation to show that for a given state of stress the stress-point (σ_u, τ_u) in a two-dimensional σ, τ space traces out, as α varies, a *circle* whose centre is on the σ-axis, as shown in Fig. A.1(c).

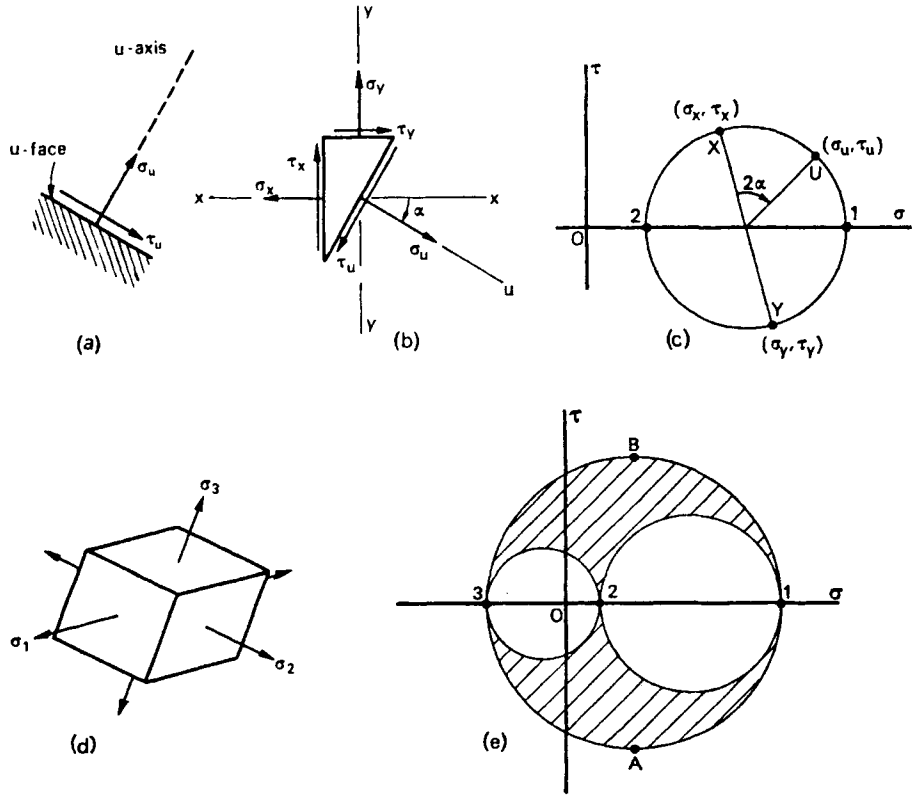

FIG. A.1. The Mohr circle of stress.

This diagram is known as the "Mohr circle of stress" after its inventor. Many observations may be made on this figure, but we shall restrict ourselves to the essential ones.

(i) The circle is defined by the points $X(\sigma_x, \tau_x)$ and $Y(\sigma_y, \tau_y)$ which lie at opposite ends of a diameter.

(ii) The circle represents the *state of stress* at a point in the body.

(iii) The relationship between the $U(\sigma_u, \tau_u)$ and X points on the circle is that they subtend angle 2α at the centre of the circle, the radius-vector to U rotating in the same sense as the axis u, but through twice the angle.

(iv) It is always possible to find two directions, perpendicular to each other, for which τ is zero on the corresponding planes. These axes and planes are called *principal* axes and planes, respectively, and the corresponding magnitudes of σ the *principal stresses*. Numerical suffices, 1 and 2, are used to denote the principal axes, as indicated in Fig. A.1(c).

So far we have been discussing two-dimensional states of stress and our single-suffix notation has been adequate. When we consider general three-dimensional states of stress we need a more comprehensive notation. However, we can make some powerful statements about three-dimensional states of stress without needing to discuss notation if we accept the result that it is always possible—for *any* state of three-dimensional stress—to choose three mutually perpendicular *principal* directions of stress. A small cube "cut out" with faces perpendicular to these directions sustains on its faces only the normal stresses, σ_1, σ_2, σ_3, as indicated in Fig. A.1(d).

The two-dimensional analysis may be applied in turn in each of the planes perpendicular to axes, 1, 2 and 3, and if the resulting three diagrams are superimposed we obtain the composite figure shown as Fig. A.1(e). Now a full analysis shows that if the direct stress and (resultant) shearing stress are worked out on *any* arbitrarily inclined plane the corresponding point in Fig. A.1(e) lies within the region shown hatched between the three circles. Rules may be worked out to locate the point in terms of angles defining the inclined plane, but we shall not discuss them here. What is important to us in our present study is that the magnitude of the largest *shearing stress* which can occur on any inclined plane for a given state of stress is readily determined in terms of principal stress and, moreover, the inclination of the relevant planes (corresponding to points A and B in Fig. A.1(e)) is readily determined. These planes are always inclined at 45° to two principal directions of stress, and are parallel to the third.

The sign convention indicated in Fig. A.1(a), which is used extensively in the book, is rather unusual. Clearly there are many possible notations and conventions, and this one has the sole merit of making the two-dimensional Mohr circle entirely unambiguous. This is clearly desirable in the present book which makes considerable detailed use of the Mohr circle in several chapters. The reader will find that a little time spent in mastering the Mohr circle construction is amply rewarded. See also Appendix V.

APPENDIX II

VIRTUAL WORK

THE principle of virtual work is indispensable in the proof of structural theorems, and it is often useful in the discussion of particular structural problems. There are many possible statements of the principle, depending on what are regarded as the basic axioms of mechanics. Here we shall take the simple view that (a) we understand what we mean by "equilibrium" of "forces" acting on a macroscopic body and (b) that three-dimension Euclidian geometry is essentially a simple business of lines, lengths and angles.

The condition of equilibrium for a set of forces acting at a point may be stated in several ways which are precisely equivalent, as follows.

(i) Forces are vectors. For a set of forces to be in equilibrium the "space polygon" formed by the vectors must close.

(ii) The algebraic sum of the *components* of the vectors in any arbitrary common direction must be zero.

(iii) Because the net unbalanced force on the point is zero, the sum of the work done by each force separately when the point moves a small distance in any arbitrary direction is zero.

This last statement, which we shall find particularly useful, involves the definition of the *work* done by a force (of constant magnitude and direction) when its point of application moves; work is the product of the force and the projection of the distance moved onto the line of action of the force—or, alternatively, the scalar product of the force and displacement vectors.

We now set out to establish the principle of virtual work for an arbitrary structure. For definiteness consider a simple two-dimensional framework of weightless bars pin-jointed to each other, and in equilibrium under loads P applied at the joints, as indicated in Fig. A.2(a). Each bar of the structure carries a tension T which is of such a magnitude that all of the joints of the structure are in equilibrium. Figure A.2(b) shows the joints of the structure and the forces acting on them, the bars having been "removed". Notice that each bar exerts equal and opposite forces at two joints.

Now suppose that each of the joints in Fig. A.2(b) is given an arbitrary small displacement in the plane, that the virtual-work equation of equilibrium is written for each joint, and that all the resulting equations are added together. In the total sum each force P will occur *once*, multiplied by the component of the displacement of the joint in the direction of the line of action of the force. On the other hand, each force T will occur *twice*, multiplied by appropriate components of displacement at two joints. Inspection shows that when the work terms corresponding to a pair of T forces are added, each T is

multiplied, effectively, by the movement of the two corresponding joints *towards each other*—all displacements being assumed "small".

Thus our overall equation may be written

$$\Sigma P_j u_j = \Sigma T_i e_i \qquad \text{(A.2)}$$

where summation is over all joints and bars respectively, u_j are the components of the (small) joint displacements in the directions of the lines of action of P_j, and e_i are the changes in *separation* of pairs of joints.

In this equation the u's and e's correspond to *any* arbitrary set of small displacements of the joints. Thus, for example, if only *one* joint is displaced, equation (A.2) gives, precisely, the equilibrium equation in the corresponding direction for one joint. Alternatively, if the joint displacements are chosen to

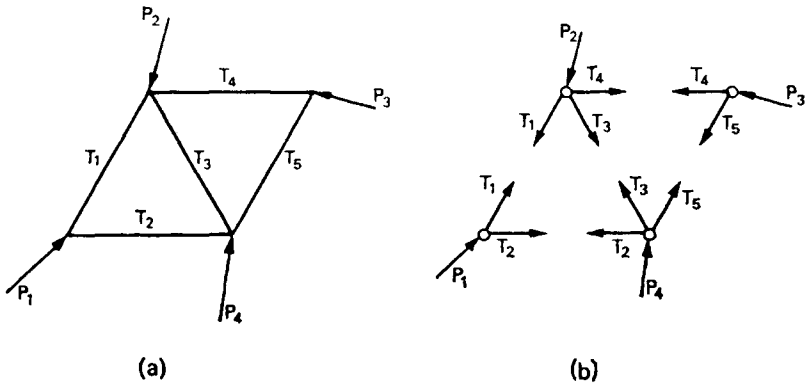

FIG. A.2. The principle of virtual work.

be such that the *relative* positions of the joints do not change, we would obtain an equilibrium equation for the truss as a whole. In other words, by suitable choice of joint displacements equation (A.2) gives, in turn, *all* equilibrium equations which can be written for the structure or any part thereof.

We obtained equation (A.2) by "dismantling" the structure and making arbitrary displacements of the detached joints. The equation is equally valid if we regard e_i as the *extensions* of the members in a general distortion of the structure without prior dismantling. The important point here is that the distortion of the structure is an *arbitrary* one which satisfies the *geometrical* requirements of continuity without any question of the extensions corresponding to the effects of *tension* in the members, rather as if we were distorting a drawing of the structure made on a rubber sheet. The "detached joint" picture is a useful one to recall if there is any difficulty in comprehending this rather subtle point.

Now the simple two-dimensional pin-jointed structure was used primarily as an illustrative example. Clearly the same arguments may be applied to three-dimensional pin-jointed structures and, moreover, to any solid three-

dimensional structure. In this case the appropriate form of the R.H.S. of equation (A.2) is

$$\int_V \sigma \epsilon \, dV \tag{A.3}$$

where integration extends over the entire volume of the body and σ, ϵ are appropriate symbolic representations of stress and strain, respectively. In fact, the virtual work equation may take many forms, depending on the variables used to describe the loading and the internal structural action (see Appendix III).

Finally we emphasize that in the virtual work equation (A.2) the forces P and tensions T form an "equilibrium set" (for the *undeformed* structure), and the small displacements u and extensions e form a geometrically "compatible set". There is no necessary mechanical relationship between T and e or between u and e as far as the virtual work equation is concerned. To emphasise the independence of the "equilibrium" and "compatible" variables it is helpful to introduce additional, obvious, symbolism into equation (A.2) as follows:

$$\overline{\left|\Sigma P_j u_j\right.} \quad = \quad \overline{\left.\Sigma T_i e_i\right|} \tag{A.4}$$

For further reading see the book by Neal listed under Structural Mechanics in the Bibliography.

APPENDIX III

"CORRESPONDING" LOADS AND DEFLECTIONS

A CENTRAL notion in the concept of virtual work (Appendix II) is that the *force* and *displacement* quantities are related to each other in the sense that the product of corresponding variables represents a quantity of *work*. If a single force P acts at a joint, the "corresponding" measure of displacement of the joint is the component of the displacement in the (positive) direction of the line of action of the force. Similarly, if the components of a force are specified, say X, Y, Z in mutually perpendicular directions, the "corresponding" displacements are the components of displacement x, y, z in the same directions, and the appropriate (scalar) product is simply $Xx + Yy + Zz$.

We are not, however, limited to discussion of loads on structures in terms of force as such. A structure may be loaded by a *couple*, for which the corresponding displacement is an angle of rotation (measured in radians); or a *pressure*, for which the corresponding displacement is a "swept volume"; or a uniform *line load*, for which the corresponding displacement is a "swept area".

Similarly (as noted in Appendix II), we are not limited to discussion of internal structural action in terms of tension or, indeed, stress: we often use the "strength of materials" variables of bending moment, twisting moment, etc. For example, where the compatible deformation involves continuous changes of curvature κ along a beam, the corresponding form of the R.H.S. of equation (A.2) is

$$\int_l M\kappa \, dl$$

where M represents bending moment, and the integration is along the length l of the beam. If, however, the compatible deformation involves "kinks" in the beam (as it may, legitimately and usefully) the corresponding term is

$$\Sigma M\theta$$

where θ is the angle of a kink and M is the bending moment at the corresponding point in the beam.

There is usually no difficulty in deciding, in any given situation, what are the corresponding displacement variables to any set of force variables.

APPENDIX IV

PROPORTIONAL LOADING

MANY structures sustain several *independent* sets of loads. For example a building structure in general sustains (a) "dead" load (its own weight plus the weight of any fixed equipment) in addition to several forms of "live" load such as (b) floor loading due to the weight of people and movable objects, (c) wind loading and (d) snow loading. It is easy to think of many other examples.

Sometimes it simplifies thinking to imagine that all loads are "geared" to each other so that when one class of loading is, say, doubled in magnitude, so also are all other classes of loading. In effect, therefore, the loading on the structure at any time is specified by a *single* (*scalar*) *parameter* under these circumstances.

Some early forms of the upper- and lower-bound theorems were established for structures sustaining such "proportional loading", and bounds were thus established on the single "load factor" at collapse. In this book, however, we do not find it necessary to impose restrictions of this sort because in general we work in terms of a "collapse load surface" in a multi-dimensional load space.

There are, of course, many important situations where analysis in terms of a single loading parameter is appropriate: forming operations, for example, fall into this category.

APPENDIX V

NOTATION FOR THREE-DIMENSIONAL STRESS

FIGURE 2.12, p. 33, shows a possible notation for a general three-dimensional state of stress, referred to arbitrary mutually perpendicular x, y, z axes; see also Fig. 6.3(a), p. 142. It is necessarily different from the specially simple notation used for the Mohr circle of stress (Appendix I). The axes x, y, z now have positive and negative senses, and τ_{xy}, for example—which is a component of shearing stress on the x faces of the cube—is directed in the positive y direction for the face of the cube on the "positive x" side.

It follows that the "complementary shear" relations (see Appendix I) are, in the present notation,

$$\tau_{xy}=\tau_{yx} \quad \text{etc.}$$

without the minus sign which occurred in our main notation.

There is, in fact, little occasion in general for confusion between the two sets of notation.

APPENDIX VI

SYMBOLS, UNITS AND CONVERSION FACTORS

THE following information, except for the abbreviations psi and tsi, is in accordance with British Standard 3763: 1964 "The International System (SI) Units".

SYMBOLS

m	metre
kg	kilogramme
s	second
N	newton (kg m/s^2)
ft	foot
in.	inch
lb	pound (mass)
lbf	pound force
tonf	ton force = 2240 lbf
psi	lbf/in^2
tsi	tonf/in^2

PREFIXES

m	milli-	= 1/1000
k	kilo-	= 1000
M	mega-	= 1,000,000
G	giga-	= 1,000,000,000

CONVERSION FACTORS

The following factors should be adequate for rough calculations. For exact conversion factors see B.S.3763: 1964.

Length: 1 ft is equivalent to 0·305 m
Mass: 1 lb „ „ 0·454 kg

Force:	1 lbf	is equivalent to	4·45 N
	1 tonf	„	„ 10 kN
Stress:	1 psi	„	„ 6·89 kN/m²
	1 tsi	„	„ 15·4 GN/m²
Density:	1 lb/ft³	„	„ 16·0 kg/m³

ANSWERS TO PROBLEMS

CHAPTER II

2.4. See the way point A (Problem 2.12) is plotted in Fig. 2.25.

2.5. $(2/3)^{\frac{1}{2}}$.

2.7. (a) $\sigma^2 + 4\tau^2 = Y^2$, (b) $\sigma^2 + 3\tau^2 = Y^2$.

2.9. $(d/l)^2$.

2.13. The state of stress in the cylindrical shell wall is equivalent to a pure shear plus a hydrostatic tension. The state of stress in the spherical shell wall is equivalent to a uniaxial compression plus a hydrostatic tension.

2.14. The eighteen points in σ_1, σ_2 space are:
(20, 0), (20, 20), (0, 20), (–20, 0), (–20, –20), (0, –20), (21, 7), (21, 14), (14, 21), (7, 21), (–7, 14), (–14, 7), (–21, –7), (–21, –14), (–14, –21), (–7, –21), (7, –14), (14, –7).

2.15. Tresca: (a) see Fig. 5.11, (b) two lines $|\sigma_1 - \sigma_2| = Y$. In this case the flow rule requires σ_3 to be intermediate between σ_1 and σ_2.
Mises: (a) the ellipse $\sigma_1^2 + \sigma_2^2 - \sigma_1\sigma_2 = Y^2$, (b) two lines $(\sigma_1 - \sigma_2)^2 = 4Y^2/3$.

CHAPTER III

3.3. $\sigma_z = \lambda pa^2/(b^2 - a^2) + (1-\lambda)(\sigma_r + \sigma_\theta)/2$, $0 \leqslant \lambda \leqslant 1$, where $p = Y \ln(b/a)$, $\sigma_r = Y \ln(r/b)$ and $\sigma_\theta - \sigma_r = Y$.
The first part of the question is solved by having, in effect, $\lambda = 1$ and expressing the condition that σ_z is intermediate between σ_θ and σ_r.

3.6. The stress trajectory in the π-plane corresponding to $a \leqslant r \leqslant c$ would be a segment of the edge $\sigma_\theta - \sigma_r = Y$ of the hexagon, instead of a single point. σ_z would have to be intermediate between σ_θ and σ_r, of course.

3.7. $b/a \leqslant 2{\cdot}2$, approximately.

3.16. The state of stress at any radius in a thick tube at collapse is a pure shear superimposed on a hydrostatic tension. (It would really be more appropriate to deal in terms of k rather than Y throughout the chapter.)

CHAPTER IV

4.1. $p = Y(1 - a/b)$.

4.2. $p = Y \ln(1 + h/a)$.

CHAPTER V

5.1. Dimensional analysis.

5.6. For example, if $a/b = 0{\cdot}2$ and hub thickness = 3 × disc thickness, the hub extends to $0{\cdot}32b$.
Volume of disc with hub = 1·09 (volume of plain disc).
Volume of disc with compact ring = 1·05 (volume of plain disc).

5.7. $A = ha(\sigma_r/Y)/(1-a^2/c^2)$.

CHAPTER VI

6.3. For circle, square and triangle, $T_p = 2/3\ Akr$, where A = area of cross-section and r = radius of inscribed circle. For rectangle $a \times b$, $b \geqslant a$, $T_p = \frac{a^2k}{2}\left(b - \frac{a}{3}\right)$.

6.5. ½ per cent.

6.6. $125/3\ ka^3$, reduced by $< 25/3\ ka^3$, i.e. < 20 per cent.

6.7. (a) $T^u = (2\pi/3)\ ka^3\ (= T^l)$, (b) $T^u = 1{\cdot}147\ (8/3)\ ka^3$.

6.8. The P, M locus consists of two parabolic segments.

6.9. $T^l = 25/12\ ka^3$.

6.10. $T_p = k((14/3)b^3 + k(b^2c/2 - b^3/6)$, $c \geqslant b$. About 2 per cent for the configuration shown.

CHAPTER VII

7.1. $F^u = 5{\cdot}52\ kb$ (i.e. 12 per cent lower than (7.3)). In the optimum configuration the band of intense shear subtends approximately 134° at the centre of the circle.

7.4. $F^u = 4\sqrt{2}\ kb = 5{\cdot}66kb$, when the "depth" of the mode is equal to $b/\sqrt{2}$.

7.8. Equation (7.23).

7.10. Mechanism (a): For equilateral triangles, $F^u_{\text{smooth}} = 10/\sqrt{3}\ kb$; $F^u_{\text{rough}} = 4\sqrt{3}\ kb$. For optimum isosceles triangles (cf. Problem 7.4) $F^u_{\text{smooth}} = 4\sqrt{2}\ kb$; $F^u_{\text{rough}} = 4\sqrt{3}\ kb$. Mechanism (b): $F^u_{\text{smooth}} = 6kb$ when $x = b/2$; $= 6{\cdot}25\ kb$ when $x = b$. $F^u_{\text{rough}} = 6{\cdot}5\ kb$ when $x = b/2$ or $x = b$. ($x/b_{\text{optimum}} = \frac{1}{2}$ (smooth); $= 1/\sqrt{2}$ (rough)).

7.11. Between successive lower-bound points in Fig. 7.21 the curve rises almost linearly, with a "jump" in ordinate of $(1 + \sqrt{2})/2n$ at $b/h = 2n\sqrt{2}$, where n is an integer.

7.12. $F^u/2kb = 1 + 0{\cdot}25\ h/b$ for smooth dies. Add $0{\cdot}25\ b/h$ for rough dies.

7.13. $F^u/2ky = 0{\cdot}42$.

CHAPTER VIII

8.1. $p = 2k\ \ln(b/a)$.

8.2. $\dot{\gamma} = V/r$. $\dot{D} = kV\alpha(b-a)$

8.3. (a) and (b): $F^u = 2kb(1 + \pi/2)$.
8.6. (a) $q = 2k(1 + \pi/2 - \theta)$
(b) $q = 2k(1 + \pi/2 + \theta)$
(c) $q = 2k(1 + \pi/2 - \theta)$.
8.7. $F = 2ka(1 + \pi/2)$.
8.8. $F^u = 2kb(1 + \pi/2)$.

CHAPTER IX

9.3. $p = 6M_0/a^2$. (Resultant of support reactions acts $2/\pi$ times radius of plate from the centre; of pressure, 2/3 times this.)
9.7. $p = 8M_0/a^2$. (Volume of "cap" = $\frac{1}{2}$ volume of circumscribing cylinder.)
9.12. $P = 2\pi M_0$, both lower and upper bounds.
9.13. $\Sigma P \geqslant 4\pi M_0$, all loads acting in the same direction.
9.14. Top steel reinforcement may be omitted over a central region whose area is fraction $M/(M + m)$ of the total area.
9.15. $a/b = 0{\cdot}62$, approximately (a root of $x^3 - x^2 - 3x + 2 = 0$).

CHAPTER X

10.3. Let $t^u/2k = f(\xi)$ for a single mode. Then for n equal sub-modes, $t^u/2k = n f(\xi/n)$.
10.4. $\alpha = \xi/2$.
10.6. $\xi = 2\alpha\sqrt{(n(n + 1))}$.
10.7. $q\, r_t = t(1 - r_t)$.
10.8. $t^u/2k = \alpha + \xi/2\alpha$ for ξ and α small: cf. equation (10.16).
10.14. Plane strain: $t^l = 2k \ln(1/s) = 2k \ln \eta$.
Axisymmetric: $t^l = Y \ln(1/s^2) = Y \ln \eta$.
Note that, written in this way, both results apply to *either* Tresca *or* Mises material.
10.15. $t^u/2k = \frac{1}{2}((s - s^{-1})\operatorname{cosec} 2\alpha - 2\cot 2\alpha)$.
Observe the *formal* relationship between this and equation (10.9) and note that it may be rewritten $t^u/2k = \frac{1}{2}\{2(\cosh \xi - \cos 2\alpha)\operatorname{cosec} 2\alpha\}$, which is formally similar to equation (10.11). Spot values may therefore readily be determined by use of the data of Fig. 10.4. For small α and ξ equation (10.16) is obtained, but for larger angles the above formulas may give much higher upper bounds than (10.9) or (10.11): consider $\alpha = 90°$, for example, and compare the mode with that of Fig. 10.8(a).
10.16.(a) $x_{opt} = s$; $t^u = k\left(s^{-1} - s\right)$.

CHAPTER XI

11.1. $W/W_0 = 0{\cdot}8/(1 - (0{\cdot}6 \pm y/l)^2)^{\frac{1}{2}}$.
11.2. $dP/dy)_0 = P_0/L\sqrt{3}$.

11.4. $ds/de)_0 = -Y$; $H = d\sigma_y/d\epsilon)_0 = Y$.

11.5. On the diagram of Fig. 2.7 construct a parabola $\sigma = C(l/l_0)^2$ which just touches the σ, l/l_0 curve for the material. Then C (the intercept of the parabola with line $l/l_0 = 1$) is the required "nominal hoop bursting stress".

11.6. $W = \dfrac{8}{l}\dfrac{Y}{4}(d^2 + y^2) = W_0\left(1 + \left(\dfrac{y}{d}\right)^2\right)$.

INDEX